SOVIET PHYSICS

JETP

A translation of the Journal of Experimental and Theoretical Physics of the USSR.

SOVIET PHYSICS JETP VOL. 34 (7), NO. 3, pp. 371-539 September, 1958

ACADEMICIAN ISAAK KONSTANTINOVICH KIKOIN

(On His 50th Birthday)

J. Exptl. Theoret. Phys. (U.S.S.R.) 34, 537-540 (March, 1958)

MARCH 28, 1958 marks the 50th birthday of the outstanding Soviet physicist, academician Isaak Konstantinovich Kikoin.

I. K. Kikoin was born on 28 March 1908 in Zhagar, a small city in what is now the Lithuanian S.S.R. His father was a schoolteacher. After completing his elementary schooling he entered the Pskov Agricultural Technical School, and in 1925 he enrolled at the Physico-Mechanical Faculty of the Leningrad Polytechnic Institute, from which he was graduated in 1930. He showed great interest in physics and mathematics even while in school. As a student of the Leningrad Polytechnic Institute Isaak Konstantinovich started working in 1928 at the Leningrad Physico-Technical Institute, with which he was continuously associated for many years, having become one of the outstanding representatives of the school of Soviet physicists, trained by academician A. F. Ioffe in that institute.

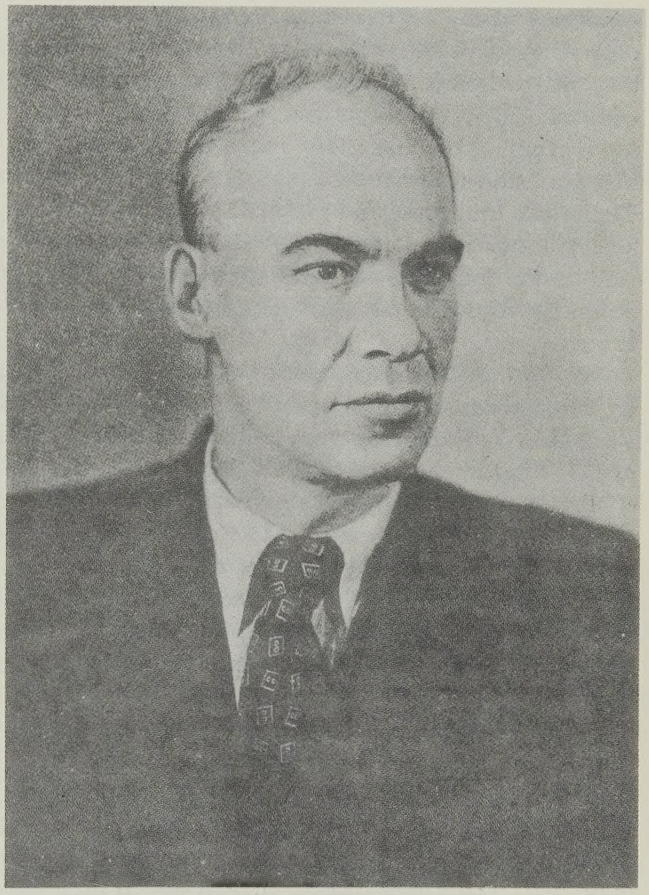

The first research performed by Isaak Konstantinovich, already in his student years (in the laboratory directed by Ia. G. Dorfman), concerned the nature of ferromagnetism.[1] Dating to that time are his first investigations of electric and galvanomagnetic properties of liquid metals[2-4,13]. These disclosed the presence of a Hall effect and of a change in the resistance in liquid metals in a magnetic field. Prior to these investigations, the presence of galvanomagnetic phenomena in liquid metals has not been ascertained; it was even assumed that these phenomena do not take place in liquid metals, which have no crystalline structure. Later, too, Isaak Konstantinovich turned to research on liquid metals. Working together with S. V. Gubar',[1] he showed experimentally that the temperature variation of the resistance of liquid metals is connected only with the change in the volume of the metal, and not with a true temperature dependence of electric conductivity.

The first investigations on the study of liquid metals were completed by Isaak Konstantinovich upon his return in 1930 from a scientific tour through Holland and Germany, where he was sent after being graduated from the Institute (he worked for some time in Munich with W. Gerlach).

In 1933 Isaak Konstantinovich started a cycle of investigations on the internal photoeffect and the Hall effect in semiconductors.[7,9] These led to the discovery (together with M. M. Noskov) of a new phenomenon — the photoelectromagnetic effect in semiconductors (the Kikoin-Noskov effect).[8,10,11,16] The investigations concerned the fundamental properties of this phenomenon — the spectral distribution and the dependence on the light intensity, on the temperature, and on the magnetic field. During the course of these investigations still another phenomenon was discovered, the so-called transverse effect, quadratic in the magnetic field, taking place when the plane of the specimen makes an angle other than zero with the direction of the magnetic field.[12]

Simultaneously with these investigations, Isaak Konstantinovich began many new projects involving the study of the properties of metals. This was connected, to a certain extent, with the founding of the Ural' Physico-Technical Institute in 1932, into which I. K. Kikoin's laboratory was also incorporated. During the first five years of its existence, this institute was housed in the Leningrad Physico-Technical Institute, and in 1936 it transferred its activities to Sverdlovsk, where it still is in operation as the Institute of Metal Physics, Academy of Sciences, U.S.S.R. as part of the Academy's Ural' branch.

In 1934 I. K. Kikoin published a large monograph on the physics of metals, written jointly with Ia. G. Dorfman.[14] For many years this was the only book of this kind in the Russian language.

Isaak Konstantinovich's investigations in metal physics involved essentially two problems: superconductivity and galvanomagnetic phenomena in ferromagnets. In the field of superconductivity he succeeded (together with B. G. Lazarev[5,6]) in establishing a correlation between superconductivity and the Hall effect. Superconducting metals were found to have a very small Hall constant (two orders of magnitude less than nonsuperconducting metals). Together with S. V. Gubar', Isaak Konstantinovich made in 1939 a very precise measurement of the gyromagnetic effect in superconductors.[17,18] The Landé factor turned out to be unity, showing the diamagnetism of superconductors to be connected with electron currents rather than, say, with electron spins.

By investigating the temperature dependence of the Hall effect in ferromagnets (nickel) down to the transition through the Curie point, Isaak Konstantinovich confirmed the fundamental fact that the Hall emf in ferromagnets is actually determined by the magnetization of the specimen, and not by the intensity of the magnetic field.[15] An original experiment made possible reliable verification of this fact, important to the theory of ferromagnetism. Further experiments on copper-nickel and palladium-nickel alloys[19] have demonstrated that the Hall constant in paramagnets is determined by the magnetization, so that in general it consists of two parts, one being an "ordinary" constant, independent of the temperature, and the second following the Curie-Weiss, law as does the magnetic susceptibility of a paramagnet.

For the past few years I. K. Kikoin has been continuing his intensive research of the transverse photoelectromagnetic effect.[22-25] He has detected here an isotropy of the effect in germanium, and has experimentally established beyond doubt a connection between this anisotropy and the crystallographic structure of germanium.

Isaak Konstantinovich's work in the Ural' has been identified with many investigations of applied nature. Jointly with D. L. Simonenko, he developed a mass-spectographic method for the analysis of gases, and together with S. V. Gubar' and V. S. Obukhov he constructed a new kind of kiloammeter based on the measurement of the magnetic field of the current-carrying conductors. In the measurement of tens of thousands of amperes dc (in electrolysis plants), this method has substantial advantages over the use of ordinary shunt instruments. Isaak Konstantinovich and his co-workers were awarded the Stalin prize for this development.[20]

In addition to the investigations mentioned above, I. K. Kikoin has led actively many other important research projects. His entire scientific activity is characterized by high creative initiative, constant originality in the approach to the solution of the studied problem, and extensive and deep erudition in problems of modern physical sciences.

From the very start of his scientific activity, Isaak Konstantinovich has been engaged in extensive pedagogical activity in academic institutions, and also in scientific-organizational work. He started teaching already while at the Physico-Mechanical Department of the Leningrad Polytechnic Institute, and continued at the Ural', where for eight years he was in charge of the Physics Faculty of the Ural Polytechnic Institute. At present he holds the rank of Professor at the Moscow State University. A brilliant lecturer, Isaak Konstantinovich has won the love of the students and the respect of his colleagues. He has introduced many novelties in the physics education of our country and prepared original modern physics courses, always attempting to eliminate all purely formal and obsolescent material from the programs.

I. K. Kikoin's scientific activity was recognized by the Soviet scientific society. In 1943 he was chosen a corresponding member of the Academy of Sciences, and became a full member in 1953. This activity was also highly valued by the government — Isaak Konstantinovich was awarded orders of the Soviet Union and has won the title of a Stalin Prize Laureate. I. K. Kikoin reaches this significant age in his life, his 50th birthday, in the full bloom of his creative activity, in energetic and fruitful work.

The editorial staff of JETP congratulates Isaak Konstantinovich and sincerely wishes him good health and new creative successes for the benefit of our Fatherland.

---

[1] The Role of Conduction Electrons in Ferromagnetism, Z. Physik **54**, 289 (1929) (with Ia. G. Dorfman).

[2] Hall Effect in Liquid Metals, Z. Physik **71**, 393 (1931) (with I. Fakidov).

[3] Change of Electric Conductivity of Liquid Metals in a Magnetic Field, Z. Physik **75**, 679 (1932) (with I. Fakidov).

[4] Effect of Transverse Magnetic Field on Resistance of Liquid Metals, J. Exptl. Theoret. Phys. (U.S.S.R.) **3**, 36 (1933); Sow. Phys. **3**, 381 (1933) (with I. Fakidov).

[5] Superconductivity and Hall Effect, J. Exptl. Theoret. Phys. (U.S.S.R.) **3**, 44 (1933); Nature **129**, 57 (1932) (with B. G. Lazarev).

[6] On the Phenomenon of Superconductivity, J. Exptl. Theoret. Phys. (U.S.S.R.) **3**, 237 (1933) (with B. G. Lazarev).

[7] Internal Photoeffect in Semiconductors and the Hall Effect, Sow. Phys. **3**, 97 (1933) (with M. M. Noskov).

[8] New Photoelectric Effect in Cuprous Oxide, Sow. Phys. **5**, 586 (1934); J. Exptl. Theoret. Phys. (U.S.S.R.) **4**, 123 (1934) (with M. M. Noskov).

[9] Hall Effect and Internal Photoelectric Effect in Cuprous Oxide, Sow. Phys **4**, 531 (1933); J. Exptl. Theoret. Phys. (U.S.S.R.) **3**, 402 (1933) (with M. M. Noskov).

[10] New Photoelectric Effect in Cuprous Oxide, Sow. Phys. **6**, 478 (1934).

[11] Effects Observed in Cuprous Oxide Illuminated in a Magnetic Field, Dokl. Akad. Nauk SSSR **2**, 71 (1934).

[12] Effects Observed in Cuprous Oxide Illuminated in a Magnetic Field, Dokl. Akad. Nauk SSSR **3**, 418 (1934).

[13] Change of Resistance of Liquid Metals in a Magnetic Field, Sow. Phys. **7**, 507 (1935); J. Exptl. Theoret Phys. **5**, 710 (1935) (with I. Fakidov).

[14] Физика металлов (Physics of Metals), GTTI, Moscow-Leningrad, 1936 (with Ia. G. Dorfman).

[15] Hall Effect in Nickel Going through the Curie Point, Sow. Phys. **9**, 1, (1936).

[16] Further Investigations of the New Photoelectric Effect in Semiconductors, J. Exptl. Theoret. Phys. (U.S.S.R.) **8**, 826 (1938).

[17] Gyromagnetic Effect in Superconductors, Dokl. Akad. Nauk SSSR **19**, 249 (1938) (with S. V. Gubar').

[18] Gyromagnetic Effect in Superconductors, J. Phys. (U.S.S.R.) **3**, 333 (1940); J. Tech. Phys. (U.S.S.R.) **16**, 129 (1946) (with S. V. Gubar').

[19] Hall Effect in Paramagnetic Metals, J. Exptl. Theoret. Phys. (U.S.S.R.) **10**, 242 (1940).

[20] New Apparatus System for the Measurement of Large Direct Currents, TEKhSO, No 183/24, 1943.

[21] Temperature Dependence of the Resistance of Liquid Metals at Constant Volume, J. Phys. (U.S.S.R.) **9**, 52 (1945) (with S. V. Gubar').

[22] New Photomagnetic Effect in Semiconductors in an Inhomogeneous Magnetic Field, Dokl. Akad. Nauk SSSR **96**, 463 (1954).

[23] Cause of EMF Produced by Illuminating a Semiconductor in an Inhomogeneous Magnetic Field, Dokl. Akad. Nauk SSSR **99**, 51 (1954) (with I. Ganev and A. Karchevskii).

[24] Transverse Photomagnetic Effect in n- and p-germanium, Dokl. Akad. Nauk SSSR **109**, 735 (1956); Izv. Akad. Nauk SSSR, ser. fiz. **21**, 801 (1957) (with Iu. Bykovskii).

[25] Anisotropy of Even (Transverse) Photomagnetic Effect in Germanium Single Crystals, Dokl. Akad. Nauk. SSSR **116**, 381 (1957) (with Iu. Bykovskii); Soviet Phys. "Doklady" **2**, 447 (1957).

Translated by J. G. Adashko
108

CLOUD CHAMBER INVESTIGATION OF THE ELECTRON-PHOTON COMPONENT NEAR THE AXIS OF EXTENSIVE AIR SHOWERS AT 3860 m ABOVE SEA LEVEL

T. V. DANILOVA, O. I. DOVZHENKO, S. I. NIKOL'SKII, and I. V. RAKOBOL'SKAIA

P. N. Lebedev Physical Institute, Academy of Sciences, U.S.S.R.

Submitted to JETP editor July 16, 1957

J. Exptl. Theoret. Phys. (U.S.S.R.) 34, 541-547 (March, 1958)

The energy spectrum of the electron-photon component of extensive air showers was investigated at 3860 m above sea level at various distances from the axis. Showers with $\overline{N} = 1.5 \times 10^5$ were recorded. The fraction of high-energy electrons and photons recorded experimentally was appreciably smaller than that computed from cascade theory, especially at small distances from the axis. A better agreement between theory and experiment was obtained at larger distances. The lateral distribution of the energy carried by the electron-photon component can be approximated by the law r^{-n}, where $n = 1.5 \pm 0.3$ for distances from the shower axis in the range 1 — 9 m and for showers with $\overline{N} = 2 \times 10^5$.

In continuation of the experiments of Ref. 1 we studied the spectrum of the electron-photon component in extensive air showers (EAS). The experiments were carried out in Autumn 1955 on Mt. Pamir (elevation 3860 m) by means of a rectangular cloud chamber[2] and a hodoscope consisting of about 1000 counters.[3] The chamber had a working volume of 60×60×30 cm and effective area equal to 0.15 m^2 for vertical showers. Seven lead plates, the first 0.5 cm thick, the second 1 cm, and the following five plates 1.5 cm each, were placed in the chamber. The top wall of the chamber was made of iron 1 cm thick.

EAS were selected by a coincidence-anticoincidence system consisting of several counter groups. The analysis of hodoscope data made it possible to find the axis position and the total number of particles for each shower.

Coincidences of discharges in four group of counters placed near the cloud chamber, 500 cm^2 in area each, were used for the selection of EAS. Anticoincidences between the central system and triple coincidences of three counter trays, 300 cm^2 in area each, placed at the vertices of a triangle at a distance of 19 m from the center of the array, were used in order to exclude showers with axes farther than 15 — 20 m from the center. In all, 300 showers with axes within a circle 9 m in radius were recorded.

Distribution of the recorded showers with respect to the number of particles is shown in Fig. 1.

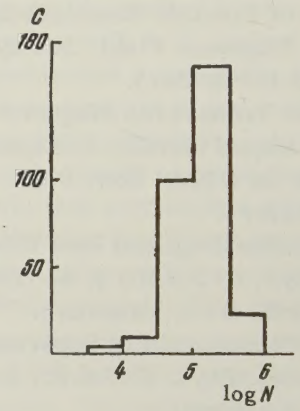

FIG. 1. Distribution of recorded extensive air showers with respect to the number of shower particles N. Number of showers recorded indicated on the y axis.

The axis position and the total number of shower particles were found from the lateral distribution of charged particles determined by means of the hodoscope.[4] The error in axis location within 5 m from the cloud chamber was ≤ 1 m, for distances larger than 5 m the error amounted to 30 — 40%.

The energy of electrons and photons initiating a shower in the lead plates in the chamber was determined by comparing the total number of shower particles observed in the sections of the chamber with the number of particles calculated according to cascade curves for lead[5] (cf. Table I). The flux of particles propagating in the forward direction within the angle of 180° was considered. We did not differentiate between cascades produced by electrons and photons, since the visibility in the

TABLE I

E, ev	Section No. 1	2	3	4	5	6	7	8	ΣN
10^8	1.3	1.6	1.4	0.6	—	—	—	—	5
$2\cdot10^8$	1.8	2.8	2.7	1.3	0.4	—	—	—	9
$3\cdot10^8$	2.2	4.1	4.1	2.1	0.6	—	—	—	13
$4\cdot10^8$	2.5	5	5.2	2.8	1	0.4	—	—	17
$5\cdot10^8$	3	5.8	6.7	3.9	1.5	0.6	—	—	21.5
$6\cdot10^8$	3.4	6.3	8	4.9	2	0.6	0.4	—	25.6
$7\cdot10^8$	4	6.8	8.8	5.7	2.6	1.1	0.5	—	29
$8\cdot10^8$	4.5	7.2	9.3	6.5	3.2	1.5	0.7	—	33
$9\cdot10^8$	5	7.8	9.8	7.3	3.8	1.8	0.8	0.4	36.7
10^9	5.5	8.2	10.3	7.9	4.3	2.3	1.2	0.6	40.5
$2\cdot10^9$	6	12	17	16	12	6	3	2	74
$4\cdot10^9$	6.5	16	30	32	24.5	15	8	4	136
$6\cdot10^9$	8.5	24	42.5	48	37.5	24.5	13	7	205
$8\cdot10^9$	10	29	55.5	65	51.5	33	19	10	273
10^{10}	12.5	35	68.5	80.5	64	43	24.5	13	341

top section of the chamber was not always satisfactory and, besides, a considerable number of photons underwent conversion in the top wall of the chamber.

The accuracy of the energy measurement was 20 — 30% for the region $2 \times 10^8 - 2 \times 10^9$ ev. The high density of particles at higher energies (Fig. 2)

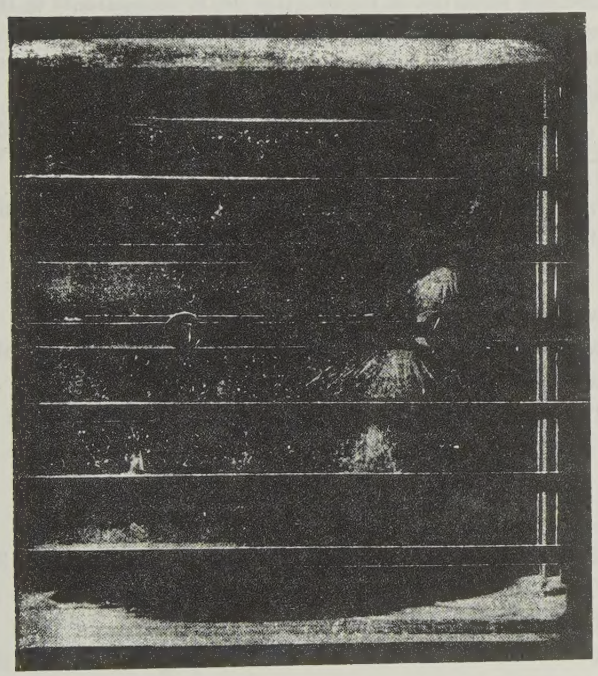

FIG. 2. Cascade shower produced in the chamber by a $\sim 10^{10}$ ev electron. The axis of the extensive air shower with $N = 1.3 \times 10^5$ fell ~ 0.8 m from the chamber.

made counting difficult and lowered the accuracy to 40 — 50%. For lower energies the accuracy was also worse because of the small number of secondary electrons.*

In 25 out of the 300 cases, the number of electrons and photons incident on the chamber was > 50. Showers produced by these particles were mixed together and difficult to separate. In these cases we found the shower cores, determined the maximum of the number of particles in each section and the number of plate in which the shower was absorbed, and comparing the results with the cascade curves, estimated the electron energy. The accuracy of energy determination was then slightly lowered. Five cases were not included in the final results because of the impossibility of separating the showers. The showers involved did not contain high-energy electrons and were characterized by a high particle flux density (~ 100) with energies $\leq 10^8$ ev.

The integral energy spectrum of electrons and photons for the region $10^8 - 10^{10}$ ev was measured for two distance intervals (0 — 4 and 4 — 9 m) for showers with the number of particles between $10^4 - 10^5$ ($\overline{N} = 6.4 \times 10^4$) and between $1.1 \times 10^5 - 10^6$ ($\overline{N} = 2 \times 10^5$). In the region $2 \times 10^8 - 10^9$ ev, the energy spectrum of the electrons and photons can be written in the form

$$N(\geqslant E) = \text{const} / E^{\gamma}.$$

The values of γ are given in Table II. In view of the absence of a marked dependence of γ on the

*Estimates of the accuracy of energy measurements were made under the assumption of a Poisson distribution of the number of particles at a given depth. Difficulties of a more exact treatment are connected with the problem of fluctuations of the number of particles in showers.

TABLE II

r	0—4 m		4—9 m	
$\bar{N}$	$6.4 \cdot 10^4$	$2 \cdot 10^5$	$6.4 \cdot 10^4$	$2 \cdot 10^5$
γ	0.63±0.07	0.60±0.06	1.3±0 3	1.3±0.3

number of particles in the shower, we grouped together showers with different number of particles for a more detailed analysis of the variation of the spectrum with the distance from axis. The results are given in Fig. 3.

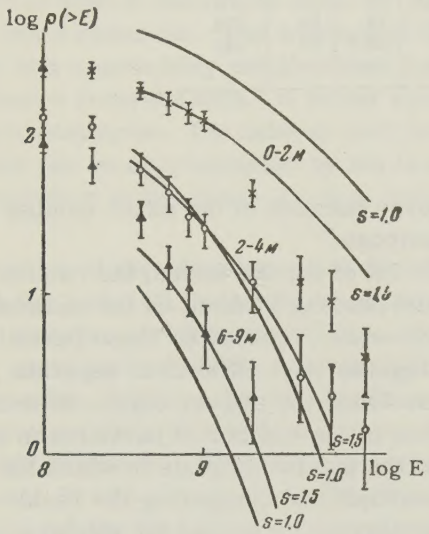

FIG. 3. Integral energy spectra of the electron-photon component of EAS in three distance intervals. Solid lines denote integral electron spectra computed from cascade theory for s = 1 and s = 1.5 (neglecting ionization losses). The experimental and the theoretical spectra are normalized for 10^9 ev and 2 – 4 m.

For comparison of the experimental results with the theoretical predictions we calculated the integral energy spectrum of electrons within a given distance interval for s = 1 and s = 1.5.* The function P (x, s) is tabulated in Ref. 7 for various values of s. The variable $x = Er_t/E_s$, where E is the electron energy in Mev, r_t is the distance from shower axis expressed in radiation units (at 3860 m one radiation unit is assumed to equal 460 m), and E_s = 21 Mev. The product $E^{2-s}P(x, s)$ is proportional to the number of particles with energy ≥ E at a given r. Integral energy spectra were calculated for s = 1 and s = 1.5 (the latter is shown in Fig. 4a). These were used for the calculation of the lateral distribution of electrons with energy ≥ E (Fig. 4b for s = 1.5)

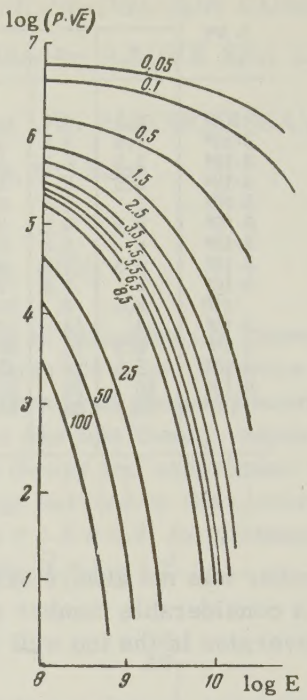

FIG. 4a

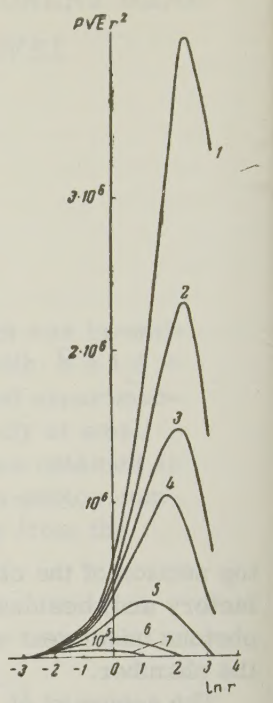

FIG. 4b

FIG. 4a. Integral energy spectrum of electrons at various distances from the axis for s = 1.5. The ordinates denote the decimal logarithm of the function $P\sqrt{E}$ proportional to the number of electrons with energy ≥ E, the x axis – log E (E in ev). Numbers at the curves denote distance from the axis (m).

FIG. 4b. Lateral distribution of electrons with energy ≥ E for s = 1.5. Distance r in meters. The function $P\sqrt{E}$ is proportional to the number of particles with energy ≥ E. The electron energies (in ev) are: 1 – 4×10^8, 2 – 6×10^8, 3 – 8×10^8, 4 – 10^9, 5 – 2×10^9, 6 – 6×10^9, 7 – 10^{10}.

which in turn were used for the determination of the number of electrons with energy ≥ E incident upon the area of the ring between the radii r_1 and r_2

$$N = 2\pi E^{2-s} \int_{r_1}^{r_2} P(x, s) r^2 d(\ln r).$$

Results of the calculations are shown in Fig. 3. The theoretical and experimental spectra are normalized for 10^9 ev at the distance of 2 – 4 m from shower axis. It can be seen from Fig. 3 that the experimental spectrum contains less high energy electrons near the axis. At larger distances this discrepancy practically disappears for the curve calculated for s = 1.5.

We calculated the ratio Δ of high-energy electrons and photons to the total number of particles in the shower for various distance intervals

*The value of s obtained from the absorption coefficient of shower particles in air is 1.2 – 1.3 (Ref. 6).

TABLE III

r, m	$\bar{N}$					
	Experimental values Δ, %				Theoretical values Δ, %	
	3860 m (1955)		100 m[1]	3260 m[5]		
	$6.4 \cdot 10^4$	$2 \cdot 10^5$	10^4—$5 \cdot 10^4$	10^5—10^6	$s = 1$	$s = 1.5$
0—2	(13±2)	(9±2)			38	15
2—4	(5.3±1.5)	(4±1)			12.5	8.5
0—4	(10±2)	(7±1.5)	(1.82±0.25)	~(11±5)	26	12
4—9	(4.2±2)	(2.0±0.5)		(5±3)	4.6	3.8

$$\Delta = \rho[E \geqslant 10^9,\ r_1,\ r_2] / \rho[E \geqslant 0,\ r_1,\ r_2].$$

where $\rho(E \geq 10^9) = N[E \geq 10^9, r_1, r_2]/C(r_1, r_2)\sigma$ is the density of electrons and photons with energy $\geq 10^9$ ev per m^2 in a shower falling within the given distance interval, $C(r_1, r_2)$ is the number of air showers in the given interval, σ is the effective area of the chamber for high-energy electrons and photons, and $N[E \geq 10^9, r_1, r_2]$ is the number of observed electrons with $E \geq 10^9$ ev in that interval. The value of $\rho(E \geq 0, r_1, r_2)$ was determined from hodoscope data. The ratio Δ determined from the experiment was compared with the results obtained from cascade theory for $s = 1$ and $s = 1.5$ under the assumption of an infinite energy of the primary particle. The results of the comparison are given in Table III and Fig. 5. It can be seen that the experiment yields a smaller fraction of high-energy electrons and photons than could be expected from cascade theory. The discrepancy is especially large for the distances 0 — 2 m for $s = 1$. This is in agreement, within the limits of the experimental errors, with the results of Hazen et al.[8] obtained by means of a cloud chamber at 3260 m above sea level. It should be noted that in Ref. 8 the electron energy was determined from the number of particles at cascade maximum and not from the sum of the number of particles in several points of the cascade curve as it was done in our work. The method used by Hazen is less accurate because of fluctuations and the energy values obtained are overestimated. Using that method, our value for Δ would be 13 — 14% instead of 10%.

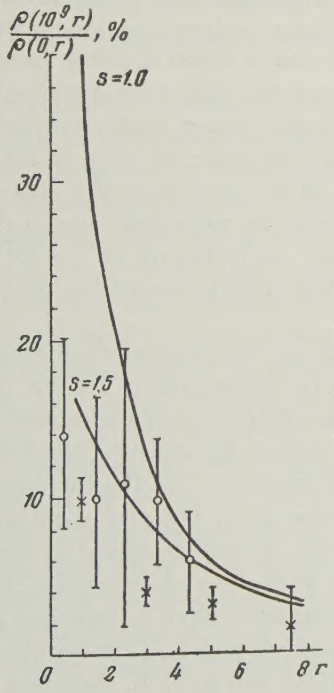

FIG. 5

FIG. 5. Ratio of the flux density of electrons and photons of $\geq 10^9$ ev to the total particle flux density in a given distance interval. o – denote data of Hazen,[8] × – of the authors.

A comparison was also made with the results of Ref. 1 (Table III). It can be seen that the fraction of high-energy electrons and photons found in experiments at 3860 and 3260 m elevation is larger than that at sea level[1] (the variation in the radiation length with altitude has been accounted for).

In 1957 we carried out new measurements with the cloud chamber at sea level, selecting events in which the EAS axis fell within 0 — 3 m from the chamber. The error in axis location amounted to ±1 m. The total number of particles in the studied showers was $\sim 10^4$. Showers of the same frequency and, evidently, the same primary energy, recorded at 3860 above sea level, have the total number of particles equal to $N = 6 \times 10^4$.*

Preliminary data indicate that the energy spectrum of electrons and photons measured at sea level coincide with that measured on the Pamir

*It can be assumed[6] that a shower of $N = 6 \times 10^4$ particles corresponds to a primary of $\sim 1.5 \times 10^{14}$ ev.

(Fig. 6), and the fraction of high-energy electrons and photons at sea level amounts to $\geq 10\%$.

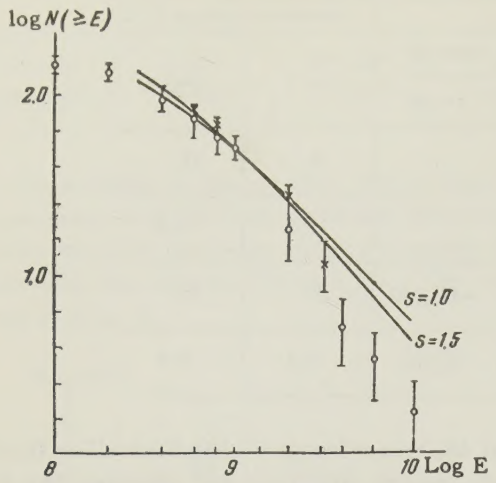

FIG. 6. Integral energy spectra of electrons and photons, × – at sea level, 0 – 4 m from axis, ○ – at 3860 m elevation, 0 – 4 m from axis. The curves represent calculations for two values of s.

At the present stage it is impossible to explain the discrepancy between the above results and those of Ref. 1. It is possible that it is partly due to the lower accuracy of shower axis location in the earlier experiments and to the larger amount of matter present in the roof of the laboratory where they were conducted. It is, however, possible that showers with different number of particles have different structure which causes the difference in the spectrum of the electron-photon component.

Using the results of the measurements at 3860 m it is possible to construct the lateral distribution of high-energy electrons and photons and the lateral distribution of the energy flux carried by the electron-photon component (ρ_E). In constructing the lateral distribution of the energy flux we accounted for electrons which did not initiate cascades in lead but which were absorbed in the first or second lead plate. Energy of such electrons was estimated from their ionization loss (cf. Ref. 1).

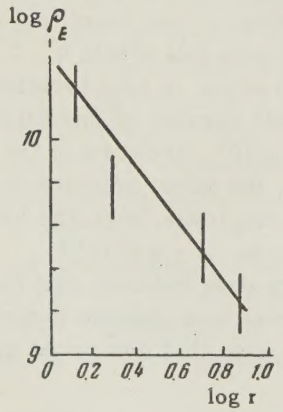

FIG. 7. Lateral distribution of the energy flux carried by the electron-photon component for showers with $\overline{N} = 2 \times 10^5$ (r in meters).

The dependence of $\overline{\rho}_E$ on r can be written in the form $\rho_E = r^{-n}$, where $n = 1.5 \pm 0.3$ for showers with $\overline{N} = 2 \times 10^5$ (Fig. 7).

In constructing the lateral distribution of high-energy electrons and photons the results were normalized for showers with $N = 10^5$ (Fig. 8). If we accept the value $s = 1.2$, then the lateral distribution of electrons and photons of $\geq 10^9$ and $\geq 2 \times 10^9$ ev cannot be explained by Coulomb scattering by air atoms only. This may be possibly connected with the influence of the angles of emission of π^0 mesons in nuclear interactions and of the lateral distribution of the nuclear-active component of EAS.

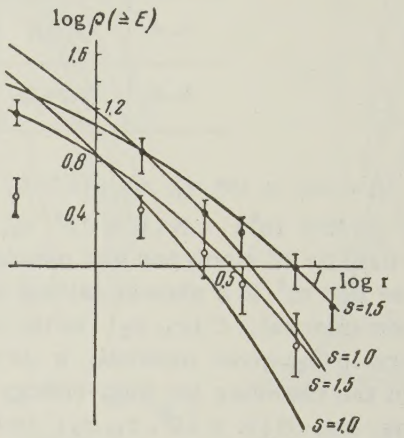

FIG. 8. Lateral distribution of electrons and photons with the energy ● – $E \geq 10^9$ ev, ○ – $E \geq 2 \times 10^9$ ev. Theoretical and experimental results are normalized for 10^9 ev at 1.5 m.

On the basis of the above experimental results one can, therefore, draw the following conclusions:

1. A deficiency of high-energy electrons and photons has been observed near the axis of EAS. This is evidently due to the presence of a flux of low-energy photons near the axis and also to the fact that nuclear-active particles of $10^{10} - 10^{12}$ ev contribute heavily to the production of the electron-photon component.

2. The spectrum of the electron-photon component of EAS produced by primaries of $\leq 2 \times 10^{14}$ ev does not vary with the altitude of observation. This fact can be explained either by equilibrium between the electron-photon component and the high-energy nuclear-active particles or by the preferential selection by the apparatus of EAS initiated at a certain effective altitude above the observation level.

In conclusion, the authors wish to express their gratitude to G. T. Zatsepin and L. I. Sarycheva for the discussion of results and to I. T. Uchaikin and D. F. Rakitin which took part in the measurements.

[1] Ivanovskaia, Kulikov, Rabobol' skaia, and Sarycheva, J. Exptl. Theoret. Phys. (U.S.S.R.) **33**, 358 (1957), Soviet Phys. JETP **6**, 276 (1958).

[2] I. A. Ivanovskaia and A. G. Novikov, J. Tech. Phys. (U.S.S.R.) **26**, 209 (1956); Soviet Phys. JTP **1**, 206 (1956).

[3] L. N. Korablev, Приборы и техника эксперимента (Instruments and Meas. Engg.) **2**, 54 (1956).

[4] Dovzhenko, Zatsepin, Murzina, Nikol' skii, Rakobol' skaia, and Tukish, Dokl. Akad. Nauk SSSR **118**, (1958).

[5] I. P. Ivanenko, Dokl. Akad. Nauk SSSR **107**, 819 (1956), Soviet Phys. "Doklady" **1**, 231 (1956).

[6] K. Greisen, Progress in Cosmic Ray Physics **3**, Amsterdam 1956, p. 1-14.

[7] V. V. Guzhavin and I. P. Ivanenko, Dokl. Akad. Nauk SSSR **115**, 1089 (1957), Soviet Phys. "Doklady" **2**, 407 (1957).

[8] Hazen, Williams, and Randall, Phys. Rev. **93**, 578 (1954).

Translated by H. Kasha
109

SOVIET PHYSICS JETP VOLUME 34 (7), NUMBER 3 SEPTEMBER, 1958

PECULIARITIES OF THE PHOTOCONDUCTIVITY IN CADMIUM SELENIDE

S. V. SVECHNIKOV

Kiev Polytechnic Institute

Submitted to JETP editor May 22, 1957

J. Exptl. Theoret. Phys. (U.S.S.R.) **34**, 548-554 (March, 1958)

Peculiarities of the photoconductivity in single crystals of cadmium selenide excited by red light of $\lambda = 7740$ A and by x-rays are considered. The first case corresponds to linear conductivity with a quantum yield $\beta^* = \text{const}$ and $\tau = \text{const}$, and the second case to nonlinear photoconductivity for which $\beta^* = \beta^*(L, J_{ph}, t)$ and $\tau = \tau(L, J_{ph})$. A two stage excitation scheme is proposed in order to explain the irregularities observed in the photoconductivity of single-crystal CdSe.

CADMIUM selenide as well as cadmium sulfide belong to those semiconducting materials with electron conductivity, which show a considerable internal photoeffect under the action of visible light as well as of other types of ionizing irradiation. From this point of view, CdSe can be quite effectively utilized for the preparation of photoresistors, whose integral sensitivity is measured in tens of amperes per lumen. With a resistance in the dark of more than 10^{14} ohms, changes in resistivity by a factor of $10^6 - 10^8$ are observed. The characteristics of the photoresistance are determined both by the technique of preparation as well as by the intrinsic properties of the semiconductor, whose internal photoeffect shows a number of peculiarities.

During the investigation of the properties of the added photoconductivity of single crystal CdSe, it was noted that the qualitative features of the internal photoeffect were similar for irradiation by visible light and by x-rays. This similarity shows up both in the statistical properties (current-voltage characteristics, nature of the light, variation of the sensitivity with applied bias, etc.) as well as in the transients in the photocurrent on switching the excitation in and out. The latter refers to the shape of the curve $J_{ph}(t)$ (Ref. 1), which determines the general features in the evolution of the process. Thus it is found that on approximating the rise and decay curves of the photocurrent by exponential functions, the time constants of these processes show the same dependence on the intensity of excitation, on the bias applied to the sample, on the temperature, etc., independent of whether the conductivity is stimulated by irradiation in the visible part of the spectrum or by x-rays. It was noted, however, that quantitatively the processes of excitation and decay of the photocurrent are substantially different in the two cases. Also, the detailed shapes of the curves prove to be different.

The samples investigated were single crystals

of cadmium selenide obtained by deposition directly from the vapor phase in a stream of argon, analogous to the growth of CdS single crystals.[2] Platinum contacts were applied to opposite ends of the sample by cathodic sputtering, after first cleaning the semiconductor surface by electron bombardment, in such a fashion that the distance between the electrodes was about 2 mm. The contacts obtained were not ohmic, but the contact barrier was small and did not appreciably affect the current-voltage characteristics of the sample, as will be shown below. The CdSe crystals grown by this technique showed a maximum photoeffect in the red region of the spectrum at $\lambda = 7700$ A (Fig. 1) and at the same time were very sensitive to x-rays.

It was noted that the kinetics of the photoconductivity of single crystals of CdSe are markedly dependent on the nature of the exciting irradiation,

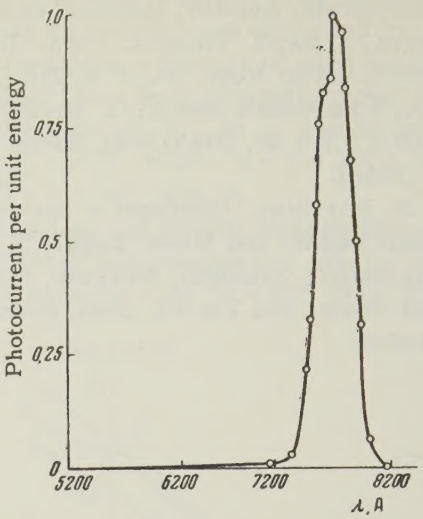

FIG. 1. Spectral sensitivity of single crystal cadmium selenide.

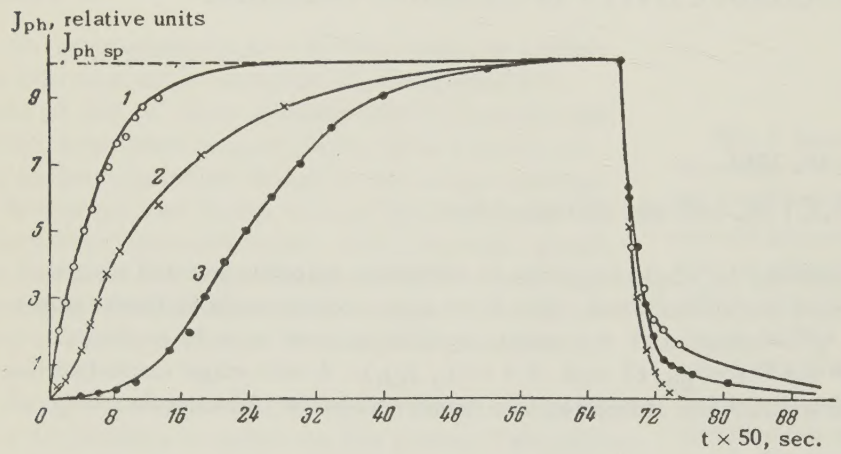

FIG. 2. Oscillograms of the photocurrent in single crystal CdSe excited by radiation of different types: 1 – $\lambda = 7740$ A, 2 – $\lambda = 7160$ A, 3 – x-rays of 50 kv max. energy.

i.e., the parameters of the excitation and decay processes of the photocurrents under otherwise identical conditions are functions of λ. This is illustrated by Fig. 2, which shows oscillograms of the photocurrent when the sample is excited with square light pulses at two different values of λ and by x-rays with a maximum energy of 50 kv. The value of the resultant photocurrent was the same for all three curves and equal to 1 μa with a bias of $U_{ph} = 13$ v applied to the sample.

From an analysis of the oscillograms shown above it follows that, of the three excitation processes studied, only the first case corresponds to a linear shape where $J_{ph}(t)$ varies exponentially with time. The second and third curves show a marked deviation from linearity in the initial rise of the photocurrent. An analysis of the initial stage shows that it corresponds to a parabolic time dependence of the photocurrent, where $J_{ph} \sim t^2$.

Thereafter the parabola degenerates into an exponential whose time constant is, however, larger by about an order of magnitude than the time constant which characterizes Curve 1. The relaxation processes do not show such a characteristic dependence on λ: As a rule, the decay of the photocurrent is exponential, with approximately equal values for the time constants of all three curves, except for the tail of the decay curves which amounts to only 10 — 15% of $J_{ph\ sp}$.

The mismatch in the shape of the curves shown above cannot be explained by a different concentration of current carriers forming in the active volume of the crystal, since the greatest deviation from linearity in the initial stages of the curves is observed under excitation by weakly absorbed light which penetrates uniformly throughout the whole crystal ($\lambda = 7740$ A and x-rays). The deviation from linearity in the photocurrent rise curve is in

this case a consequence of different mechanisms of excitation of the photoconductivity in CdSe when the crystal is illuminated by x-rays and by light of long wavelength, corresponding to the maximum of the spectral characteristics of the photocurrent.

The formal kinetic equation for the photocurrent, which determines J_{ph} as a function of t, may be presented in the form

$$dJ_{ph}/dt + TJ_{ph} = \beta^* L, \quad (1)$$

where T is defined as a quantity inversely proportional to the time constant τ for the rise or decay of the photocurrent, and β^* is a coefficient proportional to the quantum yield β and related to parameters of the photoresistance such as the mobility μ, the absorption coefficient k', the magnitude of the applied bias U_{ph} and the distance d between the electrodes by the relationship

$$\beta^* = \beta\mu ek' U_{ph}/d^2. \quad (2)$$

In the general case T and β^* may depend upon the intensity of illumination L, the current carrier concentration and the time, i.e., $T(L, J_{ph}, t)$ and $\beta^*(L, J_{ph}, t)$. In this case the kinetics of the photoconductivity will obviously be non-linear. The rise and decay curves of the photocurrents may then have different shapes with values of T differing by an order of magnitude. The condition that T and β^* are constants obviously corresponds to the linear case.

It follows from Eq. (1) that the initial stage of the rise of the photocurrent when $t \ll \tau$ is determined by

$$J_{ph} = \beta^* L t. \quad (3)$$

Every deviation from linearity in the relationship (3) is caused by the time dependence of the quantum yield $\beta^* = \beta(t)$. Expanding this expression into a series and taking into account only terms of the first order of magnitude, in the assumption that the term of zero order is equal to zero, we obtain $J_{ph} \sim t^2$; this is indeed observed experimentally under excitation by strongly absorbed light and by x-rays. Curve 1 of Fig. 2 corresponds to the condition $\beta^* = \text{const}$.

On the other hand, when the photocurrent is measured after a long interval of time, i.e., when $t \gg \tau$, it proves to be proportional to the product $\beta^*\tau$. Then the lux-ampere characteristics of the sample must be determined by a relationship of the form

$$J_{ph} = \beta^* \tau L, \quad (4)$$

where β^* and τ may themselves be functions of L, in agreement with the above.

Proceeding in the same manner as in the treatment of the time dependence of the photocurrent in the initial stage of the rise curve, it is not difficult to show that the relationship (4) of the photocurrent with $\beta^*(L)$ and $\tau(L)$ must lead to a nonlinear curve with increasing slope for $J_{ph}(L)$. This nonlinearity should be particularly marked at low intensities of illumination when the concentration of photoelectrons is small, and should change with increasing L first to a linear relationship and then to a nonlinear relationship with decreasing slope. In the case of single crystals of CdSe such a behavior of the light characteristics corresponds to excitation by x-rays as illustrated in Fig. 3. In the

FIG. 3. Light characteristics of single crystal CdSe. The dashed curves correspond to excitation by white light, the full curves correspond to excitation by x-rays. The abscissa gives L in lux for curves a and b; the ordinate for a – $J_{ph} \times 2.10^5$ amp, for b – $J_{ph} \times 10^6$ amp. The abscissa gives I in roentgens/minute for curves c and d; the ordinate for c – $J_{ph} \times 10^5$ amp, for d – $J_{ph} \times 2 \times 10^7$ amp. 1 – $U_{ph} = 0.2$; 2 – $U_{ph} = 15$; 3 – $U_{ph} = 100$ v.

diagram the full curves represent $J_{ph}(I)$ under excitation by x-rays of intensity I, and the dashed curves represent $J_{ph}(L)$ under excitation by nondispersed white light and with different biases applied to the sample.

Starting from the shape of the spectral characteristics of CdSe shown in Fig. 1 one may conclude that the characteristics of the photocurrent pro-

duced in this experiment by excitation with white light should be close to those of Curve 1, Fig. 2. Analysis of the curve $J_{ph}(L)$ showed that in this case the dependence of the photocurrent on the intensity of illumination at low values of L is linear and that it curves downwards in the region of large values of L; whereas under excitation by x-rays $J_{ph} \sim I^3$ at low intensity I, and changes first to a proportional relationship on increasing I and thereafter to a nonlinear relationship with decreasing slope. From the curves shown in Fig. 3 it follows that the nonlinearity of $J_{ph}(L)$ or $J_{ph}(I)$ in the region of intermediate and large intensities of the exciting irradiation depends also on the magnitude of the bias applied to the sample, particularly for low values of U_{ph}. At large values of U_{ph} (of the order of hundreds of volts) the curvature of the light characteristics is caused by the heating of the sample by photocurrents. In the present paper this part of the curves is not discussed further.

The above discussion leads to the conclusion that excitation by x-rays produces an essentially nonlinear curve also in the case of the statistical characteristics, whereas excitation by light in the visible part of the spectrum close to the maximum sensitivity gives an approximately linear curve. This renders evidence of the different mechanisms of the internal photoeffect in the two cases.

The variation of β^* and τ with L should obviously show up in the kinetics of the photoconductivity, mainly in the rise of the photocurrent. From this point of view, the investigated case of single crystals of CdSe appears typical, as is illustrated by the oscillograms of $J_{ph}(t)$ in Fig. 4. The oscillograms were taken under different x-ray intensities increasing from Curve 1 to Curve 4. It follows from the curves shown that the nonlinearity mentioned above, which is caused by variations of β^* and τ with L, appears only at small levels of excitation. The process becomes linear for large values of I and for large carrier concentrations in the crystal (Curves 3 and 4). This refers not only to the variation of β^* and τ with I, but also to the variation of these parameters with time. Indeed, on increasing the level of excitation the quantum yield β^* no longer depends on the time, giving evidence of the transition from a "bimolecular" to a "monomolecular" process.[3,4]

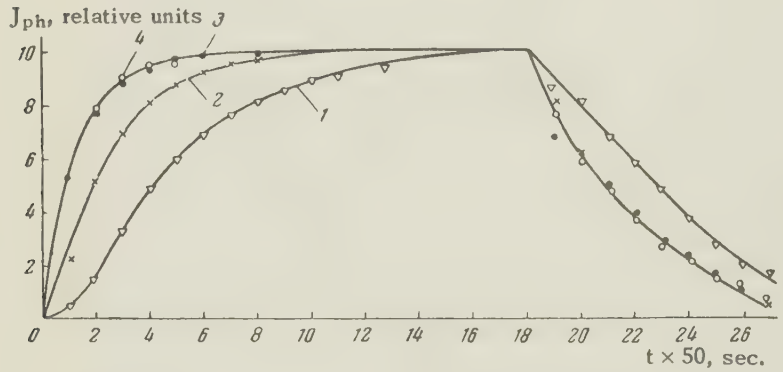

FIG. 4. Oscillograms of excitation and decay of photocurrents in single crystal CdSe for different x-ray intensities, expressed in roentgens/min: 1 – 25; 2 – 125; 3 – 250; 4 – 375. Curves 3 and 4 coalesce.

Some useful information on the hypothetical structure may be obtained from a consideration of the I—V characteristics, as is well known.[5] For CdSe single crystals these characteristics curve upwards in the absence of light and are for the most part linear under illumination regardless of the wavelength of the exciting light (Fig. 5). Such a variation of J_{ph} with U_{ph} may be explained by the presence of electron traps close to the bottom of the conduction band with quite low life times for the electrons. Consequently their role in determining the kinetics of the photoconductivity is negligibly small and did not show up in the preceding experiments. These levels should be unoccupied in darkness and are filled under illumination. The space charge localized in these traps under illumination displaces the Fermi level in the semiconductor. As a result the metal-semiconductor contact does not block the current and the $J_{ph}(U_{ph})$ curve becomes linear. This is confirmed by the temperature dependence of the photocurrent and of the dark current in single crystal CdSe as shown in Fig. 6. The temperature variation of the photocurrent was measured under illumination by red light of wavelength $\lambda = 7740$ A (Curve 1) and by x-rays (Curve 2). In accordance with expectations, at relatively low temperatures until the appearance of an appreciable dark conductivity $J_{ph}(T^\circ) \sim \exp(T_c/T^\circ)$ independent of the wavelength of the exciting illumination, where T_c is a constant for the given range T°.

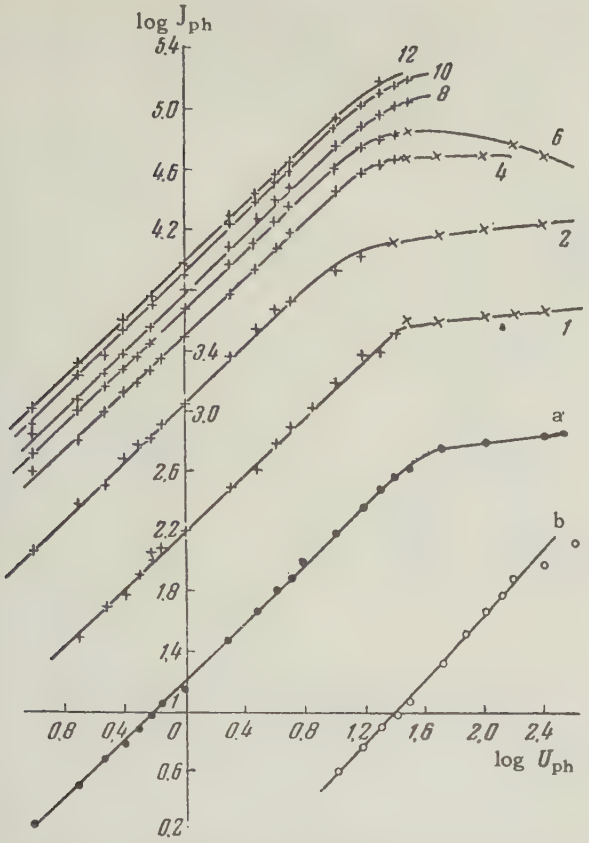

FIG. 5. Current-voltage characteristics of single crystal CdSe. Numbers placed besides the curves correspond to the flux in ma of the x-ray tube at a generating voltage of 50 kv. a – excitation with visible light; b – dark current.

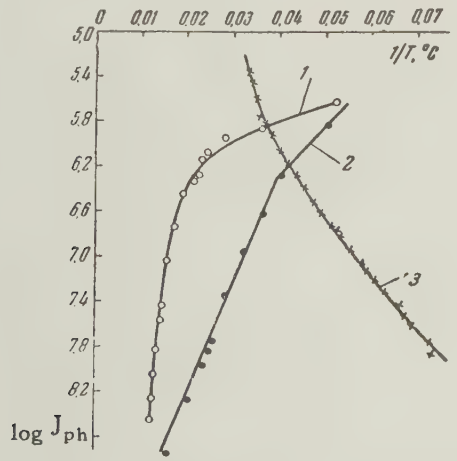

FIG. 6. Temperature dependence of the photocurrent and of the dark current in single crystal CdSe. 1 – excitation with λ = 7740 A, 2 – excitation with x-rays, 3 – dark current (for curve 3 the units of the abscissa are $1/T \times 10$).

The experimental results concerning the photoconductivity of single crystals of CdSe discussed above makes it plausible to adopt the transition scheme shown in Fig. 7. The scheme is based on a two stage mechanism for the excitation of the

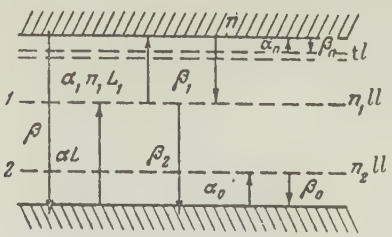

FIG. 7. Model of the proposed optical transitions in single crystal CdSe.

photoconductivity (αL and $\alpha_1 n_1 L$). As shown by Lashkarev[6] and Tolstoi,[4] the presence of such a transition causes β^* to be a function of L, J_{ph}, t and τ to be a function of L, J_{ph}. Moreover, the different character of the excitation and decay curves of the photocurrent follows from the formal treatment of a two-stage excitation. The rise curves of the photocurrent are found to depend on L, but not the decay curves. In this connection it is worth noting that the excitation process takes a longer time than the decay. These general conclusions are in good agreement with the experimental data given in the present paper.

In the scheme of Fig. 7, tl are the electron traps. As mentioned above, they do not affect the photoconductivity and play a part only in the dependence of J_{ph} on U_{ph}. The localized electron levels are marked "ll". Level 1 should be nearer the bottom of the conduction band and level 2 nearer the top of the valence band. In agreement with this scheme, the capture cross-section of level 1 for electrons is less than the capture cross-section of level 2 for electrons. For this reason level 1 may be regarded as sparsely populated by electrons, and level 2 as almost completely occupied by electrons.

Recombination from the band onto level 1 is more probable than excitation for low excitation intensities and low current carrier concentrations within the band. In this case the solution of the kinetic equations for the postulated transition scheme leads to[4] $J_{ph} \sim t^2$ for the processes taking place at the beginning of the rise curve; this is observed experimentally. For increasing excitation, the ejection $\alpha_1 n_1 L$ becomes more probable than recombination onto this level. The analysis shows that in this case $J_{ph} \sim L$ and $\tau \sim 1/L$. At large levels of excitation, partial saturation[4] must occur as a result of the two stage optical transitions.

The transition scheme shown in Fig. 7 corresponds to excitation by x-rays and strongly absorbed light. Under excitation by red light of wavelength λ = 7740 A, the transition αL should be considered as the primary transition, leading to a change in conductivity. However, such a transition suggests the possibility of conduction by local levels;[4] this has yet to be confirmed.

[1] N. A. Tolstoi and A. V. Shatilov, J. Exptl. Theoret. Phys. (U.S.S.R.) 30, 109 (1956), Soviet Phys. JETP 3, 81 (1956).

[2] M. E. Bishop and S. H. Klebson, J. Appl. Phys. 24, 660 (1953).

[3] K. W. Böer and H. V. Vogel, Ann. Physik 17, 10 (1955).

[4] N. A. Tolstoi, Радиотехника и электроника (Radio Engg. and Electronics) 1, 1135 (1956).

[5] A. Rose, Phys. Rev. 97, 1538 (1955).

[6] V. E. Loshkarev and G. A. Fedorus, Izv. Akad. Nauk SSSR, ser. fiz. 16, 81 (1952).

Translated by P. F. Schmidt
110

SOVIET PHYSICS JETP VOLUME 34(7), NUMBER 3 SEPTEMBER, 1958

MEASUREMENT OF THE MASS OF 660 Mev PROTONS

V. P. ZRELOV, A. A. TIAPKIN, and P. S. FARAGO*

Joint Institute for Nuclear Research

Submitted to JETP editor September 12, 1957

J. Exptl. Theoret. Phys. (U.S.S.R.) 34, 555-558 (March, 1958)

Measurements of the momentum p and velocity v of 660-Mev protons were conducted in the external beam of the synchrocyclotron. The mass $m_1 = p/v$ was compared with the value computed in accord with the relativistic relation $m_2 = m_0[1 - (v^2/c^2)]^{-1/2}$. Both mass values are in agreement within the limits of the experimental error. The observed relative deviation was $\Delta m/m = 0.004\,(1 \pm 0.6)$.

INTRODUCTION

THE accuracy with which the theory of relativity, now a classic one, describes high-velocity effects, as well as possible deviations from the theoretical predictions, may be rightly questioned. The existence of such deviations can, of course, be rejected from purely theoretical considerations requiring the preservation of the internal completeness of the basic theory. The decisive answer, however, indisputably belongs to the experiment. The large experimental material available confirms, on the whole, the existence of relativistic effects in nature but contains little data with respect to the degree of accuracy of the theoretical predictions. It is often claimed that the successful operation of cyclic high-energy particle accelerators gives an accurate confirmation of the relativistic dependence of the mass on velocity. Farago and Janossy,[1] however, having analyzed the corresponding experimental material, have concluded that the relativistic relation is confirmed to a considerably lesser extent than it is generally assumed. Quantitative results from accelerators now in operation are indefinite to a few percent. It was found in direct experiments with electrons[1] that the experimental error is rather large (2 — 10%). Grove and Fox[2] carried out an experiment with protons, using a 140-inch synchrocyclotron. They determined the equilibrium orbit for 385-Mev protons and measured the angular frequency on the orbit. The results are in agreement with the relativistic law of the variation of mass. An analysis of the data is, however, rendered difficult by the complex motion of protons inside the accelerator on the one hand, and by the scant information provided by the authors on the other.

The purpose of our work was to compare the proton mass calculated according to the relativistic relation $m_2 = m_0[1 - (v^2/c^2)]^{-1/2}$ (from the measured value of v) with the value $m_1 = p/v$ found from the measured proton momentum and velocity. The measurements were conducted in an external beam of protons of about 660 Mev, which made it considerably easier to determine the possible errors.

*Edinburgh, Scotland.

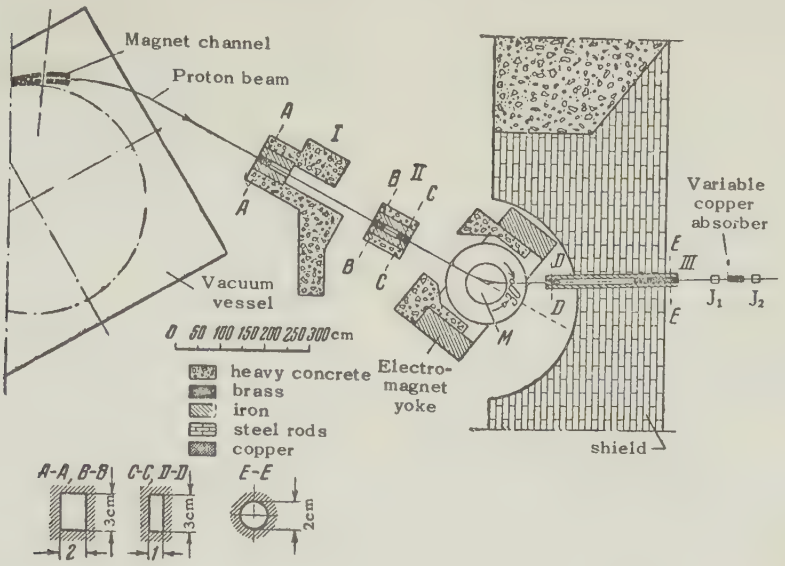

APPARATUS AND METHOD

A general diagram of the experimental arrangement is shown in the figure. The external beam of the six-meter synchrocyclotron passed through collimators I and II, was deflected in the field of electromagnet M with poles 1 m in diameter, then passed through collimator III and struck the ionization chamber J_1. The shape and dimensions of collimator openings are shown in the figure. Adjustment of the collimating system was carefully checked by exposing an x-ray film.

The current in the coils of electromagnet M was adjusted to obtain maximum counting rate in chamber J_1. The film exposed at the exit from collimator III then recorded a sharp image of the proton beam, symmetrical with respect to the collimator axis. The magnetizing current was stabilized within 0.1%. Fluctuations of the magnetic field intensity were smaller still, since the iron core was almost saturated.

An accurate determination of the momentum of protons from measurements of the magnetic field was impossible in practice, because of stray fields of the synchrocyclotron magnet and of the magnet M. The momentum of the protons of the beam traversing the collimating system was measured using the method of current carrying filament.[3-5] A Litz wire 0.2 mm in diameter was threaded through all collimators and was supported three meters from the exit from collimator III by means of a silk thread with attached weight Q on a miniature pulley. As is well known, a stretched wire carrying a current I in magnetic field assumes the form of the trajectory of a charged particle with momentum $p = aQ/I$. If the tension Q of the wire is expressed in grams and the current I in amperes, then the momentum of a singly charged particle in Mev/c will be given by the relation

$$p = 2.943\, Q / I.$$

In the above formula the weight and elastic stresses of the wire are neglected. The accuracy with which the force of the weight Q is converted into wire tension depends on the accuracy with which the pulley is centered and on the quality of its bearings. It was found experimentally, for the pulley used, that it takes a difference of 0.3 g to upset the equilibrium between two 300 g weights hanging on a thread looped over the pulley.

By varying the current continuously at a constant tension Q = 300 g, a position was found such that the thread passed freely through the collimators along their axes. The corresponding current was measured with a calibrated ammeter of 0.001 amp accuracy.

As a check, a measurement of the proton momentum was carried out in which the tension due to a weight of 300 g was transmitted to the wire by means of a pendulum suspension. For the wire tension and the force due to the weight to be equal, it was necessary that the horizontal distance from the pendulum suspension point to the point of junction with the horizontal wire be equal to the vertical distance from the point of suspension to the horizontal wire. The error in the value of tension depends only upon the accuracy of length measurements. The suspension point of the pendulum was attached to the frame of an overhead crane in the hall where the experiments were carried out. The above distances, amounting to about 5 m, were made equal to within ±5 mm. The results of these measurements were in good agreement with those obtained with the pulley.

To determine proton velocities we made use of earlier results obtained by measurement of the angle of the Cerenkov radiation.[6] The mean velocity of the protons in the external beam was found to be $v_0/c = 0.8090 \pm 0.0005$. The mean range $\overline{R}_0$ of protons in copper was determined from the Bragg curve simultaneously with the velocity measurements. In the present work only the Bragg curve and the mean range $\overline{R}$ were measured for the proton beam separated by the collimating system. As shown by Mather and Segrè,[7] the Bragg curve depends on the energy distribution of the beam particles, but the mean range is always equal to the thickness of absorber, for which the current in the ionization chamber amounts to 0.82 of the maximum value. Correction to the value of the mean proton velocity was found from the difference in the mean ranges $\Delta\overline{R} = \overline{R} - \overline{R}_0$, based on the stopping power for copper. A copper absorber with an automatically variable thickness from 254.6 to 270.7 g/cm^2 and a second ionization chamber J_2 were placed behind the first chamber for the measurement of the Bragg curve. The chambers J_1 and J_2 and the copper absorbers were those used in previous measurements, which were carried out simultaneously with the measurement of the proton velocity.

RESULTS AND DISCUSSION

In the measurements of the proton momentum by the method of the current-carrying conductor it was found that $Q = 300.0 \pm 0.3$ g and $I = 0.681 \pm 0.001$ A. Hence

$$p = 1296.5 \pm 2.3 \text{ Mev}/c.$$

A series of measurements was carried out with $Q = 200$ g. These yielded a result consistent with the first series, within the accuracy limits. This means that for $Q = 200$ g the errors arising from neglecting the weight and elasticity of the wire are no larger than the errors in the measurement of the current and tension of the wire.

It was found from the measurements of the mean range of the protons that the energy of the protons used in the experiment was slightly higher, and their range larger by 3.8 g/cm^2, than $\overline{R}_0$ measured previously. Repeated measurement of the Bragg curve showed that the accuracy of measurement of the range difference ΔR amounted to 10%. For determination of the corresponding correction to the value of proton energy, the stopping power of copper for protons of velocity $v/c = 0.81$ was found from the formula of Bethe[8] to be equal to $-dE/dx = 1.73$ Mev/g-cm^{-2}. It follows that the difference in the mean energy of protons of mean velocity v_0 and of the beam protons used in the present experiment amounts to $\Delta E_1 = 6.6$ Mev.

Since the momentum measurement pertains to protons near the magnetic analyzer and the velocity v and range were measured after the protons traversed about 5.5 m of air, it was necessary to introduce a correction for the energy loss in air. This amounted to $\Delta E_2 = 1.5$ Mev. The total correction is therefore $\Delta E = \Delta E_1 + \Delta E_2 = 8.1$ Mev.

Since the relative value of the correction amounts only to 1.2%, the error in its determination can be neglected. The corresponding correction to the velocity is calculated according to the relativistic expression for energy. Assuming the rest energy of the proton to be 938.2 Mev (Ref. 9), we obtain for the mean velocity a value $v/c = 0.8112 \pm 0.0005$. The fact that, while aiming at detecting small deviations from the basic relativistic relation $m = m_0[1 - (v^2/c^2)]^{-1/2}$, we used a relativistic relation to determine the corrections ΔE and Δv, is justified by the small magnitude of the corrections.

Using the values for the momentum and velocity of protons given above, we obtain

$$m_1 = p/v = 1598.2 \pm 3 \text{ Mev}/c^2$$

and

$$m_2 = m_0[1 - (v^2/c^2)]^{-1/2} = 1604.3 \pm 1.9 \text{ Mev}/c^2.$$

Hence

$$\Delta m = m_2 - m_1 = 6.1\,(1 \pm 0.6)$$

or

$$\Delta m/m = 0.004\,(1 \pm 0.6).$$

(the errors represent standard deviations).

The results are, within the limits of the experimental errors, in agreement with the relativistic law of the variation of mass.

In conclusion the authors wish to express their gratitude to Prof. L. Janossy for his interest in the work and their appreciation to B. S. Neganov and Iu. D. Baiukov for assistance and valuable discussion.

[1] P. S. Farago and L. Janossy, Nuovo cimento **5**, 1411 (1957).

[2] D. J. Grove and J. C. Fox, Phys. Rev. **90**, 378 (1953).

[3] J. J. Thomson, Phil. Mag. **6**, 13, 561 (1907).

[4] I. Loeb. Compt. rend. **222**, 488 (1946).

[5] M. S. Kozodaev and A. A. Tiapkin, Приборы и техника эксперимента (Instruments and Meas. Engg.) **1**, 21 (1956).

[6] V. P. Zrelov, Report, Inst. Nucl. Studies Acad. Sci. U.S.S.R., 1954.

[7] R. Mather and E. Segrè, Phys. Rev. 84, 191 (1951).

[8] M. S. Livingston and H. A. Bethe, Revs. Mod. Phys. 9, 263 (1937).

[9] Cohen, Layton, Du Mond, and Rollet, Revs. Mod. Phys. 27, 363 (1955).

Translated by H. Kasha
111

SOVIET PHYSICS JETP VOLUME 34 (7), NUMBER 3 SEPTEMBER, 1958

RANGE AND SPECIFIC IONIZATION OF MULTIPLY-CHARGED ION IN A GAS

Ia. A. TEPLOVA, V. S. NIKOLAEV, I. S. DMITRIEV, and L. N. FATEEVA

Moscow State University

Submitted to JETP editor September 20, 1957

J. Exptl. Theoret. Phys. (U.S.S.R.) 34, 559-568 (March, 1958)

The range and specific ionization in air, argon, and hydrogen have been measured for the ions from Be to Ne at velocities between 1.5×10^8 and 12×10^8 cm/sec. For $v \leq 5 \times 10^8$ cm/sec, the specific ionization and the range of an ion is approximately proportional to the particle velocity v. At higher velocities, the range is proportional to v^2 and the specific-ionization curves have a flat maximum, as in the Bragg curve for α particles. The stopping power of a substance, B, is not the same for all ions and decreases with increasing Z of the ion.

1. INTRODUCTION

In connection with the study of nuclear reactions induced by multiply-charged ions and by hypernuclei, interest has increased recently in the passage of charged ions of light elements, with atomic numbers $Z > 2$, through matter. Particularly interesting are the ranges and specific ionizations of these ions. A theoretical prediction of these characteristics is a rather complicated matter, owing to the difficulties of accounting for the charge exchange, which comes prominently into play at an ion velocity v close to the velocity of its orbital electrons. Recent publications describe the stopping of ions in photo emulsion[1-3] and in air,[3-5] using certain simplifying assumptions concerning the effective ion charge and the stopping power B of the substance. These reports need an experimental verification.

The only information available up to recently was on the ranges (referred to air) of recoil nuclei in a condensation chamber, at velocities from 2×10^8 to 7×10^8 cm/sec.[6-11] A short time ago reports were published on the ranges of many accelerated ions in gases, at velocities below 1×10^8 cm/sec,[12] and of lithium,[13] beryllium, and nitrogen[14] ions at higher velocities. The ranges of certain multiply-charged ions in photoemulsion[15-18] and of nitrogen ions in nickel[19] were also measured. As to specific ionization, there exist, in addition to a report[19] concerning its constancy at velocities from 10×10^8 to 20×10^8 cm/sec, also data (in gases) for neon and nitrogen ions in the velocity region below 3×10^8 cm/sec (Ref. 20), and also for lithium ions.[13,21]

In this investigation, we studied the ranges and the specific ionizations of ions from Be to Ne, at velocities from 1.5×10^8 to 12×10^8 cm/sec in argon, air, and hydrogen.

2. DESCRIPTION OF THE EXPERIMENT

In this work, as in the work reported in Ref. 13, we employed a focused ion beam extracted from a 72-cm cyclotron. After passing through a system of 1×10 mm slits, the beam entered the registering apparatus (Fig. 1).

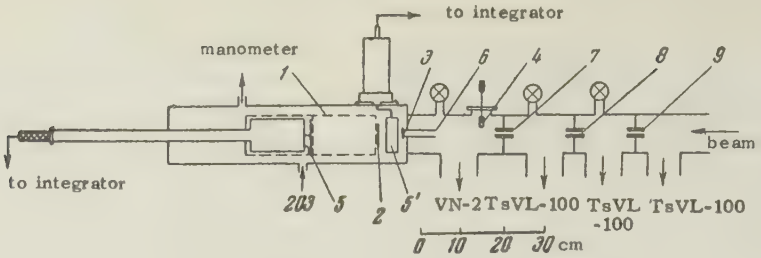

FIG. 1. Diagram of measuring apparatus.

The measurement method consisted of moving a charged-particle recorder, attached on a movable rod, along the trajectory of the beam inside the stopping chamber, to measure the relative ionization along the path. The particle speed was determined from the intensity of the field of the focusing magnet, calibrated for α particles and deuterons of known energy. The value of the field, in turn, was determined from the ranges of α particles in air and of deuterons in air and hydrogen, using tabulated data on the energy dependence of the range.[22] The accuracy of the speed determination did not exceed 2% and that of the corresponding energy determination did not exceed 4%. To obtain ions of different velocities, we varied the magnetic field intensity and the frequency of the electric field between the dees of the cyclotron. The gases BF_3, air, and Ne were introduced into the ordinary arc source of the cyclotron. Beryllium ions were obtained from a source with a beryllium plug.

The ions were stopped in chamber 1 (Fig. 1), filled with gas at pressure suitable for operation of the proportional counter and at the same time sufficient to keep the total range of the ions within the chamber. The average pressure was approximately 40 mm mercury for air, 35 for argon, and 130 for hydrogen. At low velocities ($v < 4 \times 10^8$ cm/sec), pressures up to 2 mm mercury were used, and the ions were registered in this case with an ionization chamber. An inclined mercury manometer, accurate to ± 0.3 mm Hg, was used to measure pressure from 1 to 50 mm Hg. Higher pressures were measured with an ordinary U-shaped manometer.

The vacuum portion of the cyclotron was separated from the stopping chamber with a celluloid film 3, ~ 120 $\mu g/cm^2$ thick. An identical film 4 was placed in the vacuum a certain distance away from film 3. Film 4 could be placed in the path of the beam to determine the air equivalent of the first film.

The specific ionizations and the ranges of ions with velocity from 4×10^8 to 12×10^8 cm/sec were measured with a proportional counter and a linear amplifier 2. The counter comprised a rectangular brass box with a 3×10 mm slit for the admission of the particles. The collecting electrode was a tungsten wire 60 microns in diameter, stretched parallel to the slit and placed 7 mm off the center of the slit. The counter was 6 mm deep and was not separated from the stopping chamber. The pulses at the output of the linear amplifier were measured both visually with a cathode ray oscillograph, and on the film of a loop oscillograph 60 mm wide. As a check, each series of measurement was repeated many times.

The ranges of nitrogen ions at velocities from 1.5×10^8 to 4×10^8 cm/sec were measured with a flat ionization chamber 5, recording the total current at a given portion of the ion path. A chamber approximately 3 mm deep was attached to the moving rod together with the counter. The high voltage electrode, measuring 8×2 cm, was in the form of a tungsten wire mesh 60 microns thick, the distance between wires being 1 mm. The particles entered the chamber through the mesh and moved in the chamber in the direction of the electric field. The current in the ionization chamber was measured with an integrator. The readings of the measuring chamber were related to the readings of a monitor chamber 5', located at the input to the stopping chamber, and providing passage for the entire beam. To avoid energy losses in the film, a differential vacuum system was employed with a pressure drop from 10 to 2×10^{-5} mm Hg, obtained by four stages 6 — 9, separated by 1×10 mm channels 4 to 10 cm long. To provide comparison with the results obtained with the counter, control measurements were made at 5 and 8×10^8 cm/sec, using the film instead of the differential vacuum.

3. PROCESSING OF THE RESULTS AND EXPERIMENTAL ERRORS

The measurements yielded the dependence of the pulse amplitudes (or of the ionization current) on the distance between the recorder and the point of entry of the beam into the stopping chamber. The end of the range was determined from the x-intercept of the experimental curve for the specific ionization. At a pressure of 760 mm mercury, the range was calculated from the formula

$$R = l(p/760) + \Delta R,$$

where l is the length of the ion path in the stopping chamber, p is the pressure in the chamber in mm Hg, and ΔR the equivalent of the celluloid film when operating with the counter, averaged over all measurements for the given ion and gas. This equivalent amounted to ~ 1 mm for air and argon and ~ 4 mm for hydrogen.

The measurements of the film equivalent did not show it to depend on the ion velocity, but an approximately linear dependence on the ion charge was observed. In hydrogen, the reduction in the value of the equivalent from the proton to the neon ion amounted to 30% in neon, 15% in argon, and 5% in air. Since the accuracy in the measurement of the equivalent did not exceed 15 — 30%, the observed law can be considered only approximate. In measurements with the ionization chamber, ΔR represented the effective length of channel 6, equal to $(63 \pm 3)\,(p/760)$ mm, which was calculated with the Knudsen formula for viscous flow.

The absolute values of the specific energy losses in Mev/cm was obtained from the pulse amplitude vs. distance curve by two methods: (A) normalization with respect to energy, as described in Ref. 16, and (B) comparison of the pulse from a given ion with the pulse from a proton of known energy, for identical counter positions. Both methods yielded equal values, within the limits of experimental error. Table I gives the results of the comparison for argon. To check the procedure, specific ionization vs. velocity curves were obtained for α particles and deuterons, and these curves agreed quite satisfactorily with the available data.[22,23]

The major error, both in the determination of the range and in the determination of the specific ionization, was due to the considerable spread of the pulses within a single series and between various series of measurement. Calculations have shown that in the region with $v > 3 \times 10^8$ cm/sec the spread within any one series can be accounted for almost entirely by statistical fluctuations of the coefficient of gas amplification. Differences between series was probably due to counter-voltage fluctuations. The summary error, which includes in addition to the above error also the errors in the measurements of the pressure and of the film equivalent, is shown in Figs. 2 — 4 to fluctuate between 2 and 7% for the range and between 7 and 15% for the specific ionization, depending on the ion and on the velocity (at $v > 3 \times 10^8$ cm/sec).

TABLE I

Ion	dE/dx, Mev/cm	
	A	B
$^{9}Be^{+2}$	5.0±0.4	5.2±0.5
$^{11}B^{+2}$	6.2±0.6	5.8±0.6
$^{14}N^{+3}$	9.1±0.4	8.5±0.8
$^{16}O^{+3}$	9.6±0.5	9.5±1.0

Figure 2 shows, by way of an example, the experimental points obtained by measuring the dependence of the specific ionization on the range for the ions ^{11}B and ^{14}N in air and in hydrogen. The solid line represents the average of the experimental points.

4. RESULTS

The results of the range measurement are shown in Fig. 3 in the form of the dependence of Z^2R/A on E/A, i.e., in units that are independent of the isotopic mass of the ion A. The solid lines on the graph were obtained by integrating the curves of the specific ionization and are continued dotted to the range measured at maximum energy E. The dots represent the results of direct measurement of the ion ranges at various velocities. The points fit the curves within experimental accuracy. This shows that, within the experimental error, the average energy required to produce a single pair of ions is independent of the velocity and of the type of ion, i.e., that the forms of the curves of specific ionization and of average energy loss dE/dx coincide, as was indeed assumed in the normalization of the specific-ionization curve.

Comparison of the ranges of the ions in various gases shows that, for equal velocity, the range is greater by 6% in argon and by a factor of 3.7 times in hydrogen, compared with air, and that this ratio diminishes somewhat with increasing Z of the ion (by $\sim 10 - 20\%$ as Z increases from 5 to 10). At a velocity $v < 5 \times 10^8$ cm/sec, the range of the ion is proportional to the velocity, and at higher velocities the dependence of R on v changes, the range becoming approximately proportional to v^2 at velocities $\sim 6 - 8 \times 10^8$ cm/sec.

The specific ionization, as can be seen from Fig. 5, is proportional to the velocity at $v < 5 \times 10^8$ cm/sec, and at $v \sim 6 - 8 \times 10^8$ cm/sec it has a maximum similar to the Bragg curve for α particles. At the maximum, $dE/dx \approx 1.5\,Z$ Mev/cm.

Comparison of the curves of the specific ionization in various gases shows that it is possible to employ for all ions a factor 0.92 ± 0.05 in converting from argon to air, and 0.29 ± 0.01 in converting from hydrogen to air. These coefficients, accurate to $\sim 10\%$, can be considered equal to the

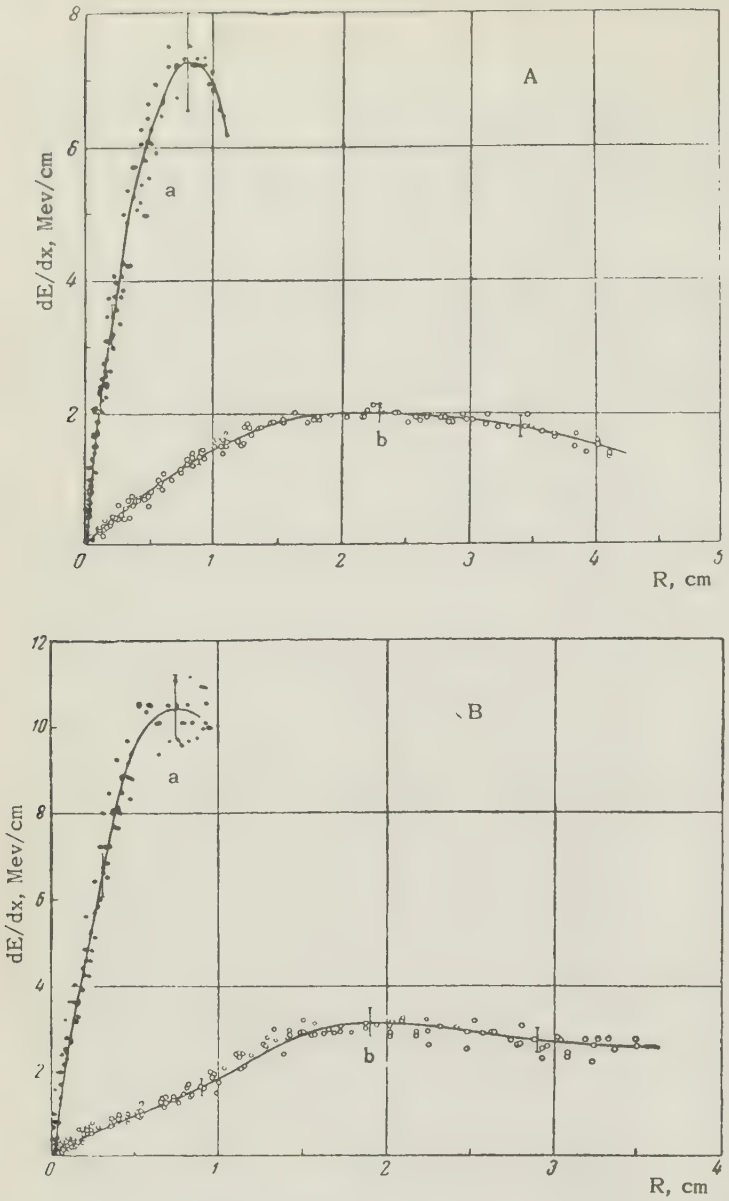

FIG. 2. Specific ionization: A – ^{11}B, B – ^{14}N; a – in air, b – in hydrogen, depending on the residual range at 760 mm Hg.

ratio of $N_0 Z_S^{2/3}$ for the given substances, where N_0 is the number of atoms per cm^3 of matter, and Z_S is the atomic number of the medium, On the whole, the dependence of the specific ionization on Z and on Z_S can be written

$$-\frac{dE}{dx} \approx N_0 Z_S^{2/3} Z f(v),$$

where f(v) is independent of the medium and of the ion within ±10 – 15%.

5. INTERPRETATION OF THE RESULTS

The ranges of ions in air, measured by means of an ionization chamber (see Fig. 4), are approximately 1 mm shorter than the ranges obtained

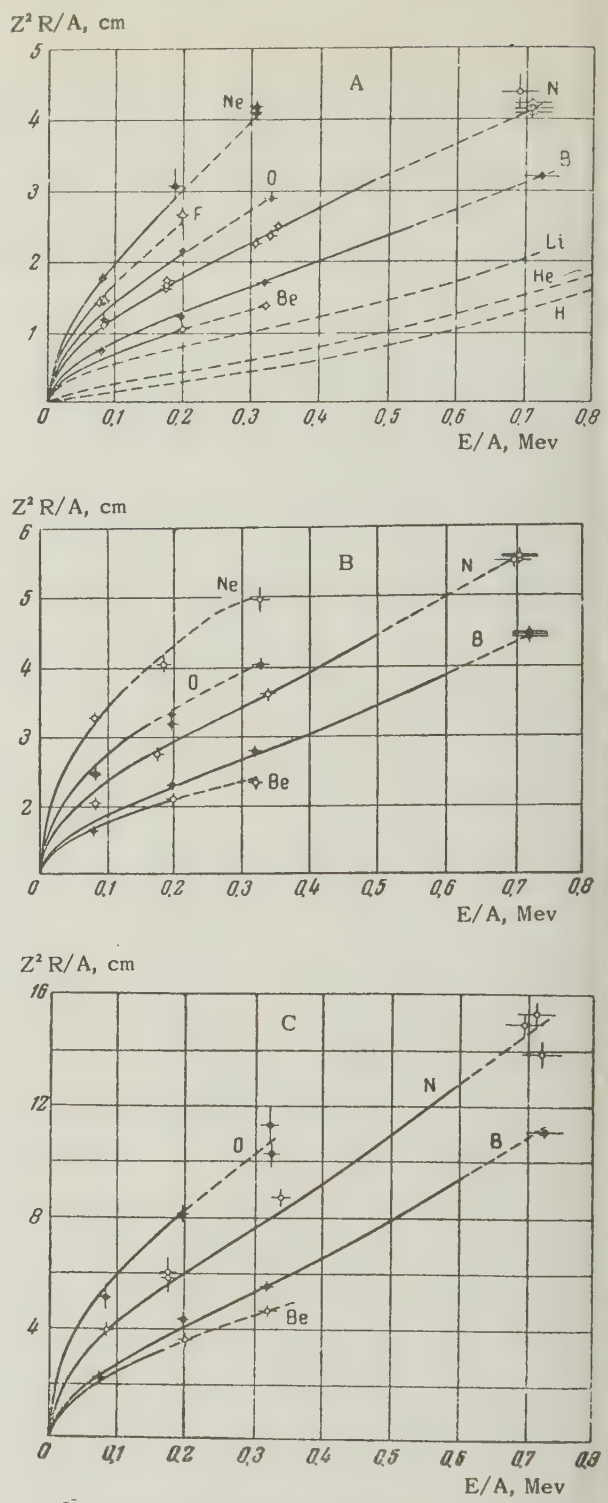

FIG. 3. Dependence of the ion ranges on the energy at a pressure of 760 mm Hg. A – in air, B – in argon, C – in hydrogen. Values of the ranges in air for the protons and the α particles were taken from Ref. 22, those for the Li ions – from Ref. 13.

with the aid of the counter. A similar difference is observed also in argon (~1 mm) and in hydrogen (~2 mm). Qualitatively this can be attributed to nuclear collisions. It is known that at the end of the range there is an increase in the number of elastic collisions between the ions and the atoms

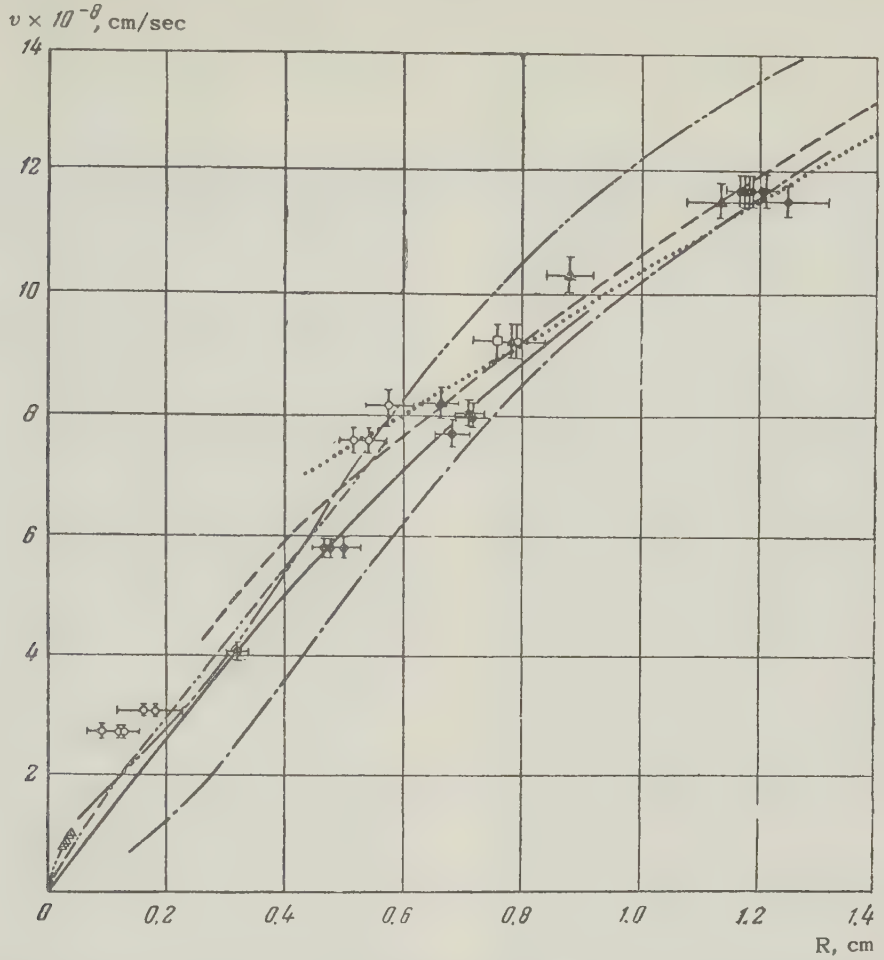

FIG. 4. Dependence of the ranges of ^{14}N ions on the velocity in air at 760 mm Hg: – our experimental results, obtained with a proportional counter, and o – with an ionization chamber; ▲– measurements in a condensation chamber,[14] Δ – values obtained in Ref. 12, ··–––·· – measurements of recoil nuclei,[6,8] ···– measurements in photoemulsion, recalculated for air.[15] Calculated curves: – – – – – from Ref. 3, –··–·· – from Ref. 4, and –·–·– from Ref. 5.

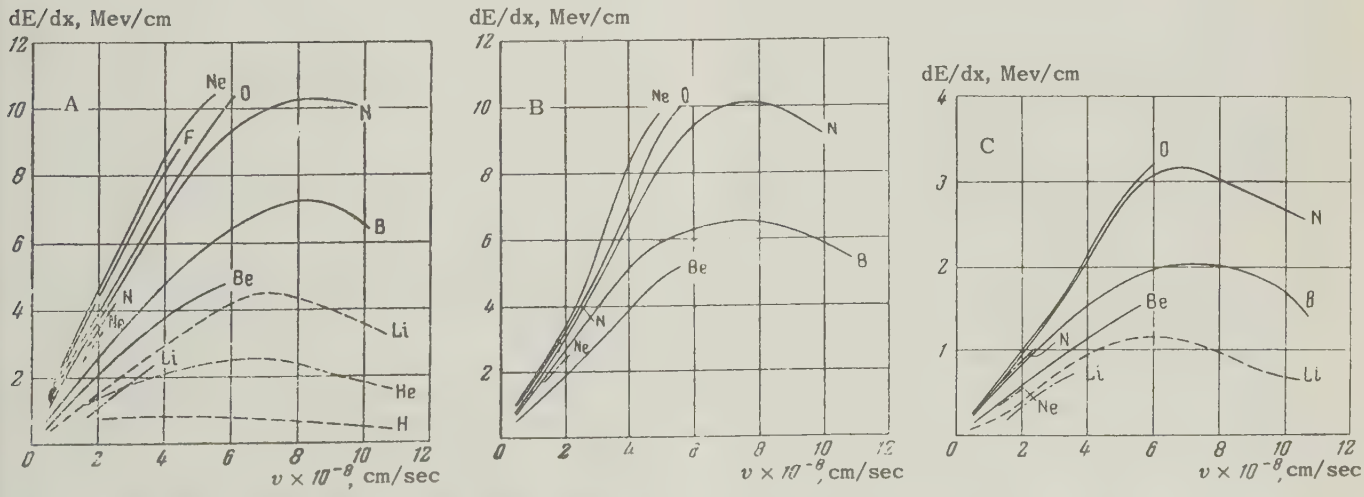

FIG. 5. Specific ionization of multiply-charged ions as function of the velocity: A – in air, B – in argon, C – in hydrogen. Solid line – results of this investigation, dotted line – from Refs. 22, 23, and 13; dash-dot line – from Refs. 21 and 20.

of the substance, leading to greater energy losses per collision and to greater deflection angles. Since the dimensions of the input slit of a proportional counter are small, the counter recorded essentially the ions that did not experience elastic collisions and whose range was greater than the range of most ions that entered into the ionization chamber. A theoretical estimate of this effect, based on the classical approximation,[24,25] leads to a range difference that is close to that observed experimentally.

Figure 4 gives all the published data on the ranges of the ^{14}N ions in air. According to Ref. 14, the ranges of accelerated nitrogen ions, measured in a condensation chamber, are approximately 5% less than our values, but this can also be attributed to the influence of nuclear collisions. The curve obtained from data on the ranges of the recoil nuclei,[6,8] a curve characterized by low statistics and large spread of individual points, differs on the average from our results by 10%. An analogous correspondence is observed also for oxygen, fluorine, and neon ions.[6-9] Only in the case of the boron ions are the ranges of the recoil nuclei (see Ref. 11) approximately 1.5 mm smaller than ours; this apparently can be attributed only partially to nuclear collisions.

Figure 4 gives also the curve for the ranges of nitrogen ions in photoemulsion,[15] recalculated for air using a value of 1800 for the stopping power. The fact that the curves agree within 15% shows that the stopping power of the photoemulsion with respect to air is the same for these ions as the stopping power for α particles.

For comparison with experiment, Fig. 4 shows three calculated curves.[3-5] The curve from Ref. 4 is close to the experimental curve for a velocity $v = 6 \times 10^8$ cm/sec, but at greater velocities it gives undervalued ranges. To the contrary, the curves from Refs. 3 and 5 do not agree with experiment at low velocities, but at $v > 7 \times 10^8$ cm/sec they agree with the experimental curve within 10%.

The measured specific-energy losses for the ^{14}N ions agree, within the limits of experimental error, with the previously obtained data[20] (Fig. 5). However, the specific-energy losses for the ^{20}Ne ions, cited in the same reference, are 30% lower than those obtained in our work. Such a discrepancy can be hardly attributed to various influences of nuclear collisions. The curve of Ref. 11 for the specific-energy losses for ^{11}B ions, calculated from the ranges, differs from our curve by not more than 10%. The value of the specific ionization calculated in Ref. 5 for nitrogen and beryllium ions is too high, and at the maximum it exceeds the experimental value by approximately 30%.

It is known that the average energy loss can be calculated from the formula

$$-dE/dx = (4\pi e^4/mv^2) i^{*2} \cdot N_0 \cdot B(v),$$

where i^* is the effective ion charge, and B is the stopping power of the substance. In the above-mentioned calculations of the ranges and specific-energy losses,[1-5] the value of B was assumed the same for all ions and was determined from the values of dE/dx and i^* for protons or α particles. The values of B calculated in our work from the values of dE/dx, and the values of the rms charge from the equilibrium distribution of the charges in the ion beam,[26] have shown that in the velocity range $v < 3-5 \times 10^8$ cm/sec B diminishes with increasing Z and is approximately 20% lower for ^{20}Ne than for the ^{11}B ions. A similar character of the dependence of B on Z follows from the known Bloch formula for the specific-energy losses,[22] according to which

$$B = Z_s[\ln(2mv^2/I) - Q],$$
$$Q = R\psi[1 + j(i^*e^2/\hbar v)] - \psi(1),$$

where ψ is the logarithmic derivative of the Γ function and $R\psi$ is the real part of ψ. As Z increases, the mean charge, and consequently also the the quantity Q (which depends on the ratio of the mean charge to the ion velocity) increases and the stopping power B diminishes.

The Bloch formula is applicable only when the ion velocity v is considerably greater than the velocity u of the orbital electrons of the atoms of the substance. At $v \sim 3-5 \times 10^8$ cm/sec, this condition is not satisfied for a considerable number of electrons. One can assume, however, that at least for those electrons with $u < v$, the dependence of the stopping power on the ion charge fits the Bloch formula, and that the contribution to the stopping produced by electrons with $u > v$ is independent of Z. As a result, we can assume that $B = B_0 - Z_s^* Q$, where B_0 is independent of Z, and Z_s^* is the effective number of electrons of the atoms of the substance, for which the Bloch formula is valid.

As the velocity increases, Z_s^* should also increase, and should approach Z_s in the limit. The dependence of Q on v in the region $v \sim 3-6 \times 10^8$ cm/sec is weak, since the value of the mean charge is approximately proportional to v (Ref. 26). At greater velocities, when the mean charge increases more slowly, Q diminishes. At the same time, as the velocity increases, the value B_0 increases rapidly, i.e., B becomes on the whole less dependent on Z.

TABLE II

Ion	Air			Argon		
	B	Q	$B+3Q$	B	Q	$B+6Q$
He	10.8±0.3	0.29	11.7±0.3	20.4±0.6	0.29	22.1±0.6
B	10.0±0.8	0.58	11.7±0.8	20.0±1.5	0.60	23.6±1.5
N	9.8±0.7	0.74	12.0±0.7	17.8±1.3	0.75	22.3±1.3
O	8.6±0.6	0.82	11.1±0.6	15.6±1.0	0.84	20.6±1.0
Ne	8.2±0.5	0.92	11.0±0.5	16.4±1.0	0.92	21.9±1.0

We determined the value of Z_S^* from the values of B and Q, corresponding to the experimental values of the mean ion charge in gases.[26] In the velocity region $v \sim 4-5 \times 10^8$ cm/sec, it turned out to be close to 3 for air, ~6 for argon, and ~1 for hydrogen, i.e., $Z_S^* \approx Z_S^{2/3}$. The values of B, Q, and $B_0 = B + Z_S^* Q$ for $v = 4 \times 10^8$ cm/sec are given in Table II (the data from the survey of Ref. 24 are used for the α particles). The values of B_0, as can be seen from the table, are the same for all ions within ±7%.

It must be noted, that the close agreement between the theoretical calculations, based on the assumption that B is independent of Z, with experiment is to certain extent fortuitous and may be due to the fact that the dependence of the mean charge on Z is assumed in these investigations to be somewhat weaker than actual.

In conclusion, I express my gratitude to S. S. Vasil'ev for interest in this work and for a discussion of its results, to the cyclotron crew headed by G. V. Kosheliaev, and also to B. M. Makuna for help in this work.

[1] J. P. Lonchamp, J. phys. et radium **14**, 89 (1953).

[2] A. Papineau, Rapport CEA, N 543 (1956).

[3] D. L. Livesey, Can. J. Phys. **34**, 203 (1956).

[4] D. Knipp and E. Teller, Phys. Rev. **59**, 659 (1941).

[5] I. S. Dmitriev, J. Exptl. Theoret. Phys. (U.S.S.R.) **32**, 570 (1957), Soviet Phys. JETP **5**, 473 (1957).

[6] P. M. S. Blackett and D. S. Lees, Proc. Roy. Soc. **A134**, 194, 658 (1932).

[7] N. Feather, Proc. Roy. Soc. **A141**, 193 (1933).

[8] W. W. Eaton, Phys. Rev. **48**, 921 (1934).

[9] J. T. McCarthy, Phys. Rev. **53**, 30 (1938).

[10] G. A. Wrenshall, Phys. Rev. **57**, 1095 (1940).

[11] A. B. Lillie, Phys. Rev. **87**, 716 (1952).

[12] Evans, Stier, and Barnett, Phys. Rev. **90**, 825 (1953).

[13] Teplova, Dmitriev, Nikolaev, and Fateeva, J. Exptl. Theoret. Phys. (U.S.S.R.) **32**, 974 (1957), Soviet Phys. JETP **5**, 797 (1957).

[14] Iu. A. Vorob'ev, Отчет НИИЯФ МГУ за 1955 г. (1955 Report, Sci. Res. Inst. for Nuclear Physics, Moscow State University).

[15] H. L. Reynolds and A. Zucker, Phys. Rev. **96**, 393 (1954).

[16] Parfanovich, Rabin, and Semchinova, J. Exptl. Theoret. Phys. (U.S.S.R.) **31**, 188 (1956), Soviet Phys. JETP **4**, 99 (1957).

[17] J. F. Miller, Progress in Nuclear Physics **4**, 215 (1955).

[18] G. Faraggi, Compt. rend. **242**, 105 (1956).

[19] Reynolds, Scott, and Zucker, Phys. Rev. **95**, 671 (1954).

[20] P. K. Weyl, Phys. Rev. **91**, 289 (1953).

[21] S. K. Allison and C. S. Littlejohn, Phys. Rev. **104**, 959 (1956).

[22] E. Segrè, ed. Experimental Nuclear Physics, vol. I, Wiley, N. Y. 1953.

[23] M. S. Livingston and H. A. Bethe, Revs. Mod. Phys. **9**, 245 (1937).

[24] S. K. Allison and S. D. Warshaw, Revs. Mod. Phys. **25**, 779 (1953).

[25] N. Bohr, Passage of Atomic Particles through Matter, Ch. II. (Russ. Transl) IIL, 1950.

[26] Nikolaev, Dmitriev, Fateeva, and Teplova, J. Exptl. Theoret. Phys. (U.S.S.R.) **33**, 1325 (1957), Soviet Phys. JETP **6**, 1019 (1958).

Translated by J. G. Adashko
112

DECAY SCHEME OF Ba^{140}

A. N. SILANT' EV

Radium Institute, Academy of Sciences, U.S.S.R.

Submitted to JETP editor September 7, 1957

J. Exptl. Theoret. Phys. (U.S.S.R.) 34, 569-573 (March, 1958)

The gamma-ray spectrum of Ba^{140} was measured with a scintillation gamma spectrometer. The spectrum was treated by the method of Maeder, Müller, and Wintersteiger. The relative intensities of gamma rays with energies of 30, 160, 305, 430, and 537 kev were respectively 0.7, 0.18, 0.12, 0.18, and 1.0. Measurements of $\gamma-\gamma$ and $\beta-\gamma$ coincidences were obtained. A decay scheme for Ba^{140} is proposed on the basis of the results of the present and previous investigations.

BEACH, Peacock and Wilkinson[1] have studied the beta spectrum of Ba^{140}, the two components of which have end-point energies of 1022 and 480 kev and relative intensities of 60 and 40%. Cork and his co-workers[2] have investigated the internal conversion electrons from the gamma rays of Ba^{140} by measuring the conversion electron energies and determining their relative intensities. The conversion electrons were ascribed to gamma rays with energies of 29.6, 118.5, 131.8, 162.1, 304, 421.8, 435.8 and 536.7 kev. Maerker and Birkhoff[3] and Rohr and Birkhoff[4] measured the internal conversion coefficient of 540-kev gamma rays from Ba^{140}, obtaining $\alpha_K = (5.6 \pm 1.9) \times 10^{-3}$ with $K/L + M = 6 \pm 2$ and 5 ± 0.5, respectively.

Kelly and Wiedenbeck[5] using a scintillation spectrometer recorded gamma rays from Ba^{140} with energies of 30, 132, 162, 304, 436 and 537 kev. Through an analysis of the gamma spectrum measured from a source inside the crystal conclusions were reached regarding $\gamma-\gamma$ coincidences. The same article gives the angular correlation of 162 and 304-kev gamma rays.

EXPERIMENTAL PROCEDURE

Radioactive Ba^{140} decays with a half life of 13 days to radioactive La^{140} which, in turn, decays with a half life of 40 hours to the stable isotope Ce^{140}. Thus the source always contains a mixture of the radioactive isotopes of Ba^{140} and La^{140}.

Chemical purification was effected by precipitating La from the Ba in solution. Drops of the filtered solution were deposited on a collodion film and dried. Gamma radiation from the prepared source was measured by means of a scintillation spectometer. $\beta-\gamma$ and $\gamma-\gamma$ coincidences were also recorded. The Ba^{140} spectrum was automatically recorded.[6] Since La^{140} is gradually accumulated in the source measurements were performed as soon as possible after preparation of the specimen and not later than 5 hours afterward.

The amount of La^{140} in the source was estimated from its 800-kev line. The La^{140} spectrum was subtracted from the spectrum of Ba^{140} containing La^{140}; the remaining spectrum is shown in Fig. 1.

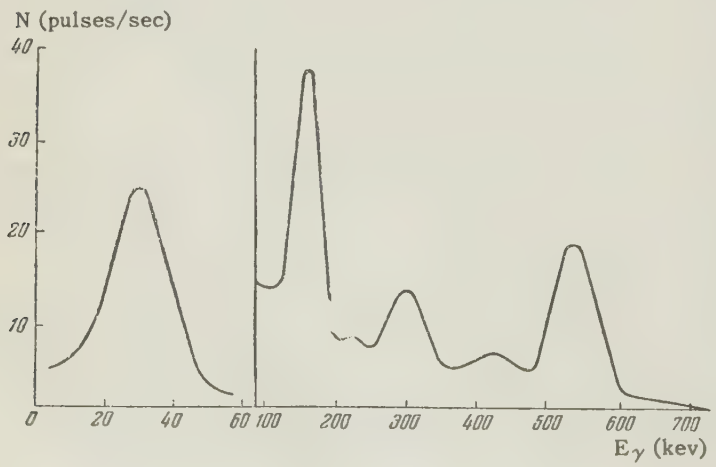

FIG. 1. Gamma-ray spectrum of Ba^{140}: E_γ – gamma-ray energy; N – counting rate (analyzer output).

In analyzing the spectrum the method of Maeder et al.[7] was employed to calculate the form of the line (the form of the photopeak and the form and magnitude of the Compton electron spectrum) from the frequency and height of the gamma-ray photopeak at a given energy. In order to ascertain that 30-kev gamma rays came from the source and did not result from secondary effects in the crystal a copper absorber with a thickness of 1 g/cm^2 was placed between the source and the crystal. This caused the 30-kev gamma peak to disappear completely while the remaining spectrum of harder gamma rays was attenuated only slightly.

TABLE I. Energies and relative intensities of gamma radiation from Ba^{140}

From Cork et al.[2]	From Kelly and Wiedenbeck[5]	Our measurements	
		Energy (kev)	Relative intensity
29.6	30	30	0.7
118.5	—	—	—
131.8	132	—	—
162.1	162	160	0.18
—	—	230	0.02
304	304	305	0.12
421.8	—	—	—
435.8	436	430	0.18
536.7	537	537	1.0

Gamma rays at about 230 kev were observed in addition to previously known gamma radiation. This is probably scattered radiation. Table I shows the measured relative intensities of the gamma rays.

Figure 2 presents three spectra of gamma rays coinciding with beta rays of different energies. The counting rate of the beta spectrometer was normalized for all three gamma spectra. The hard beta rays correspond to a transition to the ground level or first excited level of La^{140}; with the same counting rate of the beta spectrometer for different energies the $\beta-\gamma$ coincidence rate was reduced when the beta spectrometer was adjusted for the harder part of the spectrum. The 540-kev gamma rays coincide only with soft beta rays.

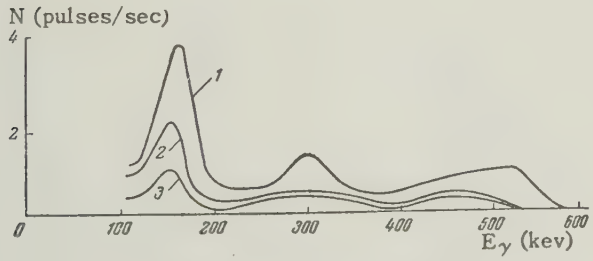

FIG. 2. Spectrum of gamma rays coinciding with: 1 – the soft part of the beta spectrum, 2 – the middle of the beta spectrum, 3 – the hard part of the beta spectrum; N is the counting rate at the output of the coincidence scheme.

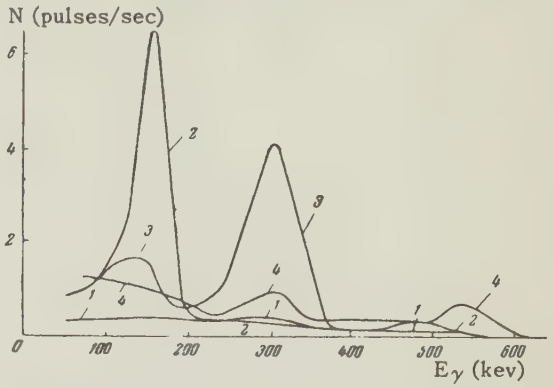

FIG. 3. Spectrum of gamma rays coinciding with other gamma rays of the following energies: 1 – 450 kev, 2 – 304 kev, 3 – 160 kev, 4 – 30 kev; N is the counting rate at the output of the coincidence scheme.

Figure 3 contains the spectra of gamma rays coinciding with other gamma rays of various energies. The following gamma-ray coincidences occur: 300-kev gamma rays coincide with those of 160 kev, while 30-kev gamma rays coincide with those of 540 and 300 kev.

CONCLUSIONS

Since we know the internal conversion coefficient of the 540-kev gamma transition[3,4] we can compare the present results with those of Cork and his co-workers[2] and attempt to estimate the internal conversion coefficients for the remaining transitions Preliminary values of the internal conversion coefficients can be taken from tables in Refs. 8 and 9, using the relative intensities of conversion electrons in Ref. 2. The latter method must be preferred because the relative intensities of conversion electrons can be determined more accurately when their energies are close than when they are separated by a large energy interval. These results are shown in Table II.

It can be seen from Table II that the x-ray contribution to the 30-kev gamma transition may be neglected. Conversion also has little effect on the relative intensities of hard gamma transitions but greatly changes the 30-kev transition. Table III gives the relative intensities of gamma transitions with the internal conversion coefficients taken into account.

In the decay scheme proposed by Kelly and Wiedenbeck[5] the 450-kev gamma transition goes to the ground level. This is contradicted by the facts given below, which permit the conclusion

TABLE II. Preliminary values of internal conversion coefficients.

Energy of gamma transition (kev)	Conversion electron level and energy (kev)	Relative intensity of electron conversion	Conversion coefficients (Ref. 8 and 9) in the ratios L_I: L_{II}: L_{III} or K:L	Conversion coefficients computed from the conversion coefficient for E=540 kev	Conversion coefficients used in the present work	Relative intensity of 39-kev x-rays
29.6	L_I 23.3	20	3.8	$5\cdot10^{-3}$	3.8	
	L_{II} 23.7	2	$3.1\cdot10^{-1}$	$5\cdot10^{-3}$	0.3	
	L_{III} 24.1	1	$6.3\cdot10^{-2}$	$2\cdot10^{-3}$	0.1 6.6	0
	M 28.2	10	—	$2\cdot10^{-2}$	1.6	
	N 29.3	5	—	$1\cdot10^{-2}$	0.8	
118.5	K 79.8	1	—	—	—	—
131.8	K 93.1	4	—	—	—	—
162.1	K 123.3	10	$2.8\cdot10^{-1}$	$1.0\cdot10^{-1}$	$2.8\cdot10^{-1}$	
	L 156.0	5	$7.5\cdot10^{-2}$	$5\cdot10^{-2}$	$0.7\cdot10^{-1}$	$1.6\cdot10^{-2}$
	M 160.8	2	—	$2\cdot10^{-2}$	$0.3\cdot10^{-1}$	
230	—	—	—	—	—	—
304	K 265.5	4	—	$6\cdot10^{-2}$	$6\cdot10^{-2}$	$0.6\cdot10^{-2}$
421.8	K 382.8	1	—	—	—	—
435.8	K 397.1	1	—	$1\cdot10^{-2}$	$1\cdot10^{-2}$	$0.16\cdot10^{-2}$
536.7	K 498.0	4	—	$6\cdot10^{-3}$	$7\cdot10^{-3}$	$0.5\cdot10^{-2}$
	L 530.0	1	—	$1\cdot10^{-3}$		
						0.03

that the transition in question goes to the first excited level at 30 kev. The analysis of $\gamma-\gamma$ coincidences shows that 540-kev and 30-kev gamma rays coincide. To account for the large relative intensity of the 30-kev transition it must be assumed that the 540-kev transition goes to the first excited state rather than to the ground level of La^{140}. The difference between the end-point energies of the two beta components is 542 kev according to Beach et al.[1] rather than the 507 kev of the decay scheme in Ref. 5. All of the other data obtained in the present work agree with the decay scheme in Ref. 5.

Figure 4 shows the decay scheme of Ba^{140} which is in accordance with the results of our present work.

The author is deeply grateful to Professor G. V. Gorshkov, in whose laboratory this work was done, for his continued interest and valuable suggestions. The author also wishes to thank V. I. Katsapov for the chemical purification of Ba to remove La.

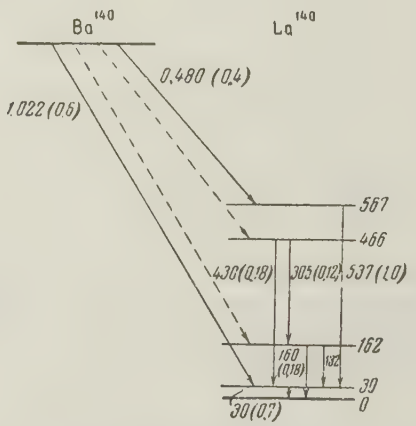

FIG. 4. Decay scheme of Ba^{140}.

TABLE III. Relative intensities of gamma transitions

Energy (kev)	Relative intensities	Energy (kev)	Relative intensities
29.6	5.3*	304	0.13
118.5	—	421.8	—
131.8	0.25	435.8	0.20
162.1		536.7	1.0
230	0.02**		

*The relative intensity of the 30-kev transition is probably too high because of inaccurate knowledge of the internal conversion coefficients.

**The 230-kev line evidently belongs to scattered radiation.

[1] Beach, Peacock and Wilkinson, Phys. Rev. **76**, 1624 (1949).

[2] Cork, LeBlanc, Stoddard, Martin, Branyan and Childs, Phys. Rev. **83**, 856 (1951).

[3] R. E. Maerker and R. D. Birkhoff, Phys. Rev. **89**, 1159 (1953).

[4] R. C. Rohr and R. D. Birkhoff, Phys. Rev. **98**, 1266 (1955).

[5] W. H. Kelly and M. L. Wiedenbeck, Phys. Rev. **102**, 1130 (1956).

[6] A. N. Silant'ev, J. Tech. Phys. (U.S.S.R.) (in press).

[7] Maeder, Müller and Wintersteiger, Helv. Phys. Acta **27**, 3 (1954).

[8] A. Sliv and I. Band, Таблицы коэффициентов внутренней конверсии гамма-излучения (Tables of Internal Conversion Coefficients of Gamma Rays), Acad. Sci. Press, 1956.

[9] G. F. Dranitsyna, Коэффициенты внутренней конверсии на L_I, L_{II}, L_{III} подоболочках (L_I, L_{II} and L_{III} Internal Conversion Coefficients), Acad. Sci. Press, 1957.

Translated by I. Emin
113

SOVIET PHYSICS JETP VOLUME 34 (7), NUMBER 3 SEPTEMBER, 1958

MEASUREMENT OF FAST NEUTRON ABSORPTION CROSS SECTIONS

T. S. BELANOVA

Submitted to JETP editor September 28, 1957

J. Exptl. Theoret. Phys. (U.S.S.R.) 34, 574-578 (March, 1958)

The absorption cross sections for 25, 220 and 830-kev photoneutrons have been found for 20 elements, using neutron transmission in strict spherical geometry.*

1. METHOD OF MEASUREMENT.

FOR the measurement of neutron absorption cross sections, we used the transmission of neutrons in strict spherical geometry (with the neutron source placed inside a sphere of absorbing material). The spherical geometry of the experiment eliminates the direct effect of elastic scattering. The effect of inelastic scattering, which is important for high energy neutrons, was scarcely evident because a long counter was used for detecting the neutrons. Thus, from relative measurements we determined the absolute value of the neutron absorption cross section.

2. EXPERIMENTAL ARRANGEMENT

The experimental arrangement is shown schematically in the figure. Three photoneutron sources, spherical in shape, were used (Sb — Be, Na — D_2O, and Na — Be). They consisted of γ sources of Sb or NaF 25 — 30 mm in diameter, embedded in spherical targets of Be or D_2O, 8 mm in thickness. After assembly, the source had a diameter of 45 — 50 mm. Table I gives the characteristics of the neutron sources used in the present work.

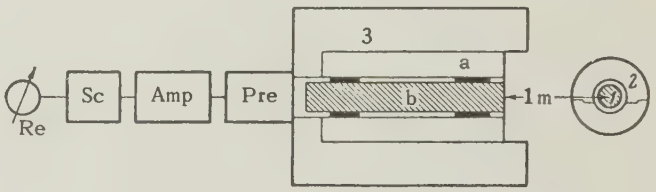

FIG. 1. Arrangement of the experiment. 1 — neutron source, 2 — absorbing sphere of sample material, 3 — long counter: a — paraffin container, b — boron counter; Pre — preamplifier, Amp — amplifier, Sc — scaler, Re — mechanical recorder.

The energy and intensity of the hard neutron group from the (Sb — Be) source was determined from the decay scheme[6] of Sb^{124} and the behavior of the (γ, n) reaction on beryllium.[7]

The samples of materials for study were in the form of spheres with outer diameter 15 — 22 cm, with a cavity 5 — 8 cm in diameter in their interior. They consisted of two hemispheres, so that the neutron source could be inserted into the cavity. The materials to be studied were taken both in cast metal and in powder form. The powders were placed in spherical brass containers having wall thickness 1 — 1.5 mm. The dimensions of the containers were the same as those of the cast spheres. The powders were thoroughly dried before filling the containers.

The neutron detector used was a long counter,[8]

*The measurements were carried out in 1952-1955.

TABLE I

Neutron source	Half-life	Angular distribution of neutrons from (γ, n) reaction	Maximum neutron energy	Average neutron energy, kev
(Sb—Be)	60 days	Isotropic[1]	29 kev[3]	25±4 (93%)[3,5] 400 (7%)
(Na—D_2O)	15 hr.	$1+4.7\sin^2\theta$[2]	270 kev[3,4]	220±20[3,4]
(Na—Be)	15 "	$1+0.8\sin^2\theta$[1]	1 Mev[3,4]	830±40[3,4]

which had the same sensitivity for neutrons of different energies. Pulses from the counter entered a wide-band amplifier and were counted in a PS-64 scale-of-64 recorder.

3. CALCULATION OF ABSORPTION CROSS SECTION

The computation was made using the formula

$$\sigma_a = \frac{(1-(N_2/N_1))\,(1-\exp\{-(R-r)/\lambda_{tr}\})}{[(R-r)\,(1-(N_2/N_1)) + \bar{l}\,((N_2/N_1)-\exp\{-(R-r)/\lambda_{tr}\})]N_0}, \quad (1)$$

where σ_a is the neutron absorption cross section, N_0 the number of atoms per cc, λ_{tr} the transport length, $\bar{l}$ the mean length of neutron path in the material, N_1 the number of neutrons recorded from the (bare) neutron source, N_2 the number of neutrons recorded with the neutron source placed inside the absorbing sphere, R the radius of the sphere, and r the radius of the cavity in the sphere. The formula was obtained on the assumption that the path lengths of neutrons that suffer elastic scattering in the absorber have an exponential distribution. This formula is valid for relatively large absorptions $\sim 25-30\%$.

The average path of the neutrons for a point source was calculated using a somewhat modified formula due to O. D. Kazachkovskii,* which takes into account the presence of the cavity in the sphere:

$$\bar{l} = \frac{1}{2}\frac{R^2}{\lambda_{tr}} + 0.7R - \frac{3}{2}\frac{r^2}{\lambda_{tr}} + \frac{r^3}{r_0\lambda_{tr}} + 0.29\left(R-\frac{r}{2}\right)\exp\left\{-0.46\left(R-\frac{r}{2}\right)/\lambda_{tr}\right\}, \quad (2)$$

where $r_0 = R + 0.7\lambda_{tr}$. For some of the elements, $\bar{l}$ was computed using the data of Barshall et al.[9] on the transport cross section σ_{tr} for 220-kev neutrons, and the data of Lovchikova[10] for 830-kev neutrons. For most of the elements, at 830-kev, we used the values of σ_{tr} found by Walt and Barschall[11] and Walt[12] at 1 Mev. In those cases where there were no experimental data for σ_{tr} for the elements under investigation, we used the value of σ_{tr} computed on the basis of the paper of Feshbach and Weisskopf.[13] From the graphs in their paper, we found the ratio σ_{tr}/σ_{tot} (where σ_{tot} is the total cross section). Using the experimental values of σ_{tot}[14], we calculated σ_{tr} for all the elements studied. Comparison of known experimental values of σ_{tr} with the computed values showed satisfactory agreement.

For 25-kev neutrons the scattering is isotropic, and for low values of σ_a we can use the total scattering cross section $\sigma_s = \sigma_{tot}$ in place of σ_{tr} in calculating $\bar{l}$.

4. CONTROL EXPERIMENTS AND CORRECTIONS

1. Because the boron counter is sensitive to γ rays from the photoneutron source, a correction was made for counting of γ quanta. The correction was of the order of $2-3\%$ of the total count.

2. A correction for fission of U^{235}, which is contained in the normal mixture of isotopes, was made on the absorption cross section of uranium. Depending on the neutron energy, this correction amounted to $3-10\%$ of the capture cross section.

3. Elastic and inelastic slowing down of the neutrons in the spheres changes the primary neutron spectrum. This can result in a change in σ_a. Measurements were made with spheres of different sizes. The values of σ_a obtained were the same for a given element within the limits of accuracy of the experiment. This means that the softening of the initial neutron spectrum is of no consequence, in first approximation.

4. An experimental correction was made for scattering of neutrons in the walls of the sample holders. The size of this correction decreased from ~ 5 to 2% with increase of neutron energy from 25 to 830 kev. The capture cross section was calculated only for those powders in which the effect of capture was greater then the correction for the container.

5. In calculating the average neutron path length, it was necessary to include σ_a in determining σ_s from σ_{tot}. A method of successive

*Private communication.

approximations was used. We first determined σ_a using σ_{tot} in place of σ_s. Then we improved σ_s by using the formula

$$\sigma_s = \sigma_{tot} - \sigma_a$$

and again calculated σ_a. Since σ_{tot} is known to an accuracy of $\sim 15-20\%$, corrections of σ_s were made for those elements in which the measured $\sigma_a > 0.1$ barns.

6. A correction was made for the finite distance between the detector and the neutron source. This experimental correction was determined in several ways. For a distance of 1 meter between the detector and neutron source, the correction was of the order of 1% for all energies.

7. The presence of a hard neutron group in the (Sb — Be) source reduces somewhat the values of the measured absorption cross sections for 25-kev neutrons. A computation showed that σ_a is reduced by 3 — 5%. This correction was not applied to the experimental values of σ_a, since the size of the correction is beyond the limits of accuracy of the computation.

There were also other effects whose contribution to the computation of the absorption cross section were so small compared to the accuracy of the method that they could be neglected. Among these effects are:

(a) multiplication of the neutrons in U^{238} (< 1% correction to σ_a for uranium);

(b) the effect of the finite dimensions of the neutron source on the size of the average neutron path in the sphere (a correction of $\sim 1-2\%$ in $\bar{\ell}$);

(c) the effect of the anisotropy of the (γ, n) reaction in $(Na - D_2O)$ and $(Na - Be)$ sources on the size of the average neutron path in the sphere (a correction of < 1% in $\bar{\ell}$);

(d) the effect of reduction of neutron energy because of backscattering in the source).

5. DISCUSSION OF RESULTS

The results of the present measurements are given in Table II. All the absorption cross sections reported up to now were measured mainly by the activation method.[14-18] They refer only to individual isotopes. The advantage of the method described here is that it does not require absolute measurements of neutron fluxes and β activity of samples, and is also applicable to isotopes which are stable after neutron capture. With the exception of a few isolated cases, the data of the present paper are in good agreement with the absorption cross sections found in the papers mentioned above.

The sensitivity of the long counter varies by

TABLE II

Element	σ_a, millibarn			Element	σ_a, millibarn		
	25±4 kev	220±20 kev	830±40 kev		25±4 kev	220±20 kev	830±40 kev
Mg	19±3	13±10	10±4	Cd	321±7	123±5	73±5
Al	17±3	6±3	<16	Sn	112±5	52±8	36±6
S	<44	<38	<40	Sb	444±4	130±10	100±8
Ca	13±10	5±10	8±10	I	1097±39	314±42	101±40
Cr	144±6	36±1	21±1	Ba	<108	<116	<114
Fe	19±2	13±2	9±2	W	422±26	133±35	40±33
Ni	50±1	26±2	19±6	Hg	202±9	108±11	43±12
Cu	32±3	18±2	19±1	Pb	13±3	8±4	<24
Zn	29±2	21±2	18±3	Th	457±4	235±6	202±6
Se	215±11	83±13	58±16	U	572±7	204±5	147±7

$\sim 18\%$ in the energy range ~ 1 Mev (Ref. 8). Such a change in sensitivity affects the value of σ_a to some extent, since in this energy range there is an effect of elastic slowing down of the neutrons in the spheres and, in addition, in the 830-kev energy region there is appreciable inelastic scattering of the neutrons for some of the elements. Reduction of the sensitivity of the counter to elastically and inelastically slowed neutrons acts as an apparent increase in the absorption effect, and consequently raises the value of the absorption cross section.

Attempts were made, both experimentally and by computation, to estimate the increase in σ_a caused by elastic and inelastic neutron collisions. Computation showed that for 830-kev neutrons σ_a may be increased by 24 — 30% because of the variation in counter sensitivity. For 220-kev neutrons, the increase in σ_a varies between 2 and 4%. For 25-kev neutrons the variation in counter sensitivity is so small that it has no effect on the value of σ_a. Separate experiments were carried out with spheres of graphite (which has no appreciable neutron absorption), thick enough to reduce the average neutron energy by a factor of two. The counting rate with the graphite sphere for 25-kev neutrons was hardly changed. For 220- and 830-kev neutrons, the counting rate was lowered by about 3 — 5%.

An analysis of all the errors of the method enables us to estimate the accuracy: for 25- and 220-kev neutrons, the method gives absorption cross sections to an accuracy of 3 — 15%, while for 830-kev neutrons the absorption cross sections are too high by 20 — 30%. In the future we plan experiments with a detector which has a more constant sensitivity in the energy range below 1 Mev (though we pay the price in poorer response at higher energies).

In conclusion, the author expresses his gratitude to O. D. Kazachkovskii for continual help in the work and for valuable advice, and to V. P. Pazovska and I. M. Kopylov who helped in the measurements.

The author is grateful to Prof. A. I. Leipunskii for continued interest in the work.

[1] Hamermesh, Hamermesh and Wattenberg, Phys. Rev. **76**, 611 (1949).
[2] E. P. Meiners, Phys. Rev. **76**, 259 (1949).
[3] A. Wattenberg, Phys. Rev. **71**, 497 (1947).
[4] D. J. Hughes and C. Eggler, Phys. Rev. **72**, 902 (1947).
[5] R. Culp and B. Hamermesh, Phys. Rev. **93**, 1025 (1954).
[6] Dzhelepov, Zhukovsky, Nedovesov, Uchevatkin and Chumin, Nucl. Phys. **2**, 408 (1956).
[7] B. Hamermesh and C. Kimball, Phys. Rev. **90**, 1063 (1953).
[8] A. O. Hanson and J. L. McKibben, Phys. Rev. **72**, 673 (1947).
[9] Barschall, Battat, Bright, Graves, Jorgensen and Manley, Phys. Rev. **72**, 881 (1947).
[10] G. N. Lovchikova, Атомная энергия (Atomic Energy) **2**, 174 (1957).
[11] M. Walt and H. H. Barschall, Phys. Rev. **93**, 1062 (1954).
[12] M. Walt, P/588, Proceedings of the International Conference on the Peaceful Uses of Atomic Energy, Geneva, 1956, Vol. 2, p. 18.
[13] H. Feshbach and V. F. Weisskopf, Phys. Rev. **76**, 1550 (1949).
[14] D. J. Hughes and J. A. Harvey, Neutron Cross Sections, New York, 1955.
[15] H. C. Martin and R. F. Taschek, Phys. Rev. **89**, 1302 (1953).
[16] V. Hummel and B. Hamermesh, Phys. Rev. **82**, 67 (1951).
[17] R. L. Henkel and H. H. Barschall, Phys. Rev. **80**, 145 (1950).
[18] L. E. Beghian and H. H Halban, Nature **163**, 366 (1949).

Translated by M. Hamermesh
114

SOVIET PHYSICS JETP VOLUME 34 (7), NUMBER 3 SEPTEMBER, 1958

ELECTRON LOSS AND CAPTURE IN COLLISIONS BETWEEN FAST HYDROGEN ATOMS AND MOLECULES OF GASES

Ia. M. FOGEL', V. A. ANKUDINOV, D. V. PILIPENKO and N. V. TOPOLIA

Physico-Technical Institute, Academy of Sciences, Ukrainian S.S.R.

Submitted to JETP editor September 30, 1957

J. Exptl. Theoret. Phys. (U.S.S.R.) **34**, 579-592 (March, 1958)

The cross sections for capture and loss of electrons in single collisions of 5-kev to 40-kev hydrogen atoms with He, Ne, A, Kr and Xe atoms and with H_2, N_2 and O_2 molecules are measured by a mass-spectrometric method.

INTRODUCTION

THE passage of fast neutral particles through a substance is accompanied by processes of electron capture and loss as the particles collide with atoms of the substance. The first of these processes can occur only if the neutral particle possesses positive electron affinity. As a result of electron capture and loss a neutral beam which has traversed a layer of matter will upon emerging contain singly charged negative ions and positive ions of various charge multiplicities in addition to neutral particles. A beam of hydrogen atoms, each of which can capture or lose only a single electron, will upon emerging include negative hydrogen ions, hydrogen atoms and protons. For thin layers of matter permitting only single collisions the composition of the emerging beam will be determined by the cross sections for electron capture (σ_{0-1}) and loss (σ_{01}) by hydrogen atoms (σ_{ik} is the cross section for a process whereby a particle with charge ie is transformed into a particle with charge ke). For thicker layers, where multiple collisions begin to play a part, the composition of the emerging beam is determined not only by the two cross sections already mentioned but also by σ_{10}, σ_{-10}, σ_{1-1} and σ_{-11}. Of these six cross sections for a hydrogen beam the cross section σ_{10} for the capture of a single elec-

tron by protons has been most completely investigated.[1-8]

The most important of the cross sections that determine the composition of a hydrogen beam is σ_{10}, since it determines the attenuation of a proton beam in its passage through matter. It is also possible to compare the experimental values of σ_{10} for protons in hydrogen and helium with a number of theoretical calculations.[9-14]

There have been several investigations to determine the cross sections σ_{01} and σ_{-10} for electron loss by hydrogen atoms[3,15,16] and by negative hydrogen ions,[4,5,7,16] respectively. The cross sections σ_{1-1} and σ_{-11} for the capture and loss of two electrons by protons and negative hydrogen ions, respectively, have also been measured.[17,18] There has been no direct measurement of the cross section σ_{0-1} for electron capture by hydrogen atoms. In Ref. 16 this cross section was calculated from measurements of σ_{-10} and $(N^-/N^0)_p$, which is the ratio of the negatively charged component to the neutral component in a beam of equilibrium composition assuming $\sigma_{1-1} = \sigma_{-11} = 0$.

The capture of electrons by neutral atoms is of considerable interest because in this case the electron is bound at the electron affinity level. There may be a definite correlation between the electron affinity of atoms that capture electrons and σ_{0-1}. Such a correlation would make it possible to determine the electron affinity, which cannot be measured easily. It is also of interest to determine to what extent electron capture by neutral particles satisfies Massey's adiabatic criterion. It should be noted that the theoretical calculation of σ_{0-1} is somewhat simplified by the absence of excited levels in many negative ions, as a result of which electrons are captured only at the ground level.

Recent investigations[19-21] have shown that the most promising method of producing a strong negative ion beam is the conversion of positive ions into negative ions by sending them through a layer of matter. The negative ions appear both through single processes $I^+ \rightarrow I^-$ (capture of two electrons by a positive ion in a single collision) and in stages: $I^+ \rightarrow I^0$ and $I^0 \rightarrow I^-$. Hence for the purpose of calculating the negative ion content of the emerging beam σ_{0-1} must be known in addition to other cross sections. It should also be noted that knowledge of the cross sections for all inelastic interactions between hydrogen particles and gas molecules will make it possible to improve the calculations of energy losses by protons of moderate energies ($E \approx E_0$) passing through gases.[22]

The foregoing considerations induced us to develop the apparatus and experimental procedure for the measurement of σ_{0-1}. As the first part of our program of measuring σ_{0-1} for H, C, O, Cl and F atoms, the present article gives measurements of σ_{0-1} for hydrogen atoms colliding with He, Ne, A, Kr and Xe atoms and H_2, N_2 and O_2 molecules. Since our procedure enabled us to measure both σ_{0-1} and also σ_{01} for electron loss by hydrogen atoms, the data for the latter are also given.

APPARATUS AND EXPERIMENTAL PROCEDURE

To obtain a beam of hydrogen atoms we neutralized protons by sending them through a mercury vapor target, which we had previously used[18,19] to produce a beam of negative hydrogen ions. Figure 1 is a diagram of the apparatus used in the present experiments. A hydrogen ion beam came from an ion gun which consisted of a high-frequency ion source 1 of the Reifenschweiler type,[23] a three-electrode lens 2 and an accelerating tube 3. The electrostatic corrector 4 was used to correct the direction of the ion beam. A monoenergetic proton beam which was selected by the magnetic mass monochromator 5 entered the mercury vapor target chamber 6, which was described in Ref. 19. The beam emerging from the mercury vapor contained protons and negative hydrogen ions in addition to hydrogen atoms. A second magnetic ana-

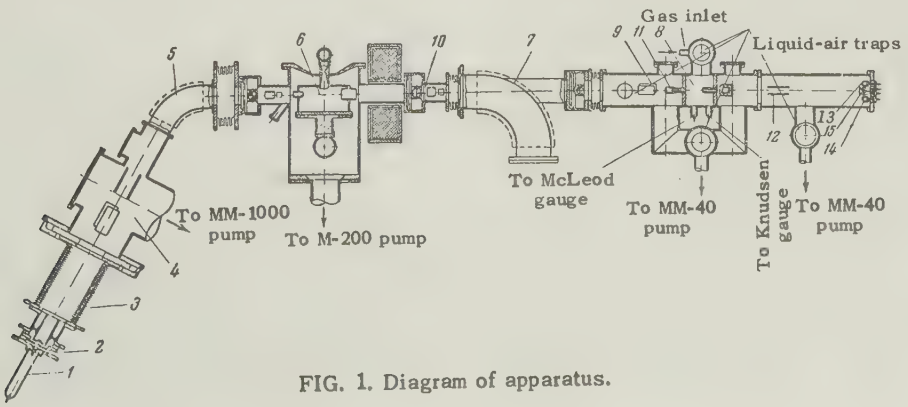

FIG. 1. Diagram of apparatus.

lyzer 7 separated the charged and neutral particles. A small admixture of charged particles in the hydrogen atom beam resulted from collisions of atoms with residual gas molecules along the path from the magnetic analyzer to the entrance diaphragm of the collision chamber 8. These charged particles were removed from the neutral beam by the plane condenser 9 placed before the entrance to the collision chamber. The neutral beam was collimated by two diaphragms 10 and 11. One of these, of 3-mm diameter aperture, was placed directly behind the mercury vapor target; the second, of 2 mm diameter, was aligned axially in front of the entrance tube of the collision chamber. This tube was 5 mm in diameter and 50 mm long. The beam emerged from the collision chamber through a tube of the same length and diameter. The distance from the exit plane of the entrance tube to the entrance plane of the exit tube was 50 mm. The equivalent current of the hydrogen atom beam entering the collision chamber was between 10^{-9} and 4×10^{-8} amperes. The beam intensity was enhanced with increasing energy of the hydrogen atoms because of better focusing of the proton beam at higher energies. To obtain 5-kev H atoms we used the process $H_3^+ \rightarrow H_1$ (a beam of 15-kev H_3^+ ions was directed at the mercury vapor target) since at 5 kev the proton beam was poorly focused on the target by the ion gun.

The beam emerging from the collision chamber was separated into neutral, positive, and negative components by the electric field of the plane condenser 12, which consisted of plates 80 mm long separated by 24 mm. The currents of the charged components were measured by means of Faraday cylinders 13 and 14. The H_1^- current was measured by an EMU-3 vacuum tube electrometer with a sensitivity of 10^{-14} amperes per division; the proton current was measured by a string electrometer with a sensitivity of 10^{-12} amperes per division. Vacuum thermocouple 15 was used to measure the intensity of the neutral component. The thermoelectric power of the thermocouple was measured by an M 107/3 mirror galvanometer with a sensitivity 2×10^{-8} volts per division.

The pressure of the gas which entered the collision chamber was measured by a Knudsen gauge calibrated against a McLeod guage. The residual gas pressure in the chamber was 2×10^{-5} mm Hg.

The cross sections σ_{0-1} and σ_{01} were determined by the mass-spectrometric method which was described in detail in Refs. 17, 18, 24 and 25. This method investigates the dependence of the ratios N^-/N^0 and N^+/N^0 on the gas pressure in the collision chamber. N^-/N^0 and N^+/N^0 are the ratios of the number of negative hydrogen ions and the number of protons, respectively, to the number of hydrogen atoms in the beam passing through gas in the collision chamber. Since different detectors were used to measure the intensities of the charged components and the neutral component of the beam, the vacuum thermocouple used to detect the neutral component had to measure the absolute intensity of the neutral beam.

For absolute measurements of the neutral beam intensity we used a vacuum thermocouple that was essentially similar to the thermocouple described in Ref. 21. The thermocouple was calibrated by means of a proton beam; simultaneous measurement was performed of the proton current strength reaching the receiver of the thermocouple and the thermoelectric power generated in the junction. The calibration factor was determined for all energies at which we were to measure the cross sections of interest.

It was essential for the correctness of the measurements of N^-/N^0 and N^+/N^0 and thus for the correctness of σ_{0-1} and σ_{01} that the entire beam of neutral particles should reach the thermocouple receiver, i.e., the beam axis had to pass through the center of the diaphragm aperture and the diameter of the beam had to be smaller than the diameter of the aperture. Otherwise the measured ratios N^-/N^0 and N^+/N^0 are too large, because the 14 mm diameter of the openings of the Faraday cups was large enough to admit the charged components of the beam entirely.

In order to verify that the entire neutral beam was reaching the thermocouple, a diaphragm with variable aperture was placed in front of the thermocouple for the purpose of determining the beam diameter. This diameter was 4.5 mm for beam energies of 5, 10 and 20 kev while the thermocouple aperture was 6 mm in diameter.

The neutral beam produced by the $H_1 \rightarrow H_1^0$ conversion from 10 to 40 kev was intense enough to cause deflections of not less than 20 to 30 divisions of the galvanometer used to measure the thermoelectric power of the thermocouple. However, at 5-kev beam energy the deflection was still very small, both because of the reduced particle energy and because at 5 kev the ion gun achieved poor focusing of the proton beam on the mercury vapor target.

The conversion $H_3^+ \rightarrow H_1^0$ can be used to produce a beam of 5-kev hydrogen atoms. A beam of 15-kev H_3^+ ions is properly focused on the mercury-vapor target by the ion gun. On the other hand, the conversion coefficient of molecular hydrogen ions transformed into atoms is larger than for protons,

as we established in our investigation of the conversion of positive to negative hydrogen ions in a mercury-vapor target.[19] In earlier work (Ref. 18) we used the $H_3^+ \rightarrow H_1^-$ conversion to produce a beam of low-energy H_1^- ions. But in using $H_3^+ \rightarrow H_1^0$ to produce a beam of hydrogen atoms, a difficulty is encountered which is absent when the dissociation of molecular ions is used to obtain negative ions. This difficulty lies in the fact that as a result of the dissociation of H_3^+ ions with energy E, in addition to H_1^0 atoms with energy $\frac{1}{3}E$, H_2^0 molecules with energy $\frac{2}{3}E$ can be produced (H_3^0 is unstable). Only when the number of H_2^0 molecules in the neutral beam emerging from the mercury-vapor target is small compared with the number of H_1^0 atoms can this beam be used to measure the cross sections of interest. It is thus necessary to have some method of determining the relative content of H_1^0 and H_2^0 in the neutral beam. The neutral beam produced after passage of H_3^+ ions through the mercury-vapor target traversed a collision chamber filled with argon at 2×10^{-4} mm Hg. Because of the loss of electrons by H_1^0 and H_2^0 through collisions with argon atoms the beam emerging from the collision chamber had to contain particles of H_1^+ with the energy $\frac{1}{3}E$ and H_2^+ with the energy $\frac{2}{3}E$, E being the energy of the H_3^+ ions striking the mercury-vapor target. The emerging beam was found to contain positively charged particles with the energies $\frac{1}{3}E$ and $\frac{2}{3}E$. These are evidently the ions H_1^+ and H_2^+ that result from collisions of H_1^0 and H_2^0 with argon atoms, with the loss of electrons. This provides confirmation of the hypothesis that the neutral beam produced by passing H_3^+ ions through a mercury vapor target consists of H_1^0 and H_2^0.

It is evident that the relative numbers of H_1^0 and H_2^0 in the neutral beam must depend on the thickness of the mercury-vapor target. Specifically, we cannot exclude the possibility of complete dissociation of the molecules into atoms in a target of sufficient thickness. In order to determine whether this occurs we investigated the relation between the H_1^+ and H_2^+ currents in the beam after the neutral beam had traversed the argon-filled chamber, and the thickness of the mercury vapor target. The target thickness was varied by changing the boiler temperature (see Ref. 26). Figure 2 shows $I_{H_1^+}$ and $I_{H_2^+}$ as functions of the boiler temperature. It can be seen that $I_{H_1^+}$ and $I_{H_2^+}$ pass through a maximum and begin to diminish with further increase of the boiler temperature; this results from scattering in the mercury vapor jet. However, $I_{H_2^+}$ diminishes much more rapidly than $I_{H_1^+}$; this apparently results from increased dissociation of

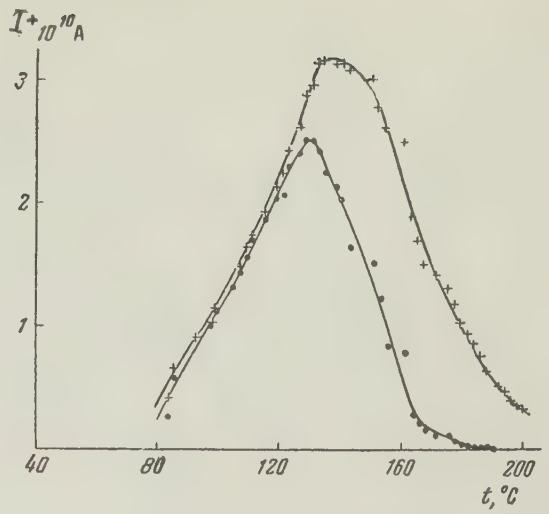

FIG. 2. The Currents $I_{H_1^+}$ and I_{H^+} as functions of the boiler temperature: + – for H_1^+; • – for $^2H_2^+$.

molecules to form atoms as the target thickness is increased. At $t_{boiler} \approx 190°C$ we have $I_{H_1^+} = 6.3 \times 10^{-11}$ amp while $I_{H_2^+} < 2 \times 10^{-13}$ amp. It thus follows that when the target thickness corresponds to $t_{boiler} = 190°C$ the neutral beam that results from passage of H_3^+ ions through the target is practically completely atomic in character. This is also confirmed by the fact that the cross sections σ_{0-1} and σ_{01} as measured with a neutral beam from 10-kev protons and with a neutral beam from 30-kev H_3^+ ions were identical within the limits of experimental error. The measurements of σ_{0-1} and σ_{01} with 5-kev neutral beams obtained from $H_3^+ \rightarrow H_1^0$ were subsequently performed at a boiler temperature of 200°C.

There are inherent systematic errors in the mass-spectrometric method which we used to measure σ_{0-1} and σ_{01}. These result from: (a) the influence of the pressure and composition of the residual gas in the apparatus on the magnitudes of the measured cross sections;[25] (b) unequal scattering of protons, atoms and negative hydrogen ions in the collision chamber; (c) unequal attenuation of the beams of protons, atoms and ions on their path from the collision chamber to the vacuum thermocouple and Faraday cups of the analyzer.

By investigating the dependence of σ_{0-1} and σ_{01} on $(N^-/N^0)_f$ and $(N^+/N^0)_f$* we have shown that the error due to residual gas in the path of the beam is small and within the limits of experimental error. In order to determine the influence of unequal scattering in the collision chamber we measured σ_{0-1} and σ_{01} with an aperture of 2 mm

*$(N^-/N^0)_f$ and $(N^+/N^0)_f$ are the values of N^-/N^0 and N^+/N^0 when no gas is admitted into the collision chamber.

diameter behind the collision-chamber outlet and axially aligned with the exit tube, as well as in the absence of this aperture.* This aperture reduced to one sixth the solid angle of emission of the particles leaving the collision chamber. Measurements were performed at beam energies of 15 and 30 kev in He and Kr. Identical values within the limits of experimental error were found for σ_{0-1} and σ_{01} with and without the use of the diaphragm aperture behind the exit tube. Thus the scattering of particles in the collision chamber does not seriously affect the measurements. The correction for unequal attenuation of the separate beams in the analyzer does not exceed a few tenths of one per cent and is unimportant. Random errors amounted to $\pm 20\%$ for σ_{0-1} and $\pm 15\%$ for σ_{01}.

The energy of the hydrogen atoms was determined from the sum of the potential differences across the ion source and accelerating tube, which were measured by electrostatic voltmeters calibrated against a resistance voltmeter. As we have shown in Ref. 18, the energy loss of the protons in traversing the mercury vapor target is very small. There was an error of $\pm 3\%$ in the measurement of the hydrogen atom energy.

RESULTS AND DISCUSSION

We measured the cross sections for electron capture and loss in collisions of hydrogen atoms at 5 to 40 kev with He, Ne, A, Kr and Xe atoms and H_2, N_2 and O_2 molecules. The collision chamber was filled with hydrogen passed through a palladium barrier, spectrally pure helium, neon, krypton and xenon, oxygen with 0.9% impurity, argon with 0.3% impurity and nitrogen with 0.03% impurity.

Figures 3 and 4 show the cross sections σ_{0-1} and σ_{01} as functions of the hydrogen atom energy for atomic and molecular gases. The cross section at each energy was obtained by averaging two measurements, and was computed per gas particle, which in the case of the molecular gases means per gas molecule.

Figures 3 and 4 show that in the investigated energy range σ_{0-1} for H atoms in He, Ne, H_2, N_2 and O_2 passes through a maximum, which with He occurs at 20 kev and with Ne_2, H_2, N_2 and O_2 at ~ 10 kev. In A, Kr and Xe σ_{0-1} decreases monotonically with rising energy. σ_{0-1} varies

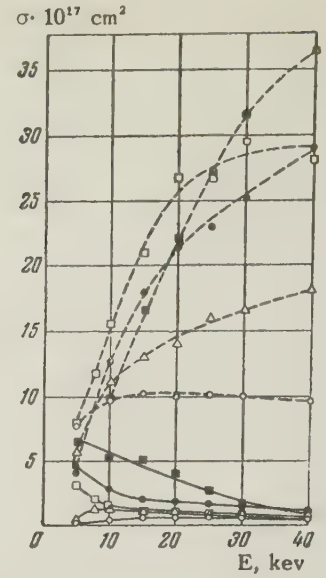

FIG. 3. σ_{0-1} (solid curves); σ_{01} (dashed curves). o – He, Δ – Ne, □ – A, ● – Kr, ■ – Xe.

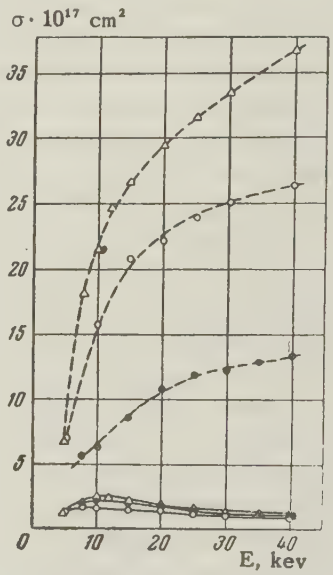

FIG. 4. σ_{0-1} (solid curves); σ_{01} (dashed curves). ● – H_2, o – O_2, Δ – N_2.

from 2.4×10^{-18} cm^2 (in He at 5 kev) to 6.6×10^{-17} cm^2 (in Xe at 5 kev). For the molecular gases σ_{0-1}, within the limits of error, does not depend on the kind of gas. For atomic gases σ_{0-1} is observed to depend on the kind of gas, especially at low energies. σ_{0-1} increases with the atomic number of the inert gas.

For all gases except He σ_{01} decreases with reduced energy of the H atoms. The maximum of σ_{01} for He occurs at 15 kev. σ_{01} varies from 4.2×10^{-17} cm^2 (in Kr at 5 kev) to 3.7×10^{-16} cm^2 (in Xe and N_2 at 40 kev). σ_{01} is about one order of magnitude larger than σ_{0-1}.

It is of interest to compare our results with

*It is not desirable to have a diaphragm directly at the exit aperture of the exit tube since this would distort the pressure distribution in the tube and change the effective length of the collision chamber.

those obtained by other investigators. As mentioned in the introduction, there were no direct measurements of σ_{0-1}. For H_2, N_2, O_2, He, Ne and A it is possible to make a comparison with the values for σ_{0-1} calculated by Stier and Barnett[16] from measurements of σ_{-10} and $(N^-/N^0)_p$ assuming small cross sections for two-electron transfers ($\sigma_{1-1} = \sigma_{-11} = 0$). For H_2 σ_{0-1} was calculated by Whittier[5] using his own measurements of $(N^-/N^+)_p$ and σ_{-10} and Bartels' measurements of $(N^+/N^-)_p$.

Our measurements of σ_{01} for H_2, N_2, O_2, He, Ne and A can be compared with those of Stier and Barnett.[16] Montague[15] also measured σ_{01} in H_2, but his data cover the energy range 45 — 329 kev, which is outside our energy range.* σ_{01} was calculated theoretically for atomic hydrogen by Bates and Griffing[28] and for helium by Bates and Williamson.[29]

Figure 5 shows σ_{0-1} and σ_{01} as functions of energy for H_2, N_2, O_2, He, Ne and A; the values obtained in the present investigation are compared with those obtained by other writers.† The figures show that our values for σ_{0-1} are in good agreement with the calculations of Stier and Barnett, but that for H_2 they differ somewhat from those computed by Whittier. The fact that these investigators calculated σ_{0-1} without taking account of two-electron transfers could not have introduced any considerable error; our measurements[17,18] have shown that the cross sections for such transfers are small compared with those for one-electron transfers.

Figure 5 shows that our values for σ_{01} are consistently lower than those measured by Stier and Barnett, although the curves have similar shapes. The beginning of Montague's curve (Fig. 5) is more consistent with our curve than with that of Stier and Barnett although the American authors all used the same method of neutral beam attenuation while our measurements were obtained by a mass-spectrometric method. When the values of σ_{0-1} and σ_{01} given by different writers are compared it must be kept in mind that the discrepancies may be caused by an admixture of excited metastable atoms in the neutral beam that enters the collision chamber. The percentage of metastable atoms in the neutral beam can differ in the various

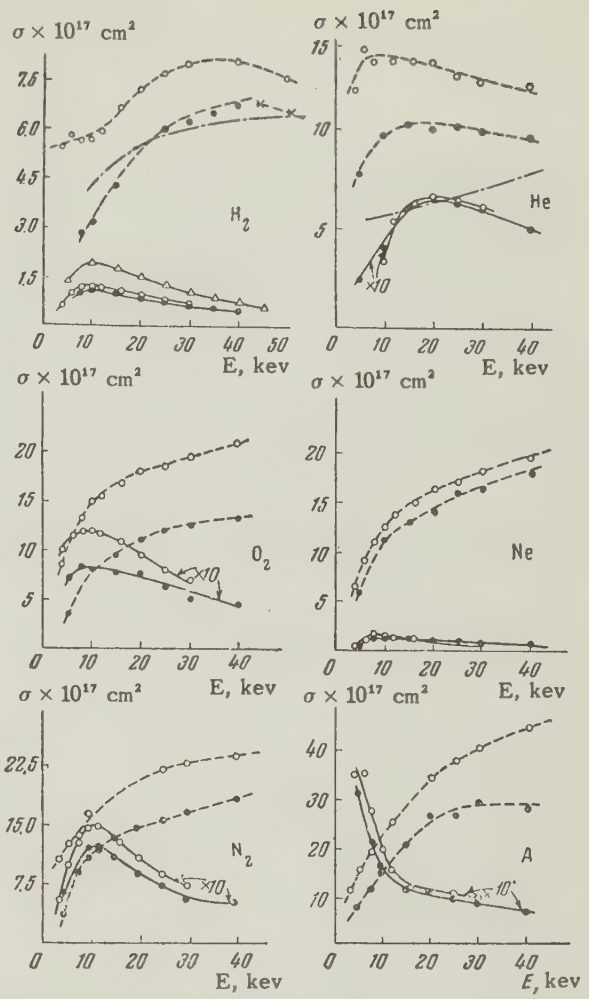

FIG. 5. σ_{0-1} (solid curves); σ_{01} (dashed curves); σ_{01} (dots and dashes) from Refs. 28 and 29. o — from Ref. 16; × — from Ref. 15; Δ — from Ref. 5; • — our present data.

experiments depending on the experimental conditions (different targets for neutralizing the original charged beam, different distances between the target and collision chamber) and thus account for the discrepancies between the results.

The foregoing considerations provide no explanation of the discrepancy between the value of σ_{01} obtained in the present work and that of Stier and Barnett.[16] Although the hydrogen atom possesses a metastable $2^2S_{1/2}$ state with a lifetime of the order of 0.1 sec, in both experiments the neutral beam before entering the collision chamber passed through the electric field of the condenser which removed charged particles. This field reduced the lifetime of the excited atoms to 2×10^{-8} sec, so that the neutral beam entered the collision chamber in an unexcited state.

A comparison of the experimental and theoretically computed values of σ_{01} (Fig. 5) shows that in the 5- to 40-kev energy range for hydrogen the

*Montague actually measured the sum $\sigma_{01} + \sigma_{0-1}$, but since $\sigma_{01} \gg \sigma_{0-1}$ this sum differs very little from σ_{01}.

†Since other authors give the cross sections per gas atom our values for σ_{0-1} and σ_{01} in the case of the molecular gases which are given in Fig. 5 were obtained by halving the measurements.

theoretical values are in good agreement with the experimental results obtained in the present work and by Montague. For helium there is considerable difference between the theoretical and experimental curves with regard to both magnitude and form. The experimental curves pass through a maximum at 10 — 12 kev, whereas the theoretical curve rises monotonically in this range.*

In the comparison of theoretical with experimental results the following circumstances must be kept in mind. σ_{01} is computed theoretically for atomic hydrogen whereas the experiments are performed with molecular hydrogen. In the comparison it is therefore assumed that a molecule of hydrogen is equivalent to two atoms. In Refs. 28 and 29 σ_{01} was calculated in a Born approximation; the values thus obtained should generally be valid for $E \gg E_0$ (E_0 = 25 kev, which is the energy at which the velocity of the hydrogen atom equals the orbital velocity of the electron). Indeed, for E > 100 kev we find good agreement between theory and the experimental results of Stier and Barnett in the case of helium. For hydrogen the agreement is not so good but is still satisfactory (see Ref. 29). Thus the disagreement between theory and experiment for helium in the vicinity of $E \approx E_0$ is not surprising, as the Born approximation is not generally applicable to this energy range. On the other hand, the good agreement between theory and experiment for hydrogen is evidence either that the experimental results for σ_{01} are inaccurate or that the Born approximation in this special instance is valid up to $E \approx E_0$. We know that the calculation of σ_{10} by the Born approximation for protons in hydrogen is in very good agreement with experiment up to energies of the order of E_0.[14] Jackson[30] has shown that this is not accidental but is associated with the fact that when the total interaction Hamiltonian is used for Z = Z′ = 1 (where Z and Z′ are the atomic numbers of the incident and struck particle, respectively) the correction to the matrix element in the second Born approximation is zero. There may be a good theoretical reason for the applicability of the Born approximation to σ_{01} near $E \sim E_0$ for hydrogen atoms in hydrogen.

As mentioned in the Introduction, the composition of a hydrogen beam that has passed through matter is determined by the six cross sections σ_{10}, σ_{01}, σ_{0-1}, σ_{-10}, σ_{1-1}, σ_{-11}. For a beam in equilibrium we have[17]

$$\left(\frac{N^-}{N^+}\right)_p = \frac{\sigma_{10}\sigma_{0-1} + \sigma_{1-1}\sigma_{01} + \sigma_{1-1}\sigma_{0-1}}{\sigma_{01}\sigma_{-10} + \sigma_{-11}\sigma_{01} + \sigma_{-11}\sigma_{0-1}}. \quad (1)$$

For a hydrogen target there have been determined in our laboratory σ_{10},[6] σ_{1-1},[17] σ_{-11},[18] σ_{01} and σ_{0-1} (the present work), and also $(N^-/N^+)_p$.* Substituting these results in Eq. (1), we can derive σ_{-10} and compare this result with the measurements in Refs. 5 and 16. Figure 6 shows good agreement between our calculation for σ_{-10} and the results in Ref. 5 but somewhat greater divergence from the results in Ref. 16. Considering the cumulative error in the calculation of σ_{-10} and the appreciable error in the measurements of σ_{-10} in Ref. 16, the discrepancy is within the limits of experimental error.

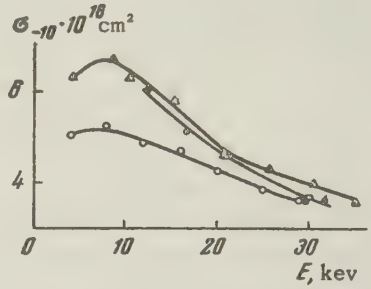

FIG. 6. ▲— data from Ref. 5; ○ — data from Ref. 16; ● — computed from Eq. (2); □ — computed from Eq. (5).

By using the solutions of the differential equations that determine the composition of a hydrogen beam [see Eq. (3) of Ref. 17], it can be shown that at very low gas pressures in the collision chamber the following relation exists between N^+/N^- and pressure:

$$N^+/N^- = \varkappa p + \Omega p^2, \quad (2)$$

where

$$\varkappa = \sigma_{-11} L / kT \quad (3)$$

$$\Omega = {}^1/_2 [\sigma_{-10}\sigma_{01} + \sigma_{-11}(\sigma_{-10} + \sigma_{-11} - \sigma_{10} - \sigma_{1-1})] (L/kT)^2. \quad (4)$$

Experiment shows that the beginning of the curve $N^+/N^- = f(p)$ always satisfies Eq. (2). By applying the method of least squares to the experimental results, we can determine Ω and then σ_{-10} from Eq. (4). We have plotted the curve $N^+/N^- = f(p)$ for H_2 and H_1^- ions of 30-kev energy† and used the foregoing method to compute σ_{-10}. This value

*The theoretical curve reaches its maximum at 60 kev (Ref. 29).

*The results given in Ref. 17 for $(N^-/N^+)_p$ in H_2 have been checked with our apparatus. Our results were 20% higher than those of Ref. 17 and were in good agreement with Whittier[5] and Stier and Barnett.[16] These results have been used for the computation of σ_{-10} through Eq. (2).

†For this purpose we used the apparatus described in Ref. 18.

of σ_{-10} in Fig. 6 is in good agreement with both the value calculated for an equilibrium beam and with experimental measurements.

The pressure dependence of N^-/N^+ over the entire pressure range as far as the equilibrium point is given [see Eq. (3) of Ref. 17] by the formula

$$\frac{N^-}{N^+} = \frac{a_0 + a_1 \exp\{-(r_1 L / kT)\, p\} + a_2 \exp\{-(r_2 L / kT)\, p\}}{b_0 + b_1 \exp\{-(r_1 L / kT)\, p\} + b_2 \exp\{-(r_2 L / kT)\, p\}}, \quad (5)$$

where r_1, r_2, a_0, a_1 etc. are functions of the six cross sections σ_{ik}. Substituting into (5) the values of these cross sections for hydrogen at 32 kev, we can calculate N^-/N^+ at various gas pressures in the collision chamber and compare the results with our experimental curve $N^-/N^+ = f(p)$. Figure 7 shows that the experimental curve and the curve plotted according to Eq. (5) are in good agreement.

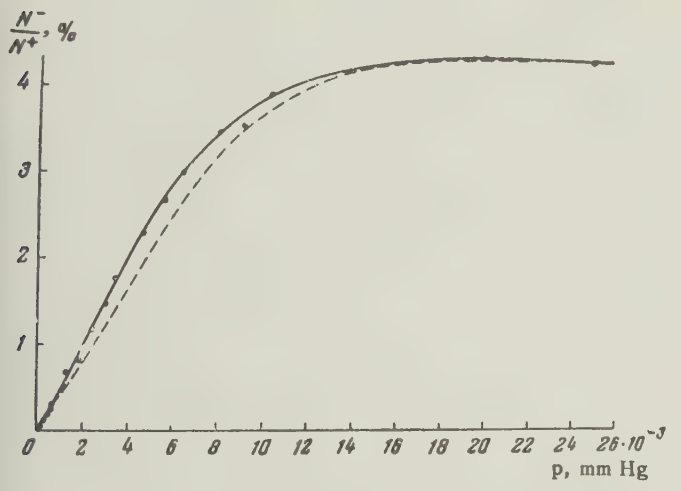

FIG. 7. $N^-/N^+ = f(p)$: dashed curve – calculated from Eq. (6); solid curve – experimental.

The comparisons which have been made show that our measurements of σ_{10}, σ_{0-1}, σ_{-11}, σ_{1-1}, σ_{01} and (N^-/N^+) do not contain large errors and can therefore be used to calculate the composition of a hydrogen beam in a hydrogen target. For calculating the composition of the beam in inert gases and in N_2 and O_2 together with our measured results for σ_{01}, σ_{0-1}, σ_{-11} and σ_{1-1} the values of σ_{10} and σ_{-10} in Refs. 7 and 16 can be used.

Our knowledge of the six cross sections for charge transfers in hydrogen particles colliding with gas particles permits us to compare these cross sections among themselves. The three electron-capture cross sections and the three electron-loss cross sections obey the following inequalities* in the investigated energy range:

$$\sigma_{1-1} < \sigma_{0-1} < \sigma_{10}, \quad (6a)$$

$$\sigma_{-11} < \sigma_{01} < \sigma_{-10}. \quad (6b)$$

Conclusions derived from these inequalities are in full agreement with expectations. It follows from (6) that: (1) the cross sections for two-electron processes are smaller than the cross sections for one-electron processes, (2) the cross section for single-electron capture increases with the binding energy of the electron in the resulting particle ($\sigma_{0-1} < \sigma_{10}$), and (3) the cross section for the loss of a single electron decreases with increase of the electron binding energy in the particle which loses the electron ($\sigma_{01} < \sigma_{-10}$).

From the numerical values of the six cross sections which determine the composition of the beam we see that σ_{10} is about two orders greater than σ_{1-1} and σ_{0-1}, and that the latter two cross sections do not differ very much from each other (σ_{1-1} amounts to from 30 to 80% of σ_{0-1}). σ_{-10} is about one order of magnitude larger than σ_{-11} and σ_{01}, which also do not differ very much (σ_{-11} is from 30 to 70% of σ_{01}). The ratios of the capture and loss cross sections in the investigated energy interval are characterized by the following numerical relationships: $\sigma_{1-1}/\sigma_{-11}$ varies between 1 and 30%; $\sigma_{0-1}/\sigma_{-10}$ is 0.5 – 2%; σ_{10}/σ_{01} for all gases except helium decreases from a magnitude on the order of 10 at the beginning of the range to the order of unity at the end of the range. For helium this ratio varies very little in the energy range under investigation and is close to unity. From the dependence of the ratios σ_{ik}/σ_{ki} on the parameter γ ($\gamma = v_i/v$, where v_i is the orbital velocity of the electron in a moving particle and v is the velocity of the particle) it can be seen that for $\gamma = 1$ $\sigma_{1-1}/\sigma_{-11}$ and $\sigma_{0-1}/\sigma_{-10}$ are very far from unity whereas σ_{10}/σ_{01} differs very little from unity for $\gamma = 1$. Therefore the hypothesis that the electron capture and loss cross sections are equal when the particle velocity equals the orbital velocity of the electron is approximately valid only for $H_1^0 \rightleftarrows H_1^+$, and is not valid for $H_1^+ \rightleftarrows H_1^-$ and $H_1^0 \rightleftarrows H_1^-$.

The maxima of the curves $\sigma_{0-1} = f(E)$ in He, Ne, H_2, N_2 and O_2 permit us to estimate the impact parameter for the corresponding processes on the basis of Massey's adiabatic criterion [see Eq. (2) of Ref. 25]. The resonance defect for electron capture by fast atoms $A + B = A^- + B^+$ can be put into the form

$$\Delta E = S_A - V_B', \quad (7)$$

where S_A is the electron affinity of particle A

*There is a single exception for σ_{-11} and σ_{01} at 5 kev in O_2 and N_2, where $\sigma_{-11} > \sigma_{01}$.

and V_B^I is the first ionization potential of particle B. In the case of molecular gases electron capture by A can occur in two ways: $A + B_2 = A^- + B_2^+$ and $A + B_2 = A^- + B^+ + B$, i.e., in the first instance a slow singly charged molecular ion is formed, while in the second instance this ion is dissociated. In the latter instance the resonance defect is calculated from the formula

$$\Delta E = S_A - (V_{B_2^+} + E_{\text{dis}}), \qquad (8)$$

where E_{dis} is the dissociation energy of B_2^+.

The table contains the values of the impact parameter which were computed by means of Massey's adiabatic criterion. The values marked with asterisks refer to cases in which the molecular ion is dissociated. The impact parameter varies very little for different target particles, especially when it is assumed that electron capture in molecular gases is accompanied by the dissociation of a slow molecular ion; the mean impact parameter in this case is 3 A. The same condition applies to the capture of a single electron[4,7] or two electrons[17,25] by singly charged positive ions; for these processes the mean impact parameter is 8 A and 1.5 A, respectively. Thus for the capture of a single electron by an atom, the particles must approach closer than for the capture of a single electron by a positive ion. The particles must approach closest for the capture of two electrons by a positive ion.

Gas	Resonance defect ΔE (ev)	Maximum		Impact parameter (A)
		E, (kev)	V, cm/sec	
He	−23.7	20	$2 \cdot 10^8$	3.4
Ne	−20.7	10	$1.4 \cdot 10^8$	2.8
H_2	−14.7	10.2	$1.4 \cdot 10^8$	4.0
	−17.3*			3.4*
N_2	−15.1	11	$1.45 \cdot 10^8$	4.0
	−23.8*			2.5*
O_2	−11.8	8	$1.24 \cdot 10^8$	4.4
	−18.2*			2.8*

The dependence of σ_{0-1} on the electron binding energy in a target atom can be expressed most directly in terms of the resonance defect $|\Delta E|$ (see Eq. (7)). Figure 8 shows the dependence of σ_{0-1} on $|\Delta E|$ for H atoms with an energy of 5 kev (curve 1) and 30 kev (curve 2). These points for $H_1^0 \rightarrow H_1^-$ in inert gases can be connected by smooth curves representing the monotonic reduction of σ_{0-1} as the resonance defect increases. The values for oxygen fit both curves well if it is assumed that electron capture from an oxygen molecule is accompanied by dissociation of the molecular oxygen ion. A point for nitrogen lies on curve 2 if, on the contrary, it is assumed that the molecular nitrogen ion does not dissociate. The same applies to hydrogen. Values for nitrogen do not lie on curve 1 whether the molecular ion is dissociated or not. There is still insufficient experimental information available for any conclusions to be drawn from the arrangement of values for molecular gases on the curve for $\sigma_{0-1} = f(|\Delta E|)$ as to which form of the process $H_1^0 \rightarrow H_1^-$ occurs in a molecular gas.

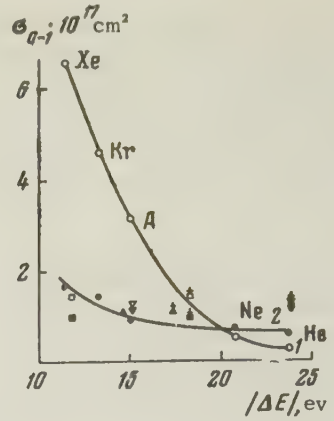

FIG. 8. Resonance defect according to Eq. (7): □, ■ – for O_2; ▲– for H_2; ▽, ▼– for N_2. The same symbols with a plus sign above give the resonance defect according to Eq. (8). The solid symbols refer to 30 kev.

The observed reduction of σ_{0-1} as the absolute value of the resonance defect increases confirms the conclusion reached regarding the reduction of this cross section as the electron binding energy in a target atom is increased. Figure 8 shows that this relationship is much more pronounced at lower velocities of the hydrogen atom.

A consideration of the curves for $\sigma_{01} = f(E)$ shows that it is not correct to postulate the same impact parameter for the process $H_1^0 \rightarrow H_1^+$ in all of the gases investigated here, because a resonance defect equal in absolute magnitude to the ionization potential of the hydrogen atom would be the same for all gases, so that the maximum cross section would be observed at the same energy for the various gases. Figures 3 and 4 show clearly that this is not the case. It is possible that the adiabatic postulate cannot be applied to electron loss by fast atoms as it can for electron loss by negative ions. An analysis of the experimental cross sections for electron capture and loss by hydrogen particles suggests that Massey's adiabatic postulate is in good agreement with electron capture processes but cannot be applied to electron loss. Any decision as to the applicability of the adiabatic postulate to electron capture and loss by fast atoms will have a firmer basis after measurements of σ_{0-1}

and σ_{01} at low energies where the slow collision condition $a|\Delta E|/hv \gg 1$ will be fulfilled. However, for measurements in this energy range the sensitivity of our experimental procedure will have to be considerably increased.

We wish to thank N. I. Bliznetsov and A. G. Shevchenko for preparing the vacuum thermocouples which were used in the present work. The authors also consider it a pleasant duty to thank Prof. A. K. Val' ter for his continued interest.

[1] J. P. Keene, Phil. Mag. 40, 369 (1949).
[2] F. L. Ribe, Phys. Rev. 83, 1217 (1951).
[3] H. Kanner, Phys. Rev. 84, 1211 (1951).
[4] J. B. Hasted, Proc. Roy. Soc. (London) A212, 235 (1952).
[5] A. C. Whittier, Can. J. Phys. 32, 275 (1954).
[6] Fogel', Krupnik, and Safronov, J. Exptl. Theoret. Phys. (U.S.S.R.) 28, 589 (1955), Soviet Phys. JETP 1, 415 (1955).
[7] J. B. H. Stedeford and J. B. Hasted, Proc. Roy. Soc. (London) A227, 466 (1955).
[8] de Heer, Huizenga, and Kistemaker, Physica 23, 181 (1957).
[9] D. R. Bates and A. Dalgarno, Proc. Phys. Soc. (London) A65, 919 (1952); A66, 972 (1953).
[10] A. Dalgarno and H. N. Yaday, Proc. Phys. Soc. (London) A66, 173 (1953).
[11] J. D. Jackson and H. Schiff, Phys. Rev. 89, 359 (1953).
[12] D. R. Bates and G. W. Griffing, Proc. Phys. Soc. (London) A66, 961 (1953).
[13] Bransden, Dalgarno, and King, Proc. Roy. Soc. (London) A67, 1075 (1954).
[14] T. Pradhan, Phys. Rev. 105, 1250 (1957).
[15] J. H. Montague, Phys. Rev. 81, 1026 (1951).
[16] P. M. Stier and C. F. Barnett, Phys. Rev. 103, 896 (1956).
[17] Ia. M. Fogel' and R. V. Mitin, J. Exptl. Theoret. Phys. (U.S.S.R.) 30, 450 (1956), Soviet Phys. JETP 3, 334 (1956).
[18] Fogel', Ankudinov, and Slabospitskii, J. Exptl. Theoret. Phys. (U.S.S.R.) 32, 453 (1957), Soviet Phys. 5, 382 (1957).
[19] Fogel', Krupnik, and Ankudinov, J. Tech. Phys. (U.S.S.R.) 26, 1208 (1956), Soviet Phys. JTP 1, 1181 (1956).
[20] J. A. Weinmann and J. R. Cameron, Rev. Sci. Instr. 27, 288 (1956).
[21] Fogel', Krupnik, Koval', and Slabospitskii, J. Tech. Phys. (U.S.S.R.) 27, 988 (1957), Soviet Phys. JTP 2, 902 (1957).
[22] A. Dalgarno and G. W. Griffing, Proc. Roy. Soc. (London) A232, 423 (1955).
[23] O. Reifenschweiler, Ann. Phys. 14, 33 (1954).
[24] Ia. M. Fogel' and L. I. Krupnik, J. Exptl. Theoret. Phys. (U.S.S.R.) 29, 209 (1955), Soviet Phys. JETP 2, 252 (1956).
[25] Fogel', Mitin, and Koval', J. Exptl. Theoret. Phys. (U.S.S.R.) 31, 397 (1956), Soviet Phys. JETP 4, 359 (1957).
[26] Fogel, Lisochkin, and Stepanova, J. Tech. Phys. (U.S.S.R.) 25, 1944 (1955).
[27] H. Bartels, Ann. Phys. 13, 373 (1932).
[28] D. R. Bates and G. W. Griffing, Proc. Phys. Soc. (London) A68, 90 (1955).
[29] D. R. Bates and A. Williams, Proc. Phys. Soc. (London) A70, 306 (1957).
[30] L. D. Jackson, Proc. Phys. Soc. (London) A70, 26, (1957).

Translated by I. Emin
115

PHOTODISINTEGRATION OF Be^9 AND C^{12} BY GAMMA-BREMSSTRAHLUNG WITH MAXIMUM ENERGY UP TO 44 Mev

I. V. CHUVILO and V. G. SHEVCHENKO

P. N. Lebedev Physics Institute, Academy of Sciences, U. S. S. R.

Submitted to JETP editor October 5, 1957

J. Exptl. Theoret. Phys. (U.S.S.R.) 34, 593-598 (March, 1958)

We present results of an investigation of the angular and energy distributions of protons from the photodisintegration of Be^9 and C^{12}. Analysis of the results leads to the conclusion that in the region of the giant resonance the interaction of γ quanta with these nuclei is satisfactorily explained by the resonance theory of the compound nucleus. For energies above the giant resonance, the interaction of the γ quanta is predominantly with individual substructures within the nuclei.

In the present work we have studied the angular and energy distributions of the protons formed in the photodisintegration of Be^9 by γ bremsstrahlung with a maximum energy of $E_{\gamma max} = 44$ Mev and in the photodisintegration of C^{12} by bremsstrahlung with maximum energies of 30 and 44 Mev.

The results were obtained using the method described in a previous paper.[1] The targets were a graphite plate of thickness 17 mg/cm^2 and a beryllium plate 15 mg/cm^2 in thickness. Impurities amounted to less than 0.3%. The protons were recorded in NIKFI Ia-2 emulsions of thickness 400 and 500 μ.

In the irradiation of C^{12} by γ rays with $E_{\gamma max} = 30$ Mev, only the protons from the $C^{12}(\gamma, p)B^{11}$ reaction were investigated. Other photoreactions on carbon in which protons are emitted have energy thresholds above 26 Mev, and the protons produced in these reactions (which have an energy less than 3 Mev) were not counted in our experiment. The contribution from the $C^{12}(\gamma,d)B^{10}$ reaction is very small at both energies since this reaction is forbidden by the isotropic spin selection rule.

We shall first consider the results obtained for beryllium. The angular distributions of protons from photodisintegration of Be^9 are shown in Fig. 1. An analysis of the distributions of the various energy groups of photoprotons shows that there is no way of explaining all of the results on the basis of a single photoreaction mechanism in this range of photon energies. The angular distribution of the 4 — 6 Mev proton group, as calculated using the model of direct interaction of γ quanta with individual nucleons in the nucleus,[2] contradicts the experimental observations.

We therefore made calculations of angular distributions of photoprotons for transitions of various types on the basis of the compound nucleus resonance model.[3] The results of the computations for transitions to the 2^+ ground state and 3^+ first excited state of the Li^8 final nucleus are given in the table.

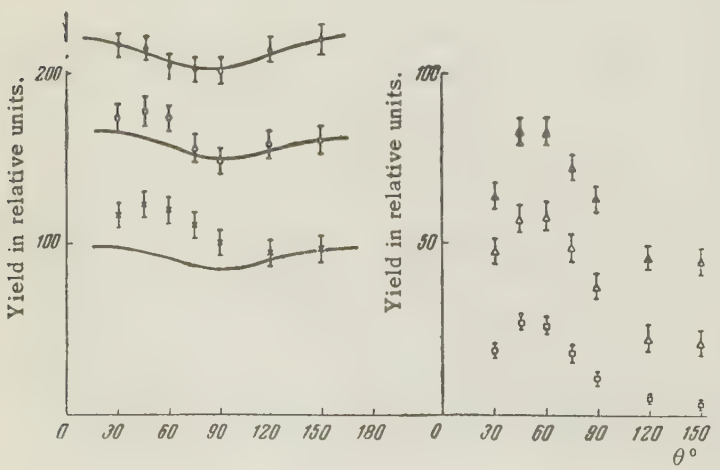

Fig. 1. Angular distributions of proton groups from photodisintegration of Be^9 by γ quanta with $E_{\gamma max} = 44$ Mev. The solid curves show the angular distributions calculated from the intermediate nucleus model, with transition to the ground 2^+ state of Li^8. ● – E_p = 4–5 Mev, ○ – E_p = 5–6 Mev, × – E_p = 6–9 Mev, ▲ – E_p = 9–12 Mev, △ – E_p = 12–15 Mev, □ – $E_p \geq 15$ Mev.

$l=0$			$l=2$		
s	I	Angular Distribution	s	I	Angular Distribution
		Li^8 left in 2^+ ground state			
3/2	5/2	const	3/2	5/2	$4+\sin^2\theta$
3/2	3/2	const	3/2	3/2	const
3/2	1/2	const	3/2	1/2	const
5/2	5/2	const	5/2	5/2	$13+3\cos^2\theta$
5/2	3/2	const	5/2	3/2	$2+\cos^2\theta$
5/2	1/2	const	5/2	1/2	const
		Li^8 left in 3^+ first excited state			
5/2	5/2	const	5/2	5/2	$13+3\cos^2\theta$
5/2	3/2	const	5/2	3/2	$2+\cos^2\theta$
5/2	1/2	const	5/2	1/2	const
7/2	5/2	const	7/2	5/2	$1.7+\cos^2\theta$
7/2	3/2	const	7/2	3/2	$6+7\cos^2\theta$
7/2	1/2	const	7/2	1/2	const

l is the relative orbital angular momentum in the final state, s is the total spin of the reaction products, I is the total angular momentum of the photon-target system.

It is not possible at present to evaluate the statistical weights of transitions with different s and I. Figure 1 shows the comparison of the computed angular distributions for photoproton groups with energies 4 — 5, 5 — 6 and 6 — 9 Mev with the experimental data, on the assumption that the statistical weights of all the transitions to the 2^+ state are the same. If these protons are produced by γ quanta absorbed by the nucleus in the region of the dipole resonance, then the assumption that the most probable transition is that to the ground state is valid. However, even if for some reason the intensity of transitions to the first excited state is comparable to the intensity of the ground state transitions, the table shows that the shape of the computed angular distribution should hardly change.

The angular distributions of the higher energy proton groups differ from those expected on the resonance theory of the compound nucleus. These deviations begin to appear even for the 5 — 6 Mev proton group, and increase with increasing proton energy. Starting with the 6 — 9 Mev proton group and higher, the experimental angular distributions have their maximum at an angle of 50°, i.e., the angular distributions are highly asymmetric around 90°, with preferential emission of the protons forward, in the direction of motion of the γ quanta. The isotropic part of the distribution decreases with increasing energy of the photoprotons, and is only one-seventh of the anisotropic part for protons with energies greater than 15 Mev. At the same time, as we see from Fig. 2, the angular distribution of the protons from Be^9 which have energies above 12 Mev is in good agreement with the angular distribution of protons from photodisintegration of the deuteron by 42 Mev γ quanta.[4] This shows that already at excitation energies of the order of 40 Mev the production of photoprotons from Be^9 occurs via a two-nucleon mechanism. Apparently the fixed position of the maximum, which is shifted markedly toward smaller angles (45° — 55°), in the angular distributions of other proton groups, shows the presence of the two-nucleon mechanism for absorption of γ quanta by Be^9 down to proton energies of 6 — 9 Mev. The complete energy spectrum of the Be^9 photoprotons is given in Fig. 3. The analysis of its high energy part is also in favor of the quasideuteron model. In the spectrum of the photoprotons with energies above 12 Mev, which is shown in Fig. 4, there is a characteristic kink whose position is in qualitative agreement with the computed kink in the spectrum of protons from photodisintegration of the deuteron. The quantitative relation between the cross sections per effective quantum for the 12 — 15 Mev proton group from the Be^9 photodisintegration and the corresponding proton group from deuteron photodisintegration is

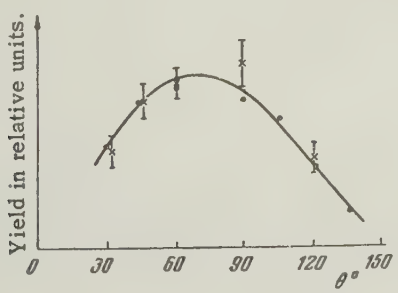

Fig. 2. Comparison of angular distribution of photoprotons from Be^9, assuming a two-nucleon interaction mechanism, with the angular distribution of the proton group of the same energy from photodisintegration of the deuteron. The data for the deuteron are shown by the solid curve. $E_{\gamma max} = 44$ Mev, $h\nu = 42$ Mev.

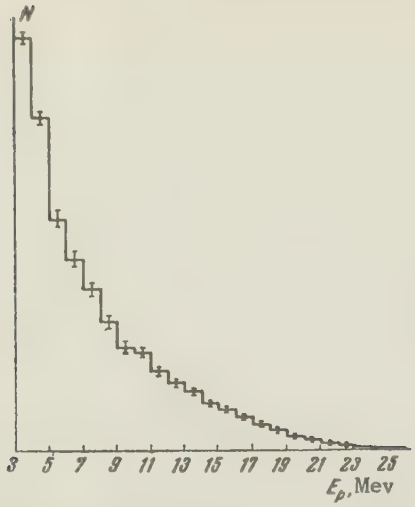

Fig. 3. Complete energy spectrum of protons from photodisintegration of Be^9; $E_{\gamma max}$ = 44 Mev.

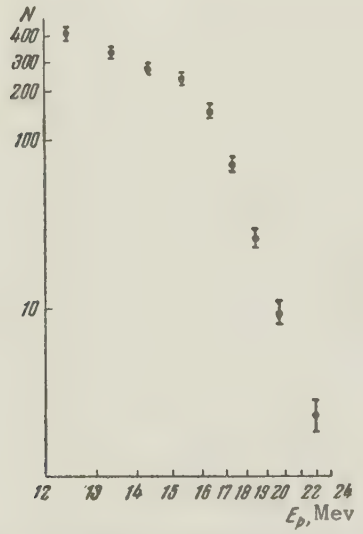

Fig. 4. Energy spectrum of protons with energies ≥ 12 Mev from photodisintegration of Be^9 (on a log-log scale); $E_{\gamma max}$ = 44 Mev.

$\sigma_{Be^9} = (1.0 \pm 0.2) A\sigma_d$. It is clear that within the limits of error the proportionality coefficient is the same as that for higher energy proton groups.[1] This is also in accord with the assumptions made above concerning the mechanism of formation of photoprotons from Be^9 at these energies.

The angular distributions of protons from photodisintegration of C^{12} by bremsstrahlung with $E_{\gamma max}$ = 30 Mev and $E_{\gamma max}$ = 44 Mev are the same (Fig. 5). Since in the first case the protons are formed only in the $C^{12}(\gamma, p)B^{11}$ reaction, the coincidence of the angular distributions is apparently related to the fact that the $C^{12}(\gamma, pn)B^{10}$ contributes little in this range of excitation energy. This is indicated also by the great similarity of the photoproton energy spectra, which are shown in Figs. 6 and 7. It is true that the maximum in the energy distribution of the protons from irradiation of C^{12} by bremsstrahlung with $E_{\gamma max}$ = 44 Mev is shifted somewhat toward lower energies compared to the energy spectrum from irradiation of C^{12} by γ quanta with $E_{\gamma max}$ = 30 Mev.

For the low energy protons (4 — 7 Mev), which are apparently produced when γ quanta are absorbed by the C^{12} nucleus in the region of the giant resonance (since the energy distribution of the protons within this energy range reproduces the shape of the cross section curve for the $C^{12}(\gamma, p)B^{11}$ reaction and the maxima of the curves also coincide), the angular distributions are in good agreement with those expected on the model of a direct photoeffect, as well as with the distribution from the resonance theory of the compound nucleus. The identity of the conclusions from both models is caused by the fact that the final B^{11} nucleus is left in either the $3/2^-$ ground state or in the $1/2^-$ first excited state. However, the experimentally observed angular distributions from C^{12} for higher energy protons (which, like those for

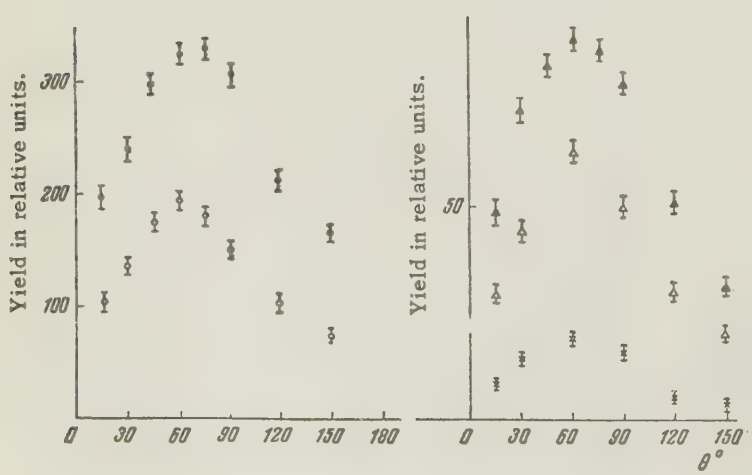

Fig. 5. Angular distributions of proton groups from photodisintegration of C^{12} by γ quanta with $E_{\gamma max}$ = 44 Mev: ● — E_p = 5–7 Mev, ○ — E_p = 7–10 Mev, ▲ — E_p = 10–13 Mev, Δ — E_p = 13–16 Mev, × — $E_p \geq 16$ Mev.

Fig. 6. Complete energy spectrum of protons from photodisintegration of C^{12} by radiation with $E_{\gamma max} = 44$ Mev.

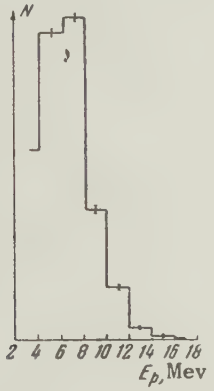

Fig. 7. Complete energy spectrum of protons from photodisintegration of C^{12} by radiation with $E_{\gamma max} = 30$ Mev.

Be^9, deviate from the resonance model) are essentially different from what would be expected from either of these models. The difference is characterized by a rapid decrease in the isotropic part of the distribution. An explanation for this is to be sought in the fact that, with increasing energy of the γ quanta, the mechanism of absorption of the γ quanta by individual substructures begins to be important. For carbon such structures are apparently quasi α particles. The angular distribution of the protons from photodisintegration of these structures has no isotropic part. Apparently the smallness of the isotropic part of the angular distributions of the high energy protons is also explained in this way.

It is of interest to note the appreciable contribution of the two-nucleon mechanism for absorption of low energy γ quanta to the photodisintegration of Be^9. This may be related to the presence of a weakly bound neutron in the Be^9 nucleus. On the other hand, in the photodisintegration of carbon, because of the high neutron binding energy (17 Mev), the two-nucleon interaction mechanism does not appear. It also does not appear at higher energies. This is shown by the angular distributions and energy spectra of photoprotons with energies above 18 Mev which are obtained from photodisintegration of C^{12} by γ quanta from bremsstrahlung with $E_{\gamma max} = 64$ Mev. In explaining this fact it should be remembered that the isotopic spin selection rule may play an important role for the interaction of γ quanta with C^{12} nuclei. In the case of the two-nucleon mechanism for absorption of γ quanta, it forbids emission of a proton and a neutron with parallel spins.

So although the analysis of the results on photodisintegration of C^{12} does not enable us to make a unique choice, the whole aggregate of experimental data on the photodisintegration of Be^9 and C^{12} are in favor of the statement that the photodisintegration of light nuclei with absorption of γ quanta in the region of the giant resonance occurs via formation of a compound nucleus. In the decay of the compound nucleus, the final nucleus is left preferentially in its ground state. With increasing energy of the γ radiation, processes begin to be important in the photodisintegration of light nuclei which owe their occurrence to absorption of the γ radiation by substructures within the nuclei. The two-nucleon mechanism for absorption of γ quanta by nuclei is already the dominant process at energies of the order of 80 Mev.

In conclusion, the authors express their sincere appreciation to G. K. Kliger and V. I. Riabinkin for assistance in the work.

[1] I. V. Chuvilo and V. G. Shevchenko, J. Exptl. Theoret. Phys. (U.S.S.R.) 32, 1335 (1957); Soviet Phys. JETP 5, 1090 (1957).

[2] E. D. Courant, Phys. Rev. 82, 703 (1951).

[3] Morita, Sugie, and Yoshida, Progr. Theor. Phys. 12, 713 (1954).

[4] L. Allen, Phys. Rev. 98, 705 (1955).

Translated by M. Hamermesh
116

GLOW OF GASES IRRADIATED BY SOFT X-RAYS

S. V. SAMOILOV, V. A. TSUKERMAN, and I. Sh. MODEL'

Submitted to JETP editor October 10, 1957

J. Exptl. Theoret. Phys. (U.S.S.R.) 34, 599-608 (March, 1958)

X-ray luminescence of air, nitrogen, argon, and gas mixtures, induced by radiation of wavelength 0.3 — 1.5 A, was investigated in the pressure range from 0.01 to 760 mm Hg. It is shown that the principal role in the excitation of gas glow is played by photoelectrons and recoil electrons, produced by interactions between x-ray quanta and gas atoms. The data obtained are explained satisfactorily by combining the gas-kinetic mechanism of extinction of the excited levels with x-ray absorption in the gas. For argon and air the experimentally-determined mean light yield, under normal conditions, is 5×10^{-4} and 2×10^{-4} light photons respectively per absorbed x-ray quantum of wavelength 1.2 A, and 9×10^{-4} and 5×10^{-4} photons respectively per quantum of wavelength 0.6 A.

No x-ray luminescence of metallic surfaces proper was observed at flux intensities up to 600 r/sec. It was established that the glow observed on a metal surface in air is due to luminescence of the thin layer of gas adjacent to the surface, induced by the photoelectrons knocked out from the metal by the x-ray quanta.

INTRODUCTION

In recent years there has been more interest in research on the glow of gases and metals under the influence of ionizing radiations. The use of gas scintillators in nuclear physics and many astrophysical problems (polar lights, glow of night sky, etc.) require a detailed study of the mechanism of glow of matter under the influence of cosmic radiation, γ rays, and fast charged particles. References 1 — 6 contain extensive experimental and theoretical material on the glow spectra, intensities, and durations of glows resulting from the interaction of various gases with slow and fast electrons, α particles, and positive ions. Refs. 7 — 11 contain the glow characteristics of noble gases used as luminophors and scintillation counters.

However, in spite of the relatively large number of investigations, the mechanism of the glow induced in gases and metals by the individual types of radiation has not been sufficiently studied. The emission of light by gases and metals under x-irradiation was investigated in only two works. In 1937 Krasnikov first observed and described these phenomena qualitatively.[12] In 1955 Spicer[13] investigated the pressure dependence of the glow intensity in air, nitrogen, and argon, and also obtained the first data on the glow spectrum. The excitation mechanism for the glow of gases and metals under the influence of x-irradiation was not discussed in these works.

The aim of the present work is a more detailed investigation of the glow of gases and metals under the influence of soft x-rays. In addition to disclosing the dependence of the glow intensity on the type and pressure of the gas, certain data have been obtained on the mechanism of transformation of x-radiation into visible light.

PROCEDURE

The source of soft x-rays was a high-power dismountable close-focus type TRB-3 x-ray tube, developed by the Institute of Physical Chemistry of the Academy of Sciences, U.S.S.R.[14] The tube operates at 50 kv and 40 ma. The distance between a focal center on the tungsten anode and the outer surface of the beryllium window is 20 mm. Under these conditions, the intensity of x-radiation in the window plane reaches 600 r/sec.

The chamber for the study of the luminosity of metals comprises a hermetically-sealed volume with two windows (Fig. 1a). The x-rays enter the lower beryllium window 1 and the luminous phenomena are observed through window 2. The investigated metal plate 3 is placed in the path of the x-ray beam against window 2.

The inner volume of the chamber can be evacuated to 10^{-2} mm Hg. The chamber for the study of gas glow (Fig. 1b) was made taller to exclude the additional illumination that might arise on the upper end of the chamber. To absorb the undesirable glow from the sidewalls, the latter were covered with black paper. In spectral investigations, win-

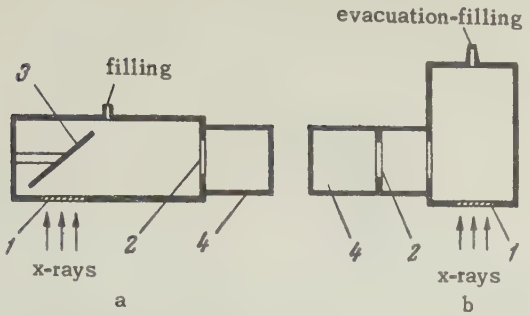

Fig. 1. Chambers for the investigation of x-ray luminescence: a – of metals and b – of gases. 1 – beryllium window; 2 – glass window; 3 – investigated metal; 4 – recording instrument.

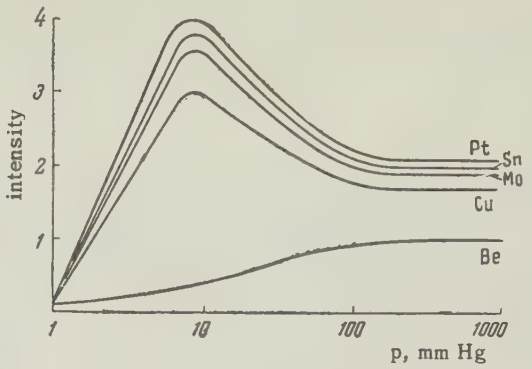

Fig. 2. Dependence of glow intensity on the air pressure in the chamber, for various metals.

dow 2 was replaced by a plate of transparent quartz 3 mm thick. The total thickness of the beryllium placed between the anode of the tube and the inner cavity of the chambers was 2.3 mm.

The luminous phenomena in the chambers were observed with the aid of a photomultiplier, a photographic camera, and a spectrograph. The first method made it possible to evaluate quantitatively the intensity of the glow as a function of the type and pressure of the gas and of other characteristics. All experiments were carried out with type FEU-19 photomultipliers, whose output signals were recorded with an EO-4 oscillograph. The photomultiplier sensitivity was 700 – 1200 amp/lu. The oscillograph gain was $10^2 - 10^5$. At maximum gain, a 1-mm deflection of the beam on the oscillograph screen corresponded to a flux of 2×10^{-11} lu on the photocathode.

The photographic camera was used to determine the spatial distribution of the glow intensity within the volume of the chamber. The relative aperture of the objective was 1:1.5, the focal distance was f = 50 mm. Using type D panchromatic motion picture film (250 – 350 GOST units), the glow could be photographed in the chambers at exposures from 5 to 200 minutes.

The spectral investigations were made with a type Q-12 Zeiss quartz spectrograph. The high intensity of the x-rays source made is possible to record glow spectra with photographic plates, without resorting to photomultipliers, as Spicer had to do.

EXPERIMENTAL RESULTS

Figure 2 shows the results of the first measurements of glow intensity as functions of the air pressure for Be, Cu, Mo, Sn, and Pt. The measurements were made with a photomultiplier using the circuit of Fig. 1a. As can be seen from the graph, the absolute light yield increases with increasing atomic number of the metal. As the pressure is reduced from 760 to 7 – 10 mm Hg, most metals exhibit an increase in glow intensity. Further reduction in pressure leads to a monotonic decrease in intensity. Finally, at approximately 10^{-2} mm Hg and below, the photomultiplier detects no noticeable light yield even at maximum gain. These unexpected results show that the observed glow is not connected with fluorescence induced in metals by the x-rays, as was proposed in Ref. 12. It has been suggested that the glow of gas in the chamber is excited by electrons, knocked out by the x-ray quanta from the metallic surface and from the gas atoms as the result of the photoeffect. Figure 3 shows photographs of the glow of the air in the chamber, confirming this suggestion. At a relatively high pressure (76 mm Hg) one observes, in addition to the glowing column of air in the lower portion of the chamber at the outlet window, also

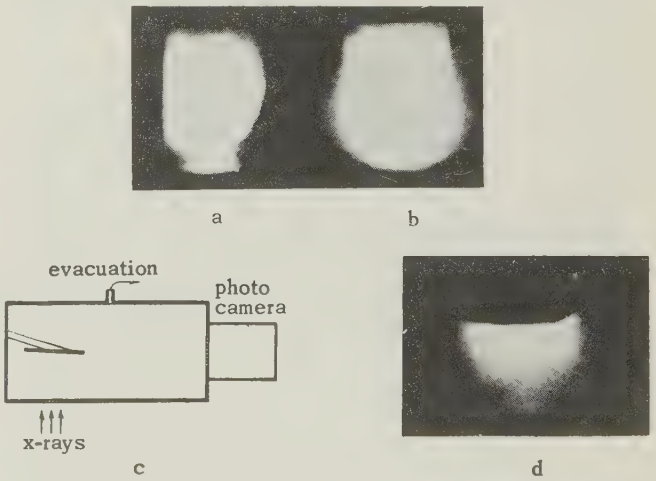

Fig. 3. Photographs of x-ray luminescence of air in the chamber of Fig. 1a: a – pressure 76 mm Hg; b – pressure 7 mm Hg; c – experimental setup for the confirmation of the electronic nature of the observed glow; d – photograph of x-ray luminescence at 7 mm Hg, using the scheme of Fig. 3c.

a bright glow of the surface of the plate (marked by an arrow in Fig. 3a). Such a photograph can readily lead to the erroneous conclusion that the metal surface fluoresces. However, the next photograph, made at 7 mm Hg, contradicts such a conclusion. Here the glowing region near the surface broadens noticeably, and merges with the glowing cone in the lower portion (Fig. 3b). Upon slight modification of the experiment, this phenomenon manifested itself even more clearly. The platinum plate was rotated in the chamber in such a way, that the objective of the camera did not "see" the surface facing the source of x-rays (Fig. 3c). In spite of this, the pressure of the glow of the air in the chamber turned out to be analogous to that of the preceding photographs (Fig. 3d).

Further confirmation of the electronic nature of the excitation of the glow of the gas under x-irradiation, and also data on the energy of the electrons that excite the glow, were obtained by photographing the glow of the air in a magnetic field. The setup of the experiment is clear from Fig. 4a. A hole 10 mm in diameter was drilled through the lower pole of a horseshoe shaped electromagnet to

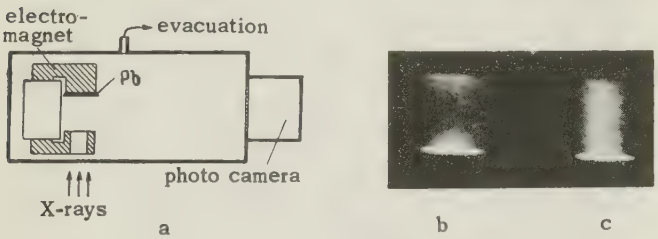

Fig. 4. X-ray luminescence of air in magnetic field. a – experimental setup, b – without magnetic field, c – with magnetic field.

permit passage of the x-rays through the gap between the poles. To increase the number of secondary electrons, the surface of the upper pole opposite the source of radiation was covered with a lead plate. With electromagnet coils energized, the field intensity in the gap between the pole is ~ 300 oersted. Photographs of the glow of the air in the gap between the poles without and with a magnetic field are shown in Figs. 4b and 4c respectively. It is seen quite distinctly that in the presence of a magnetic field the glowing region contracts towards the axis of the polepieces and assumes the shape of a glowing column. An estimate shows that the electron energy does not exceed 1000 v in a field of 300 oersted.

The pressure dependence of the intensity of the glow of air and argon, in the absence of a metallic surface in the chamber, is shown in Fig. 5 (solid curves). The experiments were made in the chamber shown in Fig. 1b. For convenience in comparison of the curves among themselves and with the results of other investigators, the ordinates represent the glow intensity in percent of the intensity at 760 mm Hg. The course of the curves is seen to be similar to that of the curves of Fig. 2. Up to pressures of 100 – 200 mm Hg for air and 300 – 400 mm Hg for argon, the glow intensity remains practically unchanged. Further reduction in pressure is accompanied by a monotonic decrease in intensity. The increased glow intensity in the 5 – 50 mm Hg region, observed in the experiments with the metallic plates, is not seen in this series of measurements. An analogous behavior of the curves was established in experiments with helium, oxygen, and nitrogen. The general character of the observed laws is in close correspondence with the pressure dependence of the glow as obtained by Spicer[13] for air (dotted curve of Fig. 5). The absolute glow intensity depends on the type of gas. At atmospheric pressure, the glow intensities of helium, oxygen, air, nitrogen, and argon are related as 1 : 2 : 10 : 35 : 1,000. The glow intensity of a gas mixture is determined by the composition and the ratio of the mixture components and by the pressure. Figure 6 shows graphs for the glow intensity of mixtures of argon with oxygen (a) and of argon with nitrogen (b). The abscissas represent the percentage of oxygen or nitrogen constant in the argon, while the ordinates represent the glow intensity in percentage of the intensity of pure argon. Three series of measurement were made for pressures p = 50, 150, and 350 mm. In all cases, a small admixture of oxygen (up to 1 – 2%) has reduced the glow intensity by a factor of several times. The "quenching" influence of the oxygen is stronger at high pressure than at low pressure. The glow of an argon-nitrogen mixture has a different character. Here a small addition (1 – 2%) of nitrogen increases the glow intensity. Further in-

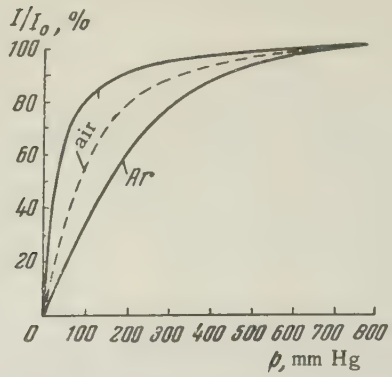

Fig. 5. Dependence of the intensity of x-ray luminescence of gas on the pressure. Solid – authors' data, dotted – Spicer's data.(Ref. 13).

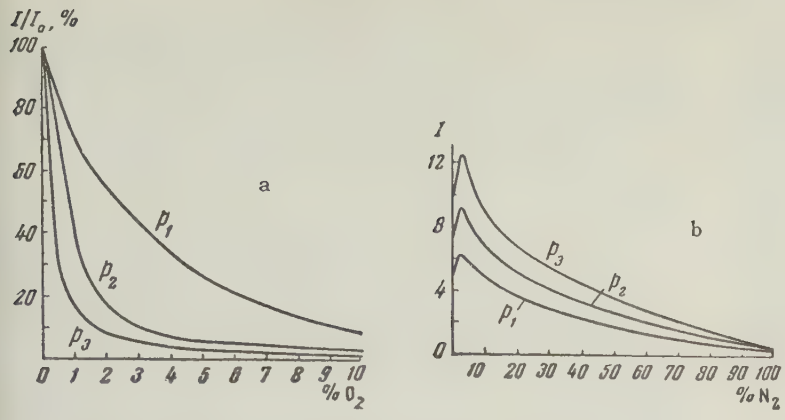

Fig. 6. Dependence of intensity of x-ray luminescence of argon on the concentration: a – of oxygen, b – of nitrogen, for pressures p_1 = 50, p_2 = 150, and p_3 = 350 mm Hg.

crease of the nitrogen concentration results in a slow decrease in intensity.

Figure 7 shows the pressure dependence of the glow intensity of a mixture of 80% argon plus 20% oxygen. For comparison, the same graph shows the pressure dependence of the glow intensity of air. The character of the two curves is practically

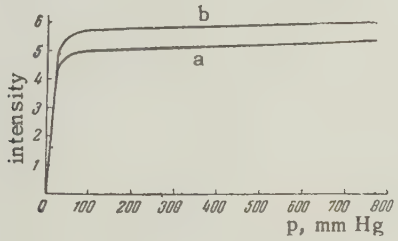

Fig. 7. Dependence of intensity of x-ray luminescence of air (a) and mixture 80% Ar + 20% O_2 (b) on the pressure.

identical. It is interesting to note that the absolute intensity of the glow of a mixture of argon with oxygen is only slightly higher than the glow intensity of air at equal pressures. This experiment refutes Spicer's point of view concerning the influence of the natural-argon content of air on the intensity of its glow.

An attempt was made to establish the connection between the glow intensity of gas and the hardness of the x-rays. For this purpose, the soft component of the x-ray spectrum was "cutoff" with the aid of aluminum filters 0.05 to 2.3 mm thick. The drop in glow intensity of air and argon had an exponential dependence on the thickness of the filter, with a variable exponent. From the resultant curves one can conclude that soft x-rays produce a more effective excitation. It must be noted that our experiments did not disclose the linear dependence of the logarithm of glow intensity on the filter thickness, as indicated by Spicer.

Figure 8 shows the result of microphotometry of a spectrogram of argon glow at atmospheric pressure. In the investigated spectral range, 6,000 – 2,500 A, seven lines were observed in the violet regions. The positions and relative intensities of these lines are in good agreement with the lines of the neutral atoms in the spectrum of argon excited by an electric discharge (shown by vertical bars).[15] The most intense lines were those at 3390, 3600, 3840, 3180, and 4180 A.

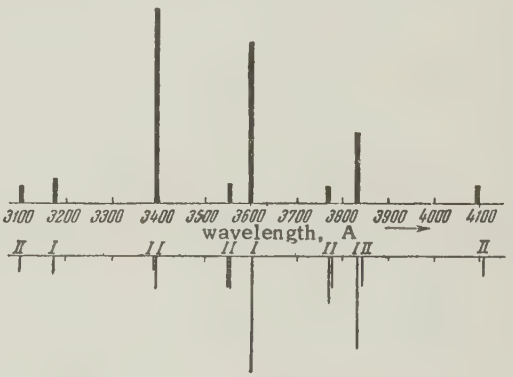

Fig. 8. Spectrum of x-ray luminescence of argon at atmospheric pressure (the lower lines are those of argon in gas discharge, coinciding with the x-ray-luminescence lines).

The data obtained on the x-ray spectrum, intensity, and spectral composition of the visible glow excited by x-rays has made it possible to estimate approximately the yield of the light photons per x-ray quantum. Such a calculation was made for argon and air at atmospheric pressure. The center line of the wavelength of the light radiation was taken to be 3500 A. The calculation results are listed in the table.

Light yield of x-ray luminescence (p = 1 atmos, t = 20°C)

Gas	wavelength of x-rays, A	light yield per absorbed x-ray quantum in photons, λ = 3500 A
Air	0.6	$5 \cdot 10^{-4}$
	1.2	$2 \cdot 10^{-4}$
Argon	0.6	$9 \cdot 10^{-4}$
	1.2	$5 \cdot 10^{-4}$

Errors in the determination of the spectra of the x-ray and optical radiations, inaccurate knowledge of the spectral characteristics of the photocathode of the multiplier, errors in the account for the geometry of the experiment, and several other factors difficult to control may cause these values to deviate from the true values by a factor of 4 — 5. These data must therefore be considered only as tentative, illustrating from the quantitative point of view the effective cross-section of x-ray luminescence in gases.

EVALUATION OF RESULTS

Let us consider the possible mechanism for the transformation of an x-ray radiation into visible light on a metallic surface. Ginzburg and Frank have described the occurrence of transition glow upon passage of fast charged particles through the separation boundary between vacuum and a metal.[16] However, to obtain a noticeable glow of a metal under the influence of electrons, their energy must be not less than several tens of kv. It is known that the energy of most photoelectrons "knocked out" from a metal by soft x-rays does not exceed 1 kv. At such energies, the probability of glow due to the transition effect is vanishingly small. It is possible to represent the occurrence of visible glow on a metallic surface as being due to the long-wave region of the bremsstrahlung spectrum. In this case the radiation of light can take place only in very thin surface layers of the metal, on the order of 10^{-6} cm. Even for soft radiation, the number of x-ray quanta converted into light in such a thin layer is negligible. The absence of a noticeable glow of metallic surfaces in vacuum confirms these qualitative considerations.

With the photomultiplier sensitivity having a maximum of 10^{-11} lu, we can state in any case that the yield of light photons from the metallic surface per x-ray quantum is less than 10^{-8}, and is at least two orders of magnitude less than the glow intensity of air, as recorded in our experiments. The apparent glow of a metallic surface in air must thus be attributed to glow of the layer of gas adjacent to the surface, induced by the electrons knocked out by x-ray quanta from the metal. Since the mean energy of such electrons is 1,000 ev, their range in air amounts to $\sim 2.5 \times 10^{-2}$ cm. A glowing layer of gas of such thickness is perceived by the observer as a glowing metallic surface.

The increase in the absolute intensity of glow with increasing Z of the metal, as indicated in Fig. 2, does not contradict this statement. The glow of the photoeffect increases with increasing Z, and the number of secondary electrons exciting the gas atoms should be greater for a heavier than for a lighter metal. There are no grounds for assuming that the mechanism of glow excitation in gas differs from the above in the absence of a metal.

An estimate of the probability of direct excitation of the levels of the argon atoms by 1.2-A x-ray quanta shows that this probability is at least 10^7 times as small than the probability of excitation of the levels of the atoms by electrons "knocked out" by the photoeffect or by recoil electrons. The observed laws of glow of gases, excited by fast electrons and other charged particles, confirm this opinion. The pressure dependence of the glow intensity obtained by Grün and Schopper[4] for nitrogen and for an argon-nitrogen mixture by irradiating these gases with α particles from polonium, is in good agreement with the laws of x-ray luminescence of gases.

The spectra of the x-ray luminescence of gases also confirm the principal role of fast electrons in the excitation of the glow. Fan has shown[1] that as the electron energy increases, the spectrum of the gas glow shifts towards the short-wave region. It is known that the most intense argon-discharge spectral lines, when the energy of the electrons does not exceed 100 v, are located in the 8100 — 8500 A and 4700 — 3900 A ranges. In our case, the most intense spectral lines lie between 3400 and 3800 A.

Let us consider in greater detail the effect of the pressure and of the composition of a gas mixture on the intensity of the gas glow. Spicer proposes that the pressure dependence of the glow intensity is determined by the change in the rate of electron-ion recombination with pressure. This assumption is not corroborated by calculations or by experimental data. The probability of direct recombination at negligibly small electron and ion concentrations (not more than 10^{12} ions per cm^3) is very small. In addition, the recombination radiation should have a continuous spectrum. Our and Spicer's experiments resulted only in line spectra. The experimental relations are explained much better by the gas-kinetic mechanism. It is known that the average lifetimes of the excited levels can vary for different gases over very wide range, from 10^{-2} to 10^{-10} sec. The probability of transitions from the excited levels with radiation of light photons increases with diminishing lifetime. For argon atoms, the fundamental levels with light radiation have average lifetimes of $10^{-7} - 10^{-9}$ sec and in addition, there exist metastable levels with a lifetime $\sim 10^{-2}$ sec. The average time interval

between collisions of argon atoms amounts to 1.64×10^{-10} sec at $p = 1$ atmos and 1.2×10^{-7} sec at $p = 1$ mm Hg ($t = 20°C$). Comparing these quantities, it is easy to note that, at pressures close to atmospheric, the time between two collisions of argon atoms is 1 — 2 orders shorter than the glow time of the ground levels. The glow intensity under such conditions, for a given number of excited argon atoms, will be less than the glow intensity for the same number of excited atoms at a pressure ~ 1 mm Hg, when the time between two atom collisions exceeds the lifetime of the excited level.

The number of excited levels n, which glow at a given pressure p, is expressed by a function of the type

$$n = N(1 - \exp\{-t_0 k/\tau_0 p\}), \quad (1)$$

where N is the total number of excited levels, τ_0 is the average lifetime of the excited level, t_0 is the average time between two collisions at $p = 1$ atmos, and k is a coefficient that accounts for the number of collisions per extinction event (ratio of gas-kinetic cross-section to the extinction cross-section). On the other hand, reducing the pressure reduces the x-ray absorption and correspondingly the number of excited levels per unit volume. This dependence is of the form

$$N \sim I_0(1 - \exp\{-\mu x p\}). \quad (2)$$

Here I_0 is the intensity of the x-rays, μ the linear coefficient of attenuation of the radiation in the gas at a pressure of 1 atmos, and x is the thickness of the gas layer absorbing the radiation. The interaction of these two opposing processes is shown in Fig. 9. Curve 1 shows the gas-kinetic extinction as a function of the pressure, in accordance with expression (1), while curve 2 shows the dependence of the absorption on the gas pressure (2). The superposition of the two laws is represented by curve 3:

$$n \sim I_0(1 - \exp\{-\mu x p\})(1 - \exp\{-t_0 k/\tau_0 p\}). \quad (3)$$

This curve has an extended horizontal section in a relatively large pressure range, in good agreement with the experimental data.

The mechanism described makes it also possible to explain the experimentally-observed increase in glow intensity in the presence of a metallic surface at pressures from 1 to 10 mm Hg (curves of Fig. 2). In contradistinction with x-ray luminescence of a pure gas, the number of secondary electrons knocked out here from the surface of the metal does not diminish with decreasing pressure, and stays at approximately the same level. Thus, in a comparatively wide pressure region, the principal role is played here by gas-kinetic extinction, and the total intensity recorded by the photomultiplier should increase with diminishing pressure. Only after the mean free path of the electron in the gas begins to exceed the dimensions of the observed glowing region does a noticeable decrease in glow intensity take place. Naturally, the quantitative relations here are determined to a great extent by the geometry of the experiment. However, a numerical estimate of the results of the graph of Fig. 2 confirms these considerations quite well.

The observed laws of the glow of gas mixtures are also in good agreement with the mechanism of gas-kinetic extinction. It is known that a small addition of oxygen exerts a considerable quenching influence on the glow of a gas discharge.[17] Oxygen is characterized by transitions from excited levels without radiation of light.[3] The large number of energy levels in this diatomic gas leads to a practically resonant "selection" of the energies of the excited levels of argon, causing an extinction of the x-ray luminescence even at small oxygen concentrations. At low pressures of argon-oxygen mixtures, the collisions between the atoms of these gases are less frequent and the quenching influence of the oxygen is less pronounced (see Fig. 6a). This process, whereby the oxygen extinguishes the excited levels of gas atoms, is apparently the decisive factor not only for argon, but also for air. A similar course of curves for the mixtures 80% Ar + 20% O_2 and $N_2 + O_2$ (air), shown in Fig. 7, confirms the above.

To the contrary, a small addition of nitrogen increases the intensity of argon glow (Fig. 6b). An analogous phenomenon was observed by Grün and Schopper,[4] where, at nitrogen concentrations in argon from 1 to 15%, an increase in glow intensity by 5 — 7 times compared with the glow intensity of pure argon was observed under the influence of α particles. The spectral investigations of the glow of argon under the influence of charged particles, performed by Bennet and Hughes,[2] have shown that a slight concentration of nitrogen in argon (0.001%) is sufficient to excite intensely the lines of the second positive group of neutral molecules of N_2. The excitation potential of the highest level of this group corresponds to the potential of the metastable state of the argon. Thus, unlike in the case of oxygen, the interaction between the excited atoms of argon with the nitrogen atoms leads to an increase in the glow intensity owing to the radiation of the metastable levels.

It is interesting to note that the laws for the glow of gases and gas mixtures under the influence

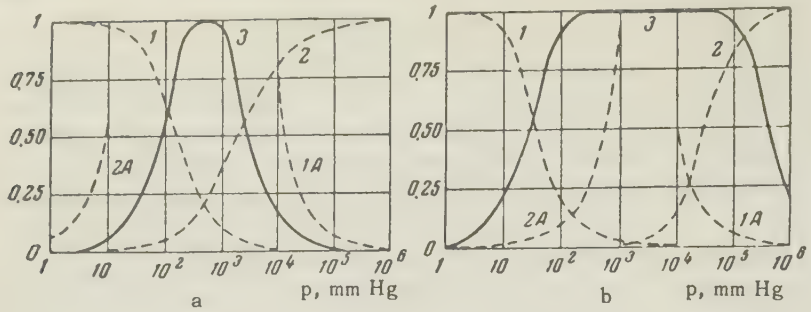

Fig. 9. Dependence of gas-kinetic extinction (1), radiation absorption (2), and total light yield of x-ray luminescence (3) on the gas pressure: a – argon, b – air.

(For portions of curves 1A and 2A, the vertical scale has been increased by 100 times.)

of ionizing radiations depends relatively little on the nature of the radiation. Fast electrons, x-rays, α particles, and other energetic radiations excite approximately equal spectra. Fan, who studied the glow spectrum of air excited by electrons, protons, and helium ions has shown that different charged particles of equal velocity, excite very similar spectra. The dependences of the glow intensity on the pressures and concentrations of mixtures of various gases turn out to be exactly similar, and show little dependence on the type of ionizing radiation.

One can consider it established that at ionizing-radiation energies that exceed by many times the ionization potential of the gas, the glow is due to the electronic transitions and is determined essentially by the atomic and molecular properties of the the gas, by its density, and by its impurities.

In conclusion, we shall mention several practical consequences of the above experiments, which are of certain interest to workers with gas scintillators. An analysis of the curves of Fig. 9 shows that a considerable increase in pressure in a gas scintillator does not lead to an increase in the luminescence intensity (in the case of registration of charged particles it may even lead to a reduction in the glow intensity). Calculations show that at a pressure of ~ 3 atmos the intensity of luminescence, excited in argon by 1-A x-rays, begins to diminish.

When the chamber is filled with a gas scintillator, it is necessary to rid the gas thoroughly of all possible impurities, which may extinguish the glow — oxygen, carbon dioxide, nitrogen oxides, etc.

It is also possible to propose the following method for increasing considerably the light output of a gas scintillator for x- and γ-rays. It is known that the ordinary gas scintillators have little sensitivity to radiations of this type. If a system of plane-parallel metal foils is placed in the scintillation chamber perpendicular to the plane of the photomultiplier cathode, then the electrons knocked out by the x- or γ-rays from the surface of the foils will produce an intense glow of the gas layers located in the gaps between the foils. By choosing suitable foil thicknesses and materials and gap thicknesses, and by choosing the kind and pressure of the gas, it is possible to increase the light yield of such a gas scintillator by many times, leaving unchanged the remaining qualitative indices, the low glow time, and the simplicity of construction.

[1] C. Y. Fan, Phys. Rev. **103**, 1740 (1956).

[2] Bennett, Wu, and Hughes, Bull. Am. Phys. Soc. **1**, 54 (1954).

[3] A. E. Grün, Z. Naturforsch. **9A**, 15 (1954).

[4] A. E. Grün and E. Schopper, Z. Naturforsch. **9A**, 134 (1954).

[5] K. Schmidt, Z. Naturforsch. **11A**, 1023 (1956).

[6] S. Lormeau, Compt. rend. **230**, 956 (1950).

[7] C. O. Muehlhause, Bull. Am. Phys. Soc. **2**, 71 (1953).

[8] R. A. Nobles, Rev. Sci. Instr. **27**, 280 (1956).

[9] Palevsky, Zimmerman, and Larsson, Rev. Sci. Instr. **27**, 323 (1956).

[10] A. E. Villaire and L. F. Wouters, Phys. Rev. **98**, 280 (1955).

[11] G. P. Boicourt and J. E. Brolley, Rev. Sci. Instr. **25**, 1218 (1954).

[12] A. I. Krasnikov, J. Exptl. Theoret. Phys. (U.S.S.R.) **8**, 1286 (1938).

[13] W. E. Spicer, Phys. Rev. **98**, 1061 (1955).

[14] Zatulovskii, Vetushkin, Nariadchikov, and Petrovskii, Сб. работ по радиационной химии Collection of Works on Radiation Chemistry, 1957 (in press).

[15] Zaidel', Prokof'ev, and Raiskii, Tables of Spectral Lines, 1952.

[16] V. L. Ginzburg and I. M. Frank, J. Exptl. Theoret. Phys. (U.S.S.R.) **16**, 15 (1946).

[17] N. A. Kaptsov, Электрические явления в газах и вакууме (Electrical Phenomena in Gases and in Vacuum), 1950.

Translated by J. G. Adashko
117

VISCOSITY OF LIQUID He^3 *IN THE RANGE 0.35 — 3.2° K AND* He^4 *ABOVE THE LAMBDA-POINT*

K. N. ZINOV'EVA

Institute for Physical Problems, Academy of Sciences, U.S.S.R.

Submitted to JETP editor October 21, 1957

J. Exptl. Theoret. Phys. (U.S.S.R.) 34, 609-615 (March, 1958)

The viscosity of liquid He^3 was measured in the temperature range 0.35 — 3.2° K by means of a capillary tube viscosimeter. A slight increase in the viscosity was observed in lowering the temperature in the range 1.0 — 3.2° K, and a strong increase was noted below 1° K. The temperature dependence of η in the range 0.5 — 1.1° K is satisfactorily described by the formula $T^{-1/2}$ and only below 0.5° K does the dependence become stronger; however, it is less strong than T^{-2}. The measurements of liquid He^4 above the λ-point show that its temperature dependence is not different from that of ordinary liquids, the region near the λ-point being excluded.

1. THE VISCOSITY OF He^3

In 1950, Pomeranchuk,[1] basing his work on the general quantum theory of liquids developed by Landau, predicted, from qualitative considerations, a viscosity coefficient for He^3 with a temperature dependence of the form $1/T^2$. Later, Abrikosov and Khalatnikov[2] considered in detail the kinetic phenomena in liquid He^3 on the basis of the theory of a Fermi liquid constructed by Landau.[3] In accord with the theory of Abrikosov and Khalatnikov, the viscosity of liquid He^3 below 0.1 — 0.2° K has a temperature dependence of the form $1/T^2$.

Up to the present time there have existed only qualitative measurements in the literature on the viscosity of He^3. These were carried out by Abraham, Osborne, and Weinstock.[4] In their research, the fluidity of liquid He^3 across a thin slit was compared with the fluidity of He^4. From their observations, the authors estimated the value of the viscosity coefficient, and established a weak temperature dependence — an increase in the viscosity from 22 to 30.4μ poise for a temperature drop from 2.79 to 1.04° K. These data were in need of verification. Moreover, we were interested in extending the range of measurement to much lower temperatures.

Recently, we learned of the measurements of Taylor and Dash[5] which were carried out by the method of the torsional vibrations of a disc. The data of Taylor and Dash, which were obtained in the range 1.3 — 2.15° K and at T = 3.34° K, agree both in absolute magnitude and in temperature dependence with the results of Abraham, Osborne, and Weinstock.

Below, we shall give a description of the method and tabulate the results of our measurements.

The Method

For the measurement of the viscosity of liquid He^3, we chose the method of the capillary viscosimeter as the most useful for research with very small quantities of the liquid. All the measurements were made in two glass thick-walled capillaries (outside diameter 4 — 5 mm), carefully selected and calibrated. With the help of a metal microscope and an ocular micrometer, we determined the shape and dimensions of the openings at the ends of the capillaries. The form of the opening was shown to be slightly elliptical, but the difference in the dimensions of the ellipses at the ends of the capillaries did not exceed 1%. The mean values of the axes of the ellipses were equal. For the first capillary, of length 35.00 mm, a = 97.8μ and b = 105.4μ; for the second capillary of length 18.13 mm, a = 74.1μ and b = 75.0μ. For verification of the form of the cross section at all points along the capillary, a definite amount of mercury was introduced and its length was measured. Such a method of checking showed that the first capillary had an almost barrel-shaped form, while the second capillary had a taper in its length of ~ 1%. Calibration of both capillaries by the flow of gaseous hydrogen and helium at room temperature gave a value of 102.1μ as the effec-

tive diameter of the first and 74.5μ for the second which, within the limits of accuracy, coincided with the values obtained from direct measurements. The error in the determination of the diameter of the capillaries amounted to ± 1%.

The principal difficulty of measurement lay in the observation of extraordinary precaution against the contamination of the capillary with foreign particles. In spite of the freedom of He^3 from carbon impurities when cooled to the temperature of liquid air, there was always a sufficient number of foreign particles which easily contaminated the capillaries if protective measures were not taken. Two arrangements (I, II) were used in the research. These are shown in their final form in Fig. 1. Measurements were carried out with apparatus I in the temperature range 1.0 — 3.2°K, while apparatus II served for measurements below 1°K. In this and the other apparatus, both capillaries were used in turn.

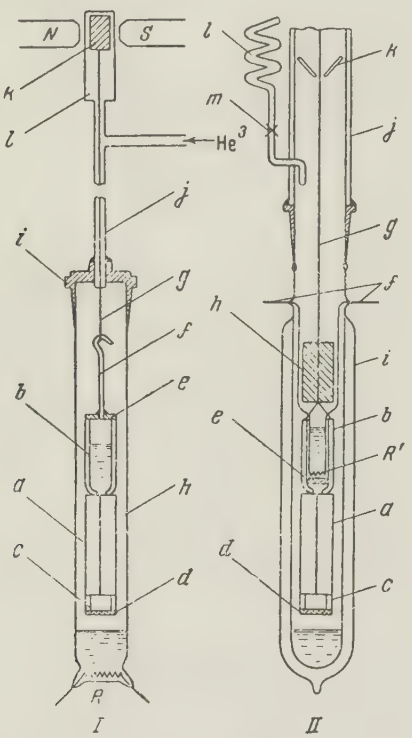

Fig. 1. Schematic drawing of apparatus for the measurement of the viscosity.

Apparatus I for measurements above 1°K contained a capillary a with a glass cylindrical reservoir b attached to it. This cylinder had an internal diameter of 5.35 mm and length 20 mm. For protection against the entrance of impurities from above, there was attached to it a covar cover e with a 1 mm diameter metal pipe f leading into it. A cylinder c of height 2 mm was cemented from below to the capillary with a filter d of fine cotton fiber cemented to its end. This filter trapped particles ~ 0.1μ. Thanks to the large area of the filter (ϕ 5 mm), its resistance was negligibly small in comparison with the resistance of the capillary (the calibration of the capillaries with gas did not reveal differences in the resistance of the capillaries when the filters were present). The reservoir was suspended by the fiber g in a cylindrical test tube h of internal diameter 8 mm, at the bottom of which was placed a resistance thermometer R of 40μ phosphor bronze. The test tube h was connected with a copper-nickel tube j by a copper connector i. The tube was of diameter 2 mm and passed through the cap of the dewar. A steel cylinder k was mounted at the upper end of the fiber and could be adjusted by the magnet NS in the tube, raising and lowering the reservoir b.

He^3 was condensed in the test tube so that the level of the liquid in the emptied capillary was lower than the highest end of the tube f. The liquid flowed into the reservoir below through the capillary, first passing the filter d. A decrease in the temperature of He^3 was achieved by pumping out the He^4 vapors in the surrounding tank. The double helium dewar had a construction similar to that described in Ref. 6. The temperature of the liquid was determined from the vapor pressure of He^3, which was measured by a mercury manometer.

The apparatus for measurements below 1°K (II, Fig. 1) consisted of a dewar i with a volume of about 3 cm^3 and diameter 8 mm, from which was carried out a pumping of the vapors of liquid He^3. The lowest temperature achieved by this method was 0.35°K. In contrast to the apparatus I, the reservoir b was open at the top and had a filter e at the entry to the capillary to serve as protection against contamination. This was in addition to the filter d. The temperature of the liquid was measured by a thirty micron phosphor-bronze resistance thermometer R′, which was located inside the reservoir b. The leads of the thermometer were taken out through the platinum bushing f. The thermometer was first calibrated by means of the vapor pressure of He^3 which was measured by a McLeod gauge. In the temperature interval 0.3 — 1.0°K, the resistance of the thirty micron phosphor-bronze has a linear temperature dependence, which was checked in a separate experiment by means of measurements of the magnetic susceptibility of a paramagnetic salt.

Just as in the apparatus I, the reservoir b was suspended by the filament g and was turned by means of a magnet. Pumping out of the He^3 vapor

was carried out by means of a mercury diffusion pump through a copper tube j of 15 mm diameter which was later changed to steel. To decrease thermal conduction inside the tube j, a copper screen k was employed. It was placed in thermal contact with the outside He^4 tank and had a temperature ~ 1°K. The He^3 vapors from the openings of the diffusion pump were condensed in the coil ℓ and the liquid He^3, cooled to 1°K, was transferred to the dewar by means of the valve m. With the exception of the lowest temperatures, the measurements in apparatus II were carried out with the pumping disconnected. In order that the temperature not change significantly during the measuring time of 1 — 2 minutes, a pellet of paramagnetic salt, cooled by the vapors of He^3, was fastened under the reservoir b. Because of its large heat capacity, the salt served as a buffer, lowering the heating rate of the liquid. With the salt in place, it required not less than three hours for the liquid to heat from 0.35 to 1°K.

The process of measurement in both pieces of apparatus was as follows. After filling the reservoir b with the liquid, the capillary was raised until its lower end did not make contact with the level of the liquid outside. Values of the position of the level in the reservoir as a function of time were determined by means of a KM-5 cathetometer and a stop watch. Usually the level in b fell off by 3 — 8 mm, depending on the diameter of the given capillary and the temperature, in the course of about two minutes. At temperatures close to the critical, where the surface tension of He^3 is small, the liquid flowed from the capillary in the form of fine strips of visible flow. At low temperatures, where the surface tension becomes appreciable, drops were formed at the end of the capillary. These were released periodically when they achieved critical dimensions. Observation was carried out with the liquid rendered visible by a luminescent lamp. The cathetometer enabled us to make measurements with the accuracy of ± 0.01 mm. Because of the distortions brought about by the optical inhomogeneities of the glass of the dewar, the errors were somewhat increased; however, they did not exceed ± 0.05 mm. This fact was specially checked by us in Ref. 7.

Results of Measurement

Determination of the coefficient of viscosity was carried out by means of the formula

$$\eta = \frac{(\rho_l - \rho_v)\, g}{2.3 \cdot 8\, l R^2} \cdot \frac{a^3 b^3}{8(a^2 + b^2)} \cdot \frac{t}{\log(H_0 / H)}, \qquad (1)$$

where a and b are the elliptical axes in the cross section of the capillary, ℓ is the length of the capillary, R = radius of reservoir b, ρ_ℓ and ρ_v are respectively the liquid and vapor densities, H = height of the liquid level in the reservoir below the lower end of the capillary, t = time, and g = acceleration due to gravity. In the research, we used He^3 with a purity not lower than 99.98%. Values of the density of the liquid and vapor He^3 in Ref. 1 were taken from the work of Kerr.[8] The temperature was determined according to the scale of Sydoriak and Roberts,[9] with accuracy down to 0.01°K. The correction required by the finite velocity of flow from the capillary, which is about 1%, was not taken into account by us. We also did not consider corrections connected with the formation of small droplets at the end of the capillary. This correction would be of the order of 0.1%.

For the calculation of the viscosity, we constructed a graph of $\log(H_0/H)$ vs. t for each point. A typical graph of this form is shown in Fig. 2. The straight-line dependence of $\log(H_0/H)$ on t, observed at all temperatures, testifies to the laminar flow of the liquid. An estimate of the Reynolds numbers for the capillaries of 102.1 and 74.5 μ gave 600 and 350, respectively.

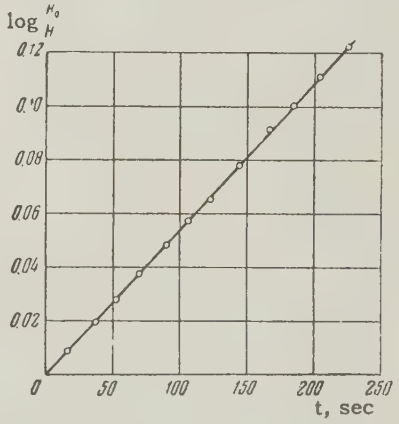

Fig. 2. Dependence of the position of the level in the reservoir on the time (in semilogarithmic plot) for the capillary of diameter 102.1μ at T = 1.105°K.

Figure 3 shows the results of measurements obtained with the two capillaries. The same dependence in logarithmic plot is shown in Fig. 4. The spread of measurements increases at the lower temperatures, which is the result of the instability of the temperature over the measuring interval (~ 0.01 — 0.02° at 0.4 — 0.5° K). The absolute values of the viscosity coefficient were determined with an accuracy to within ± 5% in the region above 1° K, and ± 10% for the very low temperatures. The mean values of η are given in Table I.

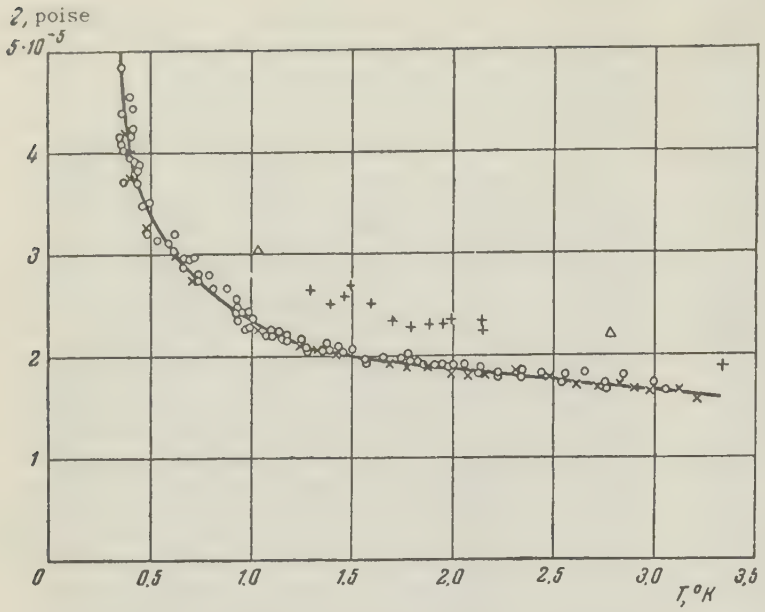

Fig. 3. Viscosity of liquid He^3: o = capillary of diameter 102.1μ, × = capillary of diameter 74.5μ, Δ = results of Abraham, Osborne and Weinstock,[4] + = data of Taylor and Dash.[5]

TABLE I. Mean Values of Viscosity of He^3

T°K	η·10⁵ poise	T°K	η·10⁵ poise	T°K	η·10⁵ poise
0.35	4.8	0.8	2.63	2.0	1.87
0.40	4.00	0.9	2.46	2.2	1.83
0.45	3.64	1.0	2.33	2.4	1.78
0.50	3.40	1.2	2.14	2.6	1.74
0.55	3.22	1.4	2.02	2.8	1.70
0.6	3.07	1.6	1.96	3.0	1.66
0.7	2.82	1.8	1.92	3.2	1.61

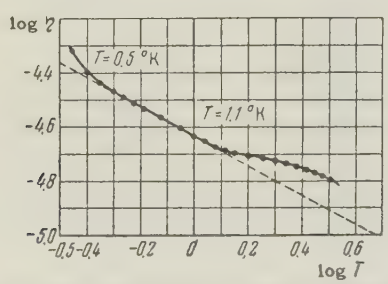

Fig. 4. Viscosity of He^3 in semilogarithmic plot.

As is seen from Fig. 3, the viscosity in the temperature range from 1 to 3.2° K increases slightly with decrease in temperature, changing from 1.6×10^{-5} to 2.32×10^{-5} poise, which is in qualitative agreement with one of the variants of the theory of Abrikosov and Khalatnikov.[2] In the temperature range below 1° K, η increases sharply, reaching a value of 4.8×10^{-5} poise at T = 0.35° K. The temperature dependence of η in the interval 1.1 — 0.5° K, as is seen from Fig. 4, is approximately described by the formula $1/\sqrt{T}$ and only below 0.5° K does the dependence become much steeper; however, it is weaker than the dependence $1/T^2$ predicted theoretically, which also agrees with the estimate given in Ref. 2.

We did not succeed in carrying out measurements of the viscosity in the immediate vicinity of the critical point. Measurements in this region are extremely difficult becuase of the small density difference $\rho_\ell - \rho_v$. It is quite evident, however, that as $T \to T_{cr}$, the viscosities of the liquid and the gas ought to approach the same value. In accord with the measurements of Becker, Misenta, and Schemissner,[10] the viscosity of gaseous He^3 at T = 3.35° K has the value of 1.25×10^{-5} poise, which agrees within 20% with our extrapolated values. In Fig. 3 we have also plotted the results of Abraham, Osborne, and Weinstock,[4] and the data of Taylor and Dash.[5] From a comparison of the results, it is evident that while the temperature dependence of the viscosity in Refs. 4 and 5 agrees with our measurements, the absolute values are approximately 20% higher, which is apparently explained by systematic errors in the determination of the constants of the apparatus.

TABLE II. Mean Values of the Viscosity of He^4

T°,K	η·10⁵ poise	T°,K	η·10⁵ poise
2.2	2.55	3.0	3.30
2.3	2.83	3.2	3.27
2.4	3.00	3.4	3.25
2.5	3.15	3.6	3.20
2.6	3.21	3.8	3.15
2.7	3.26	4.0	3.07
2.8	3.28	4.2	3.00

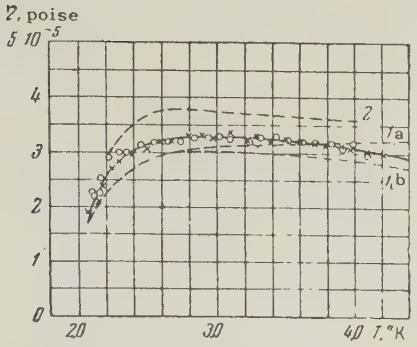

Fig. 5. Viscosity of liquid He⁴: o = capillary 102.1μ, × = capillary 74.5μ; 1a – data of Bowers and Mendelssohn;[13] 1b – the same data, recomputed by us with account of the density of the vapor; 2 – temperature curve of Taylor and Dash.[5]

2. VISCOSITY OF He⁴ ABOVE THE λ-POINT

To check our method, we simultaneously carried out measurements of the viscosity of He⁴ in the temperature range above the λ-point. The measurements were carried out with apparatus I. The dependence of $\log(H_0/H)$ on t had the form of a straight line, similar to that shown in Fig. 2. The viscosity was calculated by Eq. (1), in which the values of ρ_l were taken from the work of Kamerlingh-Onnes and Bok (see Ref. 11), the values of ρ_v from the measurements of Keesom[12] and R. Berman.*

The results of the measurements, taken with the two capillaries, are given in Fig. 5. The average values of the viscosity coefficient are tabulated in Table II. For comparison, the data of Bowers and Mendelssohn[13] (broken line 1a) are also plotted in Fig. 5. These were obtained by the same method. The results of Taylor and Dash (broken line 2) are also given. The results of our measurements agree with the data of Ref. 13 in absolute value (within the limits of error); however, instead of a monotonic increase in the viscosity, we observed a slight falling off, beginning at the temperature of 2.8°K. The cause of the divergence lies in the fact that in Ref. 13, the vapor density of He⁴ was not taken into consideration. Close to the critical point, this quantity becomes comparable with the density of the liquid. The data of Bowers and Mendelssohn, recomputed by us with account of the density correction, give the curve 1b, which in its temperature dependence does not differ from our curve. The measurements of Taylor and Dash,[5] as is seen in Fig. 5, have a temperature dependence which agrees with ours, but the absolute value of the viscosity coefficient is approximately 15% higher. We note that even in the region below the λ-point, the values of the viscosity of the normal component of He II (in the measurements of Dash and Taylor[14]) exceed by 10% our data obtained from measurements of surface attenuation of second sound.[15] It should be emphasized that the temperature dependence of the viscosity of He I, contrary to established opinion, does not differ from the same for ordinary liquids, with the exception of the region close to the λ-point. The monotonic decrease of the viscosity of He I with temperature does not contradict the value of the vapor viscosity at the critical point, which is equal to ~ 15μ poise according to the measurements of Ref. 10.

In conclusion I express my gratitude to Professor V. P. Peshkov for his discussion of the results and his constant interest in the work, and to N. I. Iakovlev, who helped in assembling the apparatus and in the measurements.

*A partial report. The author expresses his thanks to R. Berman for making his data available prior to publication.

[1] I. Ia. Pomeranchuk, J. Exptl. Theoret. Phys. (U.S.S.R.) **20**, 919 (1950).

[2] A. A. Abrikosov and I. M. Khalatnikov, J. Exptl. Theoret. Phys. (U.S.S.R.) **32**, 1083 (1956), Soviet Phys. JETP **5**, 887 (1957).

[3] L. D. Landau, J. Exptl. Theoret. Phys. (U.S.S.R.) **30**, 1058 (1956), Soviet Phys. JETP **3**, 920 (1957).

[4] Abraham, Osborne, and Weinstock, Phys. Rev. **75**, 988 (1949).

[5] R. D. Taylor and J. G. Dash, Phys. Rev. **106**, 398 (1957).

[6] V. P. Peshkov, J. Exptl. Theoret. Phys. (U.S.S.R.) **23**, 686 (1952).

[7] K. N. Zinov'eva, J. Exptl. Theoret. Phys. (U.S.S.R.) **28**, 125 (1955), Soviet Phys. JETP **1**, 173 (1955).

[8] E. C. Kerr, Phys. Rev. **96**, 551 (1954).

[9] S. G. Sydorak and T. R. Roberts, Phys. Rev. **106**, 175 (1957).

[10] Becker, Misenta, and Schmeissner, Phys. Rev. **93**, 244 (1954).

[11] W. H. Keesom, Helium, (Amsterdam, 1942), p. 207.

[12] W. H. Keesom, Helium, (Amsterdam, 1942), p. 206.

[13] R. Bowers and K. Mendelssohn, Proc. Roy. Soc. (London) A204, 366 (1950).

[14] J. G. Dash and R. D. Taylor, Phys. Rev. **105**, 7 (1957).

[15] K. N. Zinov'eva, J. Exptl. Theoret. Phys. (U.S.S.R.) **31**, 31 (1956), Soviet Phys. JETP **4**, 36 (1957).

Translated by R. T. Beyer
118

SPECIFIC HEAT OF BISMUTH BETWEEN 0.3 AND 4.4° K

I. N. KALINKINA and P. G. STREKOV

Institute for Physical Problems, Academy of Sciences, U.S.S.R.

Submitted to JETP editor October 22, 1957

J. Exptl. Theoret. Phys. (U.S.S.R.) 34, 616-621 (March, 1958)

The specific heat of spectrally pure bismuth was measured in the temperature range 0.3 — 4.4° K. Below 1.8° K, the coefficient in the T^3 term in the formula for the temperature dependence of the specific heat is $\Theta_D = 118.5 \pm 1°$ K, while the coefficient in the linear term is $\gamma = 1.6 \times 10^{-5}$ cal/deg^2-gm atom, which is an order of magnitude smaller than for most metals. The linear term is compared with the specific heat of electrons computed on the basis of the de Haas — van Alphen effect.

1. INTRODUCTION

BISMUTH has a rhombohedral lattice with two atoms per cell and a valence equal to three; consequently, the number of electrons per cell is six. Substances with an even number of electrons in the cell fill the upper band completely and are insulators. Inasmuch as bismuth always possesses metallic properties, its bands overlap and the conductivity is brought about by quasi-particles with two signs of charge — electrons and holes.

Investigation of the de Haas — van Alphen effect,[1] galvanomagnetic phenomena[2,3] and cyclotron resonance[4,5] allow us to conclude that the overlapping zone is not large and the concentration of holes and electrons $n_h = n_e \approx 10^{-5}$ electron atom^{-1}, whereas for most metals this quantity is of the order of unity. Therefore the magnitude of the linear term in the specific heat, which is related to the electron concentration, ought to be very small for bismuth, and can be determined with sufficient accuracy only for very low temperatures.

Measurements of the specific heat of bismuth have been carried out a number of times. The investigations of Keesom and van den Ende[6] were performed in the range 2 — 20° K with an accuracy of 10%. These authors found that Θ_D was not constant in the temperature range studied, but had a minimum at 9° K. They would give no judgment on the linear term of the specific heat. Keesom and Pearlman[7] measured the specific heat of bismuth in the range 1 — 4° K. The amount of impurities in the sample was estimated at 0.01%. In view of the difficulty of estimating the content of small amounts of impurities, the authors obtained data on the change in the electrical resistance of their bismuth sample as a function of temperature (Table I). The measurements showed that below 2.3° K, Θ_D is equal to 117° K. In the range 1 — 2.3° K, where the Debye law is valid, the linear specific heat term was isolated, with $\gamma = (1.9 \pm 0.7) \times 10^{-5}$ cal-deg^{-2}-gm atom^{-1}.

Ramanathan and Srinivasan[8] carried out measurements for a sample of purity 99.95% in the temperature range 1.3 — 4.1° K. The polycrystalline sample "1953" contained 0.02% Pb; 5×10^{-3}% Mn; 1×10^{-3}% Cd; 5×10^{-4}% Cu; 1×10^{-3}% Fe; As, Se, Te < 0.001%; 2×10^{-4}% Ag. The temperature of the specimen was measured by a carbon resistance thermometer, the instability of the calibration of which reduced the accuracy of the results. The temperature region in which Θ_D was established to be truly constant, was not large, which gave us no possibility of isolating the magnitude of the linear term with sufficient accuracy. Moreover, it was not evident whether one could assume that the pure bismuth will have the same values of Θ_D and γ as was obtained for these relatively contaminated samples. Therefore, the present research was undertaken with much purer metal and at much lower temperatures.

2. THE SAMPLE AND THE MEASUREMENTS

The sample investigated was a monocrystal, grown from spectrally pure bismuth,* and was several times recrystallized and outgassed in a quartz ampoule at a temperature of about 600° K in a hard vacuum. Table I allows us to judge the purity of the specimen by the magnitude of the residual resistance. The residual resistances of

*The spectrally pure bismuth was prepared by the State Institute of rare metals.

TABLE I. Relative Resistances of Samples of Bismuth

T°K		73.3	4.2	1.5
Spectrally pure specimen	Polycrystalline	0.301	0.0251	0.0247
	Monocrystalline	0.285	0.006	0.006
Hilger Co. bismuth	Polycrystalline	0.285	0.026	—
Sample of Keesom and Pearlman[7]	"	0.383	0.112	—
Sample "1953"	"	0.68	0.56	0.425

several other specimens are listed for comparison.

The construction of the calorimeter in which the determination of the specific heat was carried out and the method of measurement were similar to those described earlier.[9] The sample, of mass 267.3 gm (1.175 gm atoms), was of cylindrical shape, with diameter 18 — 19 mm and length ~ 90 mm. The surface of the specimen was covered with a thin layer of adhesive BF-2, which was polymerized for about one hour at 120° C. A constantan heater was attached on the layer thus isolated by the same adhesive BF-2. A light copper screw with a phosphor bronze thermometer wound on it was screwed into the lower part of the cylinder. The entire thermometer, the heater, etc., had less than 0.3% of the weight of the sample. Appropriate corrections were introduced in the value of the specific heat. Above 1° K, the resistance thermometers were calibrated in terms of the vapor pressure of liquid helium in degrees of the 1955 scale. For temperatures below 1° K, the calibration was carried out in terms of the susceptibility of ferric ammonium alum (mark ChDA) compacted into a cylinder of 12 mm diameter and 40 mm length. The demagnetization factor of the salt[10] was found in order to calculate the corrections. Using the data of Kürti and Simon,[11] the magnetic temperature of an equivalent spherical sample was determined; then the magnetic temperature was reduced to the thermodynamic temperature by the method of Cooke, Meyer, and Wolf.[12] The bismuth sample and block of compressed ferric ammonium alum, which served as the cold reservoir for measurements below 1° K, were supported on nylon threads in a vacuum jacket. The heat exchange of the gases before demagnetization was brought about by an adsorbing carbon pump.[13]

3. RESULTS OF MEASUREMENT

The specific heat was measured in the temperature range 0.3 — 4.4° K. The experimental points in a plot of C/T vs. T^2 below T = 1.8° K (Fig. 1) form a straight line which determines the coefficients of the equation which describes the temperature dependence of the specific heat between 0.3 and 1.8° K:

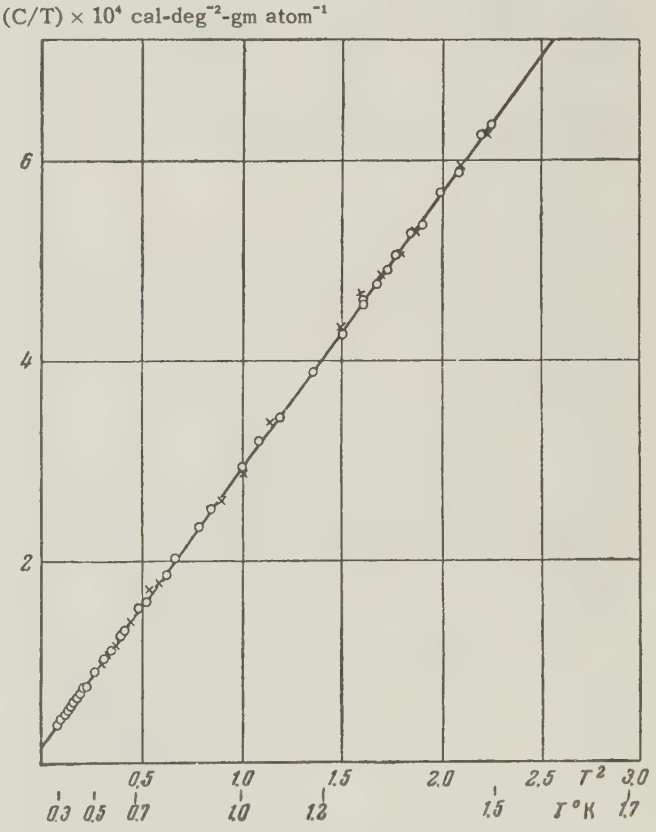

Fig. 1. C/T as a function of T^2 in the region in which the T^3 law is observed; × = measurements of 1953; ○ = spectrally pure sample.

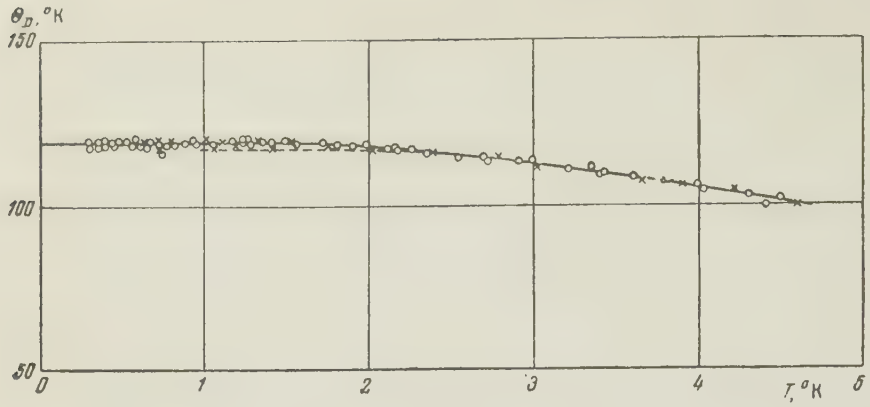

Fig. 2. Dependence of Θ_D on temperature. × = measurements of 1953; o = spectrally pure sample.

$$C = (1.6 \pm 0.1) \cdot 10^{-5} T + (2.79 \pm 0.09) \cdot 10^{-4} T^3 \text{ cal-deg}^{-1}\text{-gm atom}^{-1} \quad (1)$$

The effect of errors in measurement can be estimated by the limiting straight lines of that pencil of lines which can be drawn through the experimental points on the plot of C/T against T^2. In this way, the estimated inaccuracy of γ amounts to $\pm 0.1 \times 10^{-5}$ cal-deg^{-2}-gm atom^{-1}. The maximum possible systematic error in the values of the specific heat for temperatures near 0.3°K did not exceed 3 — 5% in our estimate.

In the interval in which the T^3 law is satisfied, i.e., between 0.3 and 1.8°K, the Debye temperature $\Theta_D = 118.5 \pm 1$°K. The change of Θ_D at much higher temperatures is shown in Fig. 2. For bismuth, the T^3 law is satisfied for $T \leq 0.015\,\Theta_D$.

4. DISCUSSION OF RESULTS

The values obtained for Θ_D and γ can be regarded as reasonably trustworthy, since they are the results of measurements taken over an extended temperature range, which allows a thoroughly accurate separation of the magnitudes of the lattice and electronic specific heats. The purity of the investigated sample was evidently sufficient, as can be judged from the data of Table II, in which no appreciable change in the values of Θ_D and γ with purity of the metal can be observed.

TABLE II. Θ and γ of the Various Bismuth Samples

Sample	Θ_D, °K	$\gamma \cdot 10^5$, cal-deg^{-2}-gm atom^{-1}
Spectrally pure, outgassed sample	118.5±1	1.6±0.1
99.99% of Keesom and Pearlman	117±1	1.87±0.7
Sample "1953"	119±1	2±0.5
99.95% of Ramanathan and Srinavasan	120±1	1.14±1.46

In Figs. 1 and 2, we have plotted experimental points which refer to bismuth with an impurity of 0.02% of lead. No systematic variation of the results that could be related to the spectrally pure sample could be noted. The reliability with which the quantity γ has been measured, allows us to attempt to make some conclusions on the contribution of the electrons and holes to the specific heat.

The coefficient for the linear term of the specific heat is determined by the value of the mean density of electron states on the Fermi surface:

$$C_e = \gamma T = \frac{\pi^2 k^2}{3} \left(\frac{dN}{dE}\right)_{E=F_0} T. \quad (2)$$

Substituting the quantity $\gamma = 1.6 \times 10^{-5}$ cal-gm atom^{-1}-deg^{-2} found experimentally, we find that the density of states on the Fermi surface is $(dN/dE)_{E=E_0} = 2.85 \times 10^{-2}$ atom-ev. Since the second band in the energy spectrum of bismuth contains a very small number of electrons, they will be found in states close to the bottom of the band and the square law of dispersion is valid for the energy. Taking anisotropy into account (which is brought about by the real bismuth lattice), Shoenberg,[1] on the basis of experimental data on the de Haas — van Alphen effect, assumed a model for the Fermi surface containing three ellipsoids which coincide with each other upon rotation by 120°. Let us calculate the electronic specific heat for this case. The number of states for a gram atom of metal, taking into account both spin directions, $N = 2VV_p/(2\pi\hbar)^3$, where V is the atomic volume, V_p = volume bounded by the Fermi surfaces in momentum space. For the three ellipsoids considered,

$$V_p = 3\,(4\pi/3)\, p_1 p_2 p_3, \text{ where } p_i = \sqrt{2m_i E}.$$

It is easy to show that in this case we obtain the same results as for the isotropic model of Sommerfeld:

$$\left(\frac{dN}{dE}\right)_{E=E_0} = \frac{3n_a N_A}{2E_0},$$

where n_a = number of electrons per atom, E_0 = bounding Fermi energy, N_A = Avogadro's number. Then

$$\gamma = \frac{\pi^2 R}{2} \frac{n_a}{T_0}. \quad (3)$$

In recent measurements of Shoenberg[1] on the de Haas — van Alphen effect for bismuth, the values $E_0/k = 205°K$, $n_a = 1.5 \times 10^{-5}$ electrons/atom were obtained; these are in excellent agreement with the calculations of Blackman,[14] based on earlier measurements of the de Haas — van Alphen effect ($n_a = 1.2 \times 10^{-5}$ electrons/atom, $E_0/k = 225°K$). Calculating the specific heat of the electrons from the data of Shoenberg according to Eq. (3), we find $\gamma_e = 0.072 \times 10^{-5}$ cal-gm atom^{-1}-deg^{-2}. This amounts to a small part of the experimental value obtained by us:

$$\gamma = 1.6\ 10^{-5} \text{ cal-gm atom}^{-1}\text{-deg}^{-2}.$$

The values of the electron concentration found from galvanomagnetic measurements[2] and from cyclotron resonance[4,5] have the same order as does the quantity obtained from the de Haas — van Alphen effect of Schoenberg. Therefore we can consider that in the case of bismuth, all the conduction electrons take part in the de Haas — van Alphen effect. All this compels us to assume that the fundamental contribution to the linear term of the specific heat is made by the holes which have a significantly larger effective mass and less boundary energy than the electrons:

$$\gamma_h = \gamma - \gamma_e = 1.53 \cdot 10^{-5} \text{ cal-gm atom}^{-1}\text{-deg}^{-2},$$

where γ_h = coefficient determined by the holes, γ_e = that determined by the electrons and γ is determined experimentally from data on the specific heat.

At the present time, we can consider it established that, for bismuth, the concentration of electrons and holes is identical.[2,3,15] Taking $n_h = n_e = 1.5 \times 10^{-5}$ electrons/atom, we can determine the boundary energy of the holes from the specific heat. Substituting in Eq. (3) the value found above for $\gamma_h = 1.53 \times 10^{-5}$ cal-gm atom^{-1}-deg^{-2}, we obtain $E_0/k = T_0 = 9.65°K$, which is about 20 times smaller than the boundary energy of the electrons. Taking the mass of the holes to be isotropic, we determine it from the equation

$$\gamma_h = 3.26 \cdot 10^{-5} (m_h/m_0) \cdot n_a^{1/3} \cdot V^{1/3} \text{ cal-gm atom}^{-1}\text{-deg}^{-2} \quad (4)$$

It is shown that $m_h = 2.5\, m_0$, i.e., two and one-half times larger than the mass of the electron.

Thus, measurements of the specific heat of bismuth down to 0.3° K have led to a value of the coefficient in the electronic term of the specific heat $\gamma = 1.6 \times 10^{-5}$ cal-gm atom^{-1}-deg^{-2}. This value is twenty times greater than the value of γ_e for electrons computed on the basis of data on the de Haas — van Alphen effect. It can be thought that the holes determine the magnitude of the linear term of the specific heat of bismuth, for which one gets $E_0/k = 9.65°K$ and $m_h = 2.5\, m_0$.

In conclusion, the authors take the occasion to thank Academician P. L. Kapitza for his unflagging interest in the research, and also Professor N. P. Sazhin and R. A. Dul'kin for supplying the spectrally pure bismuth.

[1] D. Shoenberg and J. S. Dhillon, Phil. Trans. Roy. Soc. **A248**, 1 (1955); D. Shoenberg, loc. cit. **A245**, 1 (1952).

[2] E. S. Borovik, Izv. Akad. Nauk SSSR, ser. fiz. **19**, 429 (1955).

[3] A. N. Gerritsen and W. J. Haas, Physica **7**, 802 (1940).

[4] M. Tinkham, Phys. Rev. **101**, 902 (1956).

[5] R. G. Chambers, Program of the Fifth International Conference on Low-Temperature Physics and Chemistry, August, 1957, p. 77.

[6] W. H. Keesom and J. H. Van den Ende, Leid. Comm. **18**, No. 203d (1930); **19**, No. 213c (1931).

[7] P. H. Keesom and N. Pearlman, Phys. Rev. **96**, 897 (1954).

[8] K. G. Ramanathan and T. M. Srinivasan, Phys. Rev. **99**, 442 (1955).

[9] B. N. Samoilov, Dokl. Akad. Nauk SSSR **86**, 281 (1952).

[10] K. Warmuth, Arch. f. Elektrotechnik. **33**, 734 (1939).

[11] N. Kürti and F. Simon, Phil Mag. **26**, 849 (1938).

[12] Cooke, Meyer, and Wolf, Proc. Roy. Soc. (London) **A233**, 536 (1956).

[13] P. G. Strelkov, J. Exptl. Theoret. Phys. (U.S.S.R.) **24**, 248 (1952).

[14] M. Blackman, Proc. Roy. Soc. (London) **A166**, 1 (1938).

[15] V. Heine, Proc. Phys. Soc. (London) **A69**, 505, 513 (1956).

Translated by R. T. Beyer
119

INVESTIGATION OF A SHOWER PRODUCED BY A SINGLY-CHARGED PARTICLE OF HIGH ENERGY

E. G. BOOS, A. Kh. VINITSKII, Zh. S. TAKIBAEV, and I. Ia. CHASNIKOV

Submitted to JETP editor September 10, 1957

J. Exptl. Theoret. Phys. (U.S.S.R.) 34, 622-631 (March, 1958)

A (2 + 16p) shower produced by a singly-charged particle of $(5^{+10}_{-3}) \times 10^{12}$ ev energy is analyzed. The energy spectrum of the secondary particles differs from that predicted by Landau's theory, but is consistent with Heisenberg's theory. The inelasticity coefficient is significantly smaller than unity. The fraction of energy consumed in meson production is on the order of 10 — 15%. The ratio of neutral pions to charged shower particles is $R = 0.54 \pm 0.18$, which indicates that a small fraction of the charged shower particles consists of heavy mesons and nucleons.

A (2 + 16p) event was observed in an Ilford G-5 emulsion 600μ thick, exposed in Italy in 1955 at an approximate altitude of 30 km. The energy of the primary particle, estimated by the usual kinematic method, is $(5^{+10}_{-3}) \times 10^{12}$ ev. The shower particles are contained within an angle of 1.7×10^{-1} radians. The central tracks cover a distance up to 5 cm within a single plate. This made it possible to determine the energy of 15 shower particles by direct measurement of the multiple Coulomb scattering.

1. MEASUREMENT OF MOMENTA OF SECONDARY PARTICLES

Figure 1 shows a microdiagram of the analyzed shower. The momenta of the secondary particles were determined by measuring their multiple Coulomb scattering. Measurements were made with a MBI-8M microscope of total magnification 60 × 2.5 × 15. The noise level of the stage with standard glass guide did not exceed 0.06μ per 1000-μ cell.

The geometry of the arrangement of the tracks in the shower did not permit the use of the relative-scattering measuring method. The scattering was therefore measured for each shower track separately. The directly-measured scattering $\overline{D}$ (the second difference of the coordinates of the tracks, determined over a cell length t) consists of true Coulomb scattering, D_C, and of scattering due to all other factors, n. Assuming that these quantities are independent and that they have a Gaussian distribution, we can write

$$\overline{D}_1^2 = \overline{D}_c^2 + n^2, \tag{1}$$

$$\overline{D}_c = kt^{3/2}/p\beta, \tag{2}$$

where k is a constant, p is the momentum, and β the particle velocity in terms of the velocity of light. The quantity n depends on the false scattering, due to microdistortions of the emulsion, nonlinear motion of the microscope stage, asymmetry of the track grains, inaccuracy of reading, fluctuations in microscope temperature (thermal noise), and variation of the microscope focus.

In the case of high-energy particles, n depends essentially on the microdistortions of the emulsion, which vary with a certain power of the cell length. We can therefore put $n \sim t^x$ without introducing an excessive error (Ref. 1).

The value of n can be determined by measuring the scattering of a high-energy particle by three cells along its track. For cells t_1, t_2, and t_3 with a ratio 1:2:3, Fowler et al.[1] obtained the value of x and derived a formula for n_1 on the basic cell t_1:

$$n_1 = [(27\overline{D}_1^2 - \overline{D}_3^2)/(27 - 3^{2x})]^{1/2}. \tag{3}$$

The value of x is considered constant for a given emulsion. However, the value of x for individual tracks within the same emulsion may differ considerably from the average value. In the measurement of the scattering, when $\overline{D}_C$ is not much greater than n, the elimination of each value of n is of major importance for the determination of the shower-particle energy. The method described below makes it possible to eliminate n for each track. Equation (1) for cells t_1, t_2, and t_4, with a ratio 1:2:4, can be written

$$\begin{aligned} \overline{D}_1^2 &= \overline{D}_{1c}^2 + n_1^2, \\ \overline{D}_2^2 &= \overline{D}_{2c}^2 + n_2^2 = 8\overline{D}_{1c}^2 + 2^{2x}n_1^2, \\ \overline{D}_4^2 &= \overline{D}_{4c}^2 + n_4^2 = 64\overline{D}_{1c}^2 + (2^{2x})^2 n_1^2. \end{aligned} \tag{4}$$

Such a choice of cells makes it possible to elim-

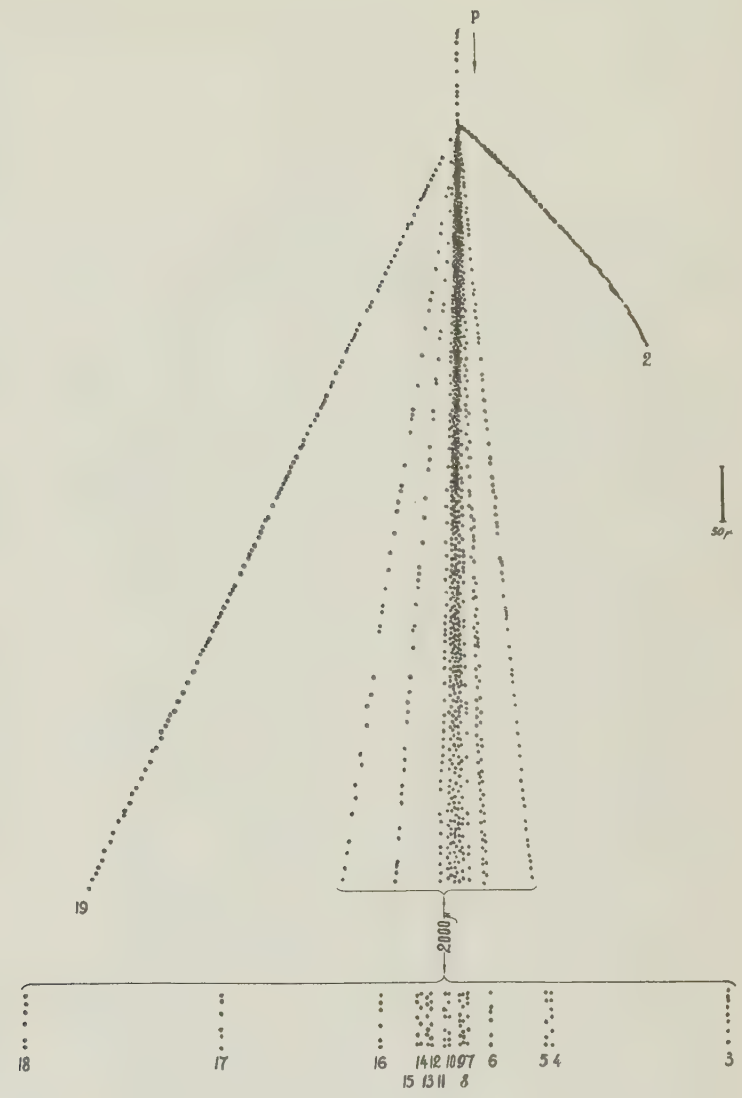

Fig. 1. Microdiagram of the shower, which is formed by a singly-charged particle (probably a proton) of energy$(5^{+10}_{-3}) \times 10^{12}$ ev.

TABLE I

No. tracks	λ	n	$10^{-3}t$, μ
12	2,2	0.25	40
15	5.6	—	10
13	5	0,13	40
11	1,73	0.38	40
10	3.6	0.07	40
8	1,75	0,46	40
9	4,5	0.18	40
7	1	0.59	40
16	5,5	—	10
6	1.9	0,34	20
5	3,2	0.19	20
14	2.8		10
4	2.7		5
17	2		5
3	1,5		5
18	1.6		5

TABLE II

Number of tracks	$p\beta c$, Bev	θ_l	E_i from Landau's theory	$p_\perp/m_\pi c$	θ'_l	E'_l, Bev
12	27±9	3′±2′	2605.1	0.16	5°36′	0,28
15	1.1±0.1	21′±3′	452,9	0,05	179°03′	0.47
13	15±4	22′±5′	434.4	0,66	46°05′	0.19
11	24±8	22′±7′	348.2	1.10	39°02′	0,28
10	14±5	28′±6′	268,3	0.81	56°47′	0.19
8	19±6	37′±1′	249.1	1.48	63°30′	0.27
9	8.3±2.3	40′±6′	217.5	0.68	83°53′	0.16
7	>25	46′±3′	154.9	—	—	—
16	1.5±0.2	1°05′±1′	124.2	0.20	175°14′	0.37
6	8.3±2.2	1°21′±4′	80.5	1.39	117°13′	0.26
5	6.0±1.5	2°03′±2′	61,3	1.84	136°22′	0,34
14	3.6±0.9	2°39′±2′	37,6	1.17	151°27′	0.37
4	1,0±0.3	4°08′±6′	29.8	0.51	173°35′	0,65
17	2,2±0,6	5°04′±2′	19.4	1.37	166°14′	0.80
3	3.3±1.1	7°16′±6′	13,8	2,94	165°35′	1,53
18	1.6±0,9	9°40′±3′	8.3	1,90	169°33′	1.50

inate x from the system of equations (4). The solution yields

$$n_1 = \frac{8\bar{D}_1^2 - D_2^2}{\sqrt{64\bar{D}_1^2 + \bar{D}_4^2 - 16\bar{D}_2^2}} \quad (5)$$

or

$$\bar{D}_{1c} = \left[\frac{\bar{D}_1^2\bar{D}_4^2 - \bar{D}_2^4}{64\bar{D}_1^2 + \bar{D}_4^2 - 16\bar{D}_2^2}\right]^{1/2}. \quad (6)$$

In our measurements, the values of n were calculated from (5). They are listed in Column 3 of Table I for the cells indicated in Column 4. For tracks where formulas (5) cannot be employed because of the small number of measurements, the value of n is assumed equal to the value obtained at the nearest track in which the above method is still applicable. In such cases no value of n is given in Column 3 of Table I. Let us note that the procedure developed here is not applicable in the case when $n \ll D_c$ or when the forward scattering varies with the length of the cell in the same ratio as the Coulomb scattering ($x = 3/2$).

The reliability of the data obtained depends on the ratio $\bar{D}/n = \lambda$ and, naturally, on the number N of independent measurements of the second differences of the coordinates of the track, when the chosen cells do not overlap. The values of λ for the cells indicated in Column 4 of Table I are given in Column 2 of the same table.

When $\lambda > 4$, the effect of the false scattering on the error in the determination of $\bar{D}$ can be neglected. For high-energy particles, owing to the insufficient length of the track, it is frequently necessary to confine oneself to $\lambda < 4$. However, when $\lambda \approx 1$, the measurement of the scattering becomes meaningless. This means physically that the observed scattering is of the same order as the false scattering. Consequently, the error in the determination of the momentum of the particles will not be less than 100% in such cases. For particle No. 7, $\lambda = 1$, and consequently this means that its energy cannot be determined. The value observed for this particle on a cell with $t = 4000\ \mu$ is $\bar{D} = 0.59 \pm 0.17\mu$. According to formula (2), this scattering corresponds to an energy of 25 Bev. Thus, the energy of this particle can be equal to or greater than 25 Bev.

The values of the energies of the other shower particles are given in Column 2 of Table II. The relative error in the quantity $p\beta$ is

$$\Delta(p\beta)/p\beta = 0.75N^{-1/2}(1-\lambda^{-2})^{-1/2}. \quad (7)$$

Measurements of the shower tracks were made in cells ranging from 500 to 4,000μ. The basic cells were taken to have $t = 500\mu$ and $t = 1{,}000\mu$. For $t = 2{,}000\mu$ and $t = 4{,}000\mu$, overlapping of the cells was employed.

2. ANGULAR AND ENERGY DISTRIBUTION OF SHOWER PARTICLES

We used the coordinate method to determine the angles θ_i of the shower particles with respect to the shower axis.

For small angles ($\tan\theta_i \approx \sin\theta_i \approx \theta_i$), the following formula holds

$$\theta_i = \sqrt{\lambda_i^2 + (\varphi_i - \varphi_0)^2}, \quad (8)$$

where φ_0 is the angle of dip of the shower relative to the plane of the emulsion, φ_i is the angle of the dip of the i-th shower particles, and λ_i the angle of the i-th particle relative to the shower axis, measured in the plane of the emulsion. Table II (Column 3) gives the angles θ_i of the shower particles.

Assuming a nucleon-nucleon collision, the energy of a primary particle is estimated from the median and geometric mean angles as well as by the method described in Ref. 2. The values of the energy E_0, estimated in this manner, are in good agreement with each other. Taking into account the possible fluctuation deviation from symmetry (forward and backward) in the distribution of the particles, in the center-of-mass system, we can indicate the following tolerances in the measurement of the energy

$$E_0 = (5^{+10}_{-3}) \cdot 10^{12}\ \text{ev}.$$

Comparison with the Landau and Heisenberg theories was made with respect to the angular and energy distributions of the shower particles.

Figure 2 shows a histogram of the angular distributions of the shower particles in the laboratory system. The ordinates represent the relative differential density of the shower particles

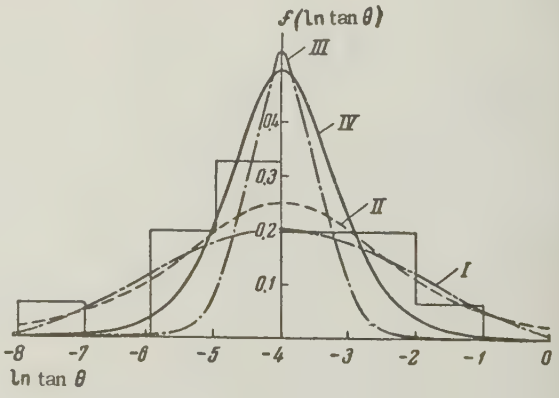

Fig. 2. Histogram of the differential angular distribution of shower particles.

$$f(\ln\tan\theta) = \frac{1}{n_s}\frac{\Delta n_s}{\Delta \ln\tan\theta},$$

as a function of $\ln\tan\theta$, where n_s is the number of charged shower particles and θ is the angle relative to the shower axis. The same diagram shows the corresponding angular-distribution functions of the Landau theory[3] (Curve I)

$$f_{\mathrm{I}}(\ln\tan\theta) = \frac{e^{-L}}{\sqrt{2\pi L}}\exp\{\sqrt{-(2L\ln\tan\theta + \ln^2\tan\theta)}\}, \quad (9)$$

and of the Heisenberg theory,[4] assuming an anisotropic (Curve II) and isotropic angular distribution of the mesons, in the c.m.s. (Curve III):

$$f_{\mathrm{II}}(\ln\tan\theta) = e^{L+\ln\tan\theta}/(1+e^{L+\ln\tan\theta})^2, \quad (10)$$

$$f_{\mathrm{III}}(\ln\tan\theta) = 3e^{3(L+\ln\tan\theta)}/[1+e^{2(L+\ln\tan\theta)}]^{3/2}. \quad (11)$$

Formula (10) is valid for large energies of colliding nucleons. The function

$$f_{\mathrm{IV}}(\ln\tan\theta) = 2e^{2(L+\ln\tan\theta)}/[1+e^{2(L+\ln\tan\theta)}]^2 \quad (12)$$

pertains to the case of a monoenergetic and isotropic distribution of the mesons in the c.m.s. (Curve IV), when the c.m.s. velocity equals the meson velocity in this system. The parameter of the angular distribution is

$$L = -\frac{1}{n_s}\sum_{i=1}^{n_s}\ln\tan\theta_i.$$

With the aid of the method of χ^2 tests,[5] we determined the probability of the symmetry of this shower to be $P(\chi^2) = 75\%$, and compared the theoretical curves I, II, III, and IV with the experimental angular distribution. The probabilities of the histogram of the experimental distribution coinciding with the above theoretical distribution are estimated at 40% (I), 60% (II), 1% (III), and 1% (IV), respectively. The angular distribution of the shower particles is in best agreement with the Heisenberg-theory distribution. However, this

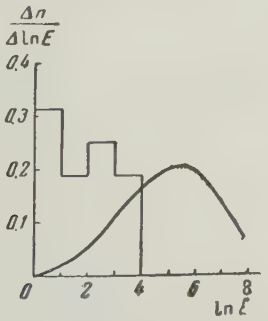

Fig. 3. Histogram of the energy distribution of shower particles in the laboratory system of coordinates. Solid line – curve obtained from the Landau theory.

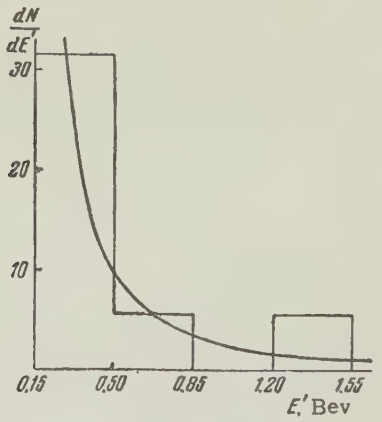

Fig. 4. Histogram of energy distribution of 15 shower particles in the c.m.s. of the colliding nucleons. Curve – energy spectrum according to the Heisenberg theory.

calculation by the χ^2-test method is only tentative, by virtue of the small number of shower particles.

To compare the energy distribution of the shower particles with the Landau theory, we plotted a histogram of the energy distribution of the shower particles in the laboratory system of coordinates, showing the distribution according to Landau (see Fig. 3). The abscissa represents the logarithm of the energy of the shower particles in units of the nucleon rest mass, and the ordinate the relative particle energy-distribution density. The intervals of the histogram ($\Delta \ln E = 1$) are much greater than the errors in the energy distribution, and therefore an account of these errors will affect very little the form of the energy distribution of the shower particles.

It follows from this comparison that the energy distribution of the particles does not correspond to the Landau theory, in that the low-energy shower particles exceed the value expected from the theory. Column 4 of Table II gives the values of the energy, calculated for the corresponding angles in accordance with Landau's theory. The comparison shows that the measured particle energy is one order of magnitude less than the theoretical values.

To compare the energy spectrum with the Heisenberg theory, we recalculated the data to the c.m.s., using a value $\gamma_c = 52$. The values of the angles θ_i' and of the energy E_i' in the c.m.s., under the assumption that all the shower particles are pions, are given in Columns 6 and 7 of Table II. Figure 4 shows the energy distribution in the c.m.s. of 15 shower particles whose energy was measured. The curve corresponds to the energy spectrum of the Heisenberg theory. In this case no discrepancy is observed between the theory and the experimental data.

The inelasticity coefficient estimated from the

total energy of the charged shower particles and of the neutral mesons (with the exception of particle No. 7), taking all the possible fluctuations of the primary-particle energy into account, is $0.10^{+0.06}_{-0.02}$ in the c.m.s. Assuming particle No. 7 to be secondary, its energy can be estimated by assuming that the mean transverse momenta in the internal and external cones are equal. The value of the average transverse momentum $\overline{p}_\perp$ of shower particles contained within the median angle is $0.9\mu c$ (without particle No. 7); for the external half of the shower particles, this value is $1.4\mu c$ (μ is the pion mass). Such an estimate gives a value of ~ 68 Bev for the energy of particle No. 7. In this case $K \sim 0.15$.

Let us note that if we assume the distribution of the generated mesons to be isotropic in the c.m.s., we can estimate the inelasticity coefficient from the angle of the cone of the shower particles.[6] This value is $K = 0.07$. Consequently, the coefficient of inelasticity ranges from 0.010 to 0.15.

Table III presents, for comparison with the experimental data, the total number of particles N, the average energy of the mesons in the c.m.s., and the inelasticity coefficients as given by the Landau and Heisenberg theories. The average energy of the shower particles in the c.m.s. is determined by using 15 particles. In the Landau theory, the fraction of the energy transferred by the mesons is close to unity, since the nucleons that participate in the collision are not separated in any manner after the collision, and have an energy close to the average value. The calculation was made for an energy of 5,000 Bev. It follows from the table that the experimental values are in better agreement with the Heisenberg theory.

TABLE III

	Total number of particles	Average energy of pions in c.m.s. (Bev)	Coefficients of inelasticity
Experiment	24	0.5	0.10—0.15
From Heisenberg's theory	18	0.6	0.1
From Landau's theory	14—15	6.7	~1

Inasmuch as the energy spectrum in the c.m.s. can be approximated by a power law (see Fig. 4), it is possible to estimate the energy of the primary particle from the relation $\gamma_c = 0.5/\theta_{1/2}$, which yields $E_0 = (1803^{+682}_{-574})$ Bev. This problem is discussed in detail by Takibaev.[7]

If one assumes[8] that the observed shower particles result from a collision between the incident nucleon and a nuclear "tunnel" of varying length, then the number of the nucleons in the tunnel is determined by the values of the median angle $\theta_{1/2}$ and the number of shower particles n_s. An analysis of this shower leads to the conclusion that the number of nucleons in the tunnel should not exceed 2. This is probable also because the excitation energy of the residual nucleus is very small (the total energy of the gray and black tracks is 220 Mev). The investigated shower can therefore be considered as produced in a nucleon-nucleon collision. If particle No. 7 is one of the colliding nucleons, the principal fraction of the energy, in the laboratory system, should be carried away by the neutron with which the collision took place.

3. SOFT COMPONENT ACCOMPANYING THE SHOWER

To study the soft component accompanying the given shower, we scanned the volume of the emulsion within a cone making a half-angle 0.15 radians with the shower axis. The scanning was performed with a total magnification $60 \times 1.5 \times 20$. In the volume scanned we found 10 electron-positron pairs (for nine of these, the distance from the center of the star is indicated in Table IV) and one trident, the data for which are indicated in Table V.

To separate the bremsstrahlung electron-positron pairs from the pairs produced by γ-quanta from the decay of the π^0 meson, we employed the

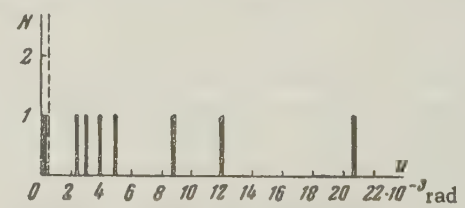

Fig. 5. Number N of electron-positron pairs as a function of the angular distance u to the nearest electron track.

criterion proposed in Ref. 9. We plotted (Fig. 5) along the ordinate the number of pairs as a function of the angular distance u to the nearest electron track of the previously-formed electron-positron pair. The pairs for which $u < 3 \times 10^{-4}$ radians were attributed to bremsstrahlung, and those with $u > 5 \times 10^{-4}$ radians to pairs directly connected with the decay of the π^0 mesons. According to this criterion, pair No. 10, produced 32,800 μ from the center of the shower, is a bremsstrahlung pair. The remaining nine pairs are produced

TABLE IV

Distance of pair from center of star, r, μ	Pair energy, determined from angle of divergence without accounting for Coulomb scattering, E_1, Bev	Energy of each electron of the pair, determined from the Coulomb scattering, ε_1 and ε_2, Bev	Pair energy, determined from Coulomb scattering, $E_2 = \varepsilon_1 + \varepsilon_2$, Bev	Pair energy, determined from the angle of divergence with allowance for the Coulomb scattering, E_3, Bev
775	$7.7^{+2.5}_{-2.6}$	2.6±0.6 3.8±0.7	6.4±1.3	5^{+11}_{-1}
1155	$22.5^{+20.5}_{-7.3}$	8.8±4.4 6.0±1.5	14.8±5.9	16^{+5}_{-2}
4290	$27.5^{+49.3}_{-10.4}$	5.6±2.1 11.7±5.8	17.3±7.9	35^{+10}_{-9}
8820	$8.7^{+1}_{-2.1}$	1.8±0.4 3.5±0.7	5.3±1.0	8^{+8}_{-1}
9875	14.3^{+4}_{-3}	1.7±0.3 1.0±0.2	2.6±0.5	
15700	$15.6^{+9.4}_{-4.9}$	3.0±0.7 14.8±5.7	17.8±6.4	30^{+50}_{-18}
19550	$0.8^{+0.1}_{-0.3}$	0.20±0.05 0.43±0.10	0.63±0.15	
19650	$1.4^{+0.1}_{-0.2}$	0.27±0.04 0.54±0.10	0.81±0.14	
20800	$8.5^{+1.0}_{-2.0}$	0.78±0.10 1.40±0.20	2.1±0.3	4^{+8}_{-1}

TABLE V

	Primary electron	First electron	Second electron	Third electron
θ_i, rad	0	$(3.5\pm1.3)\cdot10^{-3}$	$(3.8\pm1.3)\cdot10^{-3}$	$(4.3\pm1.3)\cdot10^{-3}$
α_i, rad	—	$2.4\cdot10^{-3}$	$1.2\cdot10^{-3}$	$1.2\cdot10^{-3}$
E_i, Bev	6.4±1.2	0.5±0.1	1.3±0.3	1.4±0.3

by γ-quanta from the π^0-meson decay.

Knowing the number of primary electron-positron pairs accompanying this shower, and using the law of radioactive decay, it is possible to calculate the expected number of π^0 mesons.[9,10] This number is determined from formulas

$$N_{\pi^0} = N_1 f(r)/2, \tag{13}$$

$$f(r) = \frac{1}{(1-e^{-r/\rho}) - \frac{\lambda}{\lambda-\rho}(e^{-r/\lambda} - e^{-r/\rho})}, \tag{14}$$

where N_1 is the number of γ quanta that decay at a distance r, λ is the average conversion length of the γ quanta in the photoemulsion (for the Ilford G-5 emulsion, λ = 37.5 mm), ρ is the average range of the π^0 mesons prior to decay in the photoemulsion. The average range of the π^0 mesons depends on the energy, but ρ is much less than λ and consequently the error in the determination of the average energy of the π^0 mesons is almost insignificant in the calculation of the function f(r). Starting with a resultant average energy $E^0_{\pi^0} = 15$ Bev and a lifetime of 2×10^{-15} seconds for the π^0 meson, we find $\rho = 65\mu$. Using formula (13) for three values of r, we found the ratio of the number of the neutral π^0 mesons to the number of

charged shower particles, $R = n_{\pi^0}/n_S$. For distances r of 8, 16, and 24 mm from the start of the shower, R is 0.49, 0.45, and 0.59 respectively. The mean value is $R = 0.54 \pm 0.18$; this corresponds to eight π^0 mesons.

Several methods for determining the energy of the electron-positron pairs are described in the literature. We estimated the energy of the pairs by three methods:

1. From the angle between the electron and the positron of the pair,[11] disregarding the effect of the Coulomb scattering. These data are given in Column 2 of Table IV.

2. From a direct measurement of the multiple Coulomb scattering of the electron and the positron. These measurements were made by the procedure described in Sec. 1 of this article. The energy of each electron and positron of the pair, and the energy of the entire pair, are listed in Columns 5 and 6 of Table IV.

3. From the angle between the components of the pair, taking into account the Coulomb scattering.

According to the work by Lorman,[12] the determination of the energy directly from the divergence angle can be used for an estimate of the photon energy not greater than 0.5 Bev. In this case the divergence angle of the electron and the positron can be measured at distances $\leq 100\mu$ from the point of pair production. At such a distance, the Coulomb scattering can be disregarded. For high energies, the divergence angle can be measured reliably at substantially greater distances from the point of pair production, and the contribution of the Coulomb scattering cannot be neglected. Unlike in Ref. 12, in this work we assumed equal distribution of the energy between the electron and the positron, and employed for the rms divergence angle θ a formula which takes into account, along with the Coulomb scattering, also the initial divergence of the components of the pair:

$$\bar{\theta}^2 = 4\frac{m_e^2c^4}{E_\gamma^2}\left(\ln\frac{E_\gamma}{m_ec^2}\right)^2 + 4\pi\frac{k^2t}{E_\gamma^2}. \qquad (15)$$

Here m_e is the mass of the electron, E_γ the energy of the γ-quantum producing the pair, k the constant of the Coulomb scattering, and t the distance from the point of the pair production.

The first term of the right half of Eq. (15) is the r.m.s. divergence angle of the pair, calculated in accordance with Stearns.[13] The second term is the r.m.s. divergence angle of the pair due to the relative Coulomb scattering of the pair components. Using (15), we plotted a family of curves for different energies (Fig. 6). The ordinates represent the r.m.s. divergence angle, as a function of the distance from the point of pair production, in units of 100μ. As can be seen from Fig. 6, most pairs are characterized by an undervalued angle at distances close to the point of production. This is probably due to the fact that at these distances, by virtue of the shrinkage of the emulsion during development, it is impossible to take into account the divergence of the pairs in depth. This method was used by us for pairs with energy ≥ 3 Bev. The measurement results are given in Column 6 of Table IV.

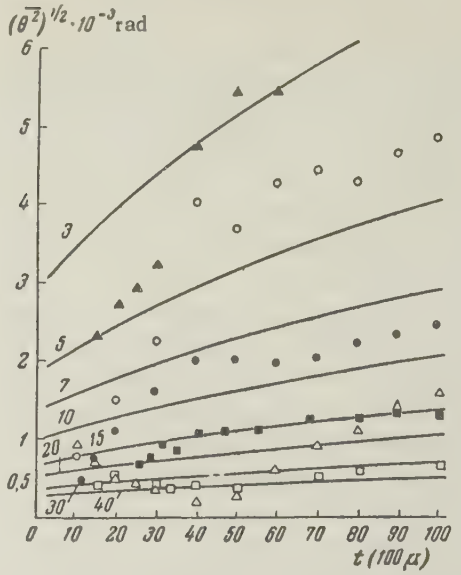

Fig. 6. Rms angle between the electron and positron of a pair as a function of the distance t to the point of pair production. ○ – pair No. 1, ■ – pair No. 2, □ – pair No. 3, ● – pair No. 4, △ – pair No. 6, ▲ – pair No. 9. Numbers on the curves represent Bev.

From the energy distribution of the γ-quanta it is possible to determine the average energy of the π^0 mesons, $\bar{E}_{\pi^0} \approx 2\bar{E}_\gamma$. Calculation of the average energy of the π^0 mesons from Columns 3 and 5 of Table IV yields accordingly

$$\bar{E}_{\pi^0} = 24^{+18}_{-6} \text{ Bev and } \bar{E}_{\pi^0} = 15 \pm 3 \text{ Bev}.$$

The average energy of the charged shower particles is 9 ± 3 Bev. Assuming that all these particles are pions (and this is confirmed by the fact that $R \approx 0.5$), a comparison with the average energy of the π^0 mesons indicates that the estimate of the energy of the γ-quanta by method 1 gives a poorer agreement than that of method 2.

Obviously, the most reliable method for determining the energy of the pairs is the measurement of the mutliple Coulomb scattering of the electron and positron. Unfortunately, this method cannot always be applied. When the energy of the pair is

small (< 1 Bev), then, as a consequence of the considerable divergence angle of the electron and the positron, the length of the track is, as a rule, too short for the application of method 2. On the other hand, in the most cases, at electron energies > 30 Bev, measurement of the Coulomb scattering is impossible. Exceptions are pairs with tracks ≥ 4 cm long within the limits of the emulsion.

It is advisable to employ method 1 at energies < 1 Bev and method 3 at energies > 30 Bev.

A trident was formed 19,355μ from the start of pair No. 1. True tridents satisfy the following criterion[10]

$$\theta_i > \bar{\alpha}_i \quad i = 1, 2, 3,$$

where θ_i is the angle that the i-th electron track of the trident makes with the continuation of the primary track; $\bar{\alpha}_i$ is the average angle of multiple scattering (including the Coulomb and all other types of scattering) of the i-th electron. It follows from Table V that this criterion is satisfied here.

On the other hand, according to the plot obtained by Kaplan and Koshiba,[10] the probability that this is a bremsstrahlung pair, less than 0.2μ away from the primary electron track, is nearly 8%. These circumstances make it possible to assert that the trident is a true one. The total length of all electron tracks in the reviewed band is 25 cm. Consequently, the average length of formation of the trident at an energy of 6 Bev is on the order of 25 cm, which is in agreement with the Bhabha theory.[14]

[1] P. H. Fowler and C. S. Waddington, Phil. Mag. **1**, 637 (1956).

[2] Dilworth, Coldsak, et al., Nuovo cimento **10**, 1261 (1953).

[3] L. D. Landau, Izv. Akad. Nauk SSSR, ser. fiz. **17**, 51 (1953).

[4] W. Heisenberg, Kosmische Strahlung, Springer, Berlin-Göttingen-Heidelberg, 1953, p. 563.

[5] I. V. Dunin-Barkovskii and N. V. Smirnov, Теория вероятностей и математическая статистика в технике (Theory of Probability and Mathematical Statistics in Engineering), GITTL, 1955.

[6] A. Vatagin, Nuovo cimento **4**, 154 (1956).

[7] Zh. S. Takibaev, Вестн. АН КазССР (Bulletin, Acad. Sci. Kazakh SSR) (in press).

[8] Zh. S. Takibaev, Вестн. АН КазССР (Bulletin, Acad. Sci. Kazakh SSR) **1**, 142 (1957).

[9] Brisbout, Danavaki, Engler, Fujimoto, and Perkins, Phil. Mag. **1**, 605 (1956).

[10] M. Koshiba and M. F. Kaplan, Phys. Rev. **97**, 193 (1955).

[11] Bradt, Kaplan, and Peters, Helv. Phys. Acta **23**, 24 (1950).

[12] E. Lohrmann, Nuovo cimento **2**, 1029 (1955).

[13] M. Stearns, Phys. Rev. **76**, 836 (1949).

[14] J. Bhabha, Proc. Roy. Soc. **A152**, 559 (1935).

Translated by J. G. Adashko
120

SOVIET PHYSICS JETP VOLUME 34 (7), NUMBER 3 SEPTEMBER, 1958

GENERAL COVARIANT EQUATIONS FOR FIELDS OF ARBITRARY SPIN

DUAN' I-SHI

Joint Institute for Nuclear Research

Submitted to JETP editor July 12, 1957

J. Exptl. Theoret. Phys. (U.S.S.R.) 34, 632-636 (March, 1958)

The Gel'fand-Iaglom field equations are extended to the general theory of relativity.

To obtain a generalized wave equation for a field in general covariant form, one must define covariant differentiation of a generalized wave function describing particles with arbitrary spin. Gel'fand and Iaglom,[1] Dirac,[2] and Fierz and Pauli[3] have studied the generalized wave equation in the special theory of relativity. In the present article, their theory is extended to the general covariant form.

1. SEMIMETRICS AND SEMIMETRIC REPRESENTATION

We introduce the metric g_{ik} in space-time with the aid of the asymmetric matrix $\|\lambda_{i(\alpha)}\|$

according to[4]

$$g_{ik} = \lambda_{i(\alpha)} \lambda_{k(\alpha)}, \quad \| \lambda_{i(\alpha)} \|^2 = \| g_{ik} \|. \tag{1}$$

Formally $\lambda_{i(\alpha)}$ may be thought of as half the metric g_{ik}. We shall call it the semimetric, and the representation shall be called the semimetric representation. The metric g_{ik} remains invariant if the semimetric $\lambda_{i(\alpha)}$ is subjected to the orthogonal transformation

$$\lambda'_{i(\alpha)} = L_{(\alpha\beta)} \lambda_{i(\beta)}, \tag{2}$$

where $\| L_{(\alpha\beta)} \|$ is an orthogonal matrix, which means that

$$L_{(\alpha\beta)} L_{(\alpha\gamma)} = \delta_{(\beta\gamma)}. \tag{3}$$

This is easily seen from (2) and (3), according to which

$$g'_{ik} = \lambda'_{i(\alpha)} \lambda'_{k(\alpha)} = \lambda_{i(\alpha)} \lambda_{k(\alpha)} = g_{ik}. \tag{4}$$

Therefore all the equations of the general theory of relativity must remain invariant with respect to two transformation groups, namely, (a) the group of general transformations of all coordinates of the form

$$x'^i = f^i (x^1, x^2, x^3, x^4), \tag{5}$$

and (b) the group of orthogonal transformations of the elements of the semimetric matrix

$$\lambda'_{i(\alpha)} = L_{(\alpha, \beta)} \lambda_{i(\beta)}. \tag{6}$$

According to Eq. (1)

$$| \operatorname{Det} \lambda_{i(\alpha)} | = + \sqrt{\operatorname{Det} g_{ik}} \neq 0. \tag{7}$$

Denoting the elements of the inverse matrix $\| \lambda_{i(\alpha)} \|^{-1}$ by $\lambda^i_{(\alpha)}$, we have

$$\lambda^i_{(\alpha)} \lambda_{i(\beta)} = \delta_{(\alpha\beta)}; \quad \lambda^i_{(\alpha)} \lambda_{k(\alpha)} = \delta^i_k. \tag{8}$$

We define

$$dx_{(\alpha)} = \lambda_{i(\alpha)} \, dx^i, \quad dx^i = \lambda^i_{(\alpha)} \, dx_{(\alpha)}. \tag{9}$$

We shall call these new coordinates $x_{(\alpha)}$ the semimetric coordinates. From (8) and (1) it follows that

$$ds^2 = g_{ik} \, dx^i \, dx^k = dx_{(\alpha)} \, dx_{(\alpha)}. \tag{10}$$

This means that in semimetric space the element of length is given by a normal quadratic form and is invariant under the linear transformation

$$x'_{(\alpha)} = L_{(\alpha\beta)} x_{(\beta)}. \tag{11}$$

From (9) we obtain

$$\lambda_{i(\alpha)} = \partial x_{(\alpha)} / \partial x^i, \quad \lambda^i_{(\alpha)} = \partial x^i / \partial x_{(\alpha)}. \tag{12}$$

It follows from (11) that

$$\frac{\partial \varphi}{\partial x_{(\alpha)}} = \frac{\partial \varphi}{\partial x^i} \frac{\partial x^i}{\partial x_{(\alpha)}} = \lambda^i_{(\alpha)} \frac{\partial \varphi}{\partial x^i},$$

so that

$$\lambda^i_{(\alpha)} \partial / \partial x^i \to \partial / \partial x_{(\alpha)}. \tag{13}$$

2. COVARIANT DERIVATIVE OF A GENERALIZED FIELD FUNCTION

Let us introduce an n-dimensional matrix vector in semimetric space, whose components $L_{(\alpha)}$ form a set of n Hermitian matrices satisfying the condition

$$[L_{(\alpha)}, \; I_{(\beta\gamma)}]_- = \delta_{(\alpha\beta)} L_{(\gamma)} - \delta_{(\alpha\gamma)} L_{(\beta)}, \tag{14}$$

where $I_{(\alpha\beta)}$ is an infinitesimal operator of a representation of the group of linear transformations of Eq. (11). These infinitesimal operators satisfy the commutation rules

$$[I_{(\alpha\beta)}, \; I_{(\gamma\delta)}]_- = \delta_{(\alpha\gamma)} I_{(\beta\delta)} + \delta_{(\beta\delta)} I_{(\alpha\gamma)} - \delta_{(\alpha\delta)} I_{(\beta\gamma)} - \delta_{(\beta\gamma)} I_{(\alpha\delta)}. \tag{15}$$

We shall denote the contravariant and covariant components of this matrix vector in Riemannian space by

$$L^i = \lambda^i_{(\alpha)} L_{(\alpha)}; \quad L_i = \lambda_{i(\alpha)} L_{(\alpha)}. \tag{16}$$

Writing

$$I_{ij} = \lambda_{i(\beta)} \lambda_{j(\gamma)} I_{(\beta\gamma)},$$

we can readily obtain from (14), (15), and (1) the relations

$$[L_i, \; I_{jk}]_- = g_{ij} L_k - g_{ik} L_j; \tag{17}$$

$$[I_{ij, kl}]_- = g_{ik} I_{jl} + g_{jl} I_{ik} - g_{il} I_{jk} - g_{jk} I_{il}. \tag{18}$$

Two complex generalized field functions ψ and $\bar{\psi}$ are called adjoint functions if the n Hermitian forms

$$\bar{\psi} L_{(\alpha)} \psi$$

make up a vector in semimetric space. Under transformations of group (a)

$$\bar{\psi}' L_{(\gamma)} \psi' = \bar{\psi} L_{(\alpha)} \psi, \tag{19}$$

the components of these vectors remain invariant. Under the transformations of group (b), we have

$$\bar{\psi}' L_{(\alpha)} \psi' = L_{(\alpha\beta)} (\psi \, L_{(\beta)} \psi). \tag{20}$$

The generalized wave functions transform among themselves according to

$$\psi' = S\psi, \; \bar{\psi}' = \psi S^{-1}, \tag{21}$$

where S is a matrix which varies from point to point and is related to $\| L_{(\alpha\beta)} \|$ by

$$S L_{(\alpha)} S^{-1} = L_{(\alpha\beta)} L_{(\beta)}, \tag{22}$$

which follows from (20). In order to derive the covariant differentiation formula for a generalized field function, we must define the concept of parallel displacement. If two points x and x + dx are separated by an infinitesimal distance, the wave functions at these points are related by the infinitesimal linear transformations

$$\psi(x+dx) = [I + \Lambda_i\, dx^i]\,\psi(x),$$
$$\bar{\psi}(x+dx) = \bar{\psi}(x)\,[I - \Lambda_i\, dx^i], \qquad (23)$$

where Λ is a certain matrix.

If (23) is to define parallel displacement, the vector $\bar{\psi}L_{(\alpha)}\psi$, which is constructed of $\bar{\psi}$ and ψ, must undergo a parallel displacement, which means that

$$A_{(\alpha)}(x+dx) = \{\delta_{(\alpha\beta)} + \eta_{\sigma\,(\alpha\beta)}\,dx^\sigma\}\,A_{(\beta)}(x). \qquad (24)$$

From (23) and (24) it follows that

$$\bar{\psi}(x)\,[I - \Lambda_i\, dx^i]\,L_{(\alpha)}\,[I + \Lambda_i\, dx^i]\,\psi(x)$$
$$= \bar{\psi}L_{(\beta)}\,\psi\,[\delta_{(\alpha\beta)} + \eta_{i\,(\alpha\beta)}\,dx^i], \qquad (25)$$

where the $\eta_{i(\alpha\beta)}$ are the components of the affine connection, which have been given by Rumer.[4]

According to Eq. (25), the Λ_i are given by

$$L_{(\alpha)}\Lambda_i - \Lambda_i L_{(\alpha)} = \eta_{i(\alpha\beta)}L_{(\beta)}. \qquad (26)$$

Multiplying (26) by $\lambda^i_{(\delta)}$, we obtain

$$L_{(\alpha)}\Lambda_{(\delta)} - \Lambda_{(\delta)}L_{(\alpha)} = \eta_{(\delta\alpha\beta)}L_{(\beta)}, \text{where}\,\Lambda_{(\delta)} = \lambda^i_{(\delta)}\Lambda_i; \qquad (27)$$

where the $\eta_{(\alpha\beta\gamma)} = \lambda^i_{(\alpha)}\eta_{i(\beta\gamma)}$ are the Ricci curvature coefficients.[5]

The general solution of Eq. (27) will be

$$\Lambda_i = {}^1/_2\,\eta_{i(\alpha\beta)}\,I_{(\alpha\beta)} + if_i I, \qquad (28)$$

where the f_i are arbitrary functions. This is easily seen by making use of (14).

Writing $f_{(\alpha)} = \lambda^i_{(\alpha)}f_i$, we obtain

$$\Lambda_{(\delta)} = {}^1/_2\,\eta_{(\delta\alpha\beta)}I_{(\alpha\beta)} + if_{(\delta)}I. \qquad (29)$$

Thus the covariant derivative of a generalized field function will be

$$\nabla_i\psi = \partial\psi/\partial x^i - \Lambda_i\psi, \quad \nabla_i\bar{\psi} = \partial\bar{\psi}/\partial x^i + \bar{\psi}\Lambda_i \qquad (30)$$

and in semimetric space

$$\nabla_{(\alpha)}\psi = \partial\psi/\partial x_{(\alpha)} - \Lambda_{(\alpha)}\psi, \quad \nabla_{(\alpha)}\bar{\psi} = \partial\bar{\psi}/\partial x_{(\alpha)} + \bar{\psi}\Lambda_{(\alpha)}. \qquad (31)$$

3. EXTENSION OF THE GEL'FAND-IAGLOM FIELD EQUATIONS TO THE GENERAL THEORY OF RELATIVITY

The covariant field equations for arbitrary spin were obtained in the special theory of relativity by Gel'fand and Iaglom,[1] and are of the form

$$L^k\,\partial\psi/\partial x^k + m\psi = 0, \qquad (32)$$

where ψ is a generalized field function describing particles with arbitrary spin, and the L^k are matrices which determine the linear transformation properties of the ψ function.

In order that Eqs. (32) become covariant with respect to all physically possible transformations, the ordinary derivatives $\partial\psi/\partial x^k$ which appear in them must be replaced by covariant derivatives $\nabla_k\psi$. Then the general covariant field equations will be

$$L^k\nabla_k\psi + m\psi = 0. \qquad (33)$$

Inserting (30) into (33) and using (28), we obtain

$$L^k\,\partial\psi/\partial x^k + m\psi - {}^1/_2 L^k\eta_{k(\beta\gamma)}I_{(\beta\gamma)}\psi = 0, \qquad (34)$$

where the L^k are matrix functions satisfying Eqs. (17). From (13), (16), and (34) one can obtain the general covariant field equations in semimetric space, namely

$$L_{(\alpha)}\,\partial\psi/\partial x_{(\alpha)} + m\psi - {}^1/_2\,\eta_{(\alpha\beta\gamma)}L_{(\alpha)}I_{(\beta\gamma)}\psi = 0, \qquad (35)$$

where the $L_{(\alpha)}$ satisfy relations (14). If $L_{(\alpha)} = \gamma_{(\alpha)}$, where the $\gamma_{(\alpha)}$ are Dirac matrices, then

$$I_{(\alpha\beta)} = {}^1/_2\,[\gamma_{(\alpha)}\gamma_{(\beta)} - \gamma_{(\beta)}\gamma_{(\alpha)}], \qquad (36)$$

and (34) become the general covariant Dirac equation

$$\gamma_{(\alpha)}\,\partial\psi/\partial x_{(\alpha)} + m\psi - {}^1/_4\,\gamma_{(\alpha)}\gamma_{(\beta)}\gamma_{(\gamma)}\eta_{(\alpha\beta\gamma)}\psi = 0, \qquad (37)$$

a special case of (34) which has been previously obtained by Fock and Ivanenko.[6] This shows that Eqs. (34) and (35) are of greater generality. The general covariant Lagrangian is in this case

$$L = {}^1/_2\left\{\bar{\psi}L^k\left(\frac{\partial\psi}{\partial x^k} - \Lambda_k\psi\right) - \left(\frac{\partial\bar{\psi}}{\partial x^k} + \Lambda_k\bar{\psi}\right)L^k\psi + 2m\bar{\psi}\psi\right\}. \qquad (38)$$

If (38) is substituted into Euler's equation, one easily obtains Eq. (34). Further, it is easily shown that the symmetric energy-momentum tensor and the current vector in general covariant form can be written, respectively,

$$T_{ik} = {}^1/_2\,\bar{\psi}L_k\nabla_i\psi + \bar{\psi}L_i\nabla_k\psi - \nabla_i\bar{\psi}L_k\psi - \nabla_k\bar{\psi}L_i\psi], \qquad (39)$$

$$j^k = ie\bar{\psi}L^k\psi. \qquad (40)$$

It should be noted that the field equations (35), as opposed to those of the special theory of relativity, contain the additional operator terms

$$\delta\hat{m} = {}^1/_2\,\eta_{(\alpha\beta\gamma)}L_{(\alpha)}I_{(\beta\gamma)},$$

acting on the spinor or tensor fields. These operators may therefore be treated as mass operators entering the theory in a natural way. They

are not introduced artificially or without any reasonable basis, as is done in many works on ordinary quantum field theory. One may hope that these operators will make it possible to eliminate the difficulties associated with divergences in field theory.

In conclusion, I express my gratitude to Professor Iu. M. Shirokov for discussing the results of the present work.

[1] I. M. Gel'fand and A. D. Iaglom, J. Exptl. Theoret. Phys. (U.S.S.R.) **18**, 703 (1948).

[2] P. A. M. Dirac, Proc. Roy. Soc. (London) **A155**, 117 (1939) [sic! Probably ... **A155**, 447 (1936)].

[3] M. Fierz and W. Pauli, Proc. Roy. Soc. (London) **A173**, 211 (1939).

[4] Iu. Rumer, J. Exptl. Theoret. Phys. (U.S.S.R.) **2**, 271 (1953).

[5] L. Eisenhart, Riemannian Geometry (Russ. Transl.), 1948.

[6] V. A. Fock and D. D. Ivanenko, Z. Physik **30**, 678 (1929).

Translated by E. J. Saletan
121

SOVIET PHYSICS JETP VOLUME 34 (7), NUMBER 3 SEPTEMBER, 1958

CIRCULAR WAVES IN AN ELECTRON-ION BEAM

R. V. POLOVIN and N. L. TSINTSADZE

Submitted to JETP editor July 31, 1957

J. Exptl. Theoret. Phys. (U.S.S.R.) **34**, 637-642 (March, 1958)

We consider circular waves in an uncompensated electron-ion beam in a cylindrical waveguide with perfectly conducting walls. The magnetic field produced by the beam current is assumed to be very strong. We treat the problem qualitatively, without an exact solution of the differential equations. It is shown that the beam is stable with respect to the oscillations being considered, and the natural frequency bands are found. The electromagnetic field is mapped.

1. The stationary state of an electron-ion beam has been examined by Bennett[1] and Budker.[2]

In the present article we consider the oscillations of an electron-ion beam in a cylindrical waveguide of radius R. We shall treat circular oscillations, which means that we assume the electromagnetic field, as well as the electron and ion densities and velocities, to be independent of z, and the dependence of these quantities on r, φ, and the time t to be given by

$$F(r, \varphi, t) = f(r)\, e^{i(\omega t - \mu\varphi)}. \qquad (1)$$

The conclusions we reach can be extended to perturbations of a more general form, namely

$$F(r, \varphi, z, t) = f(r)\, e^{i(\omega t - \mu\varphi - \gamma z)},$$

so long as the condition $\gamma R \ll 1$ is satisfied.

The amplitude of vibrations is considered small, and the equations are linearized. The problem is solved in the hydrodynamic approximation; the electrons and ions have different temperatures, which are constant in space and time.

We assume also that the magnetic field produced by the beam current is so strong that the inequalities

$$|eH_{\varphi 0}(r)/mc\omega| \gg 1, \quad |eH_{\varphi 0}(r)/Mc\omega| \gg 1 \qquad (2)$$

are fulfilled at all points within the waveguide. Here $H_{\varphi 0}(r)$ is the magnetic field strength, ω is the frequency

$$m = m_0/\sqrt{1-\beta_e^2},\ M = M_0/\sqrt{1-\beta_i^2};\ \beta_e = v_{0e}/c,\ \beta_i = v_{0i}/c,$$

m_0 and M_0 are the electron and ion rest masses, and v_{0e} and v_{0i} are the electron and ion velocities in the stationary state. Since we are dealing with a strong magnetic field, the variable components v_{er}, v_{ez}, v_{ir}, and v_{iz} of the electron and ion velocities are small.

We shall show below that the beam is stable with respect to the oscillations we are considering, and

that the μth natural frequency lies in the interval $\mu v_{iT}/R < \omega < \mu c/R$, where v_{iT} is the thermal velocity of the ions, given by $v_{iT} = \sqrt{T_i/M}$. Here T_i is the ion temperature in energy units. The thermal velocity of the ions is assumed to be less than that of the electrons, given by $v_{eT} = \sqrt{T_e/m}$.

We shall show also that at the distance $r = \mu v_{iT}/\omega$ from the beam axis the vibration amplitude of the ions has a sharp maximum. This occurs because at this radius the thermal velocity of the ions and the phase velocity of the wave are equal. A similar resonance takes place for electrons at $r = \mu v_{eT}/\omega$, so long as this value of r lies in the interval $0 < r < R$.

2. In the stationary state the electron and ion densities n_{0e} and n_{0i}, the magnetic field $H_{\varphi 0}$, and the electric field E_{r0} are of the form[1,2]

$$\begin{aligned} n_{0e}(r) &= 2[T_e(1-\beta_i^2) \\ &+ T_i(1-\beta_i\beta_e)]/\pi e^2(\beta_e-\beta_i)^2 r_0^2(1+r^2/r_0^2)^2, \\ n_{0i}(r) &= 2[T_i(1-\beta_e^2) \\ &+ T_e(1-\beta_e\beta_i)]/\pi e^2(\beta_e-\beta_i)^2 r_0^2(1+r^2/r_0^2)^2, \\ H_{\varphi 0}(r) &= 2\pi e[n_{0i}(0)\beta_i - n_{0e}(0)\beta_e]\, r/(1+r^2/r_0^2), \\ E_{r0}(r) &= 2\pi e[n_{0i}(0) - n_{0e}(0)]\, r/(1+r^2/r_0^2), \end{aligned} \tag{3}$$

where r_0 is the effective radius of the beam. All the other components of the electric and magnetic fields vanish. If the beam axis is made to coincide with the axis of the waveguide, Eqs. (3) for the electric and magnetic fields satisfy the boundary conditions $\mathbf{E} \times \mathbf{n} = 0$ and $\mathbf{H} \cdot \mathbf{n} = 0$ on the surface of the waveguide. Therefore the state of the electron-ion beam will not change if it is in a cylindrical waveguide of any radius R whatsoever.

If we use $\mathbf{E}$ and $\mathbf{H}$ to denote the variable parts of the electric and magnetic fields, and $v_{e\varphi}$, $v_{i\varphi}$, n_e, and n_i to denote the variable components of the electron and ion velocities and densities, then Maxwell's equations, the equations of motion, and the continuity equations become (the constant components cancel out)

$$\begin{aligned} -\frac{\partial H_z}{\partial r} &= \frac{1}{c}\frac{\partial E_\varphi}{\partial t} - \frac{4\pi e}{c}(n_{0e}+n_e)v_{e\varphi} + \frac{4\pi e}{c}(n_{0i}+n_i)v_{i\varphi}, \\ \frac{\partial(rE_\varphi)}{r\,\partial r} - \frac{\partial E_r}{r\partial\varphi} &= -\frac{1}{c}\frac{\partial H_z}{\partial t}, \quad \frac{\partial(rE_r)}{r\partial r} + \frac{\partial E_\varphi}{r\partial\varphi} = 4\pi e(n_i - n_e). \\ m\left(\frac{\partial v_{e\varphi}}{\partial t} + v_{e\varphi}\frac{\partial v_{e\varphi}}{r\partial\varphi}\right) &= -eE_\varphi - \frac{T_e}{n_{0e}+n_e}\frac{\partial(n_{0e}+n_e)}{r\partial\varphi}, \\ M\left(\frac{\partial v_{i\varphi}}{\partial t} + v_{i\varphi}\frac{\partial v_{i\varphi}}{r\partial\varphi}\right) &= eE_\varphi - \frac{T_i}{n_{0i}+n_i}\frac{\partial(n_{0i}+n_i)}{r\partial\varphi}, \\ \frac{\partial n_e}{\partial t} + \frac{\partial[(n_{0e}+n_e)v_{e\varphi}]}{r\partial\varphi} &= 0, \quad \frac{\partial n_i}{\partial t} + \frac{\partial[(n_{0i}+n_i)v_{i\varphi}]}{r\partial\varphi} = 0, \\ H_r = H_\varphi &= E_z = 0. \end{aligned} \tag{4}$$

In the continuity equations we have dropped terms containing v_{er} and v_{ir}, since they are small compared with $v_{e\varphi}$ and $v_{i\varphi}$. We shall not write out those equations which contain products of a large quantity $H_{\varphi 0}$, n_{0e}, or n_{0i} by a small one v_{0r}, v_{ez}, v_{ir}, or v_{iz}. These equations can be used to determine the velocities v_{er}, v_{ez}, v_{ir}, and v_{iz} in the second approximation.

When we linearize Eqs. (4) and make use of (1), we arrive at

$$-\frac{dH_z}{dr} = \frac{i\omega}{c}E_\varphi - \frac{4\pi e n_{0e}}{c}v_{e\varphi} + \frac{4\pi e n_{0i}}{c}v_{i\varphi}, \tag{5}$$

$$\frac{d(rE_\varphi)}{r\,dr} + \frac{i\mu}{r}E_r = -\frac{i\omega}{c}H_z, \tag{6}$$

$$\frac{d(rE_r)}{rdr} - \frac{i\mu}{r}E_\varphi = 4\pi e(n_i - n_e), \tag{7}$$

$$im\omega v_{e\varphi} = -eE_\varphi + i\mu T_e n_e/n_{0e}r, \tag{8}$$

$$iM\omega v_{i\varphi} = eE_\varphi + i\mu T_i n_i/n_{0i}r, \tag{9}$$

$$\omega n_e = (\mu/r)\, n_{0e} v_{e\varphi}, \tag{10}$$

$$\omega n_i = (\mu/r)\, n_{0i} v_{i\varphi}. \tag{11}$$

From these equations we eliminate the electron and ion densities, obtaining

$$\begin{aligned} v_{e\varphi} &= i\omega r^2 eE_\varphi/(\omega^2 r^2 - \mu^2 v_{eT}^2), \\ v_{i\varphi} &= -i\omega r^2 eE_\varphi/(\omega^2 r^2 - \mu^2 v_{iT}^2). \end{aligned} \tag{12}$$

Inserting (12) into Eqs. (5) — (7), we arrive at

$$\begin{aligned} -dH_z/dr &= (i\omega/c)\, q(r)\, E_\varphi, \\ d(rE_r)/dr &= i\mu q(r)\, E_\varphi, \end{aligned} \tag{13}$$

where

$$\begin{aligned} q(r) &= 1 + \Omega_e^2(r)\, r^2/(\mu^2 v_{eT}^2 - \omega^2 r^2) \\ &+ \Omega_i^2(r)\, r^2/(\mu^2 v_{iT}^2 - \omega^2 r^2), \end{aligned} \tag{14}$$

$$\Omega_e^2(r) = 4\pi e^2 n_{0e}(r)/m, \quad \Omega_i^2 = 4\pi e^2 n_{0i}(r)/M. \tag{15}$$

Eliminating $q(r)$ from (13), and integrating over r we have

$$E_r = -(\mu c/\omega r)\, H_z.$$

Inserting this expression into (6), we have

$$H_z = -\frac{i\omega c r}{\mu^2 c^2 - \omega^2 r^2}\frac{d(rE_\varphi)}{dr}. \tag{16}$$

Finally, eliminating E_r and H_z from (6), (15), and (16), we obtain the differential equation

$$\frac{d}{dr}\left[p(r)\frac{d(rE_\varphi)}{dr}\right] - q(r)E_\varphi = 0, \quad p(r) = \frac{c^2 r}{\mu^2 c^2 - \omega^2 r^2} \tag{17}$$

for E_φ, with the boundary conditions[3]

$$\begin{aligned} &E_\varphi(0) \text{ finite}, \quad E_\varphi(R) = 0 \quad \text{if} \quad \mu = 1, \\ &E_\varphi(0) = 0, \qquad E_\varphi(R) = 0 \quad \text{if} \quad \mu \geqslant 2. \end{aligned} \tag{18}$$

The frequency ω is an eigenvalue of the differential operator of Eq. (17) with the boundary con-

ditions (18).

We note that $E_\varphi(r)$ must not only satisfy the boundary conditions (18), but must also be finite in the interval $0 \le r \le R$. In addition, $v_{e\varphi}(r)$, $v_{i\varphi}(r)$, and $H_z(r)$, which are related to $E_\varphi(r)$ by (12) and (16), must also be finite in this interval.

If all the eigenvalues ω are real, the beam is stable. If, however, one or more of the eigenvalues are complex, the beam is unstable.

Since Eq. (17) cannot be solved exactly, we shall treat it in a qualitative way.

We shall first show that ω is always real. Let us assume the contrary, writing $\omega = \omega_0 + i\eta$, where $\eta \neq 0$. Then the imaginary parts of p and q are given by

$$\operatorname{Im} p = 2c^2 r\omega_0\eta/\{[\mu^2c^2 - (\omega_0^2 - \eta^2)\, r^2]^2 + 4\omega_0^2\eta^2 r^4\},$$

$$\operatorname{Im} q = \frac{2\Omega_e^2 r\omega_0\eta}{[\mu^2 v_{eT}^2 - (\omega_0^2 - \eta^2)\, r^2]^2 + 4\omega_0^2\eta^2 r^2} + \frac{2\Omega_i^2 r\omega_0\eta}{[\mu^2 v_{iT}^2 - (\omega_0^2 - \eta^2)\, r^2]^2 + 4\omega_0^2\eta^2 r^4},$$

from which it follows that Im p and Im q always have the same sign.

We may, on the other hand, by introducing the new variable $u = rE_\varphi$, write (17) in the form

$$(pu')' - qu/r = 0 \tag{19}$$

with the boundary conditions

$$u(0) = u(R) = 0. \tag{20}$$

Multiplying (19) by u^*, the complex conjugate of u, integrating over r from zero to R, and then taking the imaginary part, we arrive at

$$\int_0^R \operatorname{Im} p\, |u'|^2\, dr + \int_0^R \operatorname{Im} q\, |u|^2\, dr = 0. \tag{21}$$

Since $|u'|^2$ and $|u|^2$ are both positive, this equation cannot hold if Im p and Im q have the same signs. Thus all the eigenvalues ω are real, and the beam is stable with respect to the oscillations under consideration.

To examine (17) further, let us eliminate from it the first derivative. To do this, we make the substitution

$$y = cr\sqrt{r}\, E_\varphi/\sqrt{\mu^2c^2 - \omega^2 r^2}. \tag{22}$$

Then (17) becomes

$$d^2y/dr^2 + Q(r)\, y = 0, \tag{23}$$

where

$$Q(r) = \frac{\mu^4c^4 - 10\mu^2c^2\omega^2r^2 - 3\omega^4r^4}{4r^2(\mu^2c^2 - \omega^2r^2)^2} - \frac{\mu^2c^2 - \omega^2r^2}{c^2r^2}\, q(r); \tag{24}$$

q(r) is given by (14), and y(r) satisfies the boundary conditions

$$y(0) = y(R) = 0. \tag{25}$$

We shall first show that the frequencies ω are no greater than $\mu c/R$. To this end, let us consider the behavior of $E_\varphi(r)$, $v_{i\varphi}(r)$, $v_{e\varphi}(r)$, and $H_z(r)$ in the interval $0 \le r \le R$. Equation (23) has four singular points, namely $r = 0$, $\mu \times v_{iT}/\omega$, $\mu v_{eT}/\omega$, and $\mu c/\omega$. It can be shown that $E_\varphi(r)$, since it satisfies the boundary conditions (18), remains finite at these points. Expressions (12) and (16) show, however, that at $r = \mu v_{iT}/\omega$ and $r = \mu v_{eT}/\omega$ the velocities $v_{i\varphi}$ and $v_{e\varphi}$, respectively, become infinite, and that at $r = \mu c/\omega$ the magnetic field H_z becomes infinite.

The first two infinities are fictitious because the linearization of (27) in the neighborhoods of $r = \mu v_{iT}/\omega$ and $r = \mu v_{eT}/\omega$ is invalid. To show this, consider the nonlinear equations (4). We shall attempt to find a solution of these equations in which the desired functions contain the time t and the angle φ only in the combination $\xi = \omega t - \mu\varphi$. It follows from Eqs. (4) that at $r = \mu \times v_{iT}/\omega$

$$2v_{i\varphi}\, dv_{i\varphi}/d\xi = -(ev_{iT}/M\omega)\, E_\varphi. \tag{26}$$

This equation indicates that $v_{i\varphi}$ is of the same order as $\sqrt{E_\varphi}$. Since E_φ is small, $v_{i\varphi}$ is also small, but of lower order. In the linear approximation this means that $v_{i\varphi}$ becomes infinite if E_φ remains finite. Thus at the point $r = \mu \times v_{iT}/\omega$ the amplitude of the ion vibrations increases sharply. At the point $r = \mu v_{eT}/\omega$ there will take place a similar resonance in the electron vibrations.

As for the point $r = \mu c/\omega$, the magnetic field H_z remains infinite at this point also in the nonlinear theory. Indeed, were we to repeat the operations which led to (16), this time on the nonlinear equations (4), we would obtain

$$\frac{\partial H_z}{\partial \xi} = \frac{\omega c r}{\mu^2c^2 - \omega^2r^2}\, \frac{\partial (rE_\varphi)}{\partial r},$$

for which it follows that H_z becomes infinite at $r = \mu c/\omega$. It can also be shown that this infinity is not removed when one takes account of collisions.

It follows from this that the point $r = \mu c/\omega$ must lie outside the interval $0 \le r \le R$. In other words, it is necessary that

$$\omega < \mu c/R.$$

This inequality determines the upper bound of the eigenvalues ω.

In order to find the lower bound, we note that $Q(r)$, the function given by (24), will be negative over the whole interval $0 \leq r \leq R$ if $\omega < \mu \times v_{iT}/R$. As is known,[4] however, Eq. (23) has no solutions satisfying conditions (25) if $Q(r)$ is negative. It is therefore necessary that $\omega > \mu \times v_{iT}/R$.

We have thus proven that the eigenvalues ω cannot be complex and must lie in the interval $\mu v_{iT}/R < \omega < \mu c/R$. In the process we have assumed the existence of eigenvalues of the operator of (23) with boundary conditions (25). In other words, we have assumed that circular waves can actually exist. In order to prove the last statement, we note that as $\omega \to \mu v_{iT}/R + 0$, the function $Q(r) \to +\infty$. From this it follows that there exists an infinite number of eigenvalues.[4]

The inequality $\omega < \mu c/R$ indicates that circular waves have low frequencies, which means that they are not magnetohydrodynamic.[5,6] We note that at the resonance point $r = \mu v_{iT}/\omega$, the phase velocity of the wave is $V = r\omega/\mu$, whose form is reminiscent of the Alfven velocity[7]

$$V = H_{\varphi 0}\left[\frac{n_{0e}(1-\beta_e\beta_i) - n_{0i}(1-\beta_i^2)}{4\pi M (n_{0i}\beta_i - n_{0e}\beta_e)^2}\,\frac{r_0^2}{2r^2}\right]^{1/2}.$$

Let us go on, finally, to the mapping of the field. From the form of $p(r)$ and $q(r)$ in Eq. (17) it follows that an expansion of $E_\varphi(r)$ in powers of r contains only even powers when $\mu = 1$. Therefore $E'_\varphi(0) = 0$. In order to find the behavior of $E_\varphi(r)$ in the neighborhood of $r = \mu v_{iT}/\omega$, let us make use of (23). Since $Q(r) \to -\infty$ as $r \to \mu v_{iT}/\omega - 0$, and $Q(r) \to +\infty$ as $r \to (\mu v_{iT}/\omega) + 0$, the r dependence of y [and therefore also the function $E_\varphi(r)$] is of the form shown in Fig. 1 (when $\mu v_{eT}/\omega < R$).

When $\mu v_{eT}/\omega > R$, the graph of $E_\varphi(r)$ is of the form shown in Fig. 2. Both of these graphs are for $\mu = 1$. Figures 1 and 2 show those eigen-

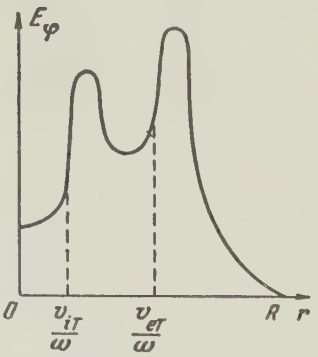

Fig. 1.

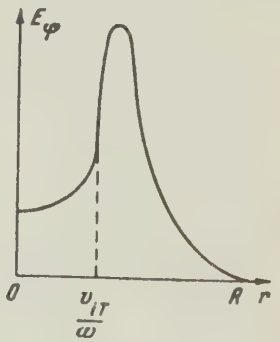

Fig. 2.

functions of the operator of (17) which belong to the largest eigenvalue ω. It can be shown that these functions have no zeros within the interval $0 < r < R$.

In conclusion, the author expresses his gratitude to Professors A. I. Akhiezer and Ia. B. Fainberg for aid in the work, and to G. Ia. Liubarskii for discussion.

[1] W. H. Bennett, Phys. Rev. **45**, 890 (1934); **98**, 1584 (1955).

[2] G. I. Budker, Атомная энергия (Atomic Energy) **5**, 9 (1956).

[3] Louis de Broglie, Electromagnetic Waves in Waveguides and Cavity Resonators (Russ. Transl.), GITTL, M. 1952.

[4] D. Sansone, Ordinary Differential Equations, (Russ. Transl.), IIL, M. 1954, Vol. 1.

[5] Al'pert, Ginzburg, and Feinberg, Распространение радиоволн (Propagation of Radio Waves), GITTL, M. 1953.

[6] L. Spitzer, Physics of Fully Ionized Gases, (Interscience, New York, 1956).

[7] H. Alfvén, Cosmical Electrodynamics, London, 1950.

Translated by E. J. Saletan
122

DEPENDENCE OF THE ALPHA-DECAY RATE ON THE ENERGY OF THE ROTATIONAL LEVELS

L. L. GOL'DIN

Submitted to JETP editor September 6, 1957

J. Exptl. Theoret. Phys. (U.S.S.R.) 34, 643-645 (March, 1958)

It is possible to separate the dependence of the probability of the α-decay on the energy and on the angular momentum carried off by the α-particle by investigating the α-decay of spin $\frac{1}{2}$ nuclei in transitions to the levels of a rotational band with $K = \frac{1}{2}$. It is shown by analyzing the case of Pu^{239} that the dependence of the α-decay on the energy for levels belonging to a particular rotational band is given by the same formula which describes the α-decay of even-even nuclei in ground state transitions.

THE energy dependence of the probability of an α-decay which leaves the daughter nucleus in its ground state is given by the Geiger-Nuttal law. It is usually given in the form

$$\log_{10}\lambda = C - D/\sqrt{E}, \qquad (1)$$

where λ is the probability of the α-decay, E is the energy of the emitted α-particles, and C and D are quantities which depend only very weakly on the atomic number Z and are the same for all isotopes of a particular element. Equation (1) was first established empirically. Later it was derived from the theory of the α-decay. The constants C and D are usually determined from experimental data. They have been tabulated by several authors (Refs. 1, 2; see also Ref. 3).

Equation (1) describes particularly well the ground state α-decays of even-even nuclei. Here the spins and parities of parent and daughter nuclei are the same, and the α-decay does not entail a reshuffling of the nucleus. For example, the probabilities of the α-decay of the nuclei Pu^{236}, Pu^{238}, Pu^{240}, and Pu^{242} are 2.4, 76, 7.6×10^3 and 4.0×10^5 years respectively, if calculated with (1); the experimental values are 2.7, 89.6, 6.58×10^3, and 3.76×10^5 years respectively. We used the values C = 53.35 and D = 147.4 (E in Mev) which according to Ref. 1 should hold for Z = 94. Thus formula (1) gives the probabilities of the α-decay of even-even nuclei with an approximate accuracy of 10%.

In odd nuclei, the observed probabilities of α-decay usually turn out to be appreciably smaller than those given by (1). This is evidently due to the change in the nucleon configuration which takes place in general in the α-decay of odd nuclei.

It would be natural to consider the branching ratio of the α-decay to the different levels of a rotational band.

It is well known that Eq. (1) gives too high values of λ for transitions to higher rotational levels. This is to be expected since the corresponding α-particles not only have a smaller energy, but also carry off a certain angular momentum. The probability λ of the α-decay there has to be not only a function of the level energy E, but also of l. For small changes of E and l one can use a series expansion:

$$\log_{10}\lambda(E, l) = \log_{10}\lambda(E_0, 0) + A(E - E_0) + Bl(l+1) + \ldots, \qquad (2)$$

It is interesting to ascertain: (i) up to which energies and angular momenta can (2) be used neglecting higher terms, and (ii) whether the energy-dependent part of (2) is equal to that of (1). It turns out that in general this question cannot be easily answered, since the dependence of λ on E cannot usually be separated from that on l. However, the case where the spin of the decaying nucleus equals $\frac{1}{2}$ can be solved at once. Here the levels of the daughter nucleus belong to the rotational band with $K = \frac{1}{2}$ (K is the projection of the angular momentum on the symmetry axis of the nucleus). It follows from kinematical considerations that a level of spin I can be reached if the α-particle carries off an angular momentum of either $I - \frac{1}{2}$ or $I + \frac{1}{2}$. Of these two possibilities, one is of necessity even and the other odd, and thus the wave function of the α-particle has to have even or odd parity. On the other hand, the parity of the wave function of the α-particle is uniquely given by the parity of the ground state of the parent nucleus and by the parity of the levels of the daughter nucleus belonging to the given rotational

α-Decay of Pu^{239} and Levels of U^{235}

Level No.	α-line	Energy of the α-particles (kev)	Energy of the levels (kev)	Intensity of the line (%)	Spin of the daughter nucleus	Angular momentum carried off by α-particle
I	α_0	5147	0	72	1/2	0
II	α_{13}	5134	13.2	16.8	3/2	2
III	α_{52}	5096	51.7	10.7	5/2	2
IV	α_{84}	5064	84	$3.7 \cdot 10^{-2}$	7/2	4
V	α_{151}	4991	151	$1.3 \cdot 10^{-2}$	9/2	4

band. Thus only one of the two possibilities, $I + \frac{1}{2}$ or $I - \frac{1}{2}$, can actually occur, namely that with the required parity. The rotational levels thus form doublets. The transitions to both members of the doublet involve the same angular momentum of the α-particle, and the branching ratio then depends only on the energy.

We consider the decay of Pu^{239}, which recently has been investigated by Novikova et al.[4] This nucleus has spin $\frac{1}{2}$. The experimental results from Ref. 4 are summarized in the table, in which all levels shown belong to the same rotational band with $K = \frac{1}{2}$.

We now shall compare Eq. (1) with the intensities of the α-decay to the levels of the doublet. The experimental ratios of the transition probabilities to the levels II and III and to the levels IV and V are

$$\lambda_{II}/\lambda_{III} = 1.57; \quad \lambda_{IV}/\lambda_V = 2.84.$$

Equation (1) yields for the same transitions

$$\lambda_{II}/\lambda_{III} = 1.75; \quad \lambda_{IV}/\lambda_V = 2.99.$$

Thus Eq. (1) gives the energy dependence of the α-decay in transitions to rotational levels with an accuracy not worse than for ground state transitions of even-even nuclei. The obtained results further show that in the expansion (2) second order terms, in particular, terms containing $[d(\log\lambda)/dE] \times \{d(\log\lambda)/d[\ell(\ell+1)]\}$ are not important for $\ell \leq 4$.

The small discrepancy between the calculated and the experimental ratios λ_i/λ_{i+1}, which is roughly the same in both cases, indicates that one should actually employ in (1) a slightly smaller value for D than given by Bohr et al.[1] Then the calculated ratios would agree with the experimental ratios within the experimental accuracy. This, incidentally, is not astonishing, since the values for C and D as proposed in Ref. 1 have been selected to yield a good fit in a slightly different case — for all isotopes of one element. The obtained accuracy of about 10% actually seems a little unexpected. One would be justified to expect, with a special choice of D, a better fit to a series of rotational levels in a particular nucleus. This conjecture actually turns out to be true.

Note added in proof (January 17, 1958). Our analysis depends essentially on the assumption that the probability of the α-decay depends explicitly only on E and ℓ. However, in principle, λ could also depend explicitly on the spin I of the daughter nucleus. In this case the above considerations are not satisfactory and there does not seem to exist any manner in which the dependence of λ on E, ℓ, and I could be determined without recourse to some kind of a model.

[1] Bohr, Fröman, and Mottelson, Kgl. Danske Videnskab. Selskab, Mat.-fys. Medd. **29**, No. 10 (1955).

[2] Ch. J. Gallacher and J. O. Rasmussen, J. Inorg. Nucl. Chem. **3**, 333 (1957).

[3] Goldin, Peker, and Novikova, Usp. Fiz. Nauk **59**, 3 (1956).

[4] Novikova, Kondrat'ev, Sobolev, and Gol'din, J. Exptl. Theoret. Phys. (U.S.S.R.) **32**, 1018 (1957), Soviet Phys. JETP **5**, 832 (1957).

Translated by M. Danos
123

STRONG AND WEAK INTERACTIONS INVOLVING HYPERONS

KHU NIN

Joint Institute for Nuclear Research

Submitted to JETP editor August 7, 1957

J. Exptl. Theoret. Phys. (U.S.S.R.) 34, 646-650 (March, 1958)

Gell-Mann's universal strong interaction theory is extended to weak interactions. It is found that the results are verified by experiment.

GELL-MANN has recently suggested[1] that the interactions of π mesons with nucleons and hyperons are universal interactions with a coupling constant about 15 times as great as the coupling constant for the interaction between K mesons and baryons. According to his model, the different baryons can be thought of as forming four degenerate doublets, which could not be distinguished if not for their interaction with K mesons. In the present article we determine the relation of this symmetry property to the charge-independent nature of the pion-baryon interaction. This same symmetry is then extended to weak interactions, and the form of the interaction function is determined. This leads in a natural way to the well known selection rule

$$\Delta T = +1/2.$$

We have not considered the possibility of parity nonconservation in weak interactions. Its inclusion, however, will not lead to any difficulties.

Let us proceed from the expressions for the meson and baryon wave functions in spinor notation. By using the representation

$$+\tau_1^{\dot\alpha\beta} = -\tau_{1\alpha\dot\beta} = \begin{pmatrix} 0 & 1 \\ 1 & 0 \end{pmatrix}, \quad +\tau_2^{\dot\alpha\beta} = -\tau_{2\alpha\dot\beta} = \begin{pmatrix} 0 & i \\ -i & 0 \end{pmatrix},$$

$$+\tau_3^{\dot\alpha\beta} = -\tau_{3\alpha\dot\beta} = \begin{pmatrix} 1 & 0 \\ 0 & -1 \end{pmatrix}, \tag{1}$$

for the Pauli matrices, we may write

$$+\pi^{\dot\alpha\beta} = -\pi_{\alpha\dot\beta} = \tau^{\dot\alpha\beta}\pi = \begin{pmatrix} \pi^0 & \sqrt{2}\,\pi^+ \\ \sqrt{2}\,\pi^- & -\pi^0 \end{pmatrix},$$

$$N_\alpha = \begin{pmatrix} N^+ \\ N^0 \end{pmatrix}, \quad \Xi^{\dot\alpha} = \begin{pmatrix} \Xi^0 \\ \Xi^- \end{pmatrix}, \quad K_\alpha = \begin{pmatrix} K^+ \\ K^0 \end{pmatrix},$$

$$\psi_{\alpha\dot\beta} = \Lambda - \tau_{\alpha\dot\beta}\,\Sigma = \begin{pmatrix} Z^0 & \Sigma^+ \\ \Sigma^- & Y^0 \end{pmatrix} = \frac{1}{\sqrt{2}} \begin{pmatrix} \Lambda + \Sigma^0 & \Sigma_1 + i\Sigma_2 \\ \Sigma_1 - i\Sigma_2 & \Lambda - \Sigma^0 \end{pmatrix},$$

$$\psi^{\dot\alpha\beta} = \Lambda - \tau^{\dot\alpha\beta}\,\Sigma = + \begin{pmatrix} Y^0 & -\Sigma^+ \\ -\Sigma^- & Z^0 \end{pmatrix}, \tag{2}$$

where the dotted indices transform as the complex conjugate of the undotted indices, and π^0, $\pi^\pm$, N^+, N^0, Σ^0, Λ, etc. are the wave functions of the corresponding particles. Since we shall consider only rotations in a three-dimensional isobaric spin space, the dotted indices will transform contravariantly with respect to the undotted indices. The expressions

$$C_{\dot\alpha}C_\alpha, \quad C^\alpha C_\alpha, \quad C^{\dot\alpha}C^\alpha, \quad C^{\alpha^*}C^\alpha,$$
$$C^*_\alpha C_\alpha, \quad C^{\dot\alpha^*}C_\alpha, \quad C^{\alpha^*}C_{\dot\alpha} \text{ etc.} \tag{3}$$

therefore, are invariant. Here the summation convention is used over repeated indices α, which can take on the values 1 and 2.

According to d'Espagnat and Prentki,[2] the strong interactions of π mesons with nucleons and cascade particles are given by the expressions

$$H_1 = g_1\bar N_\alpha i\gamma_5\pi^{\dot\alpha\beta}N_\beta, \qquad H_2 = g_2\bar\Xi^{\dot\alpha} i\gamma_5\pi^{\dot\alpha\beta}\,\Xi^{\dot\beta}. \tag{4}$$

Similarly, the interaction of π mesons with Σ and Λ particles is given by

$$H_3' = g_3\bar\psi_{\alpha\dot\beta}\, i\gamma_5\pi^{\dot\alpha\lambda}\psi_{\lambda\dot\beta} + g_4\bar\psi^{\dot\alpha\beta}\, i\gamma_5\pi^{\dot\alpha\lambda}\psi^{\dot\lambda\beta}, \tag{5}$$

In the usual notation, this can be written

$$H_3' = (g_3 - g_4)\,\bar\Lambda i\gamma_5\,(\pi\Sigma)$$
$$+ (g_3 + g_4)\,[\Sigma i\gamma_5\Sigma]\,\pi + \text{compl. conj.} \tag{5a}$$

According to Gell-Mann's model, we need now consider only the two cases, (i) $g_4 = 0$ and $g_3 \neq 0$ and (ii) $g_3 = 0$ and $g_4 \neq 0$. This follows from the fact that for all other cases, as is obvious from (5a), the mass increase due to the interaction with π mesons will not be the same for Λ and for Σ, so that it would make no sense to include both these particles in a single wave function $\psi_{\alpha\dot\beta}$. We see that only the two above-mentioned cases lead to different signs in the first term of (5a). If we bear in mind that all wave functions are given only up to an arbitrary factor of modulus 1, it is clear that these two cases transform into each other by the replacement of Λ by $-\Lambda$. They are there-

fore essentially the same, and in the future we shall consider only case (i). We can then write (5) in the form

$$H_3 = g_3 \bar{\psi}_{\alpha\dot{\beta}} i\gamma_5 \pi^{\dot{\alpha}\lambda} \psi_{\lambda\dot{\beta}}. \qquad (6)$$

Using (2), we see that (3) and (6) are invariant under rotations in isobaric spin space. This invariance property, however, is stronger than the requirement that the pion-baryon interaction be independent of the charge of the meson. For this latter requirement it is sufficient that (6) be invariant under transformations with respect to those indices contained in $\pi^{\dot{\alpha}\lambda}$. To illustrate this, let us write (6) as the sum of two terms, namely

$$H_3 = g_3 \bar{\psi}_{\alpha\dot{1}} i\gamma_5 \pi^{\dot{\alpha}\lambda} \psi_{\lambda\dot{1}} + g_3 \bar{\psi}_{\alpha\dot{2}} i\gamma_5 \pi^{\dot{\alpha}\lambda} \psi_{\lambda\dot{2}} \qquad (7)$$

The interaction will be independent of the meson charge if the two terms in (7) are separately invariant under spinor transformations with respect to the indices $\dot{\alpha}$ and λ, i.e., if $\psi_{\alpha\dot{1}}$ and $\psi_{\alpha\dot{2}}$ transform as two first-rank spinors. These ideas can be stated more exactly in the following way. Writing out (6) in detail, we obtain

$$\begin{aligned} H_3 = g_3 \{ &(\bar{\Sigma}^+ i\gamma_5 \Sigma^+ - \bar{Y}^0 i\gamma_5 Y^0)\pi^0 \\ &+ \sqrt{2}(\bar{\Sigma}^+ i\gamma_5 Y^0 \pi^+ + \bar{Y}^0 i\gamma_5 \Sigma^+ \pi^-) + (\bar{Z}^0 i\gamma_5 Z^0 - \bar{\Sigma}^- i\gamma_5 \Sigma^-)\pi^0 \\ &+ \sqrt{2}(\bar{\Sigma}^- i\gamma_5 Z^0 \pi^- + \bar{Z}^0 i\gamma_5 \Sigma^- \pi^+)\}. \end{aligned} \qquad (8)$$

We see from this that the interaction causes a transition between Σ^+ and Y^0, as well as between Σ^- and Z^0, although it causes no transition from the doublet Σ^+, Y^0 to the doublet Σ^-, Z^0. This is sufficient to prove that (if one is speaking of π-meson interactions) these two doublets differ from each other just as the doublet Ξ^0, Ξ^- differs from N^+, N^0. The hypothesis of charge invariance now means that when a π meson interacts with a hyperon, it "does not recognize" the difference between Σ^+ and Y^0 or between Σ^- and Z^0.

Thus the hyperon may be in a state which is an arbitrary superposition of Σ^+ and Y^0 or Σ^- and Z^0 without changing the interaction. There is no necessity for treating a superposition of Σ^+, Y^0, Σ^-, and Z^0, since the interaction causes no transition from the state Σ^+, Y^0 to Σ^-, Z^0. Mathematically this means that from the point of view of the π-meson interaction, Σ^+, Y^0 and Σ^-, Z^0 should be treated as two spinors, rather than as a single spinor matrix.

We may, with Gell-Mann, assume that the coupling constants g_1, g_2, and g_3 in Eqs. (3) and (7) are equal. Then the strong interactions of π mesons with different hyperons can be written in the universal form

$$H_i = g\bar{\psi}_\alpha^{(i)} i\gamma_5 \pi^{\dot{\alpha}\beta} \psi_{\dot{\beta}}^{(i)} \qquad (i = 1, 2, 3, 4); \qquad (9)$$

$$\psi^{(1)} = \begin{pmatrix} N^+ \\ N^0 \end{pmatrix}, \quad \psi^{(2)} = \begin{pmatrix} \Xi^0 \\ \Xi^- \end{pmatrix}, \quad \psi^{(3)} = \begin{pmatrix} Z^0 \\ \Sigma^- \end{pmatrix}, \quad \psi^{(4)} = \begin{pmatrix} \Sigma^+ \\ Y^0 \end{pmatrix}. \qquad (9a)$$

If we assume further that the non-renormalized masses of the N^+, N^0, Ξ, and Σ particles are initially equal (it has already been assumed that the Λ and Σ masses are equal), we obtain Gell-Mann's "global symmetry." The baryons form four pairs of degenerate doublets which cannot be differentiated except by the K-meson interaction. We see from the above that the equality of all the baryon masses is not a necessary condition for the universality of the strong interaction with π mesons. In fact, the latter requires only the equality of the non-renormalized Λ and Σ masses.

In the same way we may assume the universality of the weak pion-baryon interactions. As opposed to the strong interactions, in which the π mesons interact with only a single baryon field $\psi^{(i)}$ in an elementary act, in the weak interaction the π mesons must interact simultaneously with two different baryon fields. We assume that the universal weak interaction is given by

$$H_{Wij} = G\bar{\psi}_\alpha^{(i)} i\gamma_5 \pi^{\dot{\alpha}\beta} \psi_{\dot{\beta}}^{(j)} + \text{compl. conj.} \qquad (i \neq j), \qquad (10)$$

where G is the universal weak coupling constant. We note that expression (10) transforms in the same way as the strong interaction (9) under rotations in isobaric spin space.

Not all interaction functions (10) with different values of i and j will conserve the electric charge in the system. It is easily seen that the charge is conserved only for the two interactions

$$\begin{aligned} H_{W1} &= -G\bar{N}_\alpha \pi^{\dot{\alpha}\beta} \psi_{\beta\dot{2}} + \text{compl. conj.} \\ H_{W2} &= -G\bar{\Xi}^{\dot{\alpha}} \pi^{\dot{\alpha}\beta} \psi_{\beta\dot{1}} + \text{compl. conj.} \end{aligned} \qquad (11)$$

Before moving on, it must be emphasized that there exists also an alternate form for the weak interaction functions, satisfying all the requirements satisfied by (11). This form is

$$\begin{aligned} H_{W1} &= -G\bar{N}_\alpha \pi^{\dot{\alpha}\beta} \psi^{\dot{\beta}2} + \text{compl. conj.}, \\ H_{W2} &= -G\bar{\Xi}^{\dot{\alpha}} \pi^{\dot{\alpha}\beta} \psi^{\dot{\beta}1} + \text{compl. conj.} \end{aligned} \qquad (12)$$

As in the previously treated case, (12) reduces to (11) when Λ is replaced by $-\Lambda$. In view of the fact that the choice of Eq. (6) has eliminated the ambiguity in the sign of the Λ function, Eqs. (11) and (12) should now be different from each other. Writing (11) and (12) in the usual notation, we obtain

$$H_{W1} = G\left\{\left(\bar{N}^+ i\gamma_5 \Sigma^+ \mp \frac{1}{\sqrt{2}} \bar{N}^0 i\gamma_5 \Lambda + \frac{1}{\sqrt{2}} \bar{N}^0 i\gamma_5 \Sigma^0\right)\pi^0 + (\pm \bar{N}^+ i\gamma_5 \Lambda - \bar{N}^+ i\gamma_5 \Sigma^0)\pi^+ + \sqrt{2}\,\bar{N}^0 i\gamma_5 \Sigma^+ \pi^- + \text{compl. conj.}\right\},$$

$$H_{W2} = G\left\{\left(-\bar{\Xi}^- i\gamma_5 \Sigma^- \mp \frac{1}{\sqrt{2}} \bar{\Xi}^0 i\gamma_5 \Lambda + \frac{1}{\sqrt{2}} \bar{\Xi}^0 i\gamma_5 \Sigma^0\right)\pi^0 + (\mp \bar{\Xi}^- i\gamma_5 \Lambda + \bar{\Xi}^- i\gamma_5 \Sigma^0)\pi^- + \sqrt{2}\,\bar{\Xi}^0 i\gamma_5 \Sigma^- \pi^+ + \text{compl. conj.}\right\}, \quad (13)$$

where the upper and lower signs on Λ correspond to interactions (11) and (12). It should be noted that (11) and (12) are spinor components in isobaric spin space. Several authors[3] have already suggested and investigated the possibility that the weak interaction Hamiltonians may be spinors in isobaric spin space. This type of Hamiltonian will change the isotopic spin T by $\frac{1}{2}$. We note that no term of (13) will cause the transition $\Sigma^- \to N^0 + \pi^-$. From the form of (13), we see also that Σ particles can undergo transitions only to states with $T = +\frac{1}{2}$ (which means that $\Delta T = -\frac{1}{2}$). At first sight this would mean that (13) is not in agreement with experiment, since we know that the lifetime for the $\Sigma^- \to N^0 + \pi^-$ decay mode is comparable to that for the decay of Σ^+. We shall show that the strong interaction makes it possible for the weak interaction (13) to lead to decay of Σ^-.*

The decay process may take place through the strong interaction in the following way:

$$\Sigma^- \to \pi^- + \Lambda \to \pi^- + \pi^- + N^+ \to \pi^- + N^0; \quad (14)$$

$$\Sigma^- \to \pi^- + \Sigma^0 \to \pi^- + \pi^- + N^+ \to \pi^- + N^0. \quad (15)$$

If (11) is taken as the weak-interaction Hamiltonian and (3) and (6) are taken as the strong-interaction Hamiltonians, direct calculation shows that the transition amplitude for (14) is equal and opposite to the transition amplitude for (15). It is easily seen that for more complicated decay schemes the contribution from virtual Λ particles always annuls a similar contribution from virtual Σ^0 particles, so that the resulting transition amplitude for Σ^- decay is always zero. If, however, we take (12) as the interaction Hamiltonian, we find that the two amplitudes are always in the same direction. We therefore obtain a nonvanishing transition amplitude for Σ^- decay, with a lifetime comparable to the lifetime for Σ^+ decay.

From the above result we conclude that (12) [and not (11)] should be chosen as the universal weak interaction Hamiltonian.

We shall show below that (12) also leads to the decay of the K^0 meson. The most general form of the K-meson-baryon interaction Hamiltonian is

$$H' = f_1 \bar{\Xi}^{\dot{\alpha}} \psi_{\alpha\dot{\beta}} K^{\dot{\beta}} + f_2 \bar{\Xi}^{\dot{\alpha}} \psi^{\dot{\alpha}\beta} K^{\dot{\beta}} + f_3 \bar{N}_\alpha \psi_{\alpha\dot{\beta}} K_\beta + f_4 \bar{N}_\alpha \psi^{\dot{\alpha}\beta} K_\beta + \text{compl. conj.} \quad (16)$$

or, in the usual notation,

$$H' = (f_1 + f_2)\,\bar{\Xi}\,\tau_2 K^* \Lambda + (f_1 - f_2)\,\bar{\Xi}\,(\tau\Sigma)\,K^* + (f_3 + f_4)\,\bar{N} K \Lambda + (f_3 - f_4)\bar{N}\,(\tau\Sigma)\,K + \text{compl. conj.} \quad (17)$$

According to Gell-Mann, the coupling constants f_i are one order of magnitude less than g in Eq. (9), and the mass difference between the nucleon, Σ, Λ, and Ξ is due to the interaction (16). The decay of K^0 into $\pi^+ + \pi^-$ and $\pi^0 + \pi^0$ can go by way of the strong interactions (3) and (6), the moderately strong interaction (16), and the weak interaction (12). The simplest diagrams for such processes contain three vertices, one for each form of the interaction. The fact that the f_i are small compared to g may increase the decay time of the K^0 meson compared to the decay time of Λ and Σ, but this is compensated by the fact that the number of virtual paths is relatively large (there are about ten). Another compensating factor is the large volume in phase space of the final state. One may therefore expect that the lifetime of K^0 decay is of the same order as the Λ and Σ lifetimes, which is in agreement with experiment.

Note added in proof (February 20, 1958). A recent experiment has verified the fact that parity is not conserved in strange-particle decay. This means that the weak interaction Hamiltonian will contain terms which are pseudoscalars, rather than scalars. If Λ in (13) is replaced by $i\gamma_5\Lambda$, then all the terms containing Λ will become pseudoscalars. It is easily seen that after such a

*It should be emphasized, that due to the strong interaction, the selection rule for ΔT which follows from the weak interaction Hamiltonian is not generally the observed selection rule. For instance, the unstable strange particle under consideration may be transformed into another unstable strange particle by the strong interaction. For this new particle, the selection rule given by the interaction Hamiltonian will be different. If the initial particle decays through this second one, the selection rule for the process may be modified. As an example, the strange particle may emit virtual mesons so that the isotopic spin T′ (thought of as a space-quantized vector) of the particle in this virtual state is antiparallel to the total T. We thus obtain $\Delta T = -\Delta T'$. If the interaction Hamiltonian allows, for instance, only $\Delta T = +\frac{1}{2}$, we see immediately that a decay which takes place through this virtual state may have a change in T equal to $\Delta T = -\frac{1}{2}$.

replacement (14) and (15) will not be mutually exclusive, and the theory is again invariant under the transformation $\Lambda \to -\Lambda$, as in the case of the strong interaction.

[1] M. Gell-Mann, Phys. Rev. **106**, 1296 (1957).
[2] B. d'Espagnat and J. Prentki, Nucl. Phys. **1**, 33 (1956).
[3] J. Prentki and B. d'Espagnat, Nuovo cimento **3**, 1045 (1956); R. Gatto, Nuovo cimento **3**, 318 (1956); C. Iso and M. Kawaguchi, Progr. Theor. Phys. **16**, 177 (1956); R. H. Dalitz, Proc. Phys. Soc. (London) **A69**, 527 (1956); G. Wentzel, Phys. Rev. **101**, 1215 (1956); L. Okun', J. Exptl. Theoret. Phys. (U.S.S.R.) **31**, 333 (1956), Soviet Phys. JETP **4**, 284 (1957).

Translated by E. J. Saletan
124

SOVIET PHYSICS JETP VOLUME 34 (7), NUMBER 3 SEPTEMBER, 1958

DAMPING OF OSCILLATIONS IN A CYCLIC ELECTRON ACCELERATOR

Iu. F. ORLOV and E. K. TARASOV

Submitted to JETP editor September 6, 1957

J. Exptl. Theoret. Phys. (U.S.S.R.) 34, 651-657 (March, 1958)

Damping factors are derived for radial and phase oscillations, taking account of variation of the magnetic field along the orbit. In the case of a strong-focusing accelerator, in contrast to the case of weak focusing, the damping is independent of the variation of the gradient $\partial H_z/\partial r$ along the orbit if the field H_z is the same in all magnet sectors.

1. EQUATIONS OF MOTION

To derive the equations of motion of an electron in a cyclic accelerator, we use the well-known relations

$$\Delta L / L_s = \alpha \Delta E / E_s, \quad \Delta E = E - E_s, \quad E_s \gg mc^2; \quad (1)$$

$$\dot{\Phi} = -(2\pi q c \alpha / L_s)\, \Delta E / E_s, \quad \alpha = d \ln L / d \ln E, \quad (2)$$

where E_S and L_S are the equilibrium values of the electron energy and the orbit length, q is the harmonic number (the ratio of the rf frequency to the frequency of revolution), Φ is the phase of the accelerating voltage at the moment when the particles pass the middle of the accelerating gap. On the right side of (2), we have dropped some terms which are unimportant for the effects in which we are interested: the perturbation $\Delta\omega_r$ of the frequency of the accelerating field and the transient perturbation $2\pi q c \alpha L_S^{-1} \Delta H(t)/H_S$ of the magnetic field.

Differentiating (2) with respect to the time, we get[1]

$$\ddot{\Phi} + \frac{2\pi q c \alpha}{L_s E_s} \frac{d}{dt}(\Delta E) + \frac{\dot{E}_s}{E_s}\dot{\Phi} = 0, \quad (3)$$

where

$$\frac{d}{dt}(\Delta E) = P_0 - \left(1 - \frac{r}{\rho}\right) P_\gamma - \dot{E}_s, \qquad P_0 = \frac{ceV}{L_s} \sin \Phi, \quad (4)$$

where ρ is the radius of curvature of the orbit and P_γ the power in the radiation. Dropping the unimportant term describing the perturbation $\Delta V/V$, we have, in the linear approximation,

$$P_0 \approx P_{0s}[1 + \cot \Phi_s (\Phi - \Phi_s)], \qquad P_{0s} = ceV_0 \sin \Phi_s / L_s; \quad (5)$$

$$P_\gamma = 2e^4 E^2 H^2 / 3m^4 c^7 + p(t) = \overline{P}_\gamma + p(t), \quad (6)$$

where p(t) describes the fluctuations of the radiation, $\overline{P}_\gamma$ is the (frequency) average of the power of the radiation at a given point on the orbit; this last quantity depends on both betatron and phase oscillations. According to (6),

$$\overline{P}_\gamma = \overline{P}_{\gamma s}[1 - 2L_s \dot{\Phi} / 2\pi q c \alpha - 2nr/\rho_s], \quad (7)$$

$$n = -(\rho_s / H_s)\, \partial H_s / \partial r.$$

Substituting (5) and (7) in (3), we get the following equation for the phase oscillations in linear approximation:[2]

$$\ddot{\phi} + \frac{\dot{E}_s + 2\bar{P}_{\gamma s}}{E_s}\dot{\phi} + \Omega^2\phi + \frac{2\pi q c\alpha}{L_s}\frac{\bar{P}_{\gamma s}}{E_s}(2n-1)\frac{r}{\rho_s} = \frac{2\pi q c\alpha}{L_s E_s}p(t), \quad (8)$$

$$\phi = \Phi - \Phi_s, \quad \Omega^2 = 2\pi q c\alpha P_{0s}\cot\Phi_s / L_s E_s.$$

Here we have made use of the fact that if $<P_{\gamma S}>$ is the power of the radiation, averaged over the unperturbed orbit, $P_{0S} = <P_{\gamma S}> + \dot{E}_S$.

We write the equations for betatron oscillations in the form

$$\ddot{r} + \frac{\dot{E}_s + \bar{P}_{\gamma s}}{E_s}\dot{r} + \frac{c^2}{\rho_s^2}(1-n)r + \frac{L_s}{2\pi q c\alpha}\frac{c^2}{\rho_s^2}\dot{\phi} = \frac{c^2}{H\rho}\frac{\partial H_z}{\partial z}z - \frac{c}{H\rho}H_x\dot{z}; \quad (9)$$

$$\ddot{z} + \frac{\dot{E}_s + \bar{P}_{\gamma s}}{E_s}\dot{z} + \frac{c^2}{\rho_s^2}nz = \frac{c^2}{H\rho}\frac{\partial H_z}{\partial z}r + \frac{c}{H\rho}H_x\dot{r}. \quad (10)$$

H_X is the longitudinal component of the magnetic field.

2. DAMPING OF FREE RADIAL OSCILLATIONS*

The radiation fluctuations $p(t)$ cause phase oscillations to be set up and, because of the coupling of radial and phase oscillations [the term with $\dot{\phi}$ in (9)], also excite radial oscillations.[3] The vertical oscillations are not directly coupled to the phase oscillations. If $\partial H_Z/\partial z = H_X = 0$, they are damped according to the formula

$$\exp\left(-\frac{1}{2}\int_0^t dt'\,\frac{\dot{E} + \dot{P}_\gamma}{E}\right)$$

(cf. Ref. 2). The damping associated with the radiation is classical in character, and is caused by the fact that in the accelerating intervals the particles pass through an electric field which is intended to compensate for the radiation loss. For this reason the damping contains the term P_{0S}/E in place of the usual $\dot{E}/E$. If there were no coupling of radial and phase oscillations, the free radial oscillations would, for this same reason, have an additional damping (cf. Ref. 2) with decrement $-<P_{\gamma S}>/2E$ and the phase oscillations a damping with decrement $-<P_{\gamma S}>/E$, as is evident from Eqs. (8) and (9).*

The coupling of the oscillations leads to a redistribution of the damping strength. If no special measures are taken, the radial oscillations in a strong focusing accelerator are anti-damped with decrement $\frac{1}{2}<P_{\gamma S}>/E$, while the phase oscillations are, correspondingly, more strongly damped with decrement $-2<P_{\gamma S}>/E$. To get rid of the build-up of the radial oscillations, we can make use of their coupling to the vertical oscillations (cf. Ref. 4), for example, by introducing magnets in which there is a component H_X. However, this method is not the best, since it obviously does not enable us to obtain the oscillation damping which is needed for marked reduction of particle losses (since this method leaves the sum of the damping factors for vertical and radial oscillations equal to zero).

Later we shall show that in a strong-focusing accelerator (more precisely, when $\alpha = d\ln L/d\ln E \ll 1$) the damping factors do not depend on the variation of n along the orbit (if H_Z is the same in all the magnets), and we shall obtain a general formula for the damping of radial and phase oscillations. As we shall see, the damping depends on the variation of H_Z along the orbit, and that for any values of H_Z those magnets which have low n have no influence on the result (contrary to the erroneous statements in Refs. 2 and 4).

Since the coupling of r and z oscillations is unimportant for this problem, we shall assume that $\partial H_Z/\partial z = H_X = 0$.

Suppose that radial oscillations are excited at t = 0. Because of the dependence of the radiation in an inhomogeneous field on r [the term 2nr in (8)], the excitation will be transferred to the phase oscillations. Usually the strong inequality $\omega \gg \Omega \gg P_\gamma/E$ is satisfied, where ω and Ω are the frequencies of betatron and phase oscillations, respectively. The forced oscillation of the phase is therefore of the form

$$\ddot{\phi} \approx -\frac{2\pi q c\alpha}{L_s}\frac{\bar{P}_{\gamma s}}{E_s}(2n-1)\frac{r}{\rho_s};$$

$$\dot{\phi} \approx -\frac{2\pi q c\alpha}{L_s}\int_0^t \frac{2n-1}{\rho_s^2}\,r\,\frac{\bar{P}_{\gamma s}\rho_s}{E_s}\,dt'. \quad (11)$$

We shall use Eq. (9) for r, and shall neglect in (11), as we do throughout, the terms containing

$$P_\gamma^2/E^2,\ \dot{E}P_\gamma/E^2,\ \dot{E}^2/E^2,\ \dot{P}_\gamma/E = 4P_\gamma\dot{E}/E^2,\ \ddot{E}/E^2.$$

*The possibility of the existence of a damping mechanism due to radiation was first pointed out by A. M. Budker in 1954 (private communication).

*In addition, Ω^2 is not proportional to $\dot{E}/E$, but rather to P_{0S}/E. This also gives an additional damping of the phase oscillations.

In other words, we shall use as our basic equation

$$\ddot{r} + (c/\rho)^2 (1 - n) r = 0. \tag{12}$$

We first write $\overline{P}_{\gamma s}\rho_s$ as

$$\overline{P}_{\gamma s}\rho_s = P_{\gamma 0}\rho_0 + (\overline{P}_{\gamma s}\rho_s - P_{\gamma 0}\rho_0), \tag{13}$$

where $P_{\gamma 0}\rho_0$ is some constant. If the magnetic field is the same in all magnets with the exception of certain sections, then $P_{\gamma 0}$ and ρ_0 are the power of the radiation and the radius of curvature in the magnets of standard type, while $\overline{P}_{\gamma s}\rho_s - P_{\gamma 0}\rho_0$ is the deviation in the non-standard sections. From (12) and (13) we get

$$\dot{\phi} = -\frac{2\pi q c \alpha}{L_s}\left\{2\frac{P_{\gamma 0}\rho_0}{c^2 E}\dot{r} + \int_0^t \frac{\overline{P}_{\gamma s}}{E_s}\frac{r}{\rho_s}\,dt' + 2\int_0^t \frac{n-1}{\rho_s^2}\frac{\overline{P}_{\gamma s}\rho_s - P_{\gamma 0}\rho_0}{E_s} r\,dt'\right\}.$$

After substituting this expression for $\dot{\phi}$ in Eq. (9) for the radial oscillations, we make the substitution

$$r = a\varphi + a^*\varphi^*, \quad \dot{r} = a\dot{\varphi} + a^*\dot{\varphi}^*, \tag{14}$$

where φ and φ^* are two linearly independent solutions of (12), normalized by the condition

$$\varphi^*\dot{\varphi} - \varphi\dot{\varphi}^* = 2iW. \tag{15}$$

We then find the following equation for a:

$$\dot{a} = \frac{\varphi^*}{2iW}\left\{-\frac{\dot{E}_s + \overline{P}_{\gamma s} - 2P_{\gamma 0}\rho_0/\rho_s}{E_s}(a\dot{\varphi} + a^*\dot{\varphi}^*) + \frac{c^2}{\rho_s}\int_0^t \frac{\overline{P}_{\gamma s}}{E_s\rho_s}(a\varphi + a^*\varphi^*)\,dt' + 2\frac{c^2}{\rho_s^2}\int_0^t \frac{\overline{P}_{\gamma s}\rho_s - P_{\gamma 0}\rho_0}{E_s}\frac{n-1}{\rho_s^2}(a\varphi + a^*\varphi^*)\,dt'\right\}. \tag{16}$$

φ and φ^* are oscillating functions, which average to zero.

The frequencies of the betatron oscillations are always chosen so that there is a non-integral number of oscillations around the orbit. Because of this we see that if we are interested in only those terms of (16) which give an increase (or decrease) of a with time, we can drop oscillating functions and so throw out all the terms containing a^*. In the remaining integrals, we can take a out from under the integral sign, neglecting terms which are quadratic in the perturbation. After this, making use of the fact that only the real part of (16) gives an increase of a with time, we find by using (15),

$$a = a_0 \exp\left\{-\frac{1}{2}\int_0^t E_s^{-1} dt' \left(\dot{E}_s + \overline{P}_{\gamma s} - \frac{2P_{\gamma 0}\rho_0}{\rho_s}\right) + \frac{c^2}{2W}\operatorname{Im}\int_0^t dt' \frac{\varphi^*}{\rho_s}\int_0^{t'} dt'' \frac{\overline{P}_{\gamma s}\varphi}{E_s\rho_s} + \frac{c^2}{W}\operatorname{Im}\left(\int_0^t dt' \frac{\varphi^*}{\rho_s}\int_0^{t'} dt'' \frac{\overline{P}_{\gamma s}\rho_s - P_{\gamma 0}\rho_0}{E_s}\frac{n-1}{\rho_s^2}\varphi\right)\right\}. \tag{17}$$

Now we transform the double integrals:

$$\int_0^t \frac{\varphi^*}{\rho_s}dt' \int_0^{t'} F(t'')\varphi\,dt'' = \int_0^t F(t'')\varphi\,dt'' \int_{t''}^t \frac{\varphi^*}{\rho_s}dt' = -\int_0^t F(t'')\varphi\,dt'' \int_0^{t''} \frac{\varphi^*}{\rho_s}dt' + K(t). \tag{18}$$

Concerning the function K(t), which is the product of two integrals (one of which contains φ and the other φ^*), we can say that in any case this function unlike the double integral does not increase with time,* so that it can be dropped as unimportant in the exponential (17). On the other hand, we shall add an unimportant oscillating function to the integrand of (18), replacing the function

$$\frac{c^2}{W}\operatorname{Im}\varphi\int_0^t dt'\,\varphi^*/\rho_s$$

by the function

$$\psi = \frac{c^2}{W}\operatorname{Im}\varphi\left[\int_0^t dt'\,\varphi^*/\rho_s + \text{const}\right]. \tag{19}$$

The constant in the brackets can be chosen so that ψ is a periodic solution (with a period equal to one revolution) of the equation

$$\ddot{\psi} + (c/\rho_s)^2(1 - n)\psi = c^2/\rho_s. \tag{20}$$

The function ψ, which describes the forced radial oscillations that result from energy fluctuations, is useful since it occurs frequently in accelerator computations.

The difference $\overline{P}_{\gamma s}\rho_s - P_{\gamma 0}\rho_0$ occurring in (17) is conveniently represented as

$$\overline{P}_{\gamma s}\rho_s - P_{\gamma 0}\rho_0 = P_{\gamma 0}\rho_0 (H_s - H_0)/H_0. \tag{21}$$

Using (18), (19), and (21), we get the following final expression for the exponential damping of the free radial oscillations:

$$r_f \sim \exp\left\{-\frac{1}{2}\int_0^t \frac{dt'}{E_s}\left[\dot{E}_s + \overline{P}_{\gamma s}\left(1 + \frac{\psi}{\rho_s}\right) - 2\frac{P_{\gamma 0}\rho_0}{\rho_s} + 2P_{\gamma 0}\rho_0\frac{n-1}{\rho_s^2}\frac{H_s - H_0}{H_0}\psi\right]\right\}. \tag{22}$$

*More precisely, it is proportional to P_γ/E, whereas the other terms are proportional to $\int^t (P_\gamma/E)\,dt'$.

Let us consider the case where the field in all magnets is the same (in particular, the case of a weak-focusing accelerator). In this case the ratio ψ/ρ_S in the integrand can be replaced by its average value along the orbit. As is well known,

$$\langle\psi/\rho_s\rangle = \lim_{t\to\infty}\frac{1}{t}\int_0^t \frac{\psi}{\rho_s}\,dt' = \alpha = d\ln L/d\ln E \qquad (23)$$

(where we have replaced the momentum by the energy, assuming that $E \gg mc^2$). Thus, for $H_S = H_0$,

$$r \sim \exp\left\{-\frac{1}{2}\int_0^t \frac{dt'}{E_s}\left[\dot{E}_s + \overline{P}_{\gamma s}(\alpha - 1)\right]\right\}. \qquad (24)$$

This special case is the result already given by Kolomenskii and Lebedev.[2] In a strong-focusing accelerator ($\alpha \ll 1$) there is antidamping of the oscillations, while in a weak-focusing accelerator [$\alpha = 1/(1-n)$, $0 < n < 1$] there is damping with the decrement

$$-\frac{1}{2}\frac{n}{1-n}\frac{\langle P_\gamma\rangle}{E_s}.$$

3. DAMPING OF FREE PHASE OSCILLATIONS. DISCUSSION OF RESULTS

The result which we have found is confirmed by a simpler computation of the damping of the phase oscillations.

Suppose that phase oscillations are excited at t = 0. This leads to the development of radial oscillations. We may choose a periodic solution for r, since it differs from any other by an oscillating term which is irrelevant for the damping. Thus

$$r = \psi\Delta E/E_s = -(L_s\psi/2\pi qc\alpha)\,\dot{\phi}. \qquad (25)$$

Substituting (25) in (8) and taking account of the variation in the frequency of the phase oscillations, we get

$$\phi \sim \exp\left\{-\frac{1}{2}\int_0^t\left[\frac{\dot{\Omega}}{\Omega} + \frac{\dot{E}_s + 2\overline{P}_{\gamma s} - \overline{P}_{\gamma s}(2n-1)\psi/\rho_s}{E_s}\right]dt'\right\}. \qquad (26)$$

According to Eq. (20), which ψ satisfies,

$$\int_0^t \frac{\overline{P}_{\gamma s}\rho_s}{E_s}\frac{2n-1}{\rho_s^2}\psi\,dt' = \int_0^t \frac{dt'}{E_s}\left[\overline{P}_{\gamma s}\frac{\psi}{\rho_s} - 2P_{\gamma 0}\frac{\rho_0}{\rho_s} + 2P_{\gamma 0}\rho_0\frac{H_s - H_0}{H_0}\frac{n-1}{\rho_s^2}\psi\right] + \int_0^t d't\cdot\ddot{\psi}P_{\gamma 0}\rho_0/E_s c^2. \qquad (27)$$

The last integral can be dropped since $\ddot{\psi}$ (unlike ψ) averages to zero. Finally,

$$\phi_f \sim \exp\left\{-\frac{1}{2}\int_0^t\left[\frac{\dot{\Omega}}{\Omega} + \frac{\dot{E}_s + \overline{P}_{\gamma s}(2 - \psi/\rho_s)}{E_s} + 2P_{\gamma 0}\frac{\rho_0}{\rho_s} - 2P_{\gamma 0}\rho_0\frac{H_s - H_0}{H_0}\frac{n-1}{\rho_s^2}\psi\right]dt'\right\}. \qquad (28)$$

As was to be expected, the sum of the damping coefficients for radial and phase oscillations does not depend on the form of ψ and $(H_S - H_0)/H_0$, i.e., it does not depend on the specific form of the radial-phase coupling. The part of the sum which depends on the radiation is always

$$-\frac{3}{2}\int_0^t dt'\overline{P}_{\gamma s}/E_s.$$

For the case of weak focusing, where $H_S = H_0$, we get the familiar result of Sands:[1]

$$\phi \sim \exp\left\{-\frac{1}{2}\int_0^t\left[\frac{\dot{\Omega}}{\Omega} + \frac{\overline{P}_{\gamma s}}{E_s}\frac{3-4n}{1-n} + \frac{\dot{E}_s}{E_s}\right]dt'\right\},$$
$$\left\langle\frac{\psi}{\rho_s}\right\rangle = \alpha = \frac{1}{1-n}. \qquad (29)$$

The damping factors for r and ϕ can also be obtained by finding the characteristic roots of the system of equations (8) and (9). For this purpose, we make the substitution

$$r = x_1\varphi e^{-i\nu t} + x_2\varphi^* e^{i\nu t}, \quad x_2 = x_1^*, \quad \dot{r} = x_1\dot{\varphi}e^{-i\nu t} + x_2\dot{\varphi}^* e^{i\nu t},$$
$$\phi = x_3 + x_4, \quad \dot{\phi} = i\Omega(x_3 - x_4), \quad x_4 = x_3^*,$$

where ν is the betatron oscillation frequency, so that $\varphi e^{-i\nu t}$ and $\dot{\varphi}e^{-i\nu t}$ are periodic functions. We then get in place of (8) and (9) a set of four first order equations with periodic coefficients (which are constants for the case of weak focusing), and using first order perturbation theory we get four fundamental solutions $x_{ik}(t)$ (one index labels the solution, the other the function in the solution). If the $x_{ik}(t)$ are defined by the initial conditions

$$x_{ik}(0) = \delta_{ik},$$

the characteristic equation has the form[5]

$$|x_{ik}(T) - \lambda\delta_{ik}| = 0,$$

where T is the period of the coefficients in the equations for the $\dot{x}_{ik}(t)$. The damping factors are identical with those obtained above.

Formula (22) shows that in order to get damping of radial oscillations in a strong-focusing accelerator with a decrement equal to, say, $-\langle P_\gamma\rangle/2E_S$, which is sufficient for a marked reduction of particle losses, the approximate equality

$$\left\langle \frac{n-1}{\rho_s^2} \frac{H_s - H_0}{H_0} \psi \right\rangle \approx \left\langle \frac{1}{\rho_s} \right\rangle. \qquad (30)$$

must be satisfied. At the same time the damping factor for the phase oscillations is still sufficiently large and is equal to $-\langle P_\gamma \rangle / E_s$.

The results we have found can be visualized as follows. The additional damping of the radial oscillations occurs together with an additional antidamping of the phase oscillations, i.e., oscillations of the energy are built up. For buildup of energy oscillations it is obviously necessary that an increase in the energy of the particle be accompanied by a decrease in the radiation. This will be the case if, when the energy is increased, the trajectory of the particle changes so that the quantity $\langle H^2 \rangle \sim \langle \rho^{-2} \rangle$, averaged along the new trajectory, decreases. For example, in a weak-focusing accelerator $\langle \rho^{-2} \rangle$ always decreases with increasing energy, and the more sharply the closer n is to unity, since for $n \geq 1$ the motion becomes unstable. On the other hand, in a strong-focusing accelerator $\langle \rho^{-2} \rangle$ increases with increasing energy, even though $\langle 1/\rho \rangle$ decreases. This result is explained by the strong bending of the perturbed trajectory when $\Delta E/E > 0$ (inside the radially focusing magnets) compared with the unperturbed orbit, because of the large value of n. As a result the radial oscillations are built up in the strong-focusing accelerator (instead of being damped as they are in the weak-focusing case).

Obviously magnets with low n, introduced into a strong-focusing system, cannot change this picture, since they have practically no effect on the trajectory and do not change ρ^{-2}. As was proven above, another less obvious statement is also valid, namely that the introduction of additional magnets with arbitrarily large n but with the same field as in the other magnets does not change the dependence of $\langle \rho^{-2} \rangle$ on the energy fluctuations. When n is varied along the orbit without varying the field, the equilibrium trajectory is distorted so that

$$\langle \rho^{-2} \rangle \sim \left\langle \frac{1 - 2n\psi/\rho_s}{\rho_s^2} \right\rangle$$

is not changed for a given $\Delta E/E$.

To change the damping, it is necessary to vary the field. According to the qualitative arguments given above, to increase the damping for radial motion the field must be larger in the radially defocusing magnets ($n > 0$), since it is precisely in this case that the equilibrium trajectory straightens with increasing energy (if $\psi > 0$, which is usually the case). Formula (30) corresponds to precisely this result.

In practice, to satisfy condition (30) it is apparently more convenient to have a small number of radially focusing magnets with zero or negative field and high $n < 0$, which are designed so that they perturb the conditions of oscillation as little as possible. These requirements are satisfied, for example, by some of the proposals of Livingston and Robinson.[6]

[1] M. Sands, Phys. Rev. 97, 470 (1955).

[2] A. A. Kolomenskii and A. N. Lebedev, CERN Symposium, 1956, vol. 1, p. 477. A. A. Kolomenskii and A. N. Lebedev, Приборы и техника эксперимента (Instruments and Meas. Engg.) 1, (1957).

[3] A. A. Sokolov and I. M. Ternov, Dokl. Akad. Nauk SSSR 97, 823 (1954).

[4] A. A. Kolomenskii, Doctoral dissertation, Physics Institute, Academy of Sciences, U.S.S.R., 1957.

[5] N. G. Malkin, Теория устойчивости движения (Theory of Stability of Motion), Gostekhizdat, 1952.

[6] K. W. Robinson, CEA-4, May 15, 1956 (Report to Cambridge Electron Accelerator Group). M.S. Livingston, CERN Symposium, 1956, vol. 1, p. 442.

Translated by M. Hamermesh
125

THEORY OF GALVANOMAGNETIC AND THERMOMAGNETIC EFFECTS IN METALLIC FILMS

E. A. KANER

Institute of Radiophysics and Electronics, Academy of Sciences, Ukrainian S.S.R.

Submitted to JETP editor September 14, 1957

J. Exptl. Theoret. Phys. (U.S.S.R.) 34, 658-669 (March, 1958)

The electron distribution function, the electric conductivity, the thermal conductivity, and the Thomson coefficients have been determined for a metallic film located in a constant magnetic field directed at an arbitrary angle with respect to the surface of the film. No special assumptions are made regarding the electron dispersion law. The region of strong magnetic fields is studied in detail. Comparison of theory with experiment shows excellent agreement.

1. INTRODUCTION

THE study of the effect of shape and dimensions of a sample on the electric conductivity, thermal conductivity, and other kinetic coefficients of metals permits us to obtain data on the magnitude of the mean free path, the character of the electron energy spectrum, etc.

In Refs. 1 — 6, the conductivity of thin metallic films and wires was calculated for the absence of a magnetic field. Englman and Sondheimer[3] showed that the conductivity of an anisotropic monocrystalline film, whose thickness was much less than the mean free path length, depends not only on the angles between the current direction and the crystallographic axes, but also on the orientation of the latter with respect to the surface of the film. In Refs. 4 and 5, the conductivity of wires of circular and rectangular cross section was computed.

The conductivity of films and wires in a magnetic field was determined in Refs. 5 — 8 for various orientations of a constant magnetic field (parallel to the plane of the film and to the axis of the wire) relative to the current.

In the work of MacDonald and Sarginson,[5] the distribution function and the conductivity of the film in crossed electric and magnetic fields were found improperly (which is also noted in Ref. 7). Azbel'[7] determined the conductivity of a film in a longitudinal magnetic field, while Sondheimer[7a] has shown that the resistance of a thin film in a perpendicular magnetic field oscillates on change in the field. In the researches of Chambers[7] and Königsberg[8] on the determination of the conductivity of films and wires in a magnetic field, simple kinetic considerations were employed. These were based on a study of the trajectory of an isolated electron which enabled one to avoid the cumbersome solution of the kinetic equation (see Ref. 7).

In all these researches, with the exception of the work of Kaganov and Azbel',[2] the calculations were carried out under the assumption that the electrons in the metal were free, that is, a square law of dispersion was assumed (sometimes with anisotropic effective masses). Moreover, the anisotropy of the time of free flight was never taken into account. Also, the kinetic coefficients in thin films depend on the form of the dispersion law and the anisotropy of the collision integral. This circumstance can, in principle, be used for the study of the form of the limiting Fermi surface and the character of the electron-lattice interaction.

Insofar as the thermomagnetic effects in films are concerned, they have remained virtually unstudied.

In connection with experimental researches (for example, Refs. 5, 10), it must be noted that in almost all of them, the samples were polycrystalline. So far as we know, only in the research of Borovik and Lazarev,[9] where the effect of the shape of the specimen on the electric conductivity of bismuth was studied, were the specimens monocrystalline. In that case a plate of thickness $\ell \sim 10^{-2}$ cm was used. The plate was connected with a massive single crystal; the orientation of the crystallographic axes in the film and in the large sample were the same. The measurements were carried out simultaneously on the film and on the large monocrystal in order to eliminate the

effect of the natural anisotropy of Bi and to isolate the effect of shape in pure form. The study of the rotational diagram (the dependence of the resistance of the film on the angle between the magnetic field and the surface of the film) allowed one to determine the order of magnitude of the free path length. The results of these experiments are completely explained by the theory developed below.

The purpose of the present paper was the calculation of the kinetic coefficients of the metallic film (located in a constant magnetic field) for an arbitrary electron dispersion law. The possibility of the introduction of a relaxation time $t_0(p)$ was assumed, where p is the quasi-momentum of the electron.

2. STATEMENT OF THE PROBLEM AND SOLUTION OF THE KINETIC EQUATION

Let us first consider the electric conductivity of a layer of metal of thickness d ($0 \leq z \leq d$, the z axis being parallel to the inwardly drawn normal to the surface $z = 0$), located in a constant magnetic field H. We choose the x axis along the projection of H on the plane of the film.

We shall begin with the linearized kinetic equation[11] for the contribution of f to the equilibrium Fermi distribution function

$$v_z \partial f / \partial z + \Omega \partial f / \partial \tau + f / t_0(p) = e\mathbf{E}\mathbf{v}\, \partial f_0 / \partial \varepsilon, \qquad f_0\left(\frac{\varepsilon - \zeta}{T}\right) = \left[\exp\left(\frac{\varepsilon - \zeta}{T}\right) + 1\right]^{-1} \tag{2.1}$$

Here, we choose as variables the coordinate z, the energy of the electrons ϵ, the conserved component of the quasi-momentum $p_H = pH/H$ and the dimensionless period of the electron in its orbit $\tau = \Omega t$. The "cyclotron" frequency $\Omega = eH/mc$; $-e$ = charge, $m = (1/2\pi)\partial S(\epsilon, p_H)/\partial\epsilon$ = effective mass, $\mathbf{v} = \nabla_p \epsilon(p)$ = velocity, $\zeta(T)$ = chemical potential of the electrons; $S(\epsilon, p_H)$ = cross sectional area of the surface, $\epsilon(p) = \epsilon$ on the surface $p_H = \text{const}$; t = actual period of electron in orbit; $\mathbf{E}(z)$ = direction of the electric field inside the metal. It follows from the unperturbed equation of motion of the electron in a magnetic field $dp/dt = -(e/c)[\mathbf{v} \times \mathbf{H}]$ that the Jacobian of the transformation from the variables p_x, p_y, p_z to the variables ϵ, τ, p_H is equal to m.

The boundary conditions for Eqs. (2.1) are the periodicity of $f(z, \epsilon, \tau, p_H)$ in the variable τ with period 2π and the condition of diffuse reflection of the electrons from the boundaries of the film:

$$f(0; \mathbf{v})\big|_{v_z > 0} = 0; \quad f(d; \mathbf{v})\big|_{v_z < 0} = 0. \tag{2.2}$$

Knowledge of the distribution function $f(z; \epsilon, \tau, p_H)$ permits us to compute the current density $j(z)$

$$j(z) = -(2e/h^3) \int \mathbf{v} f\, (dp), \tag{2.3}$$

whence we find

$$\bar{j} = \frac{1}{d} \int_0^d j(z)\, dz$$

and the tensor of effective conductivity σ_{ik}. In this case, it must be taken into consideration that the components of the electric field E_x and E_y are constant along the film, while the Hall field E_z depends on z. This dependence ought to be obtained from the equation $j_z = 0$, which corresponds to the evident fact that there is an "open circuit" along the z axis. However, in what follows we shall neglect the dependence of the Hall field E_z on the coordinate z, since we shall be interested in two limiting cases: strong ($\gamma \ll 1$) and a weak ($\gamma \gg 1$) magnetic field ($\gamma = 1/\Omega t_0$) for $d \sim \ell = vt_0$. In the strong magnetic field ($\gamma \ll 1$), E_z changes appreciably only close to the boundaries of the film in a narrow range of z, $d - z \sim r \ll \ell \sim d^*$ (the contribution from which we can neglect), remaining practically constant over the thickness of the film. In the weak magnetic field ($\gamma \gg 1$), because of the small value of E_z, the Hall field can simply be neglected in the computation of the conductivity.

Starting out from physical considerations similar to those with the help of which Chambers[6] derived the formula for the conductivity of films and wires, it is not difficult to write down at once the solution of the kinetic equation (2.1), which satisfies the boundary condition (2.2):

$$f(z; \tau; \varepsilon, p_H) = \frac{e}{\Omega} \frac{\partial f_0}{\partial \varepsilon} \int_{\lambda(z;\tau)}^{\tau} \mathbf{v}(\tau_1).\mathbf{E}\left(z + \frac{1}{\Omega}\int_{\tau}^{\tau_1} v_z\, d\tau_2\right) \exp\left(\int_{\tau}^{\tau_1} \gamma\, d\tau_2\right) d\tau_1, \tag{2.4}$$

where $\lambda(z; \tau)$ denotes the closet preceding τ root of one of the following equations

$$z + \frac{1}{\Omega} \int_{\tau}^{\lambda(z;\tau)} v_z\, d\tau_2 = 0, d; \quad \lambda(z; \tau) \leqslant \tau. \tag{2.5}$$

From the periodicity requirement of f in τ with period 2π, it follows that $\lambda(z; \tau + 2\pi) = \lambda(z, \tau) + 2\pi$. If Eqs. (2.5) do not have a solution (massive

---

*$r = pc/eH$ is the radius of the electron orbit in the magnetic field, $\gamma = r/\ell$.

metal), then we must set $\lambda(z;\tau)$ equal to $-\infty$. We can show by a direct demonstration that (2.4) satisfies all the required conditions.

In the case in which the magnetic field is parallel to the surface of the film, the distribution function $f(z;\tau)$ is discontinuous, where the discontinuity occurs along the characteristic of Eq. (2.1), i.e., along the line

$$0 \leqslant z = \frac{1}{\Omega}\int^{\tau} v_z\, d\tau_2 + \text{const} \leqslant d. \qquad (2.6)$$

The presence of the discontinuity corresponds to the fact that the electrons (with given τ) reaching one of the surfaces of the film cannot penetrate directly (i.e., without collisions inside the metal) to a depth greater than $2r(\tau)$.* At the same time, the electrons (with the same value of τ) capable of penetrating to depths greater than $2r(\tau)$ do not collide directly with the boundaries of the film. Therefore, all the electrons are divided in a natural way into two groups: electrons which undergo collisions with the boundaries, and electrons which do not reach the boundaries (without collisions inside the film). The distribution function for these two groups of electrons are essentially different, which also corresponds to the presence of a discontinuity.

It is not difficult to show that the solution of Eq. (2.1) with the boundary conditions (2.2) is unique in the class of functions which achieve discontinuities along the characteristic (2.6). For this purpose it suffices to note that Eq. (2.1) with the right hand side equal to zero has its own general solution

$$f = \exp\left(-\int_0^{\tau}\gamma d\tau_2\right)\Phi\left(z - \frac{1}{\Omega}\int_0^{\tau} v_z d\tau_2\right)$$

(Φ is an arbitrary function which can have a discontinuity), which, however, does not satisfy the requirement of periodicity in τ and consequently is identically equal to zero. Thus, for finding the jump in the function f at the discontinuity, no additional conditions are required.

We can obtain (2.4) directly from (2.1). For this purpose, we continue the function $f(z;\tau)$ by setting it equal to zero for $z < 0$ and $z > d$, and apply a Laplace transformation:

$$F(p;\tau) = \int_0^{d} f(z;\tau)\, e^{-pz}\, dz;$$

$$G(p;\tau) = \int_0^{d} g(z;\tau)\, e^{-pz}\, dz \equiv \int_0^{d} \frac{e}{\Omega}\frac{\partial f_0}{\partial \varepsilon}\, vE(z)\, e^{-pz}\, dz,$$

then

$$\frac{\partial F}{\partial \tau} + \left(\gamma + \frac{pv_z}{\Omega}\right)F = G(p;\tau) + \frac{v_z}{\Omega}\left[f(0;\tau) - f(d;\tau)\, e^{-pd}\right].$$

The periodic integral of this equation is equal to

$$F(p;\tau) = \int_{-\infty}^{\tau} d\tau_1 \cdot \exp\left[\int_{\tau}^{\tau_1}\left(\gamma + \frac{pv_z}{\Omega}\right)d\tau_2\right]$$
$$\times\left\{G(p;\tau_1) + \frac{v_z(\tau_1)}{\Omega}\left[f(0;\tau_1) - f(d;\tau_1)\, e^{-pd}\right]\right\},$$

whence

$$f(z;\tau) \equiv \frac{1}{2\pi i}\int_{s-i\infty}^{s+i\infty} F(p;\tau)\, e^{pz}\, dp$$
$$= \int_{-\infty}^{\tau} d\tau_1 \exp\left(\int_{\tau}^{\tau_1}\gamma\, d\tau_2\right)\left\{g\left(z + \frac{1}{\Omega}\int_{\tau}^{\tau_1} v_z\, d\tau_2;\ \tau_1\right)\right.$$
$$+ \frac{v_z(\tau_1)}{\Omega}\left[f(0;\tau_1)\,\delta\left(z + \frac{1}{\Omega}\int_{\tau}^{\tau_1} v_z\, d\tau_2\right)\right. \qquad (2.7)$$
$$\left.\left. - f(d;\tau_1)\,\delta\left(z - d + \frac{1}{\Omega}\int_{\tau}^{\tau_1} v_z\, d\tau_2\right)\right]\right\}.$$

It follows from the boundary conditions (2.2) that

$$f(0;\tau) = -\operatorname{sgn} v_z f(0;\tau);\quad f(d;\tau) = \operatorname{sgn} v_z f(d;\tau);$$
$$\operatorname{sgn} x = \begin{cases} 1 & (x > 0) \\ -1 & (x < 0). \end{cases} \qquad (2.8)$$

Introducing

$$u(z;\tau) = \exp\left(\int_0^{\tau}\gamma\, d\tau_2\right) f(z;\tau)$$

and making use of (2.8), we get

$$u(z;\tau) + \int_{-\infty}^{\tau} d\tau_1 u\left(z + \frac{1}{\Omega}\int_{\tau}^{\tau_1} v_z\, d\tau_2;\ \tau_1\right)$$
$$\times \frac{|v_z(\tau_1)|}{\Omega}\left\{\delta\left(z + \frac{1}{\Omega}\int_{\tau}^{\tau_1} v_z\, d\tau_2\right) + \delta\left(z - d + \frac{1}{\Omega}\int_{\tau}^{\tau_1} v_z\, d\tau_2\right)\right.$$
$$\left. = \int_{-\infty}^{\tau} \exp\left(\int_0^{\tau_1}\gamma\, d\tau_2\right) g\left(z + \frac{1}{\Omega}\int_{\tau}^{\tau_1} v_z\, d\tau_2;\ \tau_1\right) d\tau_1.\right.$$

Because of the presence of the δ-function, the left side of this equation reduces to

$$u(z;\tau) + \sum_s u\left(z + \frac{1}{\Omega}\int_{\tau}^{\lambda_s(z;\tau)} v_z\, d\tau_2;\ \lambda_s(z;\tau)\right)$$

*For simplicity in the given case, we assume that the thickness of the film d is greater than the diameter of the maximum orbit max 2r(r).

$$= \int_{-\infty}^{\tau} d\tau_1 \exp\left(\int_0^{\tau_1} \gamma\, d\tau_2\right) g\left(z + \frac{1}{\Omega}\int_{\tau}^{\tau_1} v_z\, d\tau_2;\ \tau_1\right). \qquad (2.9)$$

The summation in (2.9) extends over all the roots $\lambda_s(z;\tau)$ of the equation

$$z + \frac{1}{\Omega}\int_{\tau}^{\lambda_s(z;\tau)} v_z\, d\tau_2 = 0,\ d; \quad \tau \geqslant \lambda_1 > \lambda_2 > \ldots \geqslant -\infty.$$

The solution of the functional equation (2.9), as is easy to verify, is

$$u(z;\tau) = \int_{\lambda_1(z;\tau)}^{\tau} d\tau_1 \exp\left(\int_0^{\tau_1} \gamma\, d\tau_2\right) g\left(z + \frac{1}{\Omega}\int_{\tau}^{\tau_1} v_z\, d\tau_2;\ \tau_1\right),$$

which gives Eq. (2.4) for $f(z;\tau)$. In this case, we need to take into account that, by definition,

$$\lambda_1\left(z + \frac{1}{\Omega}\int_{\tau}^{\lambda_s} v_z\, d\tau_2;\ \lambda_s\right) \equiv \lambda_{s+1}(z;\tau).$$

3. GENERAL FORMULA FOR THE EFFECTIVE CONDUCTIVITY TENSOR

To find the effective conductivity tensor, we must compute the mean value of the distribution function in terms of which the average current is expressed [see Eq. (2.3)]. From (2.1), we have

$$\frac{\partial \bar{f}(\tau)}{\partial \tau} + \gamma \bar{f} = \frac{e}{\Omega}\frac{\partial f_0}{\partial \varepsilon}\mathbf{v}\bar{\mathbf{E}} - \frac{v_z}{\Omega d}[f(d;\tau) - f(0;\tau)], \quad (3.1)$$

$$\bar{f}(\tau) = \frac{1}{d}\int_0^d f(z;\tau)\, dz; \quad \gamma = 1/\Omega t_0.$$

Making use of (2.8), we find

$$\bar{f}(\tau) = \int_{-\infty}^{\tau} d\tau_1 \exp\left(\int_{\tau}^{\tau_1} \gamma\, d\tau_2\right)\left\{\frac{e}{\Omega}\frac{\partial f_0}{\partial \varepsilon}\cdot \mathbf{v}(\tau_1)\bar{\mathbf{E}} - \frac{|v_z(\tau_1)|}{\Omega d}[f(d;\tau_1) + f(0;\tau_1)]\right\}. \qquad (3.2)$$

After substitution for $f(0;\tau)$ and $f(d;\tau)$ from (2.4), we get

$$\bar{f}(\tau) = \frac{e}{\Omega}\frac{\partial f_0}{\partial \varepsilon}\int_{-\infty}^{\tau} d\tau_1 \exp\left(\int_{\tau}^{\tau_1} \gamma\, d\tau_2\right)\left\{\mathbf{v}(\tau_1)\bar{\mathbf{E}} - \frac{|v_z(\tau_1)|}{\Omega d}\int_{s(\tau_1)}^{\tau_1} d\tau' \exp\left(\int_{\tau_1}^{\tau'} \gamma\, d\tau_2\right)\mathbf{v}(\tau')\,\mathbf{E}\left(\frac{1}{\Omega}\int_{\tau_1} v_z\, d\tau_2\right)\right\}, \quad (3.3)$$

where $s(\tau) = \lambda_1(d-0;\tau)$ for $v_z(\tau) > 0$, $s(\tau) = \lambda_1(+0;\tau)$ for $v_z(\tau) < 0$, where $s(\tau) < \tau$. It is easy to see that $s(\tau)$ coincides with the nearest preceding τ root of one of the equations

$$\frac{1}{\Omega}\left|\int_{s(\tau)}^{\tau} v_z\, d\tau_2\right| = 0; \quad \frac{1}{\Omega}\left|\int_{s(\tau)}^{\tau} v_z\, d\tau_2\right| = d.$$

Taking $\mathbf{E}(z)$ to be constant (see Sec. 2) and substituting (3.3) in (2.3), we get the final expression for the effective conductivity tensor in the very general form

$$\sigma_{ik} = \sigma_{ik}^{(0)} - \delta\sigma_{ik} \quad (\bar{j}_i = \sigma_{ik}\bar{E}_k);$$

$$\sigma_{ik}^{(0)} = -\frac{2e^2}{h^3}\int_0^{\infty}\frac{\partial f_0}{\partial \varepsilon}\, d\varepsilon \int \frac{m}{\Omega}\, dp_H \times \int_0^{2\pi} v_i(\tau)\, d\tau \int_{-\infty}^{\tau} \exp\left(\int_{\tau}^{\tau_1} \gamma\, d\tau_2\right) v_k(\tau_1)\, d\tau_1; \qquad (3.4)$$

$$\delta\sigma_{ik} = -\frac{2e^2}{h^3 d}\int_0^{\infty}\frac{\partial f_0}{\partial \varepsilon}\, d\varepsilon \cdot \int \frac{m}{\Omega^2}\, dp_H \int_0^{2\pi} v_i(\tau)\, d\tau \int_{-\infty}^{\tau} |v_z(\tau_1)|\, d\tau_1 \times \int_{s(\tau_1)}^{\tau_1} \exp\left(\int_{\tau}^{\tau'} \gamma\, d\tau_2\right) v_k(\tau')\, d\tau'.$$

In the case of several bands in (3.4), it is necessary to sum the corresponding expressions over all bands.

The tensor $\sigma_{ik}^{(0)}$ coincides with the conductivity tensor for the massive metal; the presence of $\delta\sigma_{ik}$ is brought about by the finite thickness of the film. In the limiting case of zero magnetic field, Eqs. (3.4) reduce to the corresponding equations of the researches of Fuchs[1] and Kaganov and Azbel'.[2] If the magnetic field is parallel to the surface of the film, (3.4) coincides with the results of Azbel'[7] and Königsberg.[8]

It should be noted that the Onsager relations $\sigma_{ik}(H) = \sigma_{ki}(-H)$ for the effective conductivity tensor of the film are, generally speaking, violated [it appears that $\sigma_{ik}^{(0)}(H) = \sigma_{ki}^{(0)}(-H)$]. This is not unexpected, since in the case of the film, the conductivity tensor, strictly speaking, is an operator, because of the dependence of the electric field on the coordinate z. However, in several cases (for example, a strong magnetic field parallel to the surface) we can neglect the nondiagonal components of $\delta\sigma_{ik}$ in comparison with the corresponding components in $\sigma_{ik}^{(0)}$, and then the Onsager relations will be satisfied asymptotically.

4. INVESTIGATION OF LIMITING CASES

Having in mind the comparison of the results of the present theory with the experiments of Borovik and Lazarev,[9] we consider in this section the region of strong magnetic fields ($\gamma \ll 1$) in which we consider that $d \sim \ell$. Just this case

is studied in detail in Ref. 9. With the aim of simplifying the final formulas, we shall assume the dispersion law to be isotropic and quadratic, and the relaxation time t_0 to be constant and not to depend on $\mathbf{p}$ (the residual resistance). We can show that the qualitative results (in particular, the dependence of H) do not depend on the form of the dispersion law and the collision integral.

The asymptoticity of the tensor $\sigma_{ik}^{(0)}$ in strong fields was studied in detail by Lifshitz, Azbel', and Kaganov[11] for an arbitrary form of dispersion law $\epsilon(\mathbf{p})$ and collision integral. It was shown in their work that for closed Fermi surfaces, the dispersion law and the collision integral have no effect on the dependence of $\sigma_{ik}^{(0)}$ on strong magnetic fields.

The basic difficulty in the calculation of $\delta\sigma_{ik}$ is contained in the determination of the function $s(\tau)$. Unfortunately, we did not succeed in finding a suitable analytic expression for $s(\tau)$ for arbitrary angle of inclination of H to the surface of the film. Simple formulas for $s(\tau)$ were obtained in a constant magnetic field parallel to and perpendicular to the surface of the film.

In the perpendicular field, v_z does not depend on τ and

$$s(\tau) = \tau - \Omega d/|v_z|. \tag{4.1}$$

In the parallel field two cases are distinguished: a) $d > 2r$ ($r = mvc/eH$, sufficiently strong magnetic field). In this case, the electrons which are colliding with one of the boundaries of the film cannot directly reach the other boundary (i.e., without collisions inside the film). b) $d = 2r$ (weak magnetic field or sufficiently thin film). The calculations are especially simple in case a) and are considerably complicated in case b).

For $d = 2r$, all the components of the tensor $\delta\sigma_{ik}$ are continuous. Finite jumps have a third derivative δs_{xx} with respect to H, second derivatives $\delta\sigma_{xy}$, $\delta\sigma_{yx}$, $\delta\sigma_{xz}$ and first derivatives of all the remaining components of $\delta\sigma_{ik}$.

In the perpendicular field, the nonzero components of the effective conductivity tensor are equal to

$$\frac{\sigma_{xx}}{\sigma_0} = \frac{\sigma_{yy}}{\sigma_0} = \frac{\gamma^2}{1+\gamma^2}\left\{1 - \frac{3}{8k}\frac{(\gamma^2-1)A + 2\gamma B}{1+\gamma^2}\right\};$$

$$\frac{\sigma_{zz}}{\sigma_0} = 1 - \frac{3}{4k}C; \tag{4.2}$$

$$\frac{\sigma_{xy}}{\sigma_0} = -\frac{\sigma_{yx}}{\sigma_0} = -\frac{\gamma}{1+\gamma^2}\left\{1 - \frac{3}{8k}\frac{\gamma}{1+\gamma^2}[2\gamma A + (1-\gamma^2)B]\right\},$$

where $n = 8\pi p^3/3\hbar^3$ is the density of electrons,

$$\sigma_0 = ne^2t_0/m, \quad \gamma = r/l = 1/\Omega t_0; \quad \alpha = d/r; \quad k = d/l;$$

$$A + iB = 1 - 4E_3(k + i\alpha) + 4E_5(k + i\alpha); \quad C = 1 - 4E_5(k);$$

$$E_n(x) = \int_1^\infty \xi^{-n} e^{-x\xi}\, d\xi.$$

Equations (4.2) are accurate (and coincide with the corresponding equations in Ref. 7a), as far as the equation $j_z = 0$ is satisfied by E_z, which is equal to zero, and we can introduce the tensor (and not the operator!) of the conductivity. It is obvious that in this case the Onsager relations are satisfied.

For $\gamma \ll 1$ and $k \sim 1$, Eqs. (4.2) yield

$$\sigma_{xx}/\sigma_0 = \sigma_{yy}/\sigma_0 = \gamma^2(1 + 3/8k); \quad \sigma_{zz}/\sigma_0 = 1 - 3C/4k;$$

$$\sigma_{xy}/\sigma_0 = -\sigma_{yx}/\sigma_0 = -\gamma(1 - \gamma^2 + 3\gamma^2/4k). \tag{4.3}$$

a) In a sufficiently strong parallel field ($d > 2r$), the function $s(\tau)$ is a solution of the equation

$$\frac{1}{\Omega}\int_{s(\tau)}^{\tau} v_z(\tau_2)\, d\tau_2 \equiv \frac{1}{m\Omega}[p_y(s(\tau)) - p_y(\tau)] = 0$$

(the equation

$$\frac{1}{\Omega}\left|\int_{s(\tau)}^{\tau} v_z\, d\tau_2\right| = d$$

has no solution).

Setting

$$\mathbf{v} = \mathbf{p}/m = v(\cos\vartheta, \quad \sin\vartheta\sin\tau,$$

$$\sin\vartheta\cos\tau), \quad -\pi/2 \leqslant \tau \leqslant 3\pi/2,$$

we find

$$s(\tau) = -\pi - \tau \text{ for } -\pi/2 \leqslant \tau \leqslant \pi/2, \; s(\tau)$$

$$= \pi - \tau \text{ for } \pi/2 \leqslant \tau \leqslant 3\pi/2. \tag{4.4}$$

The nonzero components of the tensor σ_{ik} have the form

$$\frac{\sigma_{xx}}{\sigma_0} = 1 - \frac{3}{8k}\left(1 - \frac{1}{2}\frac{1 + e^{-2\pi|\gamma|}}{1+4\gamma^2}\right);$$

$$\frac{\sigma_{yy}}{\sigma_0} = \frac{\gamma^2}{1+\gamma^2}\left\{1 - \frac{3}{8k(1+\gamma^2)}\left[\gamma^2 - 2\right.\right.$$

$$\left.\left. - \frac{3(6 - 5\gamma^2 + 4\gamma^4)}{2(1+4\gamma^2)(9+4\gamma^2)}(1 + e^{-2\pi|\gamma|})\right]\right\};$$

$$\frac{\sigma_{zz}}{\sigma_0} = \frac{\gamma^2}{1+\gamma^2}\left\{1 - \frac{3}{8k(1+\gamma^2)}\left[2\gamma^2\right.\right. \tag{4.5}$$

$$\left.\left. - 1 + \frac{9(1+6\gamma^2)(1+e^{-2\pi|\gamma|})}{2(1+4\gamma^2)(9+4\gamma^2)}\right]\right\}; \quad \frac{\sigma_{yz}}{\sigma_0} = -\frac{\sigma_{zy}}{\sigma_0}$$

$$= -\frac{\gamma}{1+\gamma^2}\left\{1 - \frac{9}{8k}\frac{\gamma^2}{(1+\gamma^2)}\left[1 + \frac{(7 - 8\gamma^2)(1 + e^{-2\pi|\gamma|})}{2(1+4\gamma^2)(9+4\gamma^2)}\right]\right\}.$$

Equations (4.5) have meaning only for $r \ll \ell$, $r < d/2$, when we can neglect the dependence of the Hall field E_z on the coordinates. For $\gamma \ll 1$,

$$\frac{\sigma_{xx}}{\sigma_0} = 1 - \frac{3\pi}{k}|\gamma|; \quad \frac{\sigma_{yy}}{\sigma_0} = \gamma^2\left\{1 + \frac{3}{2k} - \frac{3\pi}{4k}|\gamma|\right\}; \quad (4.6)$$

$$\frac{\sigma_{zz}}{\sigma_0} = \gamma^2\left\{1 + \frac{3\pi|\gamma|}{8k}\right\}; \quad \frac{\sigma_{yz}}{\sigma_0} = -\frac{\sigma_{zy}}{\sigma_0} = -\gamma\left\{1 - \gamma^2 - 2\frac{\gamma^2}{k}\right\}.$$

b) In the case of a weak magnetic field ($d < 2r$), the function $s(\tau)$ is determined differently for the regions $\sin\vartheta < \alpha/2$ and $\sin\vartheta > \alpha/2$. For $\sin\vartheta < \alpha/2$, $s(\tau)$ is given by Eq. (4.4), while if $\sin\vartheta > \alpha/2$, then

$$s(\tau) = -\pi - \tau \text{ for } -\pi/2 < \tau < \tau_0;$$

$$s(\tau) = \arcsin(\sin\tau - \alpha/\sin\vartheta) \text{ for } \tau_0 < \tau < \pi/2;$$

$$s(\tau) = \pi - \tau \text{ for } \pi/2 < \tau < \pi + \tau_0;$$

$$s(\tau) = \pi - \arcsin(\sin\tau + \alpha/\sin\vartheta) \text{ for } \pi + \tau_0 < \tau \leqslant 3\pi/2;$$

$$\tau_0 = \arcsin(-1 + \alpha/\sin\vartheta).$$

Let us cite the result for the conductivity of the film in a weak longitudinal magnetic field ($\mathbf{E} \parallel \mathbf{H} \parallel x$), when $\gamma \gg 1/k + k$, $\alpha \ll 1$:

$$\sigma_{xx} = \sigma_F - \sigma_0 M/\gamma^2, \quad \sigma_F/\sigma_0$$

$$= 1 - {}^3/_8 k + ({}^3/_2 k)(E_3(k) - E_5(k)). \quad (4.7)$$

Here σ_F is the conductivity of the film in the absence of a magnetic field, obtained by Fuchs,[1] while the coefficient M depends on the thickness of the film:

$$M = \frac{3}{64k}\left\{-1 + 2\left[1 + k + \frac{k^2}{6}(1-k)\right]e^{-k} + \frac{k^4}{3}E_1(k)\right\}.$$

5. SPECIFIC RESISTANCE AND THE HALL FIELD. COMPARISON WITH EXPERIMENT

By experiment one usually obtains not the direction of the electric field, but the current density and, consequently, the resistivity tensor $\rho_{ik} = \sigma_{ik}^{-1}$ rather than its inverse, the conductivity tensor. Employing the results obtained above for σ_{ik}, it is not difficult to find the dependence of the electrical resistance on H.

Let us obtain the formulas for the resistivity and the Hall field in a film located in a strong magnetic field, in the presence of two types of current carriers (electrons and "holes"). The indices 1 and 2 will refer to electrons and "holes," respectively:

1) $n_1 \neq n_2$;

$$\rho_\perp = \frac{n_1u_1 + n_2u_2 + {}^3/_8(n_1u_1/k_1 + n_2u_2/k_2)}{(n_1 - n_2)^2e^2} + O(H^{-2});$$

$$\rho_\parallel^\parallel = \rho_0\left\{1 + \frac{3\pi}{8}\rho_0\frac{ec}{H}\left(\frac{n_1}{k_1} + \frac{n_2}{k_2}\right)\right\} + O(H^{-2});$$

$$\rho_0 = \left[e^2\left(\frac{n_1}{u_1} + \frac{n_2}{u_2}\right)\right]^{-1}$$

$$\rho_\parallel^\perp = \frac{n_1u_1 + n_2u_2\,e + (3\pi c/8H)(n_1u_1^2/k_1 + n_2u_2^2/k_2)}{(n_1 - n_2)^2e^2} + O(H^{-2});$$

$$\left(\frac{E_y}{E_x}\right)_\perp = -\frac{eH}{c}\frac{n_1 - n_2}{n_1u_1 + n_2u_2 + {}^3/_8(n_1u_1/k_1 + n_2u_2/k_2)} + O(H^{-1});$$

$$\left(\frac{E_z}{E_y}\right)_\parallel = -\frac{eH(n_1 - n_2)}{c(n_1u_1 + n_2u_2)} + O(H^{-1}). \quad (5.1)$$

Here, $u_i = m_i/t_{0i}$ is the mobility of the carriers; $k_i = d/\ell_i$; the subscript symbols in all the quantities indicate the orientation of H relative to the surface of the film, while the superscript symbols for $\rho_\parallel$ denote the orientation of the current relative to the magnetic field.

2) $n_1 = n_2 = n$;

$$\rho_\perp = \frac{H^2}{nc^2[u_1 + u_2 + {}^3/_8(u_1/k_1 + u_2/k_2)]};$$

$$\rho_\parallel^\parallel = \rho_0\left\{1 + \frac{3\pi}{8}\rho_0\frac{nec}{H}\left(\frac{1}{k_1} + \frac{1}{k_2}\right)\right\};$$

$$\rho_\parallel^\perp = \frac{H^2}{nc^2[u_1 + u_2 + {}^3/_2(u_1/k_1 + u_2/k_2)]}; \quad (5.2)$$

$$\left(\frac{E_y}{E_x}\right)_\perp = \frac{c}{eH}\frac{u_1^2 - u_2^2 - {}^3/_4(u_1^2/k_1 - u_2^2/k_2)}{u_1 + u_2 + {}^3/_8(u_1/k_1 + u_2/k_2)};$$

$$\left(\frac{E_z}{E_y}\right)_\parallel = \frac{c}{eH}\frac{u_1^2 - u_2^2 + 2(u_1^2/k_1 - u_2^2/k_2)}{u_1 + u_2}.$$

The Hall constant $R = \bar{E}_z/jH = -\delta V/jHd$ in strong fields (δV = potential difference between the sides of the film) for $n_1 \neq n_2$ becomes identical asymptotically with that for the massive metal

$$R \cong 1/ec(n_1 - n_2),$$

and for $n_1 = n_2$ depends on the thickness of the film:

$$R_\parallel = \frac{u_1^2 - u_2^2 + 2(u_1^2/k_1 - u_2^2/k_2)}{nec(u_1 + u_2)[u_1 + u_2 + {}^3/_2(u_1/k_1 + u_2/k_2)]};$$

$$R_\perp = \frac{u_1^2 - u_2^2 - {}^3/_4(u_1^2/k_1 - u_2^2/k_2)}{nec[u_1 + u_2 + {}^3/_8(u_1/k_1 + u_2/k_2)]^2} \quad (5.3)$$

We proceed to a comparison of theory with experiment[9] on the effect of the shape of the specimen on the resistance of single crystals of Bi. From the fact of the increase in resistance in a strong magnetic field for massive Bi, we can draw the conclusion that $n_1 = n_2$, while it follows from experiments on the de Haas — van Alphen effect[12] that the Fermi surface for electrons in Bi is represented by a set of three uniaxial ellipsoids, located in a binary plane and turned one to the other by 120° about an axis of third order. The Fermi surface for the "holes" in Bi was little investigated, but usually it is spherical. For simplicity,

we replace the set of three ellipsoids by a single sphere (qualitative results are not changed for this case). From the equality of electrons and "holes" follows the equality of the boundary momenta and their orbital radii. The minimum resistance on the rotation diagram for $\varphi = 0$ (φ = angle between H and the film surface, $\mathbf{H} \perp \mathbf{j}$) discovered in Ref. 9 is satisfactorily explained by the formulas (5.2):

$$\frac{\rho_{\parallel}^{\perp}}{\rho_{\perp}} = \frac{d+3\bar{l}/8}{d+3\bar{l}/2} < 1; \quad 2/\bar{l} = 1/l_1 + 1/l_2; \; u_i = p/l_i.$$

It is seen from (5.2) that the increase in the resistance of the film in a strong transverse magnetic field takes place according to the same law as for the massive metal ($k_1 = \infty$), but more slowly than in the latter:*

$$\rho_{\parallel}^{\perp}(d)/\rho_{\parallel}^{\perp}(\infty) = d/(d+3\bar{l}/2) < 1;$$

$$\rho_{\perp}(d)/\rho_{\perp}(\infty) = d/(d+3\bar{l}/8) < 1.$$

The dependence of the quantity β on the magnetic field

$$\beta = \rho_{\parallel}^{\perp}/\rho_{\perp} = \frac{d+3\bar{l}/8}{d+3\bar{l}/2}\left\{1+\frac{3\pi}{4}\frac{r}{d+3\bar{l}/2}\right\}$$

$$= \frac{d+3\bar{l}/8}{d+3\bar{l}/2}\left\{1+\frac{H_0}{H}\right\}, \; H_0 = \frac{3\pi}{4}\frac{pc}{e(d+3\bar{l}/2)} \ll H, \quad (5.4)$$

agrees with that observed by Borovik and Lazarev for the decrease in this ratio in a strong field.

The presence of a discontinuity (jump in the derivative) for the quantity β at $r = d/2$ is clearly evident in Fig. 6 of Ref. 9.

Change of β with temperature is connected with the temperature dependence of the mean free path $\bar{l}$. For $\bar{l} \ll d$, (5.4) gives unity while for $\bar{l} \gg d$, $\beta \approx 1/4$. In Ref. 9, at low temperatures, when we can assume that $l \gg d$, the quantity $\beta \sim 1/2$. This difference can be connected both with the anisotropies of the dispersion law and the mean free path length, and also with the fact that $\bar{l} \sim d$ in the region of residual resistance, where $\bar{l}$ no longer depends on the temperature.

It is obvious that in such experiments only the mean free path length $\bar{l}$ can be measured, and not l_1 and l_2 separately.

Comparison with experiments on the dependence of the Hall field in the film on H is not possible because of the absence of experimental data.

*An exception is the specimen Bi-3 investigated in Ref. 9, the massive part of which (according to the way of obtaining it) was more "rougher" than the film, i.e. $\bar{l}_{mass} < d(3/2\bar{l}_f + d)/\bar{l}_f$.

6. THERMOMAGNETIC EFFECTS IN FILMS

The effect of the magnetic field on the thermal conductivity, the coefficients of Thomson, Peltier and others, in a massive metal, was studied by Azbel', Kaganov, and Lifshitz.[13] Here we shall briefly consider the thermomagnetic effects in films and establish the connection of the tensors of thermal conductivity and the Thomson coefficients with the electrical conductivity tensor.

If a temperature gradient exists in the metal; then a heat current arises, the density of which, w, is equal to

$$\mathbf{w} = 2h^{-3}\int \varepsilon \mathbf{v} f \, (d\mathbf{p}).$$

To find the kinetic coefficients, we must compute the density of the electric current j and the energy flux density w, which arises as a result of the electric field and the temperature gradient. In this case, in the right side of the kinetic equation (2.2), we have, in place of $e\mathbf{E}\cdot\mathbf{v}\,\partial f_0/\partial\epsilon$:

$$e\mathbf{E}\mathbf{v}\frac{\partial f_0}{\partial \varepsilon} - \mathbf{v}\frac{\partial f_0}{\partial T}\nabla T. \quad (6.1)$$

In those cases in which we can introduce the effective conductivity tensor (see Sec. 2—4), we have

$$\bar{j}_i = \sigma_{ik}\bar{E}_k + S_{ik}^{(0)}\partial\bar{T}/\partial x_k; \; \bar{w}_i = \xi_{ik}\bar{E}_k + S_{ik}^{(1)}\partial\bar{T}/\partial x_k, \quad (6.2)$$

where

$$\sigma_{ik} = -\int_0^\infty \frac{\partial f_0}{\partial \varepsilon}\sigma_{ik}(\varepsilon)\,d\varepsilon; \quad \xi_{ik} = e^{-1}\int_0^\infty \varepsilon\frac{\partial f_0}{\partial \varepsilon}\sigma_{ik}(\varepsilon)\,d\varepsilon;$$

$$S_{ik}^{(n)} = (-1)^n e^{-1-n}\int_0^\infty \varepsilon^n \frac{\partial f_0}{\partial T}\sigma_{ik}(\varepsilon)\,d\varepsilon, \quad (6.3)$$

while $\sigma_{ik}(\epsilon)$ is determined by the formula

$$\sigma_{ik}(\varepsilon) = \frac{2e^2}{h^3}\int_{\varepsilon(\mathbf{p})=\varepsilon}\frac{m}{\Omega}\,dp_H\int_0^{2\pi} v_i(\tau)\,d\tau\int_{-\infty}^{\tau}\exp\left(\int_{\tau}^{\tau_1}\gamma d\tau_2\right)d\tau_1$$

$$\times\left\{v_k(\tau_1) - \frac{|v_z(\tau_1)|}{\Omega d}\int_{s(\tau_1)}^{\tau_1}\exp\left(\int_{\tau_1}^{\tau'}\gamma d\tau_2\right)v_k(\tau')\,d\tau'\right\}. \quad (6.4)$$

From the law of conservation of energy, we get [and also from (6.2)]:

$$\frac{\partial Q}{\partial t} = j_i E_i - \frac{\partial w_i}{\partial x_i} = \rho_{ik} j_i j_k + \frac{\partial}{\partial x_i}\left(\varkappa_{ik}\frac{\partial T}{\partial x_k}\right) - \mu_{ik} j_i \frac{\partial T}{\partial x_k}.$$

Here Q is the internal energy density; $\rho_{ik} = \sigma_{ik}^{-1}$ the resistivity tensor;

$$\varkappa_{ik} = \xi_{ip}\rho_{pq}S_{qk}^{(0)} - S_{ik}^{(1)} \quad \text{и} \quad \mu_{ik} = \rho_{ip}S_{pk}^{(0)} + \frac{\partial}{\partial T}(\xi_{ip}\rho_{pk}) -$$

are the thermal conductivity and Thomson coefficients.

It was shown in Ref. 13 that if the collision operator was a δ-function in the energy, then for each of the components of the tensors of conductivity and thermal conductivity, the Wiedmann-Franz law is satisfied. The calculations carried out in Ref. 13 are not connected with the concrete form of σ_{ik}, μ_{ik}, κ_{ik}, and therefore we can make direct use of the results of Ref. 13 and write down at once:

$$\sigma_{ik} = \sigma_{ik}(\zeta_0; d); \quad \varkappa_{ik} = {}^1/_3\pi^2k^2T\sigma_{ik};$$
$$\mu_{ik} = \frac{\pi^2k^2T}{3e}\left(\rho_{ip}\frac{\partial\sigma_{pk}}{\partial\zeta_0} - 2\rho_{pi}\frac{\partial\sigma_{kp}}{\partial\zeta_0}\right). \qquad (6.5)$$

Here $\zeta_0 = \zeta(0)$ is the chemical potential of the electron gas at absolute zero (the limiting Fermi energy), k is Boltzmann's constant. Thus, the tensors κ_{ik} and μ_{ik} are expressed in terms of the tensor σ_{ik} studied above.

In conclusion, I take this opportunity to thank M. Ia. Azbel', E. S. Borovik, B. G. Lazarev, and I. M. Lifshitz for useful discussions and criticism of the results of the research.

[1] K. Fuchs, Proc. Cambr. Phil. Soc. **34**, 100 (1938).

[2] M. I. Kaganov and M. Ia. Azbel', J. Exptl. Theoret. Phys. (U.S.S.R.) **27**, 762 (1954).

[3] R. Englman E. H. Sondheimer, Proc. Phys. Soc. (London) **B69**, 449 (1956).

[4] R. B. Dingle, Proc. Roy. Soc. (London) **A201**, 545 (1950).

[5] D. K. Macdonald and K. Sarginson, Proc. Roy. Soc. (London) **A203**, 223 (1950).

[6] R. G. Chambers, Proc. Roy. Soc. (London) **A202**, 378 (1950).

[7] M. Ia. Azbel', Dokl. Akad. Nauk SSSR **99**, 519 (1954).

[7a] E. H. Sondheimer, Phys. Rev. **80**, 401 (1950).

[8] E. Königsberg, Phys. Rev. **91**, 8 (1953).

[9] E. S. Borovik and B. G. Lazarev, J. Exptl. Theoret. Phys. (U.S.S.R.) **21**, 857 (1951); Dokl. Akad. Nauk SSSR **62**, 611 (1948).

[10] E. R. Andrew, Proc. Phys. Soc. (London) **A62**, 77 (1949).

[11] Lifshitz, Azbel', and Kaganov, J. Exptl. Theoret. Phys. (U.S.S.R.) **31**, 63 (1956), Soviet Phys. JETP **4**, 41 (1957).

[12] B. Shoenberg, Phil. Trans. **A245**, 1 (1952).

[13] Azbel', Kaganov, and Lifshitz, J. Exptl. Theoret. Phys. (U.S.S.R.) **32**, 1188 (1957); Soviet Phys. JETP **5**, 967 (1957).

Translated by R. T. Beyer
126

SOVIET PHYSICS JETP VOLUME 34 (7), NUMBER 3 SEPTEMBER, 1958

STATIONARY CONVECTIVE FLOW OF AN ELASTICALLY CONDUCTING LIQUID BETWEEN PARALLEL PLATES IN A MAGNETIC FIELD

G. Z. GERSHUNI and E. M. ZHUKHOVITSKII

Perm State University and Perm Pedagogical Institute

Submitted to JETP editor September 19, 1957

J. Exptl. Theoret. Phys. (U.S.S.R.) **34**, 670-674 (March, 1958)

A study is made of the stationary convection of an electrically conducting liquid in the space between two parallel plates, heated to different temperatures, in the presence of a magnetic field. The distribution of velocity, temperature, and induced fields are found, and the convective heat flow is calculated.

IT is well known that currents are induced in a conducting liquid which moves in a magnetic field. The interaction of these currents with the magnetic field is the cause of the various magnetohydrodynamic effects which have been intensively studied in recent years. The magnetic field will,

of course, also have an effect on the convective flow of an electrically conducting liquid. As an example, we may cite the increased stability of the equilibrium of an electrically conducting liquid heated from below when a magnetic field is applied.[1,2] In the present paper we consider the stationary convective motion of a conducting liquid located in a magnetic field, in the space between two parallel plates heated to different temperatures.

1. The current flowing in a medium moving with velocity $\mathbf{v}$ is equal to

$$\mathbf{j} = \sigma\left(\mathbf{E} + \frac{1}{c}\mathbf{v}\times\mathbf{B}\right), \tag{1}$$

where σ is the electrical conductivity, and $\mathbf{E}$ and $\mathbf{B}$ are the field strengths. The nature of the fields and material motions are to be determined from the equations of motion for the medium (in our case these are the equations of convection) and from Maxwell's equations for the fields in the medium:

$$\frac{\partial \mathbf{v}}{\partial t} + \mathbf{v}\cdot\nabla\mathbf{v} = -\frac{1}{\rho}\nabla p + \nu\nabla^2\mathbf{v} + g\beta\gamma T + \frac{1}{\rho c}\mathbf{j}\times\mathbf{B}; \tag{2}$$

$$\partial T/\partial t + \mathbf{v}\nabla T = \chi\nabla^2 T; \tag{3}$$

$$\operatorname{div}\mathbf{v} = 0; \tag{4}$$

$$\operatorname{curl}\mathbf{H} = \frac{4\pi}{c}\mathbf{j}, \quad \operatorname{div}\mathbf{B} = 0; \tag{5}$$

$$\operatorname{curl}\mathbf{E} = -\frac{1}{c}\frac{\partial \mathbf{B}}{\partial t}, \quad \operatorname{div}\mathbf{D} = 4\pi\rho_e. \tag{6}$$

Here p is the convective pressure, T is the temperature, ρ is the density of the liquid, g is the acceleration of gravity, ν is the kinematic viscosity, β is the thermal diffusivity, χ is the thermal conductivity, $\boldsymbol{\gamma}$ is a unit vector directed vertically upward, and ρ_e is the space charge density. In accordance with the usual assumptions, we have neglected displacement currents in the equation for curl H, and the viscous and Joule dissipations in the heat transfer equation.

By eliminating the electric field strength and current density from Maxwell's equations and Eq. (1), we obtain

$$\partial\mathbf{H}/\partial t + \operatorname{curl}(\mathbf{H}\times\mathbf{v}) = \lambda\nabla^2\mathbf{H}, \quad \lambda = c^2/4\pi\mu\sigma. \tag{7}$$

Substituting the expression $(c/4\pi)\operatorname{curl}\mathbf{H}$ for the current density, we can write two of the terms in the equation of motion (2) in the form

$$-\frac{1}{\rho}\nabla p + \frac{1}{\rho c}\mathbf{j}\times\mathbf{B} = -\frac{1}{\rho}\nabla\left(p + \frac{\mu H^2}{8\pi}\right) + \frac{\mu}{4\pi\rho}\mathbf{H}\cdot\nabla\mathbf{H};$$

Here the gradient symbol operates on the total pressure (convective plus magnetic).

We now introduce dimensionless variables. Denote by $2d$ the distance between the parallel plates, by 2Θ the constant temperature difference between them, and take d and Θ as the new units of length and temperature. As the unit of field strength we choose the value of the constant, uniform, external field H_0. The units of time, velocity, and pressure are chosen as d^2/ν, ν/d, and $\rho\nu^2/d^2$. In terms of these dimensionless variables, the equations take the form

$$\frac{\partial \mathbf{v}}{\partial t} + \mathbf{v}\cdot\nabla\mathbf{v} = -\nabla\left(p + \frac{M^2}{P_m}\frac{H^2}{2}\right) + \nabla^2\mathbf{v} + G\gamma T + \frac{M^2}{P_m}\mathbf{H}\cdot\nabla\mathbf{H}; \tag{8}$$

$$\frac{\partial T}{\partial t} + \mathbf{v}\nabla T = \frac{1}{P}\nabla^2 T; \tag{9}$$

$$\frac{\partial \mathbf{H}}{\partial t} + \operatorname{curl}(\mathbf{H}\times\mathbf{v}) = \frac{1}{P_m}\nabla^2\mathbf{H}; \tag{10}$$

$$\operatorname{div}\mathbf{v} = 0, \quad \operatorname{div}\mathbf{H} = 0. \tag{11}$$

Four dimensionless parameters have been introduced into these equations: $G = g\beta\Theta d^3/\nu^2$, the Grasshof number; $P = \nu/\chi$, the Prandtl number; $M = (B_0 d/c)\sqrt{\sigma/\eta}$, the Hartmann number (here $B_0 = \mu H_0$, and $\eta = \rho\nu$ is the absolute viscosity); and $P_m = \nu/\lambda$.

The boundary conditions for Eqs. (8) to (11) will be established later.

2. Let us consider stationary convection in the space between vertical parallel plates, when an external magnetic field is applied perpendicular to the plates. We shall locate the origin of coordinates midway between the plates. The x axis is directed normal to the plates, in the direction of the colder plate; the z axis is vertically upward; and the y axis is perpendicular to the x and z axes (see Fig. 1).

If the dimensions of the plates are sufficiently large compared to the distance between them, it is possible to find an exact solution of Eqs. (8) to (11) which will describe the stationary motion at all points except near the edges of the plates. For this type of motion, (a) the velocity $\mathbf{v}$ is everywhere parallel to the z axis, (b) the temperature T depends only on x, (c) the field vector $\mathbf{H}$ is always in the xz plane, i.e., $H_y = 0$, (d) all quantities are independent of y (i.e., the problem is two-dimensional), and (e) all quantities except the pressure are independent of z.

Let us now find the profiles of temperature, velocity, and field strength for this system. From the assumptions which have been made as to the type of motion we will have, instead of Eq. (9), $d^2T/dx^2 = 0$, i.e., the temperature profile is linear. If we take the zero of our temperature scale to be the value calculated for $x = 0$, then the boundary conditions for the temperature equation

will be $T(-1) = 1$; $T(1) = -1$; and accordingly,

$$T = -x. \tag{12}$$

We now find the velocities and field strengths. From (11) it follows that $v_z = v(x)$ and $dH_x/dx = 0$; i.e., the component of magnetic field normal to the plates is a constant, and is obviously equal to the external field. Let us assume for the sake of definiteness that the direction of the external field coincides with the positive sense of the x axis. Recalling our choice of unit field strength, we have

$$H_x = 1. \tag{13}$$

The x component of Eq. (8) is

$$\frac{\partial}{\partial x}\left(p + \frac{M^2}{P_m}\frac{H^2}{2}\right) = 0, \tag{14}$$

i.e., the total pressure depends only upon z. Let us now consider the z component of Eq. (8)

$$\frac{d}{dz}\left(p + \frac{M^2}{P_m}\frac{H^2}{2}\right) = v'' + GT + \frac{M^2}{P_m}H_z'$$

(the primes represent differentiation with respect to x). Since the right-hand side is a function of x only, and the left-hand side is a function only of z, we may separate the variables, denoting the separation constant by C, and writing

$$v'' + GT + (M^2/P_m)H_z' = C. \tag{15}$$

The z component of Eq. (10) gives another equation connecting v and H_z:

$$H_z''/P_m = -v', \tag{16}$$

whence

$$H_z'/P_m = -v + C_1. \tag{17}$$

By substituting (12) and (17) into (15) we obtain an equation for v:

$$v'' - M^2 v = G(x + A), \quad A = (C - C_1M^2)/G. \tag{18}$$

The solution of (18) will contain two constants of integration which must be determined from the boundary conditions $v(-1) = v(1) = 0$. In order to determine the constant A we must know the flow of liquid through a cross-section. If the channel is closed at the top and bottom, then the liquid will circulate, rising near the warm plate and sinking near the cold one. In this case, obviously

$$\int_{-1}^{1} v\,dx = 0.$$

If A and the constants of integration are determined for this case, we obtain the velocity profile

$$v = \frac{G}{M^2}\left(\frac{\sinh Mx}{\sinh M} - x\right). \tag{19}$$

To find the induced field H_z we substitute v from (19) into (16), integrate twice, and determine the constants of integration from the boundary conditions

$$H_z(-1) = H_z(1) = 0.$$

As a result we obtain

$$H_z = \frac{GP_m}{M^2}\left(\frac{x^2-1}{2} - \frac{\cosh Mx - \cosh M}{M\sinh M}\right). \tag{20}$$

(Had the external field been in the negative x direction, H_z would have been of the opposite sign.)

Equations (12), (19), and (20) provide the solution of the given problem.

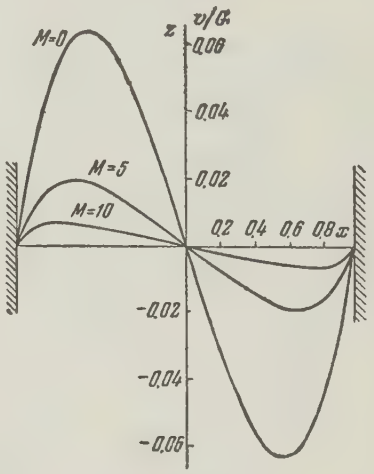

Fig. 1.

3. Figure 1 shows the velocity profiles for M = 0, 5, and 10. As an example, we may note that for mercury $\sigma = 0.945 \times 10^{16}$ sec^{-1} and $\eta = 1.55 \times 10^{-2}$ poise; consequently, $M = 0.026\,B_0 d$. Therefore if d = 1 cm, a value of M = 10 corresponds to a field B_0 of the order of 400 gauss. In the absence of a field (M = 0), Eq. (19) gives the velocity profile

$$v = Gx(x^2 - 1)/6. \tag{21}$$

As the field increases, it is evident from Fig. 1 that the flow rapidly decreases. In addition, an unusual boundary layer appears in the flow pattern; a thin layer develops near the walls in which the velocity gradient is large. (The occurrence of a boundary layer in the flow of liquids in a magnetic field was observed by Hartmann[3] while he was studying the effect of a field on Poiseuille flow.) If the thickness of the boundary layer δ is defined as the distance from the wall to the point where the velocity is a maximum, then for large values of the Hartmann number M (in prac-

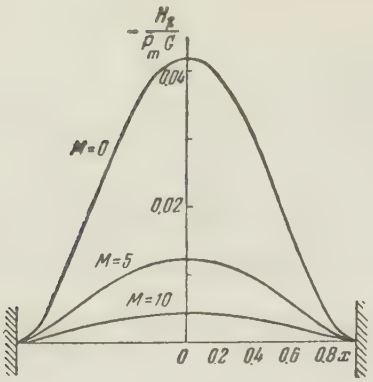

Fig. 2.

tice, when $M > 5$), we have from Eq. (19)

$$\delta = (\ln M)/M. \qquad (22)$$

The distribution of induced magnetic field over the cross-section is shown in Fig. 2. It must be noted that H_z in Eq. (20) and in Fig. 2 is the ratio of the induced (longitudinal) to the external (transverse) field. As $M \to 0$ this ratio approaches a limiting value; for large values of the Hartmann number, H_z as determined from Eq. (20) diminishes in proportion to M^{-2}. Thus, for small external fields H_0 the induced field increases proportionally to H_0, while for large H_0 it decreases as $1/H_0$. A maximum is attained at a field corresponding to $M = 3$. Note also that for moderate values of the Grasshof number the induced field is very much smaller than the external field, since the parameter P_m which enters into formula (20) has the value 10^{-7} for mercury, for example.

The induced field is equal to $j = (c/4\pi)\,\mathrm{curl}\,H$, and therefore the only non-zero component of the current density is j_y, which is proportional to dH_z/dx. The current density therefore varies in the same way as the velocity does over the cross-section.

We can also find the upward flow of heat due to convection, which is equal to

$$Q_M = c_p \rho \int_{-d}^{d} vT\,dx, \qquad (23)$$

per unit of length in the direction of the y axis, where c_p is the specific heat of the liquid, and v and T are the dimensional velocity and temperature. Evaluation of this formula gives

$$\frac{Q_M}{Q_0} = \frac{45}{M^2}\left(\frac{1}{3} - \frac{\coth M}{M} + \frac{1}{M^2}\right), \qquad (24)$$

where Q_0 is the flow in the absence of magnetic field and is equal to

$$Q_0 = 2c_p \rho g \beta \Theta^2 d^3 / 45\nu. \qquad (25)$$

The ratio Q_M/Q_0 decreases monotonically from 1 to 0 as the number M increases.

The solution derived above describes the flow in a vertical channel in the presence of a perpendicular external field. For channels inclined at an angle α to the vertical, it can easily be verified that the solution is the same as before, with $G \times \cos\alpha$ substituted for G. If the field has any arbitrary orientation with respect to the channel, its longitudinal components have no effect on the detailed motions which have been discussed.

[1] S. Chandrasekhar, Phil. Mag. **43**, 501 (1952), **45**, 1177 (1954).

[2] E. M. Zhukovitskii, Физика металлов и металловедение (Physics of Metals and Metal Research) (in press).

[3] J. Hartmann, Kgl. Danske Vidensk., Selskab. Math.-fys. Medd. **15**, 6 (1937).

Translated by D. C. West
127

STABILITY OF THE STATIONARY CONVECTIVE FLOW OF AN ELECTRICALLY CONDUCTING LIQUID BETWEEN PARALLEL VERTICAL PLATES IN A MAGNETIC FIELD

G. Z. GERSHUNI and E. M. ZHUKHOVITSKII

Perm State University and Perm State Pedagogical Institute

Submitted to JETP editor September 19, 1957

J. Exptl. Theoret. Phys. (U.S.S.R.) 34, 675-683 (March, 1958)

The effect of a constant magnetic field on the stability of the stationary convective flow of an electrically conducting liquid in the space between two parallel vertical plates is investigated. The equations for the amplitudes of the perturbations are solved by approximations, using the method of Galerkin. The study shows that a magnetic field greatly increases the stability of the stationary flow. In the case of a longitudinal field, the instability is always in the form of a "standing" perturbation. The critical Grasshof number and the critical wave number for standing and running perturbations have been determined as functions of the field strength.

IN the preceding paper[1] we considered the stationary convective flow of an electrically conducting liquid between parallel plates, heated to different temperatures, in the presence of an external magnetic field. In this paper we consider the hydrodynamical stability of this flow. (The corresponding problem for the case where the magnetic field is absent has already been solved.[2]) The effect of the magnetic field is, firstly, to slow down the stationary motion, and secondly, to hinder the growth of perturbations; both these effects should greatly increase the flow stability. Studies of hydrodynamical stability in the presence of external magnetic fields have been made for the case of plane Poiseuille flow[3,4] and for the flow between rotating cylinders.[5] No studies of the stability of stationary convective flows in a magnetic field have been made previously, to our knowledge.

In this paper we shall investigate the stability of convective flow between vertical plates. The generalization to the case of arbitrary orientation of the plates is more complex than for the stationary-flow problem, and can be carried out in a manner analogous to that of Gershuni.[6]

1. PERTURBATION EQUATIONS

Let us denote by $\mathbf{v}_0$, T_0, p_0, and $\mathbf{H}_0$ the velocity, temperature, pressure, and magnetic field strength in the stationary flow, and consider small, non-stationary perturbations $\mathbf{v}$, T, p, and $\mathbf{H}$ of these quantities. In the perturbed motion, the quantities $\mathbf{v}_0 + \mathbf{v}$, $T_0 + T$, $p_0 + p$, and $\mathbf{H}_0 + \mathbf{H}$ must satisfy Eqs. (8) to (11) of Ref. 1. Considering that the stationary solution also satisfies these equations, and neglecting the squares of the small perturbation terms, we obtain the following equations for the perturbations*

$$\frac{\partial \mathbf{v}}{\partial t} + \mathbf{v}_0 \cdot \nabla \mathbf{v} + \mathbf{v} \cdot \nabla \mathbf{v}_0 = -\nabla\left(p + \frac{M^2}{P_m}\mathbf{H}_0\mathbf{H}\right) + \nabla^2\mathbf{v} + G\gamma T + \frac{M^2}{P_m}(\mathbf{H}_0 \cdot \nabla \mathbf{H} + \mathbf{H} \cdot \nabla \mathbf{H}_0); \quad (1)$$

$$\frac{\partial T}{\partial t} + \mathbf{v}_0 \nabla T + \mathbf{v} \nabla T_0 = \frac{1}{P} \nabla^2 T; \quad (2)$$

$$\frac{\partial \mathbf{H}}{\partial t} + \operatorname{curl}(\mathbf{H} \times \mathbf{v}_0) + \operatorname{curl}(\mathbf{H}_0 \times \mathbf{v}) = \frac{1}{P_m}\nabla^2 \mathbf{H}; \quad (3)$$

$$\operatorname{div} \mathbf{v} = 0, \quad \operatorname{div} \mathbf{H} = 0. \quad (4)$$

Let us consider a plane perturbation, in which $v_y = 0$, $H_y = 0$, and all quantities depend only on x, z, and t. Then because of (4), we may introduced a flow function Ψ, connected with the velocity components by the relations

$$v_x = -\partial\Psi/\partial z, \quad v_z = \partial\Psi/\partial x, \quad (5)$$

and also a vector potential field $\mathbf{A}$ given by

$$H_x = -\partial A_y/\partial z, \quad H_z = \partial A_y/\partial x; \quad (A_x = A_z = 0). \quad (6)$$

We assume the dependence of the perturbation on z and t to be of the form

$$\Psi = \psi(x)\, e^{i(\omega t + kz)}, \quad A_y = \varphi(x)\, e^{i(\omega t + kz)}, \quad T = \theta(x)\, e^{i(\omega t + kz)}.$$

Here k is the wave number and ω is the frequency (generally complex) of the perturbation. It is well known that the sign of the imaginary part of the frequency ω determines the behavior of

*For the notation, choice of units, and orientation of coordinates axes, see Ref. 1.

small perturbations; if the imaginary part is positive, the perturbation decays with time, i.e., the stationary motion is stable. If the imaginary part of the frequency is negative, the perturbation grows — the stationary flow is unstable.

Equations for ψ, φ, and θ can be obtained if we eliminate the pressure from (1) by taking the curl of both sides, and expressing the velocity and the field in terms of the flow function and the vector potential in all equations. From this substitution we obtain differential equations for the amplitude of a perturbation. (The primes denote differentiation with respect to x):

$$(\psi^{IV} - 2k^2\psi'' + k^4\psi) - (i\omega + ikv_0)(\psi'' - k^2\psi) + ikv_0''\psi + G\theta' = -\frac{M^2}{P_m}[H_{0x}(\varphi''' - k^2\varphi') + ikH_{0z}(\varphi'' - k^2\varphi) - ikH_{0z}''\varphi]; \quad (7)$$

$$-\frac{1}{P_m}(\varphi'' - k^2\varphi) + (i\omega + ikv_0)\varphi = H_{0x}\psi' + ikH_{0z}\psi; \quad (8)$$

$$-ikT_0'\psi + (i\omega + ikv_0)\theta - \frac{1}{P}(\theta'' - k^2\theta) = 0. \quad (9)$$

Perturbations of the velocity and temperature must vanish at the boundary between the liquid and the plates, so that the boundary conditions for ψ and θ will be

$$\psi(-1) = \psi(1) = \psi'(-1) = \psi'(1) = 0,$$
$$\theta(-1) = 0(1) = 0. \quad (10)$$

The perturbations of the magnetic field are not, in general, required to vanish at the plates; the boundary conditions for the field are the usual conditions at the junction of two media. Thus, field perturbations may extend into the medium surrounding the liquid. In this case we must investigate the field in the external region also, which greatly complicates the problem. It would be possible to assume, as Fermi has done[5] in solving similar problems, that the surrounding material is an ideal conductor; such an assumption would naturally lead to very simple boundary conditions. In our case, however, it is possible, following Stuart[3] and Lock,[4] to eliminate the function $\varphi(x)$ from Eqs. (7) and (8). In order to be able to do this we must first simplify the equations by making use of the smallness of the parameter P_m.

In what follows, we shall consider two orientations of the constant external field: (1) a constant, uniform, external field perpendicular to the parallel plates, and therefore also perpendicular to the velocity vector of the stationary liquid flow (for brevity, this case will be referred to as the "transverse field" case); and (2) a constant external field in the direction of the velocity, i.e., along the z axis (the "longitudinal field" case). We shall first simplify Eqs. (7) and (8) for the transverse field case. It has been shown in Ref. 1 that the ratio H_{0z}/H_{0x} is proportional to P_m, so that for liquid metals it is extremely small, even for relatively large Grasshof numbers. Therefore in the right-hand sides of Eqs. (7) and (8) we may eliminate the terms containing the induced field H_{0z}. In the left-hand side of (8), obviously, the only important term is the one containing $1/P_m$. Thus we may write (8) in the approximate form

$$\varphi'' - k^2\varphi = -H_{0x}P_m\psi'.$$

When this substitution is made for $\varphi'' - k^2\varphi$, the right-hand side of Eq. (7) becomes $M^2\psi''H_{0x}^2$. It will be recalled that, as a result of our choice of units, H_{0x} is equal to ± 1, the two signs corresponding to the two possible directions of the perpendicular external field. Thus the right-hand side will reduce to $M^2\psi''$. This term obviously represents the effect of the magnetic field on the perturbations; its effect on the stationary flow is expressed in the dependence of the stationary profile v_0 on the magnetic field. Finally, for the transverse field case Eq. (7) takes the form

$$(\psi^{IV} - 2k^2\psi'' - M^2\psi'' + k^4\psi) - (i\omega + ikv_0)(\psi'' - k^2\psi) + ikv_0''\psi + G\theta' = 0. \quad (11)$$

In the longitudinal field case, we have $H_{0x} = 0$, and H_{0z} does not depend on x. Therefore we now have, instead of (8), keeping only the terms on the left-hand side which contain $1/P_m$,

$$\varphi'' - k^2\varphi = -ikH_{0z}P_m\psi.$$

The right-hand side of Eq. (7) is now equal to $-k^2M^2\psi$ (since $H_{0z}^2 = 1$). The equation for ψ in the longitudinal field case can be written

$$(\psi^{IV} - 2k^2\psi'' + k^4\psi + k^2M^2\psi) - (i\omega + ikv_0)(\psi'' - k^2\psi) + ikv_0''\psi + G\theta' = 0. \quad (12)$$

Thus the amplitude of the vector potential of the field perturbations, $\varphi(x)$, can be eliminated from the equations in both the longitudinal and transverse field cases. The problem reduces to the determination of the amplitudes of the flow and temperature functions $\psi(x)$ and $\theta(x)$ from Eqs. (9) and (11) or (12), with the boundary conditions (10). This is obviously an eigenvalue problem; a non-trivial solution for given values of parameters occurring in the equations will exist for only a few values of the complex number ω. The stability problem reduces to the problem of finding these characteristic frequencies ω. A neutral state, separating the regions of stability

and instability, will obviously occur when the imaginary part of the complex frequency reduces to zero.

2. STABILITY INVESTIGATION

For an approximate solution of the problem, we shall make use of the method of Galerkin.

The unknown functions $\psi(x)$ and $\theta(x)$, which are to be determined, are approximated by a linear combination of functions which satisfy the boundary conditions. The coefficients are then determined by Galerkin's method (see, for example, Kantorovich and Krylov[7]). In what follows, we shall limit ourselves to the approximation

$$\bar{\psi}(x) = a_1\psi_1 + a_2\psi_2, \quad \bar{\theta}(x) = b_1\theta_1 + b_2\theta_2, \tag{13}$$

where the approximating functions ψ_1, ψ_2, θ_1, and θ_2 must satisfy the boundary conditions (10). From the form of the equations for ψ and θ it follows that these functions are not perfectly even functions, since the unperturbed profile v_0 which enters the equations is an odd function of x. Therefore, in constructing the approximate solutions (13), we shall choose ψ_1 and θ_1 to be even functions, and ψ_2 and θ_2 to be odd. The coefficients in the approximate solutions (13) are determined from the following set of linear homogeneous equations:

$$\int_{-1}^{1} L(\bar{\psi}, \bar{\theta})\,\psi_i\,dx = 0, \quad \int_{-1}^{1} M(\bar{\psi}, \bar{\theta})\,\theta_i\,dx = 0, \quad (i = 1, 2). \tag{14}$$

Here L is an operator which corresponds to the left-hand side of Eq. (11) in the transverse field case, and of Eq. (12) in the longitudinal field case. M is the operator corresponding to the left-hand side of Eq. (9).

The condition for the existence of a non-trivial solution of (14) is that the determinant of the set of equations should equal zero. In order to express this condition more concisely, we shall first introduce the following notation:

$$A_{ik} = \int_{-1}^{1} (\psi_i^{IV} - 2k^2\psi_i'' - M^2\psi_i'' + k^4\psi_i)\,\psi_k dx \quad \text{for } H \parallel x,$$

$$A_{ik} = \int_{-1}^{1} (\psi_i^{IV} - 2k^2\psi_i'' + k^4\psi_i + k^2M^2\psi_i)\,\psi_k dx \quad \text{for } H \parallel z,$$

$$B_{ik} = -\int_{-1}^{1} (\psi_i'' - k^2\psi_i)\,\psi_k dx, \quad C_{ik}$$

$$= \int_{-1}^{1} (f_0''\psi_i - f_0\psi_i'' + k^2 f_0\psi_i)\,\psi_k dx, \qquad D_{ik} = \int_{-1}^{1} \theta_i'\psi_k dx,$$

$$a_{ik} = -\frac{1}{P}\int_{-1}^{1} (\theta_i'' - k^2\theta_i)\,\theta_k dx, \quad b_{ik} = \int_{-1}^{1} \theta_i\theta_k dx,$$

$$c_{ik} = \int_{-1}^{1} f_0\theta_i\theta_k dx, \quad d_{ik} = -\int_{-1}^{1} T_0'\psi_i\theta_k dx; \quad f_0 = \frac{v_0}{G} \tag{15}$$

Note that, by virtue of the symmetry properties of the trial functions ψ_i and θ_i and the stationary profile f_0, the integrals A_{ik}, B_{ik}, a_{ik}, b_{ik}, and d_{ik} are equal to zero for $i \neq k$; and so are the integrals C_{ik}, D_{ik}, and c_{ik} for $i = k$. Using these results and the notation of (15), the vanishing of the determinant of system (14) can be written in the form:

$$\begin{vmatrix} A_{11} + i\omega B_{11} & ikGC_{21} & 0 & GD_{21} \\ ikGC_{12} & A_{22} + i\omega B_{22} & GD_{12} & 0 \\ ikd_{11} & 0 & a_{11} + i\omega b_{11} & ikGc_{21} \\ 0 & ikd_{22} & ikGc_{12} & a_{22} + i\omega b_{22} \end{vmatrix} = 0. \tag{16}$$

This equation determines the characteristic frequencies ω of the perturbation. In order to find the conditions for a neutral perturbation state [i.e., $\mathrm{Im}(\omega) = 0$], the real and imaginary parts of determinant (16), with ω taken to be real, must be equated separately to zero. In this way we obtain two equations which we write provisionally in the form

$$L_{40}k^4G^4 + L_{04}\omega^4 + L_{22}k^2G^2\omega^2 + L_{20}k^2G^2 + L_{02}\omega^2 + L_{00} = 0, \tag{17}$$

$$\omega(N_{20}k^2G^2 + N_{02}\omega^2 + N_{00}) = 0, \tag{18}$$

the coefficients representing terms involving the coefficients in determinant (16).

For a perturbation with a given wave number, and for given values of the parameters M and P, Eqs. (17) and (18) make it possible to find the critical Grasshof number G and the real perturbation frequency ω [for, of course, only the real solutions of the set (17) — (18) have any physical meaning]. If we eliminate the real frequency ω from Eqs. (17) and (18), we define a relation between G and k which specifies the neutral curve in the G-k plane. The minimum in the curve $G = G(k)$ defines the critical wave number k_m for a perturbation and the minimum critical Grasshof number G_m.

In order to carry out all these calculations, it is necessary first to choose the trial functions in Eqs. (13). Let us take ψ_1 and ψ_2 to be polynomials which vanish, together with their first derivatives, at $x = \pm 1$:

$$\psi_1 = (1 - x^2)^2, \quad \psi_2 = x(1 - x^2)^2. \tag{19}$$

In choosing the functions θ_1 and θ_2 we note that the temperature must satisfy the boundary condition

$$\theta''(-1) = \theta''(1) = 0. \quad (20)$$

as can be seen from (9) and the boundary condition (10). Therefore we choose θ_1 and θ_2 to be polynomials which reduce to zero at $x = \pm 1$, together with their second derivatives:

$$\theta_1 = (1 - x^2)(5 - x^2), \quad \theta_2 = x(1 - x^2)(7 - 3x^2). \quad (21)$$

By using expressions (19) and (21) as the trial functions we can calculate from (15) the elements of the determinant (16), and find the coefficients in (17) and (18). In order to calculate the integrals C_{ik} and c_{ik}, which depend on the stationary velocity profile v_0, we must use expression (19) of Ref. 1 for the transverse field case and expression (21) of the same reference for the longitudinal field case, since the longitudinal field does not affect the profile.

We shall consider the results of the stability investigations separately for the transverse and longitudinal field cases.

1. Transverse Field Case

The coefficients of determinant (16) could be found from their elements, but this is a rather cumbersome method of calculation; we shall not go into details of the derivation of these complicated expressions here, since they are of no interest in themselves.

From (17) and (18) it is evident that these equations would be satisfied if $\omega = 0$ and if the value of G were a root of the equation

$$L_{40}k^4G^4 + L_{20}k^2G^2 + L_{00} = 0. \quad (22)$$

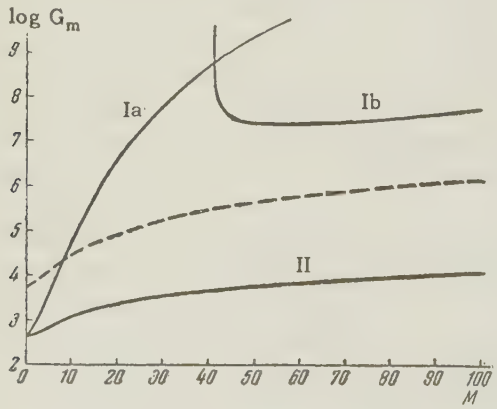

FIG. 1. Dependence of the critical Grasshof number on the Hartmann number (for P = 0.02): Ia – transverse field (standing perturbations). Ib – transverse field (running perturbations). II – longitudinal field. For comparison, the dashed line shows the dependence of the critical Grasshof number upon the field, for the onset of convection in a horizontal layer heated from below, in the presence of a transverse magnetic field.[9]

If there is a real positive root of Eq. (22), it implies that for given parameters M and P and for a given wave number k, the motion is unstable for this value of G, because at the critical point there will be a corresponding perturbation with the real part of the frequency ω equal to zero, and consequently with a phase velocity of zero. (Perturbations of this type may be called "standing," to distinguish them from "running" perturbations, for which $\omega \neq 0$.) The use of the approximation method clearly shows that the possibility of a standing perturbation, which is interesting in itself, is connected with the antisymmetry of the stationary velocity profile v_0; if the profile is completely symmetric, the imaginary part of the determinant (16) does not contain a real frequency ω as a factor, and no solution with $\omega = 0$ exists. By the same token, the existence of a standing perturbation in a flow where the mean velocity is different from zero (for example, of the Poiseuille or Couette type) is hardly possible from the physical point of view, since the existence of the perturbation would destroy the flow pattern.

Equation (22) has a real positive root for values of wave number in the interval $0 < k < \bar{k}$, where $\bar{k}$ is determined by the condition that the coefficient L_{40} should reduce to zero. The values $k = 0$ and $k = \bar{k}$ give the asymptotic neutral curves $G = G(k)$. Between these points the curve has a minimum at $k = k_m$. The critical wave number and the value of the minimum critical Grasshof number G_m have been calculated for P = 0.02 and for different values of the parameter M (i.e., as a function of the field strength). In the absence of a field (M = 0) the critical Grasshof number is equal to $G_m = 405$. This indicates a relatively low stability of the motion; for comparison, we may note that the critical Grasshof number corresponding to the onset of convection in a plane horizontal layer heated from below[8] is $G_m = 5340$ for P = 0.02. The presence of a field leads to a considerable increase in stability; as the parameter M increases the critical number G_m rises rapidly (see the table and Curve Ia in Fig. 1). For example, at M = 10 the critical number G_m is more than 100 times higher than its value in the absence of a field.

The critical wave number k_m decreases monotonically with increase in M (Curve Ia in Fig. 2), i.e., the critical wavelength of these (standing)

perturbations increases with increasing magnetic field.

In addition to the standing perturbation type of instability, described above, in the presence of a transverse magnetic field the stationary motion also exhibits instability caused by running perturbations. This type of instability takes place when the field is sufficiently high, and corresponds to a solution of (17) and (18) with $\omega \neq 0$. To find the neutral curve $G(k)$ for the running perturbations, ω must be eliminated from (17) and (18) after dividing by ω. If desired, it is also possible to find from (17) and (18) the real frequency, and hence the phase velocity, of the running perturbations. Since only the even powers of ω appear in the equations, the perturbations travel both ways along the z axis. The critical Grasshof number G_m is plotted as a function of M in Fig. 1, Curve Ib. It can be seen that for $M > 42$ a breakdown in the stationary flow can arise as the result of either standing or running perturbations, but that the critical number G_m for running perturbations is very much lower than the corresponding critical number for standing perturbations, i.e., the flow is very much less stable toward running perturbations. Nevertheless, even at very high fields there is always a possibility that the instability may set in as a standing perturbation. To make this happen, some means would have to be taken to prevent the formation of running perturbations; for instance, running perturbations obviously cannot exist in a channel with very small vertical dimensions.

Figure 2 (Curve Ib) shows the dependence of the critical wave number k_m on the field. It is evident that for $M > 42$ the critical wave number for running perturbations is greater than the critical wave number for standing perturbations. This is physically reasonable, since for large transverse fields the running perturbations lead to breakdown at lower G numbers than the standing ones; at high transverse fields the formation of a short wavelength perturbation, covering a relatively large distance in the direction of the transverse field, is energetically favored, since in this case the Joule dissipation will be less than for a long wavelength perturbation. The same reasoning explains why the critical wave number k_m for running perturbations increases with an increase in the applied field.

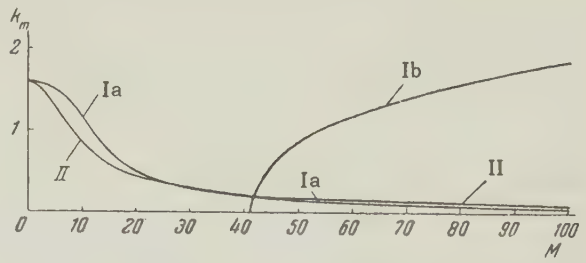

FIG. 2. Dependence of the critical wave number on the Hartmann number (for P = 0.02): Ia – transverse field (standing perturbations). Ib – transverse field (running perturbations). II – longitudinal field.

2. Longitudinal Field Case

In the case of a longitudinal field, the only possible type of instability is a standing perturbation with $\omega = 0$. If we assume that $\omega \neq 0$, then Eqs. (17) and (18) give complex roots G when ω is eliminated, indicating that with respect to running waves, the system is always stable. The critical Grasshof number G_m for standing perturbations is shown as a function of the Hartmann number M in Fig. 1, Curve II. It will be seen that the critical number G_m increases much more slowly with the field than it does in the transverse field case. At large fields, the critical number G_m increases in direct proportion to the field, in accordance with the asymptotic formula

$$G_m = 107\,M. \qquad (23)$$

A longitudinal field is much less stabilizing than a transverse field. This can be explained by the fact that a longitudinal field merely hinders the development of perturbations, while the transverse field, in addition, greatly slows down the stationary flow. The effect of this second factor on the stability is much greater – so much so that Lock,[4] in his

$\omega = 0$			$\omega \neq 0$		
M	k_m	G_m	M	k_m	G_m
0	1.6	405	41.3	0	∞
5	1.5	$3.85 \cdot 10^3$	45	0.62	$3.26 \cdot 10^7$
10	1.16	$4.64 \cdot 10^4$	50	0.87	$2.38 \cdot 10^7$
20	0.52	$3.40 \cdot 10^6$	60	1.2	$2.31 \cdot 10^7$
30	0.31	$5.70 \cdot 10^7$	70	1.4	$2.63 \cdot 10^7$
40	0.21	$4.20 \cdot 10^8$	80	1.6	$3.18 \cdot 10^7$
50	0.16	$1.80 \cdot 10^9$	90	1.75	$3.80 \cdot 10^7$
100	0.06	$2.0 \cdot 10^{11}$	100	1.9	$4.6 \cdot 10^7$

study of the stability of Poiseuille flow in a transverse field, did not even consider the effect which the field would have on the perturbations.

In the longitudinal field case the critical wave number k_m decreases monotonically as the field increases (Curve II of Fig. 2); this is a natural result, since in distinction to the transverse field case, it is the long wavelength perturbations which are energetically favored in a longitudinal field.

In conclusion, we note that the quantitative results which we have obtained could be made more accurate by using better approximations. This could be done in two way: either by an increase in the number of trial functions in (13), or by choosing the trial functions in a different way. It seems to us that the second method is more comprehensive, from the following considerations. It is known that, at high fields in stationary flows, a sort of boundary layer is formed; hence it may be expected that some such layer would also accompany a perturbation which is formed in a high field. However, the polynomial trial functions (19) and (21) which we have chosen make no provision for this kind of structural singularity in the perturbations (if such a singularity should exist). It should be noted that both of the methods for improving the accuracy of the results would greatly complicate the numerical computations.

[1] G. Z. Gershuni and E. M. Zhukhovitskii, J. Exptl. Theoret. Phys. (U.S.S.R.) **34**, 670 (1958), Soviet Phys. JETP **7**, 000 (1958).

[2] G. Z. Gershuni, J. Tech. Phys. (U.S.S.R.) **23**, 1838 (1953).

[3] J. T. Stuart, Proc. Roy. Soc. **A221**, 189 (1954).

[4] R. C. Lock, Proc. Roy. Soc. **A233**, 105 (1955).

[5] S. Chandrasekhar, Proc. Roy. Soc. **A216**, 293 (1953).

[6] G. Z. Gershuni, J. Tech. Phys. (U.S.S.R.) **25**, 351 (1955).

[7] L. V. Kantorovich and V. I. Krylov, Приближенные методы высшего анализа, (Approximation Methods in Higher Analysis), GITTL, 1949.

[8] A. Pellew and R. Southwell, Proc. Roy. Soc. **A176**, 312 (1940).

[9] S. Chandrasekhar, Phil. Mag. **43**, 501 (1952).

Translated by D. C. West
128

HYPERFINE INTERACTION AND SPIN-ELECTRON RESONANCE IN POLARONS AND EXCITONS

M. F. DEIGEN and S. I. PEKAR

Institute of Physics, Academy of Sciences, Ukrainian S.S.R.

Submitted to JETP editor September 12, 1957

J. Exptl. Theoret. Phys. (U.S.S.R.) 34, 684-687 (March, 1958)

It is shown that in polarons and excitons the energy correction due to the hyperfine interaction is zero in first approximation. Consequently, the hyperfine-interaction part of the width of the spin-electron resonance in polarons and excitons is equal to zero.

The experimentally observed narrowness of the spin-electron resonance bands in metal-ammonia solutions provides additional evidence that the current carriers in these systems are polarons.

It is shown that with intense illumination of a crystal the stationary concentration of excitons can be so large that experimental detection of paramagnetic absorption in excitons may be possible. In virtue of the optical selection rules, excitons that have absorbed a radio-frequency quantum have a very long lifetime against radiative deexcitation.

THE energy operator of the hyperfine interaction between an electron and the magnetic moments of the nuclei of a crystal is

$$\hat{U} = \sum_l \hat{U}_l; \quad \hat{U}_l = \frac{\mu\mu_l}{SI_l} \sum_{\mathbf{n}} \left(\mathbf{S},\ \text{curl curl}\ \frac{\mathbf{I}_{ln}}{\rho_{ln}} \right). \quad (1)$$

Here the index ℓ distinguishes the types of nuclei, U_ℓ is the energy operator for the hyperfine interaction of the electron with the magnetic moments of nuclei of type ℓ, $\mathbf{n}$ is the label of a point of the ℓ-th sublattice; $\mathbf{S}$ and S are the spin of the electron and its absolute value, $\mathbf{I}_{\ell\mathbf{n}}$ and I_ℓ are the spin of the $(\ell\mathbf{n})$-th nucleus and its absolute value, μ is the Bohr magneton, μ_ℓ is the magnetic moment of the nucleus, and $\rho_{\ell\mathbf{n}}$ is the distance from the $(\ell\mathbf{n})$-th nucleus to the electron. In Eq. (1) the curl operation applies to the coordinates of the electron.

We assume that in zeroth approximation the Hamiltonian of the crystal does not involve the spins of the nuclei. Then the wave function of the crystal can be written as the product of the wave function χ of the nuclear spins and a function $\psi(\mathbf{r}, \mathbf{R})$ of the coordinates $(\mathbf{r})$ of all the electrons and the coordinates $(\mathbf{R})$ of the translational motion of the nuclei.

Let χ be an eigenfunction of all the $I_{\ell\mathbf{n}z}$. Then the first-order energy correction due to the hyperfine interaction is

$$U = \sum_l U_l;$$

$$U_l = \frac{\mu\mu_l}{SI_l} \sum_{\mathbf{n}} I_{lnz} \int \left(\psi^*(r,\ R)\, \mathrm{S}\psi(r,\ R),\ \text{curl curl}\ \frac{\mathbf{i}}{\rho_{ln}} \right) (dr)\,(dR); \quad (2)$$

$$\rho_{ln} = \mathbf{r} - \mathbf{n} - \mathbf{R}_{ln}, \quad (3)$$

where $\mathbf{i}$ is a unit vector in the z direction and $I_{\ell\mathbf{n}z}$ are the eigenvalues of the z components of the nuclear spins.

It can easily be shown that the integral

$$Q_{ln} = \int \left(\psi^*(r,\ R)\, \mathrm{S}\psi(r,\ R),\ \text{curl curl}\ \frac{\mathbf{i}}{\rho_{ln}} \right) (dr)\,(dR) \quad (4)$$

does not depend on $\mathbf{n}$ if $\psi(\mathbf{r}, \mathbf{R})$ is an eigenfunction of the translation operator $T_{\mathbf{m}}$. By the operation $T_{\mathbf{m}}$ we mean a change of the coordinate system such that the electron is displaced by an integer lattice vector $\mathbf{m}$ $(\mathbf{r} \to \mathbf{r} + \mathbf{m})$ and all the deformations of the lattice are also displaced by the vector $\mathbf{m}$ $(\mathbf{R}_{\ell\mathbf{n}} \to \mathbf{R}_{\ell,\mathbf{n}-\mathbf{m}})$.

Let us apply the operation $T_{\mathbf{m}}$ to the integrand of Eq. (4); this must not change the value of the integral, since it is equivalent to a change of variables. Since ψ is an eigenfunction of the operator $T_{\mathbf{m}}$, we have

$$T_{\mathbf{m}}\psi(r,\ R) = e^{i\mathbf{k}\mathbf{m}}\psi(r,\ R).$$

Furthermore it follows from Eq. (3) that

$$T_{\mathbf{m}}\rho_{ln} = \rho_{l,\mathbf{n}-\mathbf{m}}.$$

Therefore the expression (4) goes over into

$$Q_{ln} = \int T_m \left(\psi^*(r, R)\, S\psi(r, R),\right.$$

$$\text{curl curl } \frac{1}{\rho_{ln}}\Big)(dr)(dR) = \int (\psi^*(r, R)\, S\psi(r, R),$$

$$\left.\text{curl curl } \frac{1}{\rho_{l,n-m}}\right)(dr)(dR) = Q_{l,\,n-m}. \qquad (5)$$

Thus $Q_{\ell n}$ indeed does not depend on n, and is hereafter denoted by Q_ℓ. Therefore Eq. (2) can be rewritten as follows:

$$U_l = \frac{\mu\mu_l}{SI_l} Q_l P_l;\; P_l = \sum_n I_{lnz}. \qquad (6)$$

Here P_ℓ is the z component of the total spin angular momentum of all the type ℓ nuclei in the crystal. On the average P_ℓ is zero, but actually it fluctuates slightly because the components of the nuclear spins take random values.

Since for $n \neq n'$

$$\overline{I_{lnz} I_{ln'z}} = \bar{I}_{lnz} \bar{I}_{ln'z} = 0,$$

the mean-square value of P_ℓ is given by

$$\overline{P_l^2} = N_l \overline{I_{lnz}^2}, \qquad (7)$$

where N_ℓ is the number of type ℓ nuclei in the crystal. Thus $(\overline{P_\ell^2})^{1/2}$ is proportional to $V^{1/2}$, where V is the volume of the fundamental region of the crystal.

For the polaron and exciton ψ is an eigenfunction of T_m, so that results (6) and (7) are valid. Furthermore, in these cases ψ has a normalization coefficient proportional to $V^{-1/2}$. Therefore Q_ℓ is proportional to $1/V$.

The remarks made above, and also Eqs. (6) and (7), show that as V is increased U_ℓ, and consequently also U, go to zero as $V^{-1/2}$ (it can be shown that the integral Q_ℓ converges). Consequently, the hyperfine interaction, which in the case of local electron centers was the dominant factor determining the width of the spin-resonance absorption, gives no broadening at all in the case of polarons and excitons.

This fact makes is possible to distinguish experimentally between polarons and local electron centers.

In papers by Deigen[1] it has been shown that in metal-ammonia solutions the alkali metal atoms dissociate and the liberated electrons form polarons. These latter cause the electric conductivity and optical properties of these solutions. On the basis of these ideas, quantitative explanations of many experimental facts have been obtained.

Experimental studies of the spin-electron resonance at color centers in metal-ammonia solutions[2] have shown that the width of the spin-resonance absorption region is of the order of hundredths of a gauss, i.e., 10^4 times smaller than for local electron centers (for example, F centers). This shows clearly that the color centers in question are not local electron centers. Moreover, it serves as a new proof that they are polarons.

The fact that for polarons the hyperfine interaction must be absent and the corresponding width of the spin-electron resonance must vanish was pointed out by Pekar at the All-Union Conference on the Theory of Semiconductors in February, 1955 (cf. Ref. 3). He has also emphasized that the experimentally observed extreme narrowness of the spin-electron resonance region for color centers in metal-ammonia solutions means that they are polarons.

Another view of the explanation of the small width of the spin-electron resonance in metal-ammonia solutions has been given by Kaplan and Kittel.[4] They used the model of color centers proposed by Ogg[5] (a spherical vacuum cavity in the dielectric, in which the electron is localized). The lack of physical foundation for this model has been shown in Ref. 1.

It is interesting to examine whether by illuminating a crystal it is possible to produce such a high concentration of excitons that the spin-electron absorption of radio waves by the excitons could be detected experimentally. If the deexcitation of the excitons occurred only by emission of radiation and the mean lifetime τ of the exciton were of the order of 10^{-8} sec, the stationary concentration of excitons would be given by the formula

$$n = \tau s \varkappa / \hbar\omega, \qquad (8)$$

where s is the flux of radiant energy per $cm^2 \times$ sec, κ is the coefficient of exciton absorption of light in the crystal, and ω is the frequency of the absorbed light. If $\hbar\omega \sim 1$ ev, $\kappa \sim 10^5\ cm^{-1}$, and $s \sim 1\ W/cm^2$, we get $n \sim 10^{16}\ cm^{-3}$. With such a concentration of excitons it is quite possible that the spin-resonance absorption of radio waves by them can be experimentally observed.

It is desirable to reduce the nonradiative deexcitation of the excitons to a minimum by using ideal crystals free from impurities and working at low temperatures.

It must be emphasized that the total spin of the electrons in a dielectric in its ground state is always zero. In virtue of the spin selection rules for optical transitions, the total spin remains zero when light is absorbed and an exciton is formed.

But when a radio-frequency quantum is absorbed by the exciton the total spin of the electrons becomes ± 1, so that the inverse optical transition from the exciton state to the ground state is forbidden. Thus excitons that have absorbed radio-frequency quanta have considerably longer lifetimes against radiative deexcitation than ordinary excitons.

In an entirely analogous way the lifetime in the excited state is also lengthened for local electron centers that have absorbed radio-frequency quanta.

[1] M. F. Deigen, J. Exptl. Theoret. Phys. (U.S.S.R.) **26**, 293 (1954); Укр. физ. журн. (Ukr. Phys. Journal) **1**, 245 (1956).

[2] C. A. Hutchison, Jr. and R. C. Pastor, Phys. Rev. **81**, 282 (1951); Revs. Mod. Phys. **25**, 285 (1953). M. A. Garstens and A. H. Ryan, Phys. Rev. **81**, 888 (1951). Levinthal, Rogers, and Ogg, Phys. Rev. **83**, 182 (1951).

[3] G. E. Pikus and Iu. A. Firsov, J. Tech. Phys. (U.S.S.R.) **25**, 2381 (1955).

[4] J. Kaplan and C. Kittel, J. Chem. Phys. **21**, 1429 (1953).

[5] R. A. Ogg, Jr., J. Chem. Phys. **14**, 295 (1946).

Translated by W. H. Furry
129

SOVIET PHYSICS JETP VOLUME 34 (7), NUMBER 3 SEPTEMBER, 1958

PLANE PROBLEMS IN MAGNETOHYDRODYNAMICS

G. S. GOLITSYN

Moscow State University

Submitted to JETP editor September 21, 1957

J. Exptl. Theoret. Phys. (U.S.S.R.) **34**, 688-693 (March, 1958)

The conditions for potential motion in magnetohydrodynamics are deduced and such motions are investigated. The investigations reduce to the usual hydrodynamical problems. The Prandtl-Mayer problem for a conducting gas in a magnetic field and its generalizations and applications are studied in detail.

It is of interest to ascertain what problems of magnetohydrodynamics can be solved by classical methods. In this paper only potential motions are studied.

We write the set of equations of magnetohydrodynamics for the case of an ideally conducting medium in the form

$$\frac{\partial \mathbf{v}}{\partial t} + (\mathbf{v}\nabla)\,\mathbf{v} + \frac{1}{\rho}(\nabla p + [\mathbf{h}\times\operatorname{curl}\mathbf{h}]) = 0,$$

$$\frac{\partial \ln\rho}{\partial t} + \mathbf{v}\nabla\ln\rho + \operatorname{div}\mathbf{v} = 0, \qquad \frac{\partial \mathbf{h}}{\partial t} = \operatorname{curl}[\mathbf{v}\times\mathbf{h}],$$

$$\frac{\partial}{\partial t}\left(\frac{p}{\rho^{\gamma}}\right) + \mathbf{v}\nabla\left(\frac{p}{\rho^{\gamma}}\right) = 0. \tag{1}$$

Here we use the notation $\mathbf{H} = \sqrt{4\pi}\,\mathbf{h}$. The remaining notation is standard. We limit ourselves here to adiabatic processes only.

We seek the conditions of potential flow. For this, employing a well known vector identity, we write the Euler equation in the form

$$\frac{\partial \mathbf{v}}{\partial t} + \nabla\frac{v^2}{2} - [\mathbf{v}\times\operatorname{curl}\mathbf{v}] + \frac{1}{\rho}(\nabla p + [\mathbf{h}\times\operatorname{curl}\mathbf{h}]) = 0$$

and apply the curl operator:

$$\frac{\partial}{\partial t}\operatorname{curl}\mathbf{v} = \operatorname{curl}[\mathbf{v}\times\operatorname{curl}\mathbf{v}] - \operatorname{curl}\left\{\frac{\nabla p}{\rho} + \frac{1}{\rho}[\mathbf{h}\times\operatorname{curl}\mathbf{h}]\right\} \tag{2}$$

[$\operatorname{curl}(\nabla p/\rho) = \operatorname{curl}\nabla i = 0$, where i is the specific enthalpy]. Equation (2) is satisfied identically for $\operatorname{curl}\mathbf{v} = 0$ if only

$$\operatorname{curl}\left\{\frac{1}{\rho}[\mathbf{h}\times\operatorname{curl}\mathbf{h}]\right\} = \frac{1}{\rho}\operatorname{curl}[\mathbf{h}\times\operatorname{curl}\mathbf{h}] + \left[\nabla\left(\frac{1}{\rho}\right)\times[\mathbf{h}\times\operatorname{curl}\mathbf{h}]\right] = 0.$$

This equation is valid in two cases: first, where $\mathbf{h} \parallel \operatorname{curl}\mathbf{h}$, i.e., for the so-called force-free fields;[1] second, when

$$[\mathbf{h}\,\mathrm{curl}\,\mathbf{h}] = \nabla\Phi \,\|\, \nabla(1/\rho), \tag{3}$$

where Φ is some function.

We establish the connection between the field and the density for the case of motion in the plane to which the field is everywhere perpendicular. We write the continuity and field equations in the form

$$\partial\rho/\partial t + \rho\,\mathrm{div}\,\mathbf{v} + \mathbf{v}\nabla\rho = 0,$$
$$\partial\mathbf{h}/\partial t + \mathbf{h}\,\mathrm{div}\,\mathbf{v} + (\mathbf{v}\nabla)\,\mathbf{h} = 0. \tag{4}$$

In writing down the latter equation, we have used the fact that $\mathrm{div}\,\mathbf{h} = 0$ and $(\mathbf{h}\nabla)\,\mathbf{v} = 0$, because the field has only a z component, which often has no velocity.

Equations (4) are identical relative to ρ and h; therefore, as a consequence of the adiabaticity of the motion under consideration, we can write

$$h/\rho = b = \mathrm{const}. \tag{5}$$

It is easy to see that for the plane motions being considered, Eq. (3) is satisfied; hence $\Phi = \mathbf{h}^2/2$. We also obtain exactly this same case later.

In all the remaining cases, with the exception of the one dimensional, the motion will be vortical. In particular, any three dimensional motion and any motion in the case of a finite conductivity will be vortical, since then h is a function not only of ρ but also of the time and the coordinates.

Upon observance of condition (3), all the classical theorems on vortices are satisfied.

If the fluid is incompressible and the motion is potential, then the velocity potential φ satisfies Laplace's equation. There is nothing essentially new in this case in comparison with ordinary hydrodynamics.

Plane magnetohydrodynamic problems also reduce to the corresponding ordinary gasdynamic problems if the motion is isentropic. We make the following transformation:

$$\frac{1}{\rho}(\nabla p + [\mathbf{h}\times\mathrm{curl}\,\mathbf{h}]) = \frac{1}{\rho}\nabla\left(p + \frac{h^2}{2}\right)$$
$$= \frac{1}{\rho}\frac{d}{d\rho}\left(p + \frac{h^2}{2}\right)\nabla\rho = c_m^2\,\nabla\ln\rho.$$

The set (1) reduces to two equations

$$\frac{\partial\mathbf{v}}{\partial t} + (\mathbf{v}\nabla)\,\mathbf{v} + c_m^2\,\nabla\ln\rho = 0,$$
$$\frac{\partial\ln\rho}{\partial t} + \mathbf{v}\nabla\ln\rho + \mathrm{div}\,\mathbf{v} = 0, \tag{6}$$

which differ from the usual equations of gas dynamics only in the replacement of the sound velocity c by the effective sound velocity in our medium c_m. The results of Staniukovich[2] and many others can be transformed without any change.

As an example, let us consider a class of motions which does not occur in ordinary gas dynamics; these are the simple, nonstationary generalization of the Prandtl-Mayer motion.[3] We also consider in detail the problem of the motion of a gas close to the base line — the Prandtl-Mayer problem.

If the motion is non-isentropic, then c_m is a function of ρ. It is appropriate to transform to the independent variables t, x, $z = \ln\rho$.

Setting $u = u(z)$ and $v = v(z)$, and writing out Eq. (6) in terms of components, we get

$$u_z(uy_x - y_t + v) - c_m^2 y_x = 0,$$
$$v_z(uy_x - y_t + v) + c_m^2 = 0,$$
$$uy_x - y_t + v + v_z + u_z y_x = 0. \tag{7}$$

Let

$$y = xf_1(z) - tf_2(z) + f_3(z), \tag{8}$$

where f_1, f_2, f_3 are arbitrary functions. Introducing the function

$$F = uf_1 + f_2 + v,$$

we can put the set (7) in another form:

$$F - f_1 c_m^2\frac{dz}{du} = 0, \qquad F + c_m^2\frac{dz}{dv} = 0,$$
$$F + \frac{dv}{dz} + f_1\frac{du}{dz} = 0.$$

From this it is possible to obtain the following relations:

$$du = \pm f_1 c_m dz/\sqrt{1+f_1^2}, \quad dv = \mp c_m dz/\sqrt{1+f_1^2},$$
$$f_2 = \pm c_m\sqrt{1+f_1^2} - uf_1 - v. \tag{9}$$

From the first two equations of (9), we can obtain

$$(du)^2 + (dv)^2 = (c_m d\ln\rho)^2, \tag{10}$$

which is the relation along the characteristics.

If $f_2 \equiv 0$, then the flow will be stationary. The corresponding solution will be of the form of the general solution of Prandtl-Mayer. Then

$$y = xf_1 + f_3. \tag{11}$$

If u and v are given on any line $u = \bar{u}(z)$, $v = \bar{v}(z)$, then we also have

$$f_1 = \frac{\bar{u}\,\bar{v} \pm [(\bar{u}\,\bar{v})^2 - (\bar{u}^2 - c_m^2)(\bar{v}^2 - c_m^2)]^{1/2}}{c_m^2 - \bar{u}^2}. \tag{12}$$

If $f_3 \equiv 0$ also, then we obtain the Prandtl-Mayer solution which describes the rarefaction

wave. The generalized solution (11) corresponds to the stationary simple wave.[3] Formula (11) determines a family of characteristics — a pencil of straight lines. These straight lines intersect at each point of the line of flow at an angle equal to the angle of the perturbation, the sine of which is equal to $c_m/|v|$. Along these lines, all the quantities remain constant.

Construction of a simple wave for supersonic flow around a given profile is carried out exactly the same as for ordinary gasdynamics.[3]

In view of its importance and great physical interest, the Prandtl-Mayer problem will now be considered in more detail.

Let the field be perpendicular to the plane of motion. The assumptions relative to the remaining quantities are the same as for the classical statement of the problem.[3]

For stationary motion of the gas near the base line, we can assume that all the quantities depend only on the angle φ, and, writing down Eq. (6) in polar coordinates, we obtain

$$\frac{dv_r}{d\varphi} - v_\varphi = 0, \qquad v_\varphi \frac{dv_\varphi}{d\varphi} + v_r v_\varphi + c_m^2 \frac{d\ln\rho}{d\varphi} = 0,$$

$$v_\varphi \frac{d\ln\rho}{d\varphi} + \frac{dv_\varphi}{d\varphi} + v_r = 0. \tag{13}$$

From the two previous equations, we can obtain the equality

$$(dv_\varphi/d\varphi + v_r)(1 - v_\varphi^2/c_m^2) = 0.$$

Equating the first bracket to zero, we obtain the solution which describes the homogeneous flow. Equating the second bracket to zero, we obtain $v_\varphi = \pm c_m$. This solution will describe the rarefaction wave. Insofar as this is actually the case, we can verify by carrying out considerations similar to those of the classical problem. We only remark that the field disappears along with the density. We write out the principal results:

$$\frac{1}{2}(v_\varphi^2 + v_r^2) + \int c_m^2 d\ln\rho = i_{0m} = \text{const}; \quad v_\varphi = c_m, \tag{14}$$

$$\varphi = -\int \frac{d(\rho c_m)}{\rho v_r} = \int \frac{dv_r}{v_\varphi} = \int \frac{d\sqrt{2(i_{0m} - i_m) - c_m^2}}{c_m}, \tag{15}$$

where

$$i_m = \int c_m^2 d\ln\rho = \frac{c^2}{\gamma - 1} + \frac{h^2}{\rho} = \frac{c^2}{\gamma - 1} + b^2\rho$$

has the meaning of a generalized enthalpy. We transform the equation for i_m and c_m with the aid of the Poisson adiabatic

$$\rho c^{-2/(\gamma-1)} = A = \text{const}.$$

Then

$$i_m = \frac{c^2}{\gamma - 1} + Ab^2 c^{2/(\gamma-1)} = \frac{c^2}{\gamma - 1} + \eta \frac{c^{2/(\gamma-1)}}{c_0^{2(2-\gamma)/(\gamma-1)}},$$

$$c_m^2 = c^2 + Ab^2 c^{2/(\gamma-1)} = c^2 + \eta \frac{c^{2/(\gamma-1)}}{c_0^{2(2-\gamma)/(\gamma-1)}},$$

$$\eta = Ab^2 c_0^{2(2-\gamma)/(\gamma-1)}; \tag{16}$$

c_0 is the sound velocity where the gas is at rest. The parameter η, which characterizes the field, has the simple physical meaning of the square of the ratio of the Alfven velocity $V_0 = h_0/\sqrt{\rho_0}$ to the sound velocity $c_0 = \sqrt{\gamma p_0/\rho_0}$, determined where $v = 0$.

We return to the computation of the integral (15). We introduce the independent variable $x = c/c_0$ and, carrying out differentiation with respect to x in the integrand, and taking (6) into account, we get

$$\varphi = -\frac{1}{\gamma - 1} \tag{17}$$

$$\times \int \frac{[\gamma + 1 + 3\eta x^{2(2-\gamma)/(\gamma-1)}]\,dx}{(1 + \eta x^{2(2-\gamma)/(\gamma-1)})\left[\frac{2}{\gamma - 1} - \frac{\gamma + 1}{\gamma - 1}x^2 + \eta(2 - 3x^{2/(\gamma-1)})\right]}$$

This integral is taken in two limiting cases $\eta = 0$ and $\eta \to \infty$. In the first case we obtain the well known result:

$$x = \sqrt{\frac{2}{\gamma + 1}} \cos \sqrt{\frac{\gamma - 1}{\gamma + 1}}\,\varphi. \tag{18}$$

In the other limiting case, taking the integral and solving for x, we obtain

$$x = \left(\frac{2}{3}\cos^2 \frac{\varphi}{\sqrt{3}}\right)^{(\gamma-1)/2}. \tag{19}$$

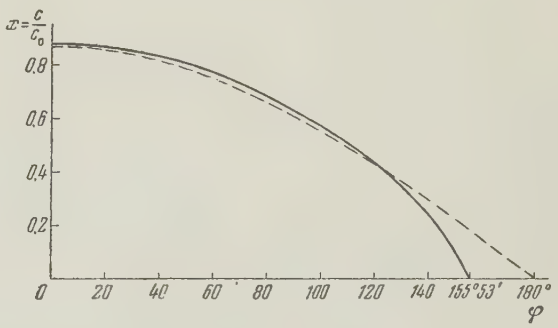

FIG. 1. Change of the sound velocity as a function of the angle φ for the limiting values: dashed line, $\eta = 0$, continuous line, $\eta \to \infty$.

Both the dependencies (18) and (19) for $\gamma = 5/3$ are shown in Fig. 1. It is interesting to note that the limiting possible angle between the weak discontinuities which limit the rarefaction wave, decrease from $(\pi/2)\sqrt{(\gamma + 1)(\gamma - 1)}$ (220° 27′ for $\gamma = 1.4$ and 180° for $\gamma = 5/3$) up to $\pi\sqrt{3}/2 = 155°\,53'$. Consequently, the maximum possible turning angle of the vector velocity in the rarefaction wave de-

creases to 65° 53′ against 130° 27′ or 90° in the absence of a field.

Calculations in the intermediate case $0 < \eta < \infty$ are carried out for $\gamma = 5/3$. Then

$$\varphi = -\int \frac{(4 + 4.5\eta x)\,dx}{\sqrt{(1+\eta x)\,[3 - 4x^2 + \eta\,(2 - 3x^3)]}}. \qquad (17')$$

The question arises as to the limits of change of x. The upper limit ought to be zero — the boundary with a vacuum. The lower limit is determined by the requirement of the reality of the integrand, i.e., the root x_0 of the polynomial in square brackets. Upon change in η over the infinite range, x_0 changes from $\sqrt{3/4} = 0.86603$ to $(2/3)^{1/3} = 0.87358$; i.e., the change is very small. However, since x_0 determines the limit of integration, then the error ϵ in the determination of x_0 itself gives an error of the order of $\sqrt{\epsilon}$ in the integration of our expression; therefore, it is necessary to determine x_0 with a sufficiently great degree of accuracy. We give a table of the dependence on η of the root x_0 by the equation

$$3 - 4x^2 + \eta(2 - 3x^3) = 0,$$

where η was computed from the given x_0.

η	x_0	η	x_0
0	0.86603	1.9560	0.8710
0.15061	0.8670	3.8332	0.8720
0.35963	0.8680	12.177	0.8730
0.65965	0.8690	94.115	0.8735
1.12694	0.8700	∞	0.87358

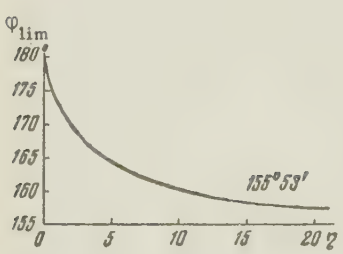

FIG. 2. Dependence on $\eta = H_0^2/4\pi\rho_0 c_0^2$ of the limiting possible angle between weak discontinuities.

The integral (17′) can, in principle, be expressed by elementary and elliptic functions; however, the method of numerical integration is much less difficult: from 0 to 0.72 the integral is computed by Simpson's rule;[4] thereafter, the integrand is represented in the form $(x_0 - x)^{-1/2} h(x)$ and $h(x)$ is expanded in a Taylor series, after which the integration becomes elementary. For calculation with accuracy up to 5 places, it is always sufficient to find only four terms in the expansion. It is not possible to apply numerical methods directly to the calculation of the entire integral, since it is not a proper one. The results of the integration are given in Fig. 2.

Finally, when the dependence $c/c_0 = x = x(\varphi)$ is found, it is of no difficulty to find other quantities as functions of the angle φ. Thus, for $\gamma = 5/3$,

$$\frac{\rho}{\rho_0} = \left(\frac{c}{c_0}\right)^{2/(\gamma-1)} = x^3; \quad \frac{p}{p_0} = \left(\frac{c}{c_0}\right)^{2\gamma/(\gamma-1)} = x^5;$$

$$\frac{c_m}{c_{m_0}} = x\sqrt{\frac{1+\eta x}{1+\eta}}; \quad \frac{v}{c_0} = \sqrt{3\,(1-x^2) + 2\eta\,(1-x^3)};$$

$$\chi = \varphi + \arctan\left[x\left(\frac{1+\eta x}{3 - 4x^2 + \eta\,(2-3x^3)}\right)^{1/2}\right].$$

Graphs are given in Figs. 3 and 4 for these quantities for $\eta = 1.127$. The dashes show the change in the corresponding quantities in the absence of field.

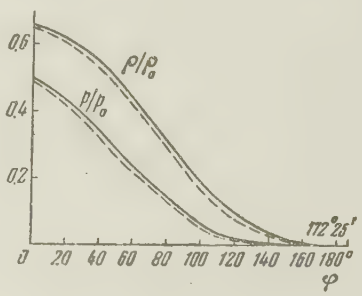

FIG. 3. Change of the density and pressure in a rarefaction wave in dependence on the angle φ for $\eta = 1.12694$.

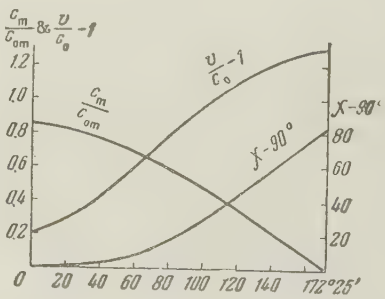

FIG. 4. Change in the magnetogasdynamical sound velocity, velocity and angle of its turn χ in dependence on the angle φ for $\eta = 1.2694$.

The results obtained can be applied without any principal difficulties to the problem of the flow angle, to the consideration of plane stationary motion.

In conclusion, I express my thanks to my director K. P. Staniukovich for suggesting the topic and for discussion of the results. I also express my gratitude to A. I. Morozov for his help in numerous suggestions for the solution of the Prandtl-Mayer problem.

[1] S. Lundquist, Arkiv. f. Fysik **5**, 297 (1952).
[2] K. P. Staniukovich, Dokl. Akad. Nauk SSSR **112**, 595 (1957).

[3] L. D. Landau and E. M. Lifshitz, Механика сплошных сред (Mechanics of Continuous Media), Secs. 101, 107, GITTL, 1954.

[4] G. M. Fikhtengol'ts, Курс дифференциального и интегрального исчисления (Course in Differential and Integral Calculus), Vol. 2, GITTL, 1951.

Translated by R. T. Beyer
130

SOVIET PHYSICS JETP VOLUME 34 (7), NUMBER 3 SEPTEMBER, 1958

FRACTIONAL PARENTAGE COEFFICIENTS FOR THE WAVE FUNCTION OF FOUR PARTICLES

G. I. ZEL'TSER

Leningrad Agricultural Institute

Submitted to JETP editor September 26, 1957

J. Exptl. Theoret. Phys. (U.S.S.R.) 34, 694-699 (March, 1958)

General formulas are obtained for the fractional parentage expansion of type $<n|n-2, 2>$ for the wave function of four nucleons in j-j coupling, with inclusion of effects of isotopic spin. The normalized fractional parentage coefficients (both for nonequivalent and for equivalent particles) are expressed in terms of the Hope χ functions, i.e., essentially in terms of Wigner 9j symbols. The results can also be applied directly to the case of LS coupling in atoms.

WHEN two-particle interactions are taken into account in the individual-particle nuclear model it turns out to be necessary to calculate the matrix elements of symmetric two-particle operators (of the type $G = \sum_{i<k} g_{ik}$) between antisymmetric states of n particles with prescribed total angular momentum and total isotopic spin. The wave functions of these states are constructed by vector composition from the functions for the individual particles. When the number n of particles is larger than two, the functions obtained by vector composition are not automatically antisymmetric, so that subsequent antisymmetrization is necessary.

In calculating the matrix elements of operators of the type G by the methods of the Racah algebra of tensor operators[1] it is convenient to possess a representation of the antisymmetric wave functions of n particles in the form of an expansion in terms of functions formed by vector composition from antisymmetric functions of the first $n-2$ particles and of the last two particles. The coefficients in this expansion are called fractional parentage coefficients of the type $<n|n-2, 2>$. Together with the analogous coefficients of the type $<n|n-1, 1>$, they were first introduced by Racah[2] for the case of equivalent electrons.

For small values of n general expressions for the fractional parentage coefficients can be obtained in terms of the Racah coefficients (Wigner 6j symbols) and more complicated invariants formed from the Clebsch-Gordan coefficients. The general expression for the coefficients $<3|2, 1>$ for three equivalent or nonequivalent nucleons with inclusion of isotopic spin effects was given by Redlich;[3] Schwartz and de-Shalit[4] gave the formula for the case of four equivalent particles in the j-j coupling scheme. The problem of the fractional parentage coefficients $<4|2, 2>$ is dealt with in a paper by Jahn[5] (see also the related paper of Englefield[6]). In this paper the fractional parentage expansion is indicated for a function of arbitrary symmetry (belonging to an arbitrary representation of the permutation group, but depending on only one type of

spin). Jahn's fractional parentage expansion enables one, for example, to obtain directly separate expressions for spatial-spin function in j-j coupling and for isotopic spin functions. By forming an antisymmetric combination of these one can obtain the complete wave function for four nucleons. But such a construction obviously does not lead to a single general formula, since the expressions obtained by Jahn do not show explicitly what the necessary relation is between the symmetry types of the functions from which the complete antisymmetric function is to be constructed.

In the present note we wish to show that the general fractional parentage coefficient $<4|2,2>$ for the complete wave function of four equivalent or nonequivalent nucleons can be obtained directly, without previous separate construction of the spatial-spin and isotopic spin expansions. For this we shall not require detailed use of the apparatus of the theory of permutation groups, on which Jahn bases his exposition.

To obtain the antisymmetric wave function of four nucleons we choose a function

$$\Psi\{[j_1j_2(J_1T_1)]_a,\ [j_3j_4(J_2T_2)]_a,\ JTMM_T\}, \tag{1}$$

constructed by vector composition:

$$\mathbf{j}_1+\mathbf{j}_2=\mathbf{J}_1,\ \mathbf{t}_1+\mathbf{t}_2=\mathbf{T}_1,\ \mathbf{j}_3+\mathbf{j}_4=\mathbf{J}_2,\ \mathbf{t}_3+\mathbf{t}_4=\mathbf{T}_2,$$
$$\mathbf{J}_1+\mathbf{J}_2=\mathbf{J},\ \mathbf{T}_1+\mathbf{T}_2=\mathbf{T}\ (t_1=t_2=t_3=t_4={}^1/_2).$$

The notation $[\ ]_a$ means that the function in the brackets is antisymmetrized. The indices on the j's number the different angular momenta. If the numbering of the particles is not indicated explicitly, then $\mathbf{j_ij_k}\dots\mathbf{j_lj_m}$ means $\mathbf{j}_i(1)\,\mathbf{j}_k(2)\dots\mathbf{j}_l(3)\,\mathbf{j}_m(4)$.

We must completely antisymmetrize the function (1) and then expand it in terms of functions analogous to (1), but in general, with different angular momenta.

It is not hard to show that the operator of complete antisymmetrization

$$A(1234)=\frac{1}{\sqrt{4!}}\sum_P(-1)^P P \tag{2}$$

can be written in the form

$$A(1234)=BA(12)\,A(34), \tag{3}$$

where

$$A(12)=(1-P_{12})/\sqrt{2},\ A(34)=(1-P_{34})/\sqrt{2}; \tag{4}$$

$$B=(1+P_{21}P_{13}-P_{13}-P_{14}-P_{23}-P_{24})/\sqrt{6} \tag{5}$$

(P_{ik} means transposition of particles i and k).

For what follows it is essential that

$$A(12)\,A(34)\,B=BA(12)\,A(34). \tag{6}$$

The function (1) can be written in the form

$$\Psi\{[j_1j_2(J_1T_1)]_a,\ [j_3j_4(J_2T_2)]_a,\ JTMM_T\}$$
$$=A(12)\,A(34)\,\Psi\{j_1j_2(J_1T_1),\ j_3j_4(J_2T_2),\ JTMM_T\}. \tag{7}$$

The function on the right is simply the product of a spatial-spin function by a function of the isotopic spins

$$\Psi\{j_1j_2(J_1T_1),\ j_3j_4(J_2T_2),\ JTMM_T\}$$
$$=\varphi(j_1j_2(J_1),\ j_3j_4(J_2),\ JM)\,\varphi_T({}^1/_2\,{}^1/_2(T_1),\ {}^1/_2\,{}^1/_2(T_2),\ TM_T). \tag{8}$$

We can now define a completely antisymmetric function of the four particles by the expression

$$\Psi\{j_1j_2(J_1T_1),\ j_3j_4(J_2T_2),\ JTMM_T\}_a$$
$$=B\Psi\{[j_1j_2(J_1T_1)]_a,\ [j_3j_4(J_2T_2)]_a,\ JTMM_T\}$$
$$=A(12)\,A(34)\,B\Psi\{j_1j_2(J_1T_1),\ j_3j_4(J_2T_2),\ JTMM_T\}. \tag{9}$$

The action of the operator B on a function of the type (8) is easily expressed by means of the Hope χ function,[7-9] which can be defined by the relation

$$P_{23}\varphi(j_1j_2(J_1),\ j_3j_4(J_2),\ JM)\equiv\varphi(j_1(1)\,j_2(3)(J_1),\ j_3(2)\,j_4(4)\ (J_2),\ JM)=\sum_{J_3J_4}\varphi(j_1j_3(J_3),\ j_2j_4(J_4),\ JM)\,\chi\begin{pmatrix}j_1j_2J_1\\ j_3j_4J_2\\ J_3J_4J\end{pmatrix}. \tag{10a}$$

The function χ is a normalized Wigner 9j symbol and can be expressed in terms of 6j symbols (or Racah W coefficients):

$$[(2J_1+1)(2J_2+1)(2J_3+1)(2J_4+1)]^{-1/2}\chi\begin{pmatrix}j_1j_2J_1\\ j_3j_4J_2\\ J_3J_4J\end{pmatrix}=\begin{Bmatrix}j_1j_2J_1\\ j_3j_4J_2\\ J_3J_4J\end{Bmatrix}=\sum_\lambda(-1)^{2\lambda}(2\lambda+1)\begin{Bmatrix}j_1j_3J_3\\ J_4J\lambda\end{Bmatrix}\begin{Bmatrix}j_2j_4J_4\\ j_3\lambda J_2\end{Bmatrix}\begin{Bmatrix}J_1J_2J\\ \lambda j_1j_2\end{Bmatrix};$$

$$\begin{Bmatrix}j_1j_2j_3\\ l_1l_2l_3\end{Bmatrix}=(-1)^{j_1+j_2+l_1+l_2}W(j_1j_2l_2l_1;j_3l_3). \tag{11}$$

Using Eq. (10a) and the relation

$$\varphi(j_1(1)\,j_2(2)\,JM) = (-1)^{j_1+j_2-J}\,\varphi(j_2(2)\,j_1(1)\,JM), \tag{12}$$

one easily obtains the relations

$$P_{14}\varphi(j_1j_2(J_1),\ j_3j_4(J_2),\ JM) = \sum_{J_3J_4}\varphi(j_4j_2(J_4),\ j_3j_1(J_3),\ JM)\,\chi\begin{pmatrix} j_1j_2J_1\\ j_3j_4J_2\\ J_3J_4J\end{pmatrix}(-1)^{j_1+j_2+j_4+J_4-J}; \tag{10b}$$

$$P_{13}\varphi(j_1j_2(J_1),\ j_3j_4(J_2),\ JM) = \sum_{J_3J_4}\varphi(j_3j_2(J_4),\ j_1j_4(J_3),\ JM)\,\chi\begin{pmatrix} j_1j_2J_1\\ j_4j_3J_2\\ J_3J_4J\end{pmatrix}(-1)^{j_2+2j_3+j_4-J_2+J_3-J}; \tag{10c}$$

$$P_{24}\varphi(j_1j_2(J_1),\ j_3j_4(J_2),\ JM) = \sum_{J_3J_4}\varphi(j_1j_4(J_3),\ j_3j_2(J_4)\,JM)\,\chi\begin{pmatrix} j_1j_2J_1\\ j_4j_3J_2\\ J_3J_4J\end{pmatrix}(-1)^{j_2+2j_3+j_4-J_2-J_4} \tag{10d}$$

$$P_{24}P_{13}\varphi(j_1j_2(J_1),\ j_3j_4(J_2)\,JM) = (-1)^{J_1+J_2-J}\,\varphi(j_3j_4(J_2),\ j_1j_2(J_1),\ JM). \tag{10e}$$

Similar relations are, of course, valid for the functions φ_T in Eq. (8).

Substituting the expressions (10) into Eq. (9) we find [after a slight transformation of some of the terms by means of Eq. (12)]

$$\Psi\{j_1j_2(J_1T_1),\ j_3j_4(J_2T_2),\ JTMM_T\}_a = A(12)\,A(34)\,\frac{1}{\sqrt{6}}\Big\{\Psi\{j_1j_2(J_1T_1),\ j_3j_4(J_2T_2),\ JTMM_T\}$$

$$+(-1)^{J_1+J_2-J+T_1+T_2-T}\Psi\{j_3j_4(J_2T_2),\ j_1j_2(J_1T_1),\ JTMM_T\} - \sum_{J_3J_4T_3T_4}\chi\begin{pmatrix} j_1j_2J_1\\ j_3j_4J_2\\ J_3J_4J\end{pmatrix}\chi\begin{pmatrix} 1/2\ 1/2\ T_1\\ 1/2\ 1/2\ T_2\\ T_3T_4T\end{pmatrix}\Big[\Psi\{j_1j_3(J_3T_3),\ j_2j_4(J_4T_4),\ JTMM_T\}$$

$$+(-1)^{J_3+J_4-J+T_3-T+T_4}\Psi\{j_2j_4(J_4T_4),\ j_1j_3(J_3T_3),\ JTMM_T\}\Big] - (-1)^{j_3+j_4-J_2-T_2}\sum_{J_3J_4T_3T_4}\chi\begin{pmatrix} j_1j_2J_1\\ j_4j_3J_2\\ J_5J_6J\end{pmatrix}\chi\begin{pmatrix} 1/2\ 1/2\ T_1\\ 1/2\ 1/2\ T_2\\ T_5T_6T\end{pmatrix}$$

$$\times\Big[\Psi\{j_1j_4(J_5T_5),\ j_2j_3(J_6T_6),\ JTMM_T\} + (-1)^{J_3+J_4-J+T_4+T_3-T}\Psi\{j_2j_3(J_6T_6),\ j_1j_4(J_5T_5),\ JTMM_T\}\Big]\Big\} \tag{13}$$

If all the j's are different and the original functions are normalized, then the function we have obtained will also be normalized in virtue of the relation

$$\sum_{J_3J_4}\chi\begin{pmatrix} j_1j_2J_1\\ j_3j_4J_2\\ J_3J_4J\end{pmatrix}\chi\begin{pmatrix} j_1j_2J_1'\\ j_3j_4J_2'\\ J_3J_4J\end{pmatrix} = \delta(J_1J_1')\,\delta(J_2J_2'), \tag{14}$$

which expresses the unitary property of the (real) transformation (10a).

Thus we immediately obtain the fractional parentage expansion for the case of different j's:

$$\Psi\{j_1j_2(J_1T_1),\ j_3j_4(J_2T_2),\ JTMM_T\}_a = \frac{1}{\sqrt{6}}\Big\{\Psi\{[j_1j_2(J_1T_1)]_a,\ [j_3j_4(J_2T_2)]_a,\ JTMM_T\}$$

$$+(-1)^{J_1+J_2-J+T_1+T_2-T}\Psi\{[j_3j_4(J_2T_2)]_a,\ [j_1j_2(J_1T_1)]_a,\ JTMM_T\}$$

$$-\sum_{J_3J_4T_3T_4}\chi\begin{pmatrix} j_1j_2J_1\\ j_3j_4J_2\\ J_3J_4J\end{pmatrix}\chi\begin{pmatrix} 1/2\ 1/2\ T_1\\ 1/2\ 1/2\ T_2\\ T_3T_4T\end{pmatrix}\Big[\Psi\{[j_1j_3(J_3T_3)]_a,\ [j_2j_4(J_4T_4)]_a,\ JTMM_T\}$$

$$+(-1)^{J_3+J_4-J+T_3+T_4-T}\Psi\{[j_2j_4(J_4T_4)]_a,\ [j_1j_3(J_3T_3)]_a,\ JTMM_T\}\Big] - (-1)^{j_3+j_4-J_2-T_2}\sum_{J_3J_4T_3T_4}\chi\begin{pmatrix} j_1j_2J_1\\ j_4j_3J_2\\ J_5J_6J\end{pmatrix}\chi\begin{pmatrix} 1/2\ 1/2\ T_1\\ 1/2\ 1/2\ T_2\\ T_5T_6T\end{pmatrix} \tag{15a}$$

$$\times\Big[\Psi\{[j_1j_4(J_5T_5)]_a,\ [j_2j_3(J_6T_6)]_a\ JTMM_T\} + (-1)^{J_3+J_4-J+T_3+T_4-T}\Psi\{[j_2j_3(J_6T_6)]_a,\ [j_1j_4(J_5T_5)]_a,\ JTMM_T\}\Big]\Big\}.$$

If there are equal values among the angular momenta j, then in carrying out the application of the antisymmetrizing operators in Eq. (13) we must note that, for example, for equivalent particles 1 and 2

$$A(12)\psi(j^2J_1T_1) = \delta_p(T_1,\ 2j - J_1)\sqrt{2}\,\psi(j^2J_1T_1), \tag{16}$$

where the function $\delta_p(x, y)$ is defined for integer values of its arguments by the relation[5]

$$\delta_p(x, y) = {}^1/_2(1 + (-1)^{x+y}). \tag{17}$$

When equal j's occur the functions obtained from Eq. (13) will not be automatically normalized, so that the normalizing factors have to be determined by further calculations. We give the final normalized expressions

$$\Psi\{j_1j_2(J_1T_1),\ j_3^2(J_2T_2),\ JTMM_T\}_a = \frac{1}{\sqrt{6}}\,\delta_p(T_2,\ 2j_3 - J_2)\Big\{\Psi\{[j_1j_2(J_1T_1)]_a,\ j_3^2(J_2T_2),\ JTMM_T\}$$

$$+ (-1)^{J_1+J_2-J+T_1+T_2-T}\Psi\{j_3^2(J_2T_2),\ [j_1j_2(J_1T_1)]_a,\ JTMM_T\} - \sqrt{2}\sum_{J_3J_4T_3T_4}\chi\begin{pmatrix} j_1j_2J_1\\ j_3j_3J_2\\ J_3J_4J\end{pmatrix}\chi\begin{pmatrix} {}^1/_2\,{}^1/_2\,T_1\\ {}^1/_2\,{}^1/_2\,T_2\\ T_3T_4T\end{pmatrix}$$

$$\times\Big[\Psi\{[j_1j_3(J_3T_3)]_a, [j_2j_3(J_4T_4)]_a, JTMM_T\} + (-1)^{J_3+J_4-J+T_3+T_4-T}\Psi\{[j_2j_3(J_4T_4)]_a,\ \ [j_1j_3(J_3T_3)]_a, JTMM_T\}\Big]\Big\}; \tag{15b}$$

$$\Psi\{j_1^2(J_1T_1),\ j_2^2(J_2T_2),\ JTMM_T\}_a = \frac{1}{\sqrt{6}}\,\delta_p(T_1, 2j_1 - J_1)\,\delta_p(T_2,\ 2j_2 - J_2)\Big\{\Psi\{j_1^2(J_1T_1),\ j_2^2(J_2T_2), JTMM_T\} + (-1)^{2j_1+2j_2+J+T}$$

$$\times\{j_2^2(J_2T_2),\ j_1^2(J_1T_1),\ JTMM_T\} - 2\sum_{J_3J_4T_3T_4}\chi\begin{pmatrix} j_1j_1J_1\\ j_2j_2J_2\\ J_3J_4J\end{pmatrix}\chi\begin{pmatrix} {}^1/_2\,{}^1/_2\,T_1\\ {}^1/_2\,{}^1/_2\,T_2\\ T_3T_4T\end{pmatrix}\times\Psi\{[j_1j_2(J_3T_3)]_a, [j_1j_2(J_4T_4)]_a, JTMM_T\}\Big\}; \tag{15c}$$

$$\Psi\{j_1^2(J_1T_1),\ j_1j_2(J_2T_2),\ JTMM_T\}_a = N_1\frac{1}{\sqrt{6}}\,\delta_p(T_1, 2j_1 - J_1)\Big\{\Psi\{j_1^2(J_1T_1),\ [j_1j_2(J_2T_2)]_a,\ JTMM_T\}$$

$$+ (-1)^{J_1+J_2-J+T_1+T_2-T}\Psi\{[j_1j_2(J_2T_2)]_a,\ \ j_1^2(J_1T_1),\ JTMM_T\} - 2\sum_{J_3J_4T_3T_4}\chi\begin{pmatrix} j_1j_1J_1\\ j_1j_2J_2\\ J_3J_4J\end{pmatrix}\chi\begin{pmatrix} {}^1/_2\,{}^1/_2\,T_1\\ {}^1/_2\,{}^1/_2\,T_2\\ T_3T_4T\end{pmatrix}\delta_p(T_3,\ 2j_1 - J_3)$$

$$\times\Big[\Psi\{j_1^2(J_3T_3),\ [j_1j_2(J_4T_4)]_a,\ JTMM_T\} + (-1)^{J_3+J_4-J+T_3+T_4-T}\Psi\{[j_1j_2(J_4T_4)]_a,\ \ j_1^2(J_3T_3),\ JTMM_T\}\Big]\Big\}; \tag{15d}$$

$$\Psi\{j^2(J_1T_1),\ j^2(J_2T_2),\ JTMM_T\}_a = N_2\frac{1}{\sqrt{6}}\,\delta_p(T_1,\ 2j - J_1)\,\delta_p(T_2,\ 2j - J_2)$$

$$\times\Big\{\Psi\{j^2(J_1I_1), j^2(J_2T_2), JTMM_T\} + (-1)^{J+T}\Psi\{j^2(J_2T_2), j^2(J_1T_1), JTMM_T\}$$

$$- 4\sum_{J_3J_4T_3T_4}\chi\begin{pmatrix} j\ j\ J_1\\ j\ j\ J_2\\ J_3J_4J\end{pmatrix}\chi\begin{pmatrix} {}^1/_2\,{}^1/_2\,T_1\\ {}^1/_2\,{}^1/_2\,T_2\\ T_3T_4T\end{pmatrix}\delta_p(T_3,\ 2j - J_3)\,\delta_p(T_4,\ 2j - J_4)\times\Psi\{j^2(J_3T_3),\ j^2(J_4T_4),\ JTMM_T\}\Big\}; \tag{15e}$$

$$N_1 = \left[1 - 2\chi\begin{pmatrix} j_1j_1J_1\\ j_1j_2J_2\\ J_1J_2J\end{pmatrix}\chi\begin{pmatrix} {}^1/_2\,{}^1/_2\,T_1\\ {}^1/_2\,{}^1/_2\,T_2\\ T_1T_2T\end{pmatrix}\right]^{-1/2}; \tag{18a}$$

$$N_2 = \left[1 + (-1)^{J+T}\delta(J_1, J_2)\,\delta(T_1, T_2) - 4\chi\begin{pmatrix} j\ j\ J_1\\ j\ j\ J_2\\ J_1J_2J\end{pmatrix}\chi\begin{pmatrix} {}^1/_2\,{}^1/_2\,T_1\\ {}^1/_2\,{}^1/_2\,T_2\\ T_1T_2T\end{pmatrix}\right]^{-1/2}. \tag{18b}$$

All the normalizing factors are easily obtained by means of Eq. (14) and the relations

$$\sum_{J_3J_4}\chi^2\begin{pmatrix} j_1j_1J_1\\ j_1j_2J_2\\ J_3J_4J\end{pmatrix}(-1)^{J_4} = (-1)^{2j_1}\chi\begin{pmatrix} j_1j_1J_1\\ j_1j_2J_2\\ J_1J_2J\end{pmatrix}; \tag{19}$$

$$\sum_{J_3J_4}\chi^2\begin{pmatrix} j\ j\ J_1\\ j\ j\ J_2\\ J_3J_4J\end{pmatrix}(-1)^{J_3+J_4} = (-1)^J\delta(J_1, J_2). \tag{20}$$

The relation (19) can be verified by using the expansion (11). It is easy to prove Eq. (20), starting with Eq. (14) and the symmetry properties of χ functions.

The fractional parentage expansions given here have been obtained for the purpose of using them for calculations of two-particle interactions in nuclei. They can also be applied in atomic spectroscopy (after the replacements $j_i \rightarrow \ell_i$, $J \rightarrow L$, $T \rightarrow S$).

[1] G. Racah, Phys. Rev. **62**, 438 (1942).
[2] G. Racah, Phys. Rev. **63**, 367 (1943).
[3] M. G. Redlich, Phys. Rev. **99**, 1427 (1955).
[4] C. Schwartz and A. de-Shalit, Phys. Rev. **94**, 1257 (1954).
[5] H. A. Jahn, Phys. Rev. **96**, 989 (1954).
[6] M. J. Englefield, Phys. Rev. **98**, 1213 (1955).
[7] H. A. Jahn and J. Hope, Phys. Rev. **93**, 318 (1954).
[8] A. de-Shalit, Phys. Rev. **91**, 1479 (1953).
[9] A. R. Edmonds, Angular Momentum in Quantum Mechanics, CERN 55-26, Geneva, 1955.

Translated by W. H. Furry
131

SOVIET PHYSICS JETP VOLUME 34 (7), NUMBER 3 SEPTEMBER, 1958

ON THE THEORY OF PHOTONUCLEAR REACTIONS

V. M. AGRANOVICH and V. S. STAVINSKII

Submitted to JETP editor September 30, 1957

J. Exptl. Theoret. Phys. (U.S.S.R.) **34**, 700-706 (March, 1958)

The cross section is computed for the capture of gamma rays by nuclear matter at giant resonance energies.

In theoretical investigations of giant resonance in photonuclear reactions, extensive use has been made of two models for interactions between gamma rays and nuclei. Migdal',[1] Goldhaber and Teller[2] and others regarded giant resonance as the result of an interaction between gamma rays and the collective dipole vibrations of nuclei. In contrast with this collective aspect, Wilkinson[3] and Burkhardt[4] have used the shell model in a detailed study of the mechanism of gamma-ray capture as the result of the excitation of single nucleons. However, neither model provides an explanation of all of the experimental data. For example, recent calculations based on the collective model[5] give a width of giant resonance in (γ, n) reactions which is much smaller than the observed width. On the other hand, the shell model gives incorrect frequencies for giant resonance.[4*] The principal defect of the calculations that have been mentioned is apparently the use of incorrect wave functions to describe highly excited nuclear states.

It is shown in several papers[6-9] that experiments on slow neutron scattering by medium and heavy nuclei can be interpreted satisfactorily if in constructing wave functions for highly excited states account is taken of the possibility that the excitation energy of a single particle is redistributed among other degrees of freedom. In our calculation of the photonuclear absorption cross section we shall use herein the method of Lane, Thomas, and Wigner[7] for constructing the wave functions of excited states, taking the above mentioned possibility into account.

1. CALCULATION OF THE PHOTONUCLEAR ABSORPTION CROSS SECTION

The nonrelativistic operator for the interaction between an electromagnetic field and a system of nucleons is

$$H' = -\sum_n \left[\left(\frac{e}{Mc}\right) \mathrm{pA} \left(\frac{1}{2} - t_{z_n}\right) + \left\{ \mu_p \left(\frac{1}{2} - t_{z_n}\right) + \mu_n \left(\frac{1}{2} + t_{z_n}\right) \right\} \sigma \nabla \times \underline{A} \right]. \quad (1)$$

If Ψ_0 and Ψ_{E_γ} are the wave functions of the nu-

*Note added in proof. The computed giant-resonance frequencies are close to the observed frequencies when the effective nucleon mass is set equal to half of the true mass for all excitation energies,[19] but there is no other basis for this assumption.

cleonic system that represent the ground level and an excited level which is higher by the energy of the absorbed gamma ray, the gamma-ray absorption probability per second[10] is

$$P = \frac{2\pi}{\hbar} |H'_{0,E_\gamma}| \rho(E_\gamma), \quad (2)$$

where $\rho(E_\gamma)$ is the density of levels with excitation energy E_γ and

$$H'_{0,E_\gamma} = \int \Psi_0^* H' \Psi_{E_\gamma} d\tau. \quad (3)$$

For the sake of simplicity we shall consider a system of A nucleons in a sufficiently large volume V. In the self-consistent field model the ground level of this system is represented by a completely filled Fermi sphere with the maximum wave number k_F. The self-consistent potential which corresponds to an excited level of the system differs from the self-consistent potential for the ground level. For this reason, and also because of the strong correlation between nucleons in a nucleus, the wave function Ψ_{E_γ} can be represented as follows:

$$\Psi_{E_\gamma} = \sum_b C_b \Phi_b, \quad (4)$$

where $\{\Phi_b\}$ denotes different Slater determinants composed of single-particle wave functions that represent the motion of single nucleons in a constant potential which is self-consistent for the ground state of the nucleus.* Following Ref. 7, it is assumed that the principal contributions to Eq. (4) come from states Φ_b which represent energies ϵ_b in a range of width W around E_γ. The width W, which is defined by

$$W^2 = \sum_b (E_\gamma - \varepsilon_b)^2 |C_b|^2, \quad (5)$$

is directly related to the imaginary part of the optical potential.[7-9] We shall also assume that it is sufficient to limit ourselves in (4) to states Φ_b which represent the emergence of only a single nucleon above the Fermi surface.

Using (4), (3), and (2), we find

$$P = \frac{2\pi}{\hbar} \rho(E_\gamma) \sum_b |C_b|^2 |M_{b0}|^2, \quad (6)$$

where

$$M_{b0} = \int \Phi_b^* H' \Phi_0 d\tau. \quad (7)$$

In (6), following Refs. 7 and 11, we have omitted the interference terms containing the products $C_b C_b^*$. Going from a sum to an integral in (6), we obtain

$$P = \frac{2\pi}{\hbar} \rho(E_\gamma) \int_0^\infty |C_b|^2 \rho(\varepsilon_b) \overline{|M_{b0}|^2} \, d\varepsilon_b. \quad (8)$$

In (8) $\overline{|M_{b0}|^2}$ is the square of the absolute value of the transition matrix element averaged over all levels of energy ϵ_b. From the normalization of Ψ_{E_γ} it follows that

$$\int_0^\infty |C_b|^2 \rho(\varepsilon_b) \, d\varepsilon_b = 1. \quad (9)$$

Using the assumption of Ref. 7 that the principal contributions to (4) come from the states Φ_b with energy ϵ_b close to E_γ within a range of width W, as was done in Ref. 8, we put

$$|C_b|^2 \rho(\varepsilon_b) = \frac{B(E_\gamma)}{\Omega} \exp\{-(E_\gamma - \varepsilon_b)^2 / \Omega^2\}. \quad (10)$$

In (10), which satisfies (9),

$$B(E_\gamma) = \frac{2}{\sqrt{\pi}} [1 + \Phi(x)]^{-1}, \quad (11)$$

where

$$x = E_\gamma / \Omega, \quad \Phi(x) = \frac{2}{\sqrt{\pi}} \int_0^x e^{-t^2} dt.$$

The function $\Omega \equiv \Omega(E_\gamma)$ in the approximation represented by (10) is, in virtue of (5), related to $W(E_\gamma)$ as follows:

$$W^2(E_\gamma) = \frac{\Omega^2(E_\gamma)}{2[1 + \Phi(x)]} \left\{ 1 + \Phi(x) - \frac{2x}{\sqrt{\pi}} e^{-x^2} \right\}. \quad (12)$$

In calculating the matrix element (7) we neglect the interaction of the electromagnetic field with the nucleonic magnetic moments. In this approximation

$$|M_{0b}|^2 = \frac{Z^2 e^2 \hbar^2}{M^2 c^2} (\mathbf{A}_0 \mathbf{k}_1)^2 \delta_{\mathbf{k}_2, \mathbf{k}_1 + \mathbf{Q}}. \quad (13)$$

Here $\mathbf{k}_1$ and $\mathbf{k}_2$ are wave vectors that represent a hole inside the Fermi sphere and a nucleon outside. These wave vectors are related* as follows ($|\mathbf{k}_2| > k_F > |\mathbf{k}_1|$):

$$\hbar^2 k_2^2 / 2M^* - \hbar^2 k_1^2 / 2M^* = \varepsilon_b. \quad (14)$$

In deriving (13) the vector potential was assumed to have the form

$$\mathbf{A} = \mathbf{A}_0 \exp\left\{ i \frac{E_\gamma t}{\hbar} + i\mathbf{Q}\mathbf{r} \right\}. \quad (15)$$

*In the approximation used below $\Psi_0 = \Phi_0$.

Here M is the effective mass of a nucleon in the nucleus.

By definition,

$$\overline{|M_{0b}|^2}_{\varepsilon_b} = \sum_{b,\varepsilon=\varepsilon_b} |M_{0b}|^2 / g_{\varepsilon_b}, \tag{16}$$

where g_{ϵ_b} is the number of states Φ_b with excitation energy ϵ_b. It follows from (13) and (14) that not all levels with ϵ_b give a non-vanishing matrix element M_{0b}. It also follows from these equations that when (14) is fulfilled $M_{0b} \neq 0$ when*

$$k_{1z} = M^*\varepsilon_b/\hbar^2 Q - Q/2 \equiv k_0. \tag{17}$$

Also, from the condition $k_0^2 \leq k_F^2$ it follows that M_{0b} can be non-vanishing only for values of ϵ_b within the limits

$$0 < \varepsilon_b < \frac{\hbar^2 Q}{M^*}\left(k_F + \frac{Q}{2}\right) \equiv \varepsilon'. \tag{18}$$

For a fixed value of ϵ_b the range of variation of $\mathbf{k}_1$ is bounded by

$$k_F^2 \geqslant k_1^2 \geqslant k_F^2 - 2M^*\varepsilon_b/\hbar^2 \equiv k_{\min}^2, \tag{19}$$

which follows from (14) and the Pauli principle ($k_2^2 > k_F^2$). From (17) and (19) we find that the end of the vector $\mathbf{k}_1$, for states Φ_b ($\mathbf{k}_2 = \mathbf{k}_1 + \mathbf{Q}$) which give a non-vanishing matrix element M_{0b}, lies within a circular ring S in the plane $k_{1Z} = k_0$. The radii of the ring are

$$\rho_{\max} = \sqrt{k_F^2 - k_0^2}, \tag{20}$$

$$\rho_{\min} = \begin{cases} \sqrt{k_F^2 - 2M^*\varepsilon_b/\hbar^2 - k_0^2}, & \text{for } 0 < \varepsilon_b < \varepsilon'', \\ 0 & \text{for } \varepsilon'' < \varepsilon_b < \varepsilon', \end{cases}$$

where

$$\varepsilon'' = \frac{\hbar^2 Q}{M^*}\left(k_F - \frac{Q}{2}\right). \tag{21}$$

Therefore†

$$\sum_{b,\varepsilon=\varepsilon_b} |M_{0b}|^2 = \frac{Z^2e^2\hbar^2}{M^2c^2} |\mathbf{A}_0|^2 \sum_S k_{1x}^2$$

$$= \frac{Z^2e^2\hbar^2 |\mathbf{A}_0|^2}{M^2c^2} \frac{V^{1/3}}{(2\pi)^2\, 4}(\rho_{\max}^4 - \rho_{\min}^4). \tag{22}$$

In computing the total number of states with energy ϵ_b it must be kept in mind that (14) is the only limitation on the magnitude of $\mathbf{k}_2$. Therefore

$$g_{\varepsilon_b} = \frac{V^{1/3}}{(2\pi)^5}(4\pi)^2 \left\{\frac{k_F^5 - k_{\min}^5}{5} + \frac{2M^*\varepsilon_b}{\hbar^2}\frac{k_F^3 - k_{\min}^3}{3}\right\}. \tag{23}$$

Thus, from (16), (22), and (23) we obtain

$$\overline{|M_{0b}|^2} = \left(\frac{Ze\hbar\,|\mathbf{A}_0|}{Mc}\right)^2 \times \frac{5\pi^2}{8V}\frac{(\rho_{\max}^4 - \rho_{\min}^4)}{k_F^5 - k_{\min}^5 + (10\,M^*\varepsilon_b/3\hbar^2)(k_F^3 - k_{\min}^3)}. \tag{24}$$

Substituting (10) and (24) into (8) and integrating, we obtain

$$P = \left(\frac{Ze\hbar\,|\mathbf{A}_0|}{Mc}\right)^2 \frac{\pi^3 (M^*c/\hbar k_F)^2}{V\hbar k_F}\, \varphi_2(x)\, \rho(E_\gamma), \tag{25}$$

where

$$\varphi_2(x) = \frac{1}{1+\Phi(x)}\left\{\left[\left(\frac{\hbar k_F}{M^*c}\right)^2 - 1 - x^2\left(\frac{2M^*\Omega}{\hbar^2 k_F^2}\right)^2 \frac{1}{16}\left(\frac{\hbar k_F}{M^*c}\right)^4\right]\right.$$

$$\times[\Phi(x) - \Phi(\gamma x)] + \frac{\sqrt{2}}{x}[(2-\gamma)\,\Phi_1(x\gamma\sqrt{2}) - \Phi_1(x\sqrt{2})]$$

$$\left. - \frac{1}{2x^2}[\Phi(x) - \Phi(\gamma x)]\right\}, \tag{26}$$

where, in turn,

$$\Phi_1(t) = \frac{1}{\sqrt{2\pi}} e^{-t^2/2}, \quad \gamma = 1 - \frac{\hbar k_F}{M^*c} + \frac{1}{2}\left(\frac{\Omega}{M^*c^2}\right)x.$$

Before proceeding from P to the gamma-ray absorption cross section we shall determine the density of final levels. The density of states Φ_b with energy E_γ is given by

$$\rho(E_\gamma) = dL(E_\gamma)/dE_\gamma,$$

where $L(E_\gamma)$ is the number of states Φ_b with $\epsilon_b \leq E_\gamma$. For the determination of $L(E_\gamma)$ it is necessary to compute the number of phase cells contained in the phase volume of the nucleon and the holes corresponding to all states Φ_b with $\epsilon_b \leq E_\gamma$. In this case, as is shown by a simple calculation,

$$\rho(E_\gamma) = \frac{3V^2}{8\pi^4}\left(\frac{2M^*}{\hbar^2}\right)^3 \Omega^2 x^2 \int_{\xi(x)}^{\sqrt{\nu(x)}} y^2 (1+y^2)^{1/2}\, dy, \tag{27}$$

where

$$\nu(x) = \hbar^2 k_F^2/2M^*\Omega x,$$

$$\xi(x) = \begin{cases} \sqrt{\nu(x) - 1}, & \nu(x) > 1 \\ 0, & \nu(x) < 1 \end{cases}.$$

Before going from (25) to the cross section, (25) must be divided by the flux c/V. Then, using (27), we obtain

$$\sigma(E_\gamma) = 0.11 \cdot 10^{-26} AZ^2 F(x)\ \text{cm}^2. \tag{28}$$

Here

$$F(x) = \left(\frac{M^*}{M}\right)^5 \varphi_2(x) \int_{\xi(x)}^{\sqrt{\nu(x)}} y^2 (1+y^2)^{1/2}\, dy \left(\frac{\Omega}{1.1\ \text{Mev}}\right). \tag{29}$$

2. DISCUSSION OF RESULTS

In Fig. 1, F(x) is plotted for different values

*The z axis is chosen to be in the direction Q.

†The x axis is in the direction of $\mathbf{A}_0$.

of Ω and M^*/M. In all cases the photonuclear absorption cross section given by (28) shows strong resonance, the frequency and width of which depend essentially on Ω. In Ref. 7 a first estimate was obtained for W, which is related to Ω by Eq. (12); the result was $W \approx 23$ Mev ($\Omega \approx 32$ Mev). Later and more accurate calculations gave $W = 6 - 10$ Mev, which corresponds to $\Omega = 8.4 - 14$ Mev. Because of this indefiniteness in the magnitude of Ω, in Fig. 1 $F(x)$ is given for two values of Ω (10 Mev and 25 Mev). The magnitude of Ω depends generally on E_γ and increases somewhat with E_γ. However, since the form of the function $\Omega(E_\gamma)$ is unknown the curves in Fig. 1 were plotted with Ω assumed to be constant. Even if the slight dependence of Ω on E_γ were taken into account, the curves of $F(x)$ would not be essentially changed. The question of the effective mass of a nucleon in a nucleus has been discussed widely in the literature (see Refs. 13 and 14, for example).

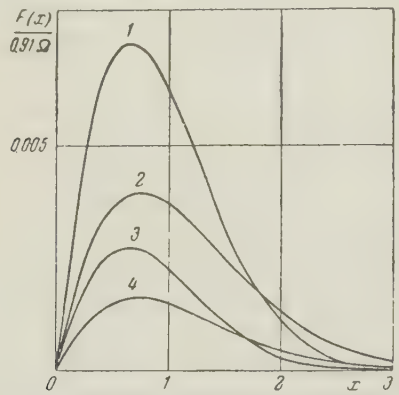

FIG. 1. 1 – $\Omega = 10$, $M^*/M = 1$; 2 – $\Omega = 10$, $M^*/M = ½$; 3 – $\Omega = 25$, $M^*/M = 1$; 4 – $\Omega = 25$, $M^*/M = ½$.

It has thus been shown that $\frac{1}{2}M < M^* < M$, where M is the mass of a free nucleon. The curves of $F(x)$ for each value of Ω were plotted for the two limiting values of the effective mass. Figure 1 shows that independently of the magnitude of Ω, when the effective mass is reduced from $M^* = M$ to $M^* = M/2$ the cross section is reduced by one half at the peak while the half width increases by 20 – 30%. The resonance frequency and the width depend slightly on M^*, which is in disagreement with Ref. 15. For different values of Ω these quantities change considerably. It is difficult to make a numerical comparison of the foregoing calculation with experimental findings, because for no single nucleus have the cross sections been measured for all processes that pass through the compound nucleus stage as a result of excitation by gamma rays* in the considered energy range ($E_\gamma < 50$ Mev). The available experiments with medium and heavy nuclei (the only nuclei for which it is meaningful to compare theory and experiment) are not qualitatively in disagreement with the foregoing calculation. Thus the observed resonance frequencies for the (γ, n), $(\gamma, 2n)$, (γ, p), etc. reactions correspond to $\Omega \sim 15$ Mev. For this value of Ω the half width of the cross section curve is 17 – 28 Mev, as follows from Fig. 1, which exceeds the observed half width for (γ, n) by a factor of 2 to 3,[17] and for (γ, γ) and (γ, γ') by a factor of 1.5 to 2. This discrepancy of the half widths can be accounted for by the following considerations:

(a) The theoretical cross section for photonuclear absorption when E_γ is below the Bethe-Hurwitz characteristic level[18] ($E_{B\text{-}H} \sim 4 - 6$ Mev for non-fissioning nuclei) appears too large, because in this energy range there occurs resonance scattering of gamma rays at particular levels which experiment[16] shows to be considerably below the result calculated above. This reduces the calculated photonuclear absorption half width by ≈ 5 Mev.

(b) The cross sections for (γ, x) reactions which pass through the compound nucleus stage are obtained by multiplying the cross section of (28) by the relative probability of the respective process.

Since the thresholds of these reactions (E_x) lie above the Bethe-Hurwitz level by 2 – 3 Mev,

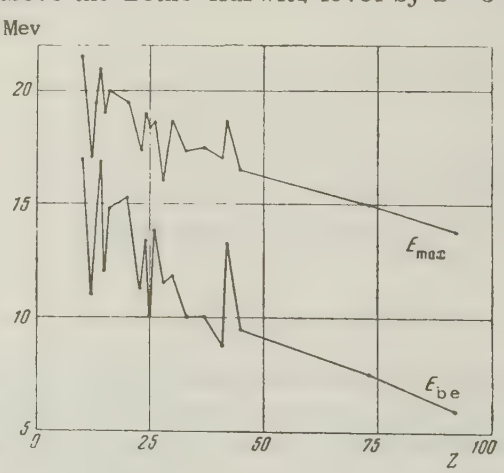

FIG. 2

the half width of the (γ, x) curve is less than that of the photoabsorption curve by 2 – 3 Mev and is thus 9 – 14 Mev. This is still greater than the

*Thus, there is a complete absence of data on the (γ, γ') threshold below the (γ, n) threshold.

observed half width of 6 — 8 Kev. The agreement between theory and experiment is somewhat improved by taking into account the dependence $\Omega(E_\gamma)$, which follows from Eq. (26). When $E_\gamma < E_x$ only the processes (γ, γ) and (γ, γ') can occur. However, the (γ, γ) cross sections in this energy range are small[16] compared with the calculated photoabsorption cross section, which apparently indicates that in this energy range considerable inelastic scattering of photons should be observed. Unfortunately, the requisite measurements are not yet available. Since, according to Ref. 7, Ω depends slightly on atomic weight, the maximum and half width of the photonuclear absorption cross section should also depend slightly on A. Therefore, we should observe a correlation between the frequency at the (γ, n) cross section maximum and the binding energy of the emitted neutron (with increasing E_{be}, E_{max} should increase and vice versa). The available experimental data actually reveal this tendency (Fig. 2).*

The model of infinite nuclear matter which has been used cannot yield the observed relation between the cross section for gamma-ray capture and A. This is due principally to the fact that the level density which has been calculated above depends more strongly on the number of particles than the density of the corresponding levels in real nuclei. In addition, the same circumstance increases by more than one order of magnitude the maximum of the gamma-ray capture cross section. Thus for $A = 100$, $\sigma_\gamma(E_{max}) \approx 6$ barns, and for $A = 200$, $\sigma_\gamma(E_{max}) = 50$ barns. Better agreement between theory and experiment results from consideration of a finite nucleus.

In conclusion the authors wish to thank A. S. Davydov and A. I. Leipunskii for their interest and for discussion of the results.

*The experimental data were taken from the review article, Ref. 17.

[1] A. B. Migdal, J. Exptl. Theoret. Phys. (U.S.S.R.) **15**, 81 (1945).

[2] M. Goldhaber and E. Teller, Phys. Rev. **74**, 1046 (1948).

[3] D. H. Wilkinson, Physica **22**, 1039 (1956).

[4] J. L. Burkhardt, Phys. Rev. **91**, 420 (1953).

[5] J. Fujita, Progr. Theoret. Phys. (Japan) **14**, 4, 400 (1955).

[6] Feshbach, Porter, and Weisskopf, Phys. Rev. **96**, 448 (1954).

[7] Lane, Thomas, and Wigner, Phys. Rev. **98**, 693 (1955).

[8] V. M. Agranovich and A. S. Davydov, J. Exptl. Theoret. Phys. (U.S.S.R.) **32**, 1429 (1957), Soviet Phys. JETP **5**, 1164 (1957).

[9] C. Bloch, Nucl. Phys. **3**, 137 (1957).

[10] L. Landau and E. Lifshitz, Квантовая механика (Quantum Mechanics), Vol. I, 1948.

[11] T. Teichmann and E. P. Wigner, Phys. Rev. **87**, 123 (1952).

[12] E. Vogt and Lascoux, CRT-679, Atomic Energy of Canada Ltd., Chalk River Project, Chalk River, Ont.

[13] H. A. Bethe and J. Goldstone, Proc. Roy. Soc. (London) **A238**, 551 (1956).

[14] W. Wada and K. A. Brueckner, Phys. Rev. **103**, 1008 (1956).

[15] V. F. Weisskopf, Nucl. Phys. **3**, 423 (1957).

[16] J. S. Levinger, Phys. Rev. **84**, 523 (1951).

[17] N. Kul' chitskii, Проблемы современной физики (Problems of Contemp. Phys.) No. 6, 5 (1957).

[18] H. A. Bethe and H. Hurwitz, Phys. Rev. **81**, 898 (1951).

[19] S. Rand, Phys. Rev. **107**, 208 (1957).

Translated by I. Emin
132

OPTICAL PROPERTIES OF METALS IN THE INFRARED REGION

V. P. SILIN

P. N. Lebedev Physical Institute, Academy of Sciences, U.S.S.R.

Submitted to JETP editor October 1, 1957

J. Exptl. Theoret. Phys. (U.S.S.R.) **34**, 707-713 (March, 1958)

Landau's theory of a Fermi liquid is employed to describe the optical properties of metals in the infrared region. It is shown that the results obtained differ substantially from the corresponding results of the ordinary electron theory of metals.

1. In the region of infrared radiation ($\omega/2\pi = 10^{12}$ to 3×10^{14} sec^{-1}), great interest (from the viewpoint of obtaining information on the properties of the conduction electrons of a metal[1]) attaches to the range of frequencies much less than the frequencies of quantum absorption, and at the same time frequencies which are large in comparison with the collision frequency $1/\tau$ (τ is the characteristic time of free flight of the electrons*). For many metals, the frequency of quantum absorption is of the same order of magnitude as the frequency† $\omega_0 = \sqrt{4\pi e^2 N/m} \approx \sqrt{3 \times 10^9 N}$ of plasma oscillations of the conduction electrons, which value appreciably exceeds the upper limit of the infrared region. Therefore we shall consider frequencies which satisfy the inequality

$$\omega_0 \gg \omega \gg 1/\tau. \qquad (1)$$

The optics of metals in such a region were studied by a number of authors.[1,3,4] In these researches, as is usually done in conduction theory, the representation of the conduction electrons as a gas of noninteracting particles is employed as one of the principal assumptions. In reality, the interaction between the electrons is by no means small, and they ought to be considered as a degenerate electron liquid. The latter is now possible with the use of the theory of a Fermi liquid formulated by Landau[5] and extended in Ref. 6 to an electron liquid.

An essential difference was discovered in Ref. 2 of the complex dielectric constant of a metal in the infrared region and the corresponding expression for ordinary theory.[1,3] However, only the real part of the complex dielectric constant was considered in that work. Below, we have obtained an expression for the imaginary part of the constant in the case in which such exists (see Ref. 1). In the case of an anomalous skin effect in the infrared region, an expression is obtained below for the surface impedance of the metal. In all these cases, the theory of the Fermi liquid modifies considerably the description of the properties of the metals.

We note that in the region of small frequencies, in which we can make use of the statistical characteristics of the metal, the theory of conductivity, which starts out from assumptions on the electron liquid, does not differ from the usual theory. The same also applies to the prominent anomalous skin effect.[2]

2. The electrons — quasi-particles produced by the electrons of the liquid — are described by the equation

$$\frac{\partial n}{\partial t} + \frac{\partial n}{\partial \mathbf{r}}\frac{\partial \varepsilon}{\partial \mathbf{p}} - \frac{\partial n}{\partial \mathbf{p}}\frac{\partial \varepsilon}{\partial \mathbf{r}} + e\left(\mathbf{E} + \frac{1}{c}\left[\frac{\partial \varepsilon}{\partial \mathbf{p}}\mathbf{H}\right]\right)\frac{\partial n}{\partial \mathbf{p}} = I(n) \qquad (2)$$

in the theory of a Fermi liquid.[5,6] Here n is the distribution function, $I(n)$ is the collision integral, and ϵ is the energy of the quasi-particle. In this case,

$$\delta\varepsilon = \int d\mathbf{p}'\Phi(\mathbf{p}, \mathbf{p}')\,\delta n'. \qquad (3)$$

The latter relation is useful because we are almost always interested in states which differ slightly from equilibrium, in which

$$n = n_0 + \delta n, \quad |\delta n| \ll n_0 = \frac{2}{(2\pi\hbar)^3}\left[\exp\left\{\frac{\varepsilon_0 - \mu}{kT}\right\} + 1\right]^{-1}; \qquad (4)$$

$$\varepsilon = \varepsilon_0 + \delta\varepsilon.$$

In this case the theory of the Fermi liquid gives the following expression for the density of the electric current:

$$\mathbf{j} = e\int d\mathbf{p}\, n\frac{\partial \varepsilon}{\partial p} = e\int d\mathbf{p}\left\{\delta n - \delta\varepsilon\frac{\partial n_0}{\partial \varepsilon_0}\right\}\frac{\partial \varepsilon_0}{\partial \mathbf{p}}. \qquad (5)$$

*At room temperature, τ 0.3×10^{-13} sec.

†For determination of N, see Refs. 1, 2. For many metals, N is of the order of 0.5×10^{23} cm^3 and, consequently, $\omega_0 \sim 10^{16}$ sec^{-1}

with the accuracy considered by us, where $Z_x^{(0)}$, $R_x^{(a)}$, $R_{xy}^{(a)}$ are defined respectively by Eqs. (16), (23), and (25), while $R_x^{(H)}$ and $R_{xy}^{(H)}$ can easily be obtained from Eqs. (8), (11), and (19).

5. The difference of Eqs. (8), (13), (23), and (25) from the corresponding relations of the research of Kaganov and Slezov[9] is due to the function Φ. It is natural to attempt to make clear what evidence can be obtained on this function from experiments in the infrared region. However, we can point out at once that the results which we have obtained above are always complicated by the anisotropies of the metal. Therefore, without a knowledge of the Fermi surface, it is difficult to obtain information on the function Φ from experiments in the infrared region. Evidently, for the determination of effects which distinguish the conduction electrons from the Fermi gas, we must first determine the form of the Fermi surface with the aid of experiments in the radio-frequency range for the case of a sharply defined anomalous skin effect.[9]

The results obtained above are greatly simplified when the metal can be regarded as isotropic.[1] The latter is quite natural for polycrystalline samples. We shall consider this case in more detail below. Under such an assumption, we have, in place of Eq. (8),

$$\operatorname{Re}\varepsilon' = -\frac{4\pi e^2 N}{m\omega^2}, \quad N = \frac{8\pi p_0^2 v_0 m}{3(2\pi\hbar)^3}\{1 + p_0^2\int d\Omega \cos\chi F(\cos\chi)\};$$

$$F = [2/(2\pi\hbar)^3]\,\Phi(p, p')/v_0, \qquad (8'')$$

where p_0 and v_0 are the momentum and velocity of the electron on the Fermi surface, m = mass of the free electron. Such an expression for the real part of the complex dielectric constant was obtained in Ref. 2. The non-diagonal elements of the tensor of the real part of the complex dielectric constant tensor in the approximation under consideration are equal to zero. In the absence of a magnetic field, the imaginary part ϵ', which is defined by Eq. (19), is also diagonal and is equal to

$$\operatorname{Im}\varepsilon' = \frac{8\pi e^2 p_0^2}{3\omega^3(2\pi\hbar)^3}\int\frac{d\Omega}{v}\,\mathbf{V}J(\mathbf{V}). \qquad (19')$$

We note that formulas which contain the collision integral are valid even in the quantum case,[10] in which the frequency of the light is comparable to, or becomes larger than $kT/\hbar$. In this case, only the value of the collision integral changes.

In the isotropic case, only the nondiagonal terms arise, as a result of the constant magnetic field. Directing H_0 along the z axis, we have

$$\operatorname{Im}\varepsilon'_{xy} = -\operatorname{Im}\varepsilon'_{yx}$$

$$= -\frac{4\pi}{\omega}\frac{8\pi e^2 p_0^2 v_0}{3(2\pi\hbar)^3\omega^2}\frac{ev_0H_0}{p_0}\left\{1 + p_0^2\int d\Omega\cos\chi F\right\}^2. \qquad (19'')$$

The presence of a magnetic field has no effect on the other components.

Finally, for an isotropic metal, Eq. (25) vanishes, while (23) takes on the form

$$R_x = \frac{3\pi}{4}\frac{v_0}{c^2}\left\{1 + p_0^2\int d\Omega\cos\chi F(\cos\chi)\right\}. \qquad (23')$$

As was shown in Ref. 2, the relation (8), along with data on the electronic heat capacity of the metal and the results of experiments in the radio-frequency region, in the case of a sharply defined anomalous skin effect, permits us to establish the value of $p_0^2\int d\Omega\cos\chi\,F(\cos\chi)$. In other words, the possibility is shown of determining the first coefficient in the expansion of $F(\cos\chi)$ in Legendre polynomials. Equation (23) points up the possibility of a similar estimate of this coefficient. Of course, it should be observed that all such estimates are essentially connected with the possibility of using the isotropic model of the metal, and this in each case must be done with caution.[2] We note that in the collision with the surface, the part (2) of the electrons can be scattered specularly. In this case, the expression obtained above for $R^{(a)}$ must be changed by a factor of $(1 - q)$.

In conclusion, I am pleased to express my thanks to L. D. Landau for useful discussions of the problem, explained in the Appendix.

APPENDIX

In order to clarify the form of the collision integral in the theory of a Fermi liquid for the nonequilibrium state, we consider as an example collisions with impurities. In this case, the collision integral has the form

$$I(n) = \int W(n; p, p')\{n(p')[1 - n(p)]$$
$$- n(p)[1 - n(p')]\}\,\delta\{\varepsilon(p) - \varepsilon(p')\}\,dp'.$$

Taking (4) into account, we can represent $I(n)$ in the form of a sum $I_1 + I_2$, where

$$I_1 = \int W(n_0; p, p')\{\delta n(p) - \delta n(p')\}\,\delta\{\varepsilon_0(p) - \varepsilon_0(p')\}\,dp',$$

$$I_2 = \int W(n_0; p, p')\{n_0(p') - n_0(p)\}\,\delta\{\varepsilon_0(p)$$
$$+ \delta\varepsilon(p) - \varepsilon_0(p') - \delta\varepsilon(p')\}dp'.$$

Here, I_1 is a quantity which coincides with the

collision integral of ordinary theory.

Further, it is convenient to transform I_2 somewhat. In this case, we take it into consideration that

$$n_0(\varepsilon_0) \approx n_0(\varepsilon_0 + \delta\varepsilon) - \delta\varepsilon \partial n_0 / \partial \varepsilon_0.$$

Thanks to the fact that in the law of conservation of energy, $\epsilon = \epsilon_0 + \delta\epsilon$, terms containing only $n_0(\epsilon)$ fall out, and there are left terms proportional to $\delta\epsilon$. For the remaining small terms, the difference between ϵ and ϵ_0 in the conservation law is no longer significant. Therefore,

$$I(n_0 + \delta n) = \int W(n_0; \mathrm{p}, \mathrm{p}') \left\{ \left(\delta n' - \delta\varepsilon' \frac{\partial n_0}{\partial \varepsilon_0'} \right) - \left(\delta n - \delta\varepsilon \frac{\partial n_0}{\partial \varepsilon_0} \right) \right\} \delta(\varepsilon_0 - \varepsilon_0') d\mathrm{p}'.$$

Thus it can be shown that the collision integral for states which differ only slightly from the equilibrium can be obtained by the substitution in the conservation law of the equilibrium value of the energy, and the replacement of n by $n_0 + \delta n - \delta\epsilon\, \partial n_0/\partial\epsilon_0$.

From these considerations, it is obvious that this result does not depend on the particular form of the collision integral selected by us, and also holds for collisions of electrons with phonons, electrons with electrons, etc. In all cases, the difference from the ordinary theory of a Fermi gas reduces to the fact that we have $\delta n - \delta\epsilon \times \partial n_0/\partial\epsilon_0$ in place of δn in the collision integral.

[1] V. L. Ginzburg and G. P. Motulevich, Usp. Fiz. Nauk **55**, 460 (1955); Fortschr. d. Phys. **3**, 309 (1955).

[2] V. P. Silin, J. Exptl. Theoret. Phys. (U.S.S.R.) **33**, 1282 (1957), Soviet Phys. JETP **6**, 985 (1958).

[3] M. I. Kaganov and V. V. Slezov, J. Exptl. Theoret. Phys. (U.S.S.R.) **32**, 1496 (1957), Soviet Phys. JETP **5**, 1216 (1957).

[4] R. B. Dingle, Physica **19**, 311, 348, 729 (1953).

[5] L. D. Landau, J. Exptl. Theoret. Phys. (U.S.S.R.) **30**, 1058 (1956), Soviet Phys. JETP **3**, 920 (1957).

[6] V. P. Silin, J. Exptl. Theoret. Phys. (U.S.S.R.) **33**, 495 (1957), Soviet Phys. JETP **6**, 387 (1958).

[7] V. P. Silin, Физика металлов и металловедение (Physics of Metals and Metal Research) (1958) (in press).

[8] K. Fuchs, Proc. Cambr. Phil. Soc. **34**, 100 (1938).

[9] A. B. Pippard, Proc. Roy. Soc. (London) **A224**, 273 (1954); M. I. Kaganov and M. Ia. Azbel', Dokl. Akad. Nauk SSSR **102**, 49 (1955).

[10] T. Holstein, Phys. Rev. **96**, 535 (1954); R. N. Gurzhi, J. Exptl. Theoret. Phys. (U.S.S.R.) **33**, 660 (1957); Soviet Phys. JETP **6**, 506 (1958).

Translated by R. T. Beyer
126

with the accuracy considered by us, where $Z_x^{(0)}$, $R_x^{(a)}$, $R_{xy}^{(a)}$ are defined respectively by Eqs. (16), (23), and (25), while $R_x^{(H)}$ and $R_{xy}^{(H)}$ can easily be obtained from Eqs. (8), (11), and (19).

5. The difference of Eqs. (8), (13), (23), and (25) from the corresponding relations of the research of Kaganov and Slezov[9] is due to the function Φ. It is natural to attempt to make clear what evidence can be obtained on this function from experiments in the infrared region. However, we can point out at once that the results which we have obtained above are always complicated by the anisotropies of the metal. Therefore, without a knowledge of the Fermi surface, it is difficult to obtain information on the function Φ from experiments in the infrared region. Evidently, for the determination of effects which distinguish the conduction electrons from the Fermi gas, we must first determine the form of the Fermi surface with the aid of experiments in the radio-frequency range for the case of a sharply defined anomalous skin effect.[9]

The results obtained above are greatly simplified when the metal can be regarded as isotropic.[1] The latter is quite natural for polycrystalline samples. We shall consider this case in more detail below. Under such an assumption, we have, in place of Eq. (8),

$$\operatorname{Re}\varepsilon' = -\frac{4\pi e^2 N}{m\omega^2}, \quad N = \frac{8\pi p_0^2 v_0 m}{3(2\pi\hbar)^3}\{1 + p_0^2\int d\Omega \cos\chi F(\cos\chi)\};$$

$$F = [2/(2\pi\hbar)^3]\,\Phi(\mathbf{p}, \mathbf{p}')/v_0, \qquad (8'')$$

where p_0 and v_0 are the momentum and velocity of the electron on the Fermi surface, m = mass of the free electron. Such an expression for the real part of the complex dielectric constant was obtained in Ref. 2. The non-diagonal elements of the tensor of the real part of the complex dielectric constant tensor in the approximation under consideration are equal to zero. In the absence of a magnetic field, the imaginary part ϵ', which is defined by Eq. (19), is also diagonal and is equal to

$$\operatorname{Im}\varepsilon' = \frac{8\pi e^2 p_0^2}{3\omega^3(2\pi\hbar)^3}\int\frac{d\Omega}{v}\mathbf{V}J(\mathbf{V}). \qquad (19')$$

We note that formulas which contain the collision integral are valid even in the quantum case,[10] in which the frequency of the light is comparable to, or becomes larger than $kT/\hbar$. In this case, only the value of the collision integral changes.

In the isotropic case, only the nondiagonal terms arise, as a result of the constant magnetic field. Directing H_0 along the z axis, we have

$$\operatorname{Im}\varepsilon'_{xy} = -\operatorname{Im}\varepsilon'_{yx}$$

$$= -\frac{4\pi}{\omega}\frac{8\pi e^2 p_0^2 v_0}{3(2\pi\hbar)^3\omega^2}\frac{ev_0H_0}{p_0}\left\{1 + p_0^2\int d\Omega\cos\chi F\right\}^2. \qquad (19'')$$

The presence of a magnetic field has no effect on the other components.

Finally, for an isotropic metal, Eq. (25) vanishes, while (23) takes on the form

$$R_x = \frac{3\pi}{4}\frac{v_0}{c^2}\left\{1 + p_0^2\int d\Omega\cos\chi F(\cos\chi)\right\}. \qquad (23')$$

As was shown in Ref. 2, the relation (8), along with data on the electronic heat capacity of the metal and the results of experiments in the radio-frequency region, in the case of a sharply defined anomalous skin effect, permits us to establish the value of $p_0^2\int d\Omega\cos\chi F(\cos\chi)$. In other words, the possibility is shown of determining the first coefficient in the expansion of $F(\cos\chi)$ in Legendre polynomials. Equation (23) points up the possibility of a similar estimate of this coefficient. Of course, it should be observed that all such estimates are essentially connected with the possibility of using the isotropic model of the metal, and this in each case must be done with caution.[2] We note that in the collision with the surface, the part (2) of the electrons can be scattered specularly. In this case, the expression obtained above for $R^{(a)}$ must be changed by a factor of $(1 - q)$.

In conclusion, I am pleased to express my thanks to L. D. Landau for useful discussions of the problem, explained in the Appendix.

APPENDIX

In order to clarify the form of the collision integral in the theory of a Fermi liquid for the nonequilibrium state, we consider as an example collisions with impurities. In this case, the collision integral has the form

$$I(n) = \int W(n; \mathbf{p}, \mathbf{p}')\{n(\mathbf{p}')[1 - n(\mathbf{p})]$$
$$- n(\mathbf{p})[1 - n(\mathbf{p}')]\}\,\delta\{\varepsilon(\mathbf{p}) - \varepsilon(\mathbf{p}')\}\,d\mathbf{p}'.$$

Taking (4) into account, we can represent $I(n)$ in the form of a sum $I_1 + I_2$, where

$$I_1 = \int W(n_0; \mathbf{p}, \mathbf{p}')\{\delta n(\mathbf{p}) - \delta n(\mathbf{p}')\}\,\delta\{\varepsilon_0(\mathbf{p}) - \varepsilon_0(\mathbf{p}')\}\,d\mathbf{p}',$$

$$I_2 = \int W(n_0; \mathbf{p}, \mathbf{p}')\{n_0(\mathbf{p}') - n_0(\mathbf{p})\}\,\delta\{\varepsilon_0(\mathbf{p})$$
$$+ \delta\varepsilon(\mathbf{p}) - \varepsilon_0(\mathbf{p}') - \delta\varepsilon(\mathbf{p}')\}d\mathbf{p}'.$$

Here, I_1 is a quantity which coincides with the

collision integral of ordinary theory.

Further, it is convenient to transform I_2 somewhat. In this case, we take it into consideration that

$$n_0(\varepsilon_0) \approx n_0(\varepsilon_0 + \delta\varepsilon) - \delta\varepsilon \partial n_0 / \partial \varepsilon_0.$$

Thanks to the fact that in the law of conservation of energy, $\epsilon = \epsilon_0 + \delta\epsilon$, terms containing only $n_0(\epsilon)$ fall out, and there are left terms proportional to $\delta\epsilon$. For the remaining small terms, the difference between ϵ and ϵ_0 in the conservation law is no longer significant. Therefore,

$$I(n_0 + \delta n) = \int W(n_0; \mathbf{p}, \mathbf{p}') \left\{ \left(\delta n' - \delta\varepsilon' \frac{\partial n_0}{\partial \varepsilon_0'} \right) - \left(\delta n - \delta\varepsilon \frac{\partial n_0}{\partial \varepsilon_0} \right) \right\} \delta(\varepsilon_0 - \varepsilon_0') d\mathbf{p}'.$$

Thus it can be shown that the collision integral for states which differ only slightly from the equilibrium can be obtained by the substitution in the conservation law of the equilibrium value of the energy, and the replacement of n by $n_0 + \delta n - \delta\epsilon\, \partial n_0/\partial\epsilon_0$.

From these considerations, it is obvious that this result does not depend on the particular form of the collision integral selected by us, and also holds for collisions of electrons with phonons, electrons with electrons, etc. In all cases, the difference from the ordinary theory of a Fermi gas reduces to the fact that we have $\delta n - \delta\epsilon \times \partial n_0/\partial\epsilon_0$ in place of δn in the collision integral.

[1] V. L. Ginzburg and G. P. Motulevich, Usp. Fiz. Nauk **55**, 460 (1955); Fortschr. d. Phys. **3**, 309 (1955).

[2] V. P. Silin, J. Exptl. Theoret. Phys. (U.S.S.R.) **33**, 1282 (1957), Soviet Phys. JETP **6**, 985 (1958).

[3] M. I. Kaganov and V. V. Slezov, J. Exptl. Theoret. Phys. (U.S.S.R.) **32**, 1496 (1957), Soviet Phys. JETP **5**, 1216 (1957).

[4] R. B. Dingle, Physica **19**, 311, 348, 729 (1953).

[5] L. D. Landau, J. Exptl. Theoret. Phys. (U.S.S.R.) **30**, 1058 (1956), Soviet Phys. JETP **3**, 920 (1957).

[6] V. P. Silin, J. Exptl. Theoret. Phys. (U.S.S.R.) **33**, 495 (1957), Soviet Phys. JETP **6**, 387 (1958).

[7] V. P. Silin, Физика металлов и металловедение (Physics of Metals and Metal Research) (1958) (in press).

[8] K. Fuchs, Proc. Cambr. Phil. Soc. **34**, 100 (1938).

[9] A. B. Pippard, Proc. Roy. Soc. (London) **A224**, 273 (1954); M. I. Kaganov and M. Ia. Azbel', Dokl. Akad. Nauk SSSR **102**, 49 (1955).

[10] T. Holstein, Phys. Rev. **96**, 535 (1954); R. N. Gurzhi, J. Exptl. Theoret. Phys. (U.S.S.R.) **33**, 660 (1957); Soviet Phys. JETP **6**, 506 (1958).

Translated by R. T. Beyer
126

SYMMETRY OF THE COORDINATE WAVE FUNCTION OF A MANY-ELECTRON SYSTEM

Iu. N. DEMKOV

Leningrad State University

Submitted to JETP editor October 14, 1957

J. Exptl. Theoret. Phys. (U.S.S.R.) 34, 714-716 (March, 1958)

The relation between the two main methods for constructing the wave function of a many-electron system, the group-theoretical method and Fock's method, is considered. It is shown that the coordinate function obtained from the first method satisfies Fock's condition of cyclic symmetry.

ASSUME that the coordinate and spin variables separate in the energy operator of an n-electron system and, in addition, that the spin part H_S of the energy operator is spherically symmetric:

$$H = H_0(1, 2, \ldots, n) + H_s(\sigma_1, \sigma_2, \ldots, \sigma_n).$$

Then we construct a total wave function, which satisfies the Pauli principle and is an eigenfunction of the square of the total spin S^2, if we know the coordinate eigenfunction $\psi(1, 2, \ldots, n)$ of the operator H_0 and the spin eigenfunction $\chi(\sigma_1, \sigma_2, \ldots, \sigma_n)$ of the operator H_S. This construction can be done either by using the methods of group theory[1] or by the method proposed by Fock.[2] In both methods, both the coordinate and the spin functions must satisfy definite symmetry conditions with respect to permutation of their arguments. It is obvious that the two methods of construction must be equivalent, so there should be a connection between the two kinds of symmetry conditions. We shall treat this relation.

It follows from group theory that the symmetry of the coordinate wave function must be defined by a Young tableau having two columns (see figure). This means that a function of the required symmetry can be obtained from an arbitrary function if we first symmetrize with respect to the pairs of variables in each row of the tableau, i.e., $(1, k+1)$, $(2, k+2)$, $\ldots$, $(k, 2k)$, and then antisymmetrize with respect to the columns, i.e., with respect to the variables $(1, 2, \ldots, k)$ and $(k+1, k+2, \ldots, n)$. If we denote the symmetrizer and antisymmetrizer in the set of variables $(\alpha_1, \alpha_2, \ldots, \alpha_m)$ by $S(\alpha_1, \alpha_2, \ldots, \alpha_m)$ and $A(\alpha_1, \alpha_2, \ldots, \alpha_m)$ respectively, the Young operator can be written as

$$J(1, 2, \ldots, k \mid k+1, k+2, \ldots, n) = A(1, 2, \ldots, k) \times A(k+1, k+2, \ldots, n) \sum_{i=1}^{k} S(i, k+i) = A_1 A_2 S.$$

(Obviously the sequence of variables in the Young tableau may be different; we would then get different operators; the number of linearly independent operators determines the dimensionality of the representation of the symmetric group which is related to the given Young pattern.) The symmetry of the corresponding spin function must be determined by the transposed Young tableau. It is obvious that $k \leq n/2$. The total spin is $n/2 - k$.

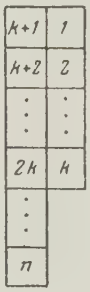

In Fock's method, the coordinate wave function must satisfy the following three conditions: (a) antisymmetry in the variables $1, 2, \ldots, k$, (b) antisymmetry in the variables $k+1, k+2, \ldots, n$, (c) cyclic symmetry: the operator

$$\Phi = 1 - P_{k,k+1} - P_{k,k+2} - \ldots - P_{k,n},$$

must annihilate the coordinate wave function. P_{ij} is the operator for transposition of the variables i and j.

A function which is symmetrized according to the Young scheme obviously satisfies conditions (a) and (b). We shall show that such a function also satisfies the cyclic symmetry condition (c), i.e., that the identity

$$\Phi J = 0.$$

is satisfied. We shall verify this by showing that all the terms in the product $\Phi A_1 A_2 S$ cancel in pairs. Consider one of the $k!(n-k)!$ terms in

the product A_1A_2. It can be written as a permutation

$$\pm\begin{pmatrix} 1, 2, \ldots, k & | & k+1, k+2, \ldots, n \\ \alpha_1, \alpha_2, \ldots, \alpha_k & | & \alpha_{k+1}, \alpha_{k+2}, \ldots, \alpha_n \end{pmatrix},$$

where $\alpha_1, \alpha_2, \ldots, \alpha_k$ is a permutation of the sequence 1, 2, ..., k; $\alpha_{k+1}, \alpha_{k+2}, \ldots, \alpha_n$ is a permutation of the sequence k + 1, k + 2, ..., n; the sign is determined by the parity of the permutation.

We now apply to this term one of the transpositions in the operator Φ. The following identity is easily shown:

$$\begin{pmatrix} k, & a \\ a, & k \end{pmatrix}\begin{pmatrix} \ldots b \ldots & | & \ldots b+k \ldots d \ldots \\ \ldots k \ldots & | & \ldots \quad c \quad \ldots a \ldots \end{pmatrix}$$
$$= \begin{pmatrix} k, c \\ c, k \end{pmatrix}\begin{pmatrix} \ldots b \ldots & | & \ldots b+k \ldots d \ldots \\ \ldots k \ldots & | & \ldots \quad a \quad \ldots c \ldots \end{pmatrix}\begin{pmatrix} b, & b+k \\ b+k, & b \end{pmatrix};$$

where

$$1 \leqslant b \leqslant k,\ k+1 \leqslant a \leqslant n,\ k+1 \leqslant c \leqslant n,\ k+1 \leqslant d \leqslant n.$$

The second factors on both sides of the identity are contained in the product A_1A_2, and differ only in a single transposition, so that they appear in the product with opposite signs. The first factors on each side are contained in the operator Φ. Finally, the operator

$$P_{b,\ b+k} = \begin{pmatrix} b, & b+k \\ b+k, & b \end{pmatrix},$$

does not change the operator S. It follows that the corresponding terms in the product ΦA_1A_2S cancel against one another.

A special case occurs when a = c, and consequently b + k = d. Then we can use the identity

$$\begin{pmatrix} k, a \\ a, k \end{pmatrix}\begin{pmatrix} \ldots b \ldots & | & \ldots b+k \ldots \\ \ldots k \ldots & | & \ldots \quad a \quad \ldots \end{pmatrix}$$
$$= \begin{pmatrix} \ldots b \ldots & | & \ldots b+k \ldots \\ \ldots k \ldots & | & \ldots \quad a \quad \ldots \end{pmatrix}\begin{pmatrix} b, & b+k \\ b+k, & b \end{pmatrix},$$

from which it follows that such a term in the product cancels against the product of the first term in the operator Φ (the identity operator) with the same term in the product A_1A_2. We have thus proven our assertion. So every function which is symmetrized by using the Young operator satisfies Fock's conditions.

The reverse relation is obviously more complicated since a function which satisfies conditions (a), (b), and (c) corresponds in general to a set of Young tableaus with all possible permutations of the variables k + 1, k + 2, ..., n. Any linear combination of the corresponding operators (among which there may be a linear dependence), when acting on an arbitrary function, gives a function which satisfies Fock's three conditions.

In comparing the two methods we note that symmetrization by means of the Young operator is convenient when we have to construct a function with particular symmetry properties from some unsymmetric function. But if the function is already known, it is easier to check whether or not it satisfies Fock's symmetry conditions than to make the analogous check using the Young operator. Fock's conditions do not give us a specific recipe for constructing a function which satisfies them; recipes for various special cases have been given.[2,3] From our proof it follows that the general recipe is to symmetrize by using the Young operator.

Thus the two methods, which are basically equivalent, supplement one another in various cases.

The methods for constructing the total wave function from the coordinate and spin functions using the method of Fock or the group theory method are also different. The relation between these methods requires further consideration.

In conclusion I thank G. F. Drukarev; the present note was written as a result of discussions with him about this class of problems.

[1] H. Weyl, Theory of Groups and Quantum Mechanics (Dover). E. Wigner, Gruppentheorie und ihre Anwendung auf die Quantenmechanik der Atomspektren, Braunschweig, 1931. L. D. Landau and E. M. Lifshitz, Квантовая механика (Quantum Mechanics), Vol. 1, §61, Gostekhizdat, 1948.

[2] V. A. Fock, J. Exptl. Theoret. Phys. (U.S.S.R.) **10**, 961 (1940).

[3] I. V. Abrenkov, Вестн. ЛГУ (Bulletin, Leningrad State University) No. 10, 43 (1956). G. F. Drukarev, J. Exptl. Theoret. Phys. (U.S.S.R.) **31**, 288 (1956), Soviet Phys. JETP **4**, 309 (1957).

Translated by M. Hamermesh
134

A GROUP-THEORETICAL CONSIDERATION OF THE BASIS OF RELATIVISTIC QUANTUM MECHANICS. IV. SPACE REFLECTIONS IN QUANTUM THEORY

Iu. M. SHIROKOV

Moscow State University

Submitted to JETP editor October 22, 1957

J. Exptl. Theoret. Phys. (U.S.S.R.) 34, 717-724 (March, 1958)

The problem of invariance of relativistic quantum theory with respect to space reflections is investigated from the most general group-theoretical point of view, without the use of a specific form of the equations of motion. A complete classification is obtained for all the unitary and nonunitary irreducible representations of the improper inhomogeneous Lorentz group. In treating the problem of distinguishing representations according to parity, essential use is made of the concept of a universal covering group, which makes possible a rigorous proof of the previously mentioned[2] impossibility of simultaneous existence of spinor particles whose wave functions transform according to representations of different types.

An analysis is made of the experiment of Wu,[3] which is currently regarded as a proof of nonconservation of parity in weak interactions.[4] From the group-theoretical point of view developed here, experiments like those of Wu and Lederman[5] do not contradict parity conservation but merely conservation of charge conjugation, and consequently prove the electric charge is a pseudoscalar and that the electromagnetic potential is a pseudovector.

1. THE RELATION BETWEEN REPRESENTATIONS OF THE PROPER AND IMPROPER LORENTZ GROUPS

IN the preceding papers I—III of this series,* we found all the irreducible representations of the inhomogeneous Lorentz group, i.e., all the possible laws of transformation under four-dimensional rotations and displacements for the wave functions of a relativistic quantum theory. The purpose of the present paper is to find all the irreducible representations of the improper group, which includes space reflections. The transition to the improper inhomogeneous Lorentz group G_S is accomplished by adjoining to the elements of the proper group G the inversion operation I_S, which satisfies the relations (I.34):

$$[I_s, p_0]_- = 0,\ [I_s, \mathbf{p}]_+ = 0,\ [I_s, \mathbf{M}]_- = 0,\ [I_s, \mathbf{N}]_+ = 0. \quad (1)$$

The first of these relations is a statement of the law of conservation of parity. Like the law of conservation of linear momentum, it is based on the fact that space and time variables are independent. According to (1), inversion changes the sign of the operators $\mathbf{p}$, $\mathbf{N}$ and leaves $\mathbf{M}$ and p_0 unchanged,

$$\mathbf{p} \to -\mathbf{p},\quad p_0 \to p_0,\ \mathbf{M} \to \mathbf{M},\quad \mathbf{N} \to -\mathbf{N}. \quad (2)$$

It is easy to show that if the operators $\mathbf{p}$, p_0, $\mathbf{M}$, $\mathbf{N}$ form a representation P of the group G, the operators $-\mathbf{p}$, p_0, $\mathbf{M}$, $-\mathbf{N}$ also satisfy the commutation laws (I.33) and consequently also form a representation of the proper group, which we shall denote by $I_S P$.

If the representation $I_S P$ is equivalent to P, then by definition there exists a non-degenerate matrix I_{S0} such that

$$I_{s0}^{-1}\mathbf{M}I_{s0} = \mathbf{M},\quad I_{s0}^{-1}p_0 I_{s0} = p_0,$$

$$I_{s0}^{-1}\mathbf{N}I_{s0} = -\mathbf{N},\quad I_{s0}^{-1}\mathbf{p}I_{s0} = -\mathbf{p},$$

or,

$$[\mathbf{M}, I_{s0}]_- = 0,\ [p_0, I_{s0}]_- = 0,\ [\mathbf{N}, I_{s0}]_+ = 0,\ [\mathbf{p}, I_{s0}]_+ = 0. \quad (3)$$

Comparison of (1) and (3) shows that in this case the representation P is also a representation of the improper group G_S, in which the inversion operator is, except for a numerical factor λ_S, equal to the operator I_{S0} in (3),

$$P_s = P,\ I_s = \lambda_s I_{s0}. \quad (4)$$

But if the representation P is not equivalent to $I_S P$, then it can no longer be a representation of

*Notations introduced without explanation are the same as in the preceding papers of this series,[1] which are cited in the text as I, II, III. References like (I.33) refer to the corresponding formula in I.

the improper group G_S. In this case the representation P_S of the group G will be the direct sum of the representations P and $I_S P$:

$$P_s = P + I_s P. \tag{5}$$

The dimension of P_S is twice that of P, and the operators for the angular momentum $M^S_{\mu\nu}$, the momentum p^S_λ and the inversion I_S will have the form

$$M^s = \begin{pmatrix} M & 0 \\ 0 & M \end{pmatrix}, \quad p_0^s = \begin{pmatrix} p_0 & 0 \\ 0 & p_0 \end{pmatrix}, \quad p^s = \begin{pmatrix} p & 0 \\ 0 & -p \end{pmatrix},$$

$$N^s = \begin{pmatrix} N & 0 \\ 0 & -N \end{pmatrix}; \tag{6}$$

$$I_s = \mu_s \begin{pmatrix} 0 & I \\ I & 0 \end{pmatrix} \tag{7}$$

P_S is irreducible with respect to G_S if P is irreducible with respect to G and is not equivalent to $I_S P$. Thus, for each irreducible representation P of the proper group G, either P is equivalent to $I_S P$ and constitutes an irreducible representation of the group G_S; or P is not equivalent to $I_S P$, and an irreducible representation of G_S is given by the direct sum $P + I_S P$. Later we shall show that the converse theorem is also true, i.e., any representation which is irreducible with respect to G_S is either irreducible with respect to G or is a direct sum of the type of (5) of two irreducible representations.

2. INVARIANTS OF THE IMPROPER INHOMOGENEOUS LORENTZ GROUP

From (I.34) and (I.42) it follows that I_S^2 and the fundamental invariants p_μ^2 and Γ_σ^2 of the improper group G_S. In II and III it was shown that for certain classes of representations there are additional invariants, which were discussed in Sec. 12 of I. These were the operator for the sign of the energy $S_H = p_0/|p_0|$ (II, Sec. 3), the operator for the sign of the fourth component of the intrinsic angular momentum $S_\Gamma = \Gamma_0/|\Gamma_0|$ (II, Sec. 4), the operator Σ of (III.16), (III.17), and finally the operators

$$F = {}^1/_2 M_{\mu\nu}^2, \quad W = (1/4\pi i)\, \varepsilon_{\mu\nu\lambda\sigma} M_{\mu\nu} M_{\lambda\sigma}$$

of (III.24), (III.25) for the class O_0. Of these operators, S_H, Σ, and F are scalars and commute with I_S, and consequently if they are invariants with respect to G, they are invariants with respect to G_S. The pseudoscalar operators S_Γ and W anticommute with I_S, and can be invariant relative to G without being invariant relative to G_S. However, if in a certain representation one of the pseudoscalar operators is invariant with respect to G, then its square is invariant with respect to G_S. We should also note that, according to the tables in II, III, the operators S_Γ, W are not simultaneously invariant in any of the irreducible representations of G.

3. STRUCTURE OF THE IRREDUCIBLE REPRESENTATIONS OF THE IMPROPER INHOMOGENEOUS LORENTZ GROUP

The irreducible representations of the proper group G, which were enumerated in II and III, can be divided into the following four types:

(1) $p_\mu \neq 0$, $W \neq \text{inv}$, $S_\Gamma \neq \text{inv}$,
(2) $p_\mu \neq 0$, $W \neq \text{inv}$, $S_\Gamma = \text{inv}$,
(3) $p_\mu = 0$, $W = \text{inv} \neq 0$,
(4) $p_\mu = 0$, $W = 0$.

In the first (fourth) case, there are no non-zero pseudoscalar operators in the representation which are invariant with respect to G and not with respect to G_S. In representations of this type, the operators $M_{\mu\nu}$, p_λ coincide with the corresponding operators in the representation of G, while the inversion operator has the form (4). In the second (third) case, the group contains one pseudoscalar operator $S_\Gamma(W)$, which is invariant with respect to G and not with respect to G_S. Then the operator $S^2_\Gamma(W^2)$ is invariant relative to G_S, and in an irreducible representation has a fixed numerical value $S^2_{\Gamma_0}(W_0^2)$. Thus a representation which is irreducible with respect to G_S can contain only two different irreducible representations of the group G, which differ in the values $\pm S_{\Gamma_0}(\pm W_0)$ of the pseudoscalar operator $S_\Gamma(W)$. The operator $S_\Gamma(W)$ changes sign under inversion, and the representation $P_\Gamma(P_W)$ of the group G changes into the representation $P_{-\Gamma}(P_{-W})$ which coincides with $I_S P_\Gamma(I_S P_W)$ to within an equivalence transformation I_{S0}. In accordance with (5) — (7), in this case the representation which is irreducible with respect to G_S is the direct sum

$$P_s = P_\Gamma + P_{-\Gamma} (P_s = P_{+W} + P_{-W}), \tag{8}$$

while the operators $M_{\mu\nu}$, p_λ, I_S will have the form

$$M_{\mu\nu} = \begin{pmatrix} M^\Gamma_{\mu\nu} & 0 \\ 0 & M^{-\Gamma}_{\mu\nu} \end{pmatrix}, \quad p_\mu = \begin{pmatrix} p^\Gamma_\mu & 0 \\ 0 & p^{-\Gamma}_\mu \end{pmatrix}, \tag{9}$$

$$I_s = \mu_s \begin{pmatrix} 0 & I \\ I & 0 \end{pmatrix}, \tag{10}$$

and correspondingly for P_W. In (10), μ_S is a number and I_{S0} is the equivalence transformation connecting $P_{-\Gamma}$ with $I_S P_\Gamma$ (P_{-W} with $I_S P_W$).

We have thus proved the assertion made at the end of Sec. 1 that any irreducible representation of G_S is either irreducible with respect to G or is the direct sum of two irreducible representations.

Let us now construct explicitly the operator I_{S0} of (4) or (10). It is not difficult to see that for representations in the classes P_m, P_Π, P_0, this operator is the operator which changes the sign of the momentum:

$$I_{s0}\Omega(p) = \Omega(-p) \quad \text{for } P_m, P_\Pi, P_0. \tag{11}$$

In the class O_0, the basic functions of the irreducible representation $S^c_{k_0}$ have the form Ω^ν_k, where $\nu = -k, -k+1, \ldots, k$; $k = k_0, k_0+1, \ldots$ The angular momentum operator is diagonal with respect to k:

$$M^{\nu\nu'}_{kk'} = \delta_{kk'} M^{\nu\nu'}_k, \tag{12}$$

while the operator N has the form (cf., for example, Ref. 6)

$$N^{\nu\nu'}_{kk'} = A^{\nu\nu'}\delta_{kk'-1} + WB^{\nu\nu'}\delta_{kk'} + C^{\nu\nu'}\delta_{kk'+1}, \tag{13}$$

where $A^{\nu\nu'}$, $B^{\nu\nu'}$, $C^{\nu\nu'}$ depend on F, W^2, k, ν, ν', (but not on W!). From (12) and (13) it follows that for $W = 0$ the operator

$$(I_{s0})_{kk'} = \delta_{kk'}(-1)^{k-k'} \tag{14}$$

commutes with M and anticommutes with N, i.e., can be used as the operator I_{S0} in (4). For $W \neq 0$, the operator (14) is also suitable for use as I_{S0}, but now of course, for (10). This is easily verified using (I.34), (12) and (13). In order to complete the construction of the irreducible representations of the group G_S, there remains for us only to determine the possible values of the factor λ_S in (4) and (10). However, for a rigorous treatment of this question, a more detailed investigation of the double-valued representations is necessary.

4. DOUBLE-VALUED REPRESENTATIONS AND UNIVERSAL COVERING GROUP

The double-valued representations are not representations in the strict sense of the word. It is, however, known that one can give a group for which these representations become single-valued (i.e., true) representations. This group is the universal covering group of the inhomogeneous Lorentz group. It is essential to note that the universal covering group is uniquely determined by the topological properties of the corresponding continuous group and is locally isomorphic to it (cf., for example, Ref. 7). The transition to the universal covering group is accomplished by adjoining to the transformations of the group G an element $I_{2\pi}$ of rotation through an angle 2π, which commutes with all the elements of the group and satisfies the relations

$$I^2_{2\pi} = I, \quad \lim I_\varphi = I_{2\pi} \quad \text{for } \varphi \to 2\pi \tag{15}$$

for one of the spacial rotations. Since the spinor representations are true representations not of the Lorentz group G, but of its universal covering group which we shall denote by $\tilde{G}$, it is the latter group with respect to which the equations and wave functions of quantum theory are covariant. The element $I_{2\pi}$ is an invariant of the group $\tilde{G}$. It is equal to 1 for single-valued, and -1 for double-valued representations.*

In accordance with our previous remarks, the operation of inversion should be introduced into the group $\tilde{G}$. Twofold application of the inversion brings the system back into its original state, which can be interpreted as a rotation through either 0 or 2π. In the first case the square of the inversion operator is unity:

$$I_s^2 = I, \tag{16}$$

while in the second,

$$I_s^2 = I_{2\pi}. \tag{17}$$

We emphasize that the relations (16), (17) do not define different representations of the same group, but rather different groups, which we denote by $\tilde{G}_S$ and $\tilde{G}'_S$ respectively. In other words, the relations (16), (17) give two types of structures of the space, and not of the individual particles.

5. THE SEPARATION OF REPRESENTATIONS OF THE GROUPS G_S, G'_S ACCORDING TO PARITY

In this section, we shall determine the possible values of the factors λ_S, μ_S in (4), (11) and thus complete the classification of the irreducible representations of the improper groups $\tilde{G}_S$, $\tilde{G}'_S$. For single-valued (unprimed) representations P, two-fold application of the inversion gives the identity

$$I_s^2 = \lambda_s^2 = I. \tag{18}$$

so that

$$\lambda_s = \pm 1. \tag{19}$$

*We shall continue to use the usual terms "single-valued" and "double-valued" representations, even though all representations are single-valued with respect to $\tilde{G}$.

The representations corresponding to $\lambda_S = 1$ and $\lambda_S = -1$ are not equivalent to one another if (4) holds for them. They are said to be even and odd, respectively, and will be denoted by $+P$ and $-P$. The occurrence of the parity assignment doubles the number of possible single-valued irreducible representations of each of the groups $\tilde{G}_S$, $\tilde{G}'_S$ for the case when (4) applies. This is the case for the representations in the classes

$$P^s_{\pm m},\ P^a_{\Pi},\ P^s_{\Pi},\ P^b_{\Pi},\ P^{\alpha}_{\Pi},\ P^c_{\pm 0},\ P^{-c}_{\pm 0},\ P^{\alpha}_{\pm 0}$$

and those representations of the class O_0 for which $W = 0$ (this set includes, in particular, four-dimensional vectors and tensors).

The double-valued representations of the groups $\tilde{G}_S$ and $\tilde{G}'_S$ differ from one another. For the double-valued representations of $\tilde{G}_S$,

$$I_s^2 = \lambda_s^2 = 1,\ \lambda_s = \pm 1, \tag{20}$$

while for $\tilde{G}'_S$,

$$I_s^2 = \lambda_s^2 = I_{2\pi} = -1,\ \lambda = \pm i \tag{21}$$

The double-valued representations of the group $\tilde{G}_S$ with $\lambda_S = 1$ and $\lambda_S = -1$ have opposite parity and are not equivalent to one another. For example, the direct product of two representations with $\lambda_S = 1$ is different from the product of a representation with $\lambda_S = 1$ and a representation with $\lambda_S = -1$. At the same time, a well-defined parity cannot be assigned to either of the representations, since for each of them there exist two operators I_S and $I_S I_{2\pi}$, one of which multiplies the wave function by 1, the other by -1, and each of them has an equal right to be regarded as the inversion operator. Therefore, for the two-valued representations we can speak only of mutual or relative parity. As pointed out in Ref. 8, this situation was first noted by Landau. An analogous situation occurs for the double-valued representations of the group $\tilde{G}'_S$ with $\lambda_S = i$ and $\lambda_S = -i$, which we shall denote by $+iP'$ and $-iP'$, respectively. Since the representations $\pm P'$ and $\pm iP'$ refer to different groups, it is meaningless to talk of direct products of the type $\pm P' \times \pm iP'$. This means that in real space only those physical systems can occur whose wave functions transform according to double-valued representations of the type $\pm P'$ alone, or of the type $\pm iP'$ alone. Arguments concerning the impossibility of simultaneous existence of spinors which are multiplied by ± 1 and by $\pm i$ under inversion have been given previously by Shapiro.[2] The use of the concept of the universal covering group enables us to formulate these arguments as a rigorous proof. Another difference between our treatment and that of, say, Shapiro, is that in this paper we investigate the irreducible representations of the group G_S rather than the Dirac equation. Thus the results obtained are applicable to particles of arbitrary spin.

We emphasize that a distinction according to parity exists only for representations which satisfy (4). When condition (10) is satisfied, the concept of parity of the representation cannot be introduced, since the representations corresponding to $\mu_S = 1$ and $\mu_S = -1$ are related by the equivalence transformation $\begin{pmatrix} 0 & I \\ I & 0 \end{pmatrix}$. This is the situation for the representations

$$P^{\Sigma}_{\pm 0} = P^{+\Sigma}_{\pm 0} + P^{-\Sigma}_{\pm 0},\ P^{l}_{\Pi} = P^{+l}_{\Pi} + P^{-l}_{\Pi} \tag{22}$$

and those representations of the class O_0 which have $W \neq 0$ (and which include the Dirac bispinor as a special case).

For completeness of our discussion, we remark that in both $\tilde{G}_S$ and $\tilde{G}'_S$ there is still one nontrivial one-dimensional irreducible representation, the representation of the factor group of G_S with respect to the subgroup G. For this representation, which we denote by J_S:

$$M_{\mu\nu} = 0,\ p_\lambda = 0,\ I_s = -1.$$

It is easily shown that

$$-P = J_s \times (+P),\ -P' = J_s \times (+P'),$$
$$-iP' = J_s \times (+iP'). \tag{23}$$

6. INTERNAL PARITY OF ELEMENTARY PARTICLES

So far, we have treated parity defined as the eigenvalue of the operator of inversion with respect to the coordinate origin. Such a definition is used in treating collisions and other similar processes, where the origin is chosen to be the center of inertia of the physical system. In addition to this, we can define for each individual particle an internal parity which is an invariant characteristic of the particle. The internal parity λ_S of a particle can be introduced by means of the relation

$$\lambda_s = I_s I_{s0}, \tag{24}$$

where I_S is the usual (external) parity, and I_{S0} is the operator for the Lorentz transformation which takes the 4-momentum $(\mathbf{p}, ip_0)$ into $(-\mathbf{p}, ip_0)$. For $\mathbf{p} = 0$, $I_{S0} = 1$ and the external parity coincides with the internal. Obviously if I_{S0} in (4) is chosen in the form of (11), the factor λ_S in (4) will determine the internal parity. The concept of internal parity exists only for particles with non-zero rest mass, which are described by the

representations P^{s}_{m}, P'^{s}_{m} satisfying (4). Particles with zero rest mass do not possess an internal parity, since their wave functions transform according to the representations P^{Σ}_{+0}, P'^{Σ}_{+0}, which satisfy (10) and not (4). Thus, for example, it is meaningless to speak of a photon as being a vector or pseudovector particle.

7. CONSERVATION OF PARITY IN WEAK INTERACTIONS

In pseudo-Euclidean space-time, the inversion and time displacement transformations commute, so that it automatically follows that the inversion operator I_S commutes with the Hamiltonian, i.e., I_S is conserved. Consequently, since the experiments of Wu,[3] Lederman,[5] and others do not contradict the pseudo-Euclidean character of space-time,[4,9] they cannot contradict the law of conservation of parity, but merely show that the present definition of parity is incorrect. In fact, by definition parity is the eigenvalue of the inversion operator, which is used to transform the wave function when all three space coordinates are reflected. The inversion operator must therefore necessarily satisfy the commutation relations (1), which are simply a mathematical statement of the definition of parity.

For example, let us consider from this point of view the experiments on the β-decay of polarized nuclei which were proposed by Lee and Yang[4] and carried out by Wu.[3] In these experiments, the angular distribution of electrons emitted by Co^{60} nuclei polarized in a magnetic field was studied. An asymmetry of the cross section with respect to the plane perpendicular to the field was observed. It follows that the angular distribution must contain a term proportional to the scalar product of the magnetic field $\mathbf{H}$ and the electron momentum $\mathbf{p}$,

$$\sigma \sim a + b\mathbf{p}\cdot\mathbf{H}. \qquad (25)$$

We emphasize that the quantity which is directly observable is $\mathbf{p}\cdot\mathbf{H}$ and not $\mathbf{p}\cdot\mathbf{s}$, where $\mathbf{s}$ is the spin of the nucleus. Since the cross section is a scalar, the quantity $\mathbf{p}\cdot\mathbf{H}$ is also a scalar, but since according to (1) $\mathbf{p}$ is a vector, the magnetic field $\mathbf{H}$ must also be a vector. The results of Wu's experiment also essentially reduce to this assertion. Up to now the magnetic field was considered to be a pseudovector and not a vector. However, until the experiment of Wu there was no possibility of establishing the law of transformation of the electromagnetic field under inversion. In fact, in the Maxwell equations and the expression for the Lorentz force density f_μ:

$$\Box A_\mu = -4\pi j_\mu, \quad f_\mu = F_{\mu\nu} j_\nu$$

A_μ and j_μ can be regarded as being either vectors or pseudovectors. If we take the second point of view, charge should be treated as a pseudoscalar, the electric field as a pseudovector, etc. The question whether A_μ and j_μ are actually vectors or pseudovectors cannot be answered within the framework of electrodynamics, since it reduces to equations which are satisfied in both cases. The two possible laws of reflection are different for an operation which consists in the simultaneous change of sign of A_μ and j_μ, i.e., for charge conjugation. Thus the occurrence of two possible laws for inversion in electrodynamics is related to its invariance under charge conjugation. These statements remain valid in a quantum theory. The Wu experiment shows that weak interactions are not invariant with respect to charge conjugation, and that in electrodynamics the second of the possible choices for the reflection operation, which has been called combined inversion,[9] is the correct one, and that, in particular, charge is a pseudoscalar.

Since charge is a pseudoscalar, it anticommutes with the inversion. Therefore for charged particles the parity cannot have a definite value. However, because of the invariance of strong interactions with respect to charge conjugation, the product of true inversion and charge conjugation is an approximate integral of the motion of such particles. This operator commutes with the charge, and its eigenvalues, which are incorrectly called the parity, can have definite values for charged particles also.

To a considerable extent, these considerations have a methodological character. However, the bringing of clarity into the definition of the concept of parity is necessary at the present time because of the widespread use of the, from our point of view, extremely misleading term "nonconservation of parity in weak interactions," when we are actually dealing with the nonconservation of charge conjugation and the problem of correct choice of the inversion operation for specific equations of motion.

---

[1] Iu. M. Shirokov, J. Exptl. Theoret. Phys. (U.S.S.R.) **33**, 861, 1196, 1208 (1957), Soviet Phys. JETP **6**, 664, 919, 929 (1958).

[2] I. S. Shapiro, Usp. Fiz. Nauk **53**, 7 (1954). Wick, Wightman, and Wigner, Phys. Rev. **88**, 101 (1952).

[3] Wu, Ambler, Hayward, Hoppes, and Hudson, Phys. Rev. **105**, 1413 (1957).

[4] T. D. Lee and C. N. Yang, Phys. Rev. **104**, 254 (1956); **105**, 1671 (1957).

[5] Garwin, Lederman, and Weinrich, Phys. Rev. **105**, 1415 (1957).

[6] M. A. Naimark, Usp. Fiz. Nauk **9**, 19 (1954); Amer. Math. Soc. Transl. Ser. 2, Vol. 6, 1957.

[7] L. S. Pontriagin, Непрерывные группы (Continuous Groups), Gostekhizdat, 1954; cf. also the English translation of the first edition: Topological Groups, Princeton University Press, 1946.

[8] V. B. Berestetskii and I. Ia. Pomeranchuk, J. Exptl. Theoret. Phys. (U.S.S.R.) **19**, 756 (1949).

[9] L. D. Landau, J. Exptl. Theoret. Phys. (U.S.S.R.) **32**, 405 (1957), Soviet Phys. JETP **5**, 336 (1957); Nucl. Phys. **3**, 127 (1957).

Translated by M. Hamermesh
135

EQUALITY OF THE NUCLEON AND ANTINUCLEON TOTAL INTERACTION CROSS SECTION AT HIGH ENERGIES

I. Ia. POMERANCHUK

Submitted to JETP editor October 24, 1957

J. Exptl. Theoret. Phys. (U.S.S.R.) 34, 725-728 (March, 1958)

The dispersion relations are used to show that the total interaction cross sections are equal for particles and antiparticles at high energies.

FROM the dispersion relations for elastic scattering of nucleons through angle zero[1-3] one can establish that the total interaction cross sections for nucleons and antinucleons must be equal at sufficiently high energies.

To be specific, let us consider scattering of protons and antiprotons through the angle zero. The dispersion relations for the scattered amplitudies, averaged over spins, are of the form

$$D_+(E) = \frac{1}{2}\left(1+\frac{E}{M}\right)D_+(M) + \frac{1}{2}\left(1-\frac{E}{M}\right)D_-(M) + \frac{p^2}{4\pi^2}\int_M^\infty \frac{dE'}{p'}\left[\frac{\sigma_+(E')}{E'-E} + \frac{\sigma_-(E')}{E'+E}\right] + \frac{f^2}{\mu^2}\frac{p^2}{M-\mu^2/2M-E} + \frac{p^2}{4\pi^2}\int_0^M \frac{idE'}{p'}\left[\frac{\sigma_+(E')}{E'-E} + \frac{\sigma_-(E')}{E'+E}\right]; \quad (1)$$

$$D_-(E) = \frac{1}{2}\left(1+\frac{E}{M}\right)D_-(M) + \frac{1}{2}\left(1-\frac{E}{M}\right)D_+(M) + \frac{p^2}{4\pi^2}\int_M^\infty \frac{dE'}{p'}\left[\frac{\sigma_-(E')}{E'-E} + \frac{\sigma_+(E')}{E'+E}\right] + \frac{f^2}{\mu^2}\frac{p^2}{M-\mu^2/2M+E} + \frac{p^2}{4\pi^2}\int_0^M \frac{idE'}{p'}\left[\frac{\sigma_+(E')}{E'+E} + \frac{\sigma_-(E')}{E'-E}\right]. \quad (1')$$

Here $D_+(E)$ is the real part of the elastic scattered amplitude, averaged over spins, for a proton of energy E scattered by a proton at rest, $D_-(E)$ is the real part of the elastic scattered amplitude for an antiproton of energy E scattered by a proton at rest, $\sigma_+(E)$ is the total scattering cross section for a proton with energy E, and $\sigma_-(E)$ is the total scattering cross section for an antiproton with energy E. For energies from zero to M, the function $\sigma_+(E)$ is the analytic continuation of $\sigma_+(E)$ for energies $E > M$, and $\sigma_-(E)$ is the analytic continuation of $\sigma_-(E)$ into the "nonphysical" region $E < M$.

As the energy E approaches infinity, $\sigma_+(E)$ and $\sigma_-(E)$ approach the constant values $\sigma_+(\infty)$ and $\sigma_-(\infty)$. This follows simply from the fact that all strong interactions approach zero exponentially for large values of the impact parameter ρ (here the form of the factor multiplying the exponential is entirely insignificant). Had we wished to consider the electromagnetic interaction of a proton or antiproton with a proton, we could have taken into account the screening of the target proton charge at large distances by the atomic electrons, and also obtained a constant total cross section at sufficiently high energies. It is true that in this way a constant cross section would be obtained only at energies of the order of $E \sim M^2/me^2 \sim 10^{14}$ ev. If, however, we were not to take into account the weak electromagnetic interaction, then up to a quantity of order $e^2 \ln(E/M)$ the total cross section would reach a constant value even at an energy of the order of 10^{10} ev. Allowing E to approach infinity and maintaining only the largest terms, Eqs. (1) and (1') lead to

$$D_+(E) = \frac{E}{2M}[D_+(M) - D_-(M)] - \frac{f^2}{\mu^2}E + \frac{E}{4\pi^2}\int_0^M \frac{idE'}{p'}[\sigma_-(E') - \sigma_+(E')] + \frac{p^2}{4\pi^2}\int_M^\infty \frac{dE'}{p'}\left[\frac{\sigma_+(E')}{E'-E} + \frac{\sigma_-(E')}{E'+E}\right]; \quad (2)$$

$$D_-(E) = \frac{E}{2M}[D_-(M) - D_+(M)] + \frac{f^2E}{\mu^2} + \frac{E}{4\pi^2}\int_0^M \frac{idE'}{p'}[\sigma_+(E') - \sigma_-(E')] + \frac{p^2}{4\pi^2}\int_M^\infty \frac{dE'}{p'}\left[\frac{\sigma_-(E')}{E'-E} + \frac{\sigma_+(E')}{E'+E}\right]. \quad (2')$$

In these equations let us first consider the integral from M to ∞. Starting at a certain energy ϵ, both cross sections σ_+ and σ_- may be considered constant and equal to $\sigma_+(\infty)$ and

$\sigma_-(\infty)$. We may therefore write $(E \gg \epsilon)$*

$$\frac{E^2}{4\pi^2}\int_M^\infty \left[\frac{\sigma_+(E')}{E'-E}+\frac{\sigma_-(E')}{E'+E}\right]dE'\frac{1}{1+E^2/M^2}$$

$$=\frac{E^2}{4\pi^2}\int_M^\varepsilon \left[\frac{\sigma_+(E')}{E'-E}+\frac{\sigma_-(E')}{E'+E}\right]\frac{dE'}{p'} \qquad (3)$$

$$+\frac{E^2}{4\pi^2}\int_\varepsilon^\infty \frac{dE'}{E'}\left[\frac{\sigma_+(\infty)}{E'-E}+\frac{\sigma_-(\infty)}{E'+E}\right]=\frac{E}{4\pi^2}\int_M^\varepsilon [\sigma_-(E')-\sigma_+(E')]\frac{dE'}{p'}$$

$$+\frac{E^2}{4\pi^2}\int_\varepsilon^\infty \frac{dE'}{E'}\left[\frac{\sigma_+(\infty)}{E'-E}+\frac{\sigma_-(\infty)}{E'+E}\right].$$

When $E \gg \epsilon$, the asymptotic value of (3) is

$$\frac{E}{4\pi^2}\left(\ln\frac{E}{\varepsilon}\right)[\sigma_-(\infty)-\sigma_+(\infty)] \qquad (4)$$

[where we have assumed that $\sigma_-(\infty) \neq \sigma_+(\infty)$]. The integral from M to ϵ is, with our conditions, proportional to E:

$$\frac{E}{4\pi^2}\int_M^\varepsilon [\sigma_-(E')-\sigma_+(E')]\frac{dE'}{p'}. \qquad (5)$$

By combining (3), (4), and (5), Eqs. (2) and (2′) become

$$D_+(E)=E\left\{\frac{D_+(M)-D_-(M)}{2M}-\frac{f^2}{\mu^2}\right.$$

$$+\frac{1}{4\pi^2}\int_0^M \frac{idE'}{p'}[\sigma_-(E')-\sigma_+(E')] \qquad (6)$$

$$\left.+\frac{1}{4\pi^2}\int_M^\varepsilon \frac{dE'}{p'}[\sigma_-(E')-\sigma_+(E')]+\frac{1}{4\pi^2}[\sigma_-(\infty)-\sigma_+(\infty)]\ln\frac{E}{\varepsilon}\right\},$$

$$D_-(E)=E\left\{\frac{D_-(M)-D_+(M)}{2M}+\frac{f^2}{\mu^2}\right.$$

$$+\frac{1}{4\pi^2}\int_0^M \frac{idE'}{p'}[\sigma_+(E')-\sigma_-(E')] \qquad (6')$$

$$\left.+\frac{1}{4\pi^2}\int_M^\varepsilon \frac{dE'}{p'}[\sigma_+(E')-\sigma_-(E')]+\frac{1}{4\pi^2}[\sigma_+(\infty)-\sigma_-(\infty)]\ln\frac{E}{\varepsilon}\right\}.$$

We see that if $\sigma_+(\infty) \neq \sigma_-(\infty)$, the principal term which determines $D_+(E)$ and $D_-(E)$ increases faster than E, and is proportional to $E \times \ln(E/\epsilon)$. This result contradicts the conclusion that the interaction decays exponentially for large distances. Let us write out the general expression for the elastic scattered amplitude $A(0)$ for the angle zero. For simplicity, we shall not take account of spin, noting that the orbital quantum number l is very large at high energies, so that the replacement of l by $l \pm 1$, which must be made in order to account for spin, will change nothing in the following considerations.

At high energies, when $l \gg 1$, we have

$$A(0)=\frac{1}{2E}\sum_l (e^{2i\eta_l}-1)\,l, \qquad (7)$$

where η_l is the phase of the wave with orbital angular momentum l. For large l we may use the semiclassical impact parameter l/E. When l/E is much larger than the radius of the interaction ρ (which is of the order of the Compton wavelength of the π meson), η_l decays exponentially with l. It follows from this that the effective upper limit in Eq. (7) is a quantity of order $E\rho$. (This result is independent of the form of the factor multiplying the exponential of the interaction.)

Since the modulus of $e^{2i\eta_l}-1$ is no greater than 2, the order of magnitude of the modulus of $A(0)$ is

$$|A(0)| \leqslant CE\rho^2, \quad C \sim 1. \qquad (8)$$

It follows from this that $D_\pm(E)$ cannot contain terms proportional to $[\sigma_+(\infty)-\sigma_-(\infty)]E\ln(E/\epsilon)$. Therefore*

$$\sigma_+(\infty)=\sigma_-(\infty). \qquad (9)$$

Thus at large energies the total antiproton and proton cross sections are equal. When we recall that at energies of several hundreds of Mev these cross sections are very different (σ_- is much greater[4,5] than σ_+), it becomes evident that at large energies we should expect one or both of these cross sections to be highly energy dependent.

An equation similar to (9) should hold also for the asymptotic values of the total cross sections $\sigma_n(\infty)$ and $\sigma_{\bar{n}}(\infty)$ for neutrons and antineutrons on protons, namely

$$\sigma_{\bar{n}}(\infty)=\sigma_n(\infty). \qquad (10)$$

From statistical considerations and the requirement of isotopic invariance,[6] we may establish the equality of $\sigma_n(\infty)$ and $\sigma_+(\infty)$, as well as that of $\sigma_{\bar{n}}(\infty)$ and $\sigma_-(\infty)$. At high energies, therefore, the proton, the neutron, the antiproton, and the antineutron should all have the same lim-

*Let us bear in mind that we take the principal part of the integral at the point $E' = E$. The same is true with respect to the singularity at $E = M$ (where σ_- approaches ∞ as $1/v$, with v being the velocity). In treating this singularity, one must treat simultaneously the intervals from zero to M and from M to ϵ.

*Equation (9) has been derived in a different way by B. V. Medvedev and D. V. Shirkov.

iting values for their cross sections.

Similar considerations hold also for K mesons. This means that at sufficiently high energies (of the order of 10^{10} ev, if electromagnetic interactions are not taken into account) the K^+, K^-, K^0, and $\overline{K}^0$ mesons should all have the same total cross section. Similarly, the π^+ and π^- cross sections should also approach equality as $E \to \infty$.[7] If we apply our result to hyperons, we obtain the following.

(1) The Λ and anti-Λ (i.e., the $\overline{\Lambda}$) have the same cross section $\sigma_\Lambda(\infty)$.

(2) The Σ^+, Σ^-, Σ^0, $\overline{\Sigma}^+$, $\overline{\Sigma}^-$, and $\overline{\Sigma}^0$ cross sections approach the common value $\sigma_\Sigma(\infty)$ as $E \to \infty$.

(3) The Ξ^-, Ξ^0, $\overline{\Xi}^-$, $\overline{\Xi}^0$ have the same cross section $\sigma_\Xi(\infty)$.

We note also that from (2), (2′), and (9) it follows that at large energies the main contributions to $D_+(E)$ and $D_-(E)$ are proportional to E and differ only in sign. This together with (9) shows that the differential cross sections for elastic scattering of nucleons and antinucleons by nucleons through the angle zero approach equality as $E \to \infty$.

In conclusion, I should like to thank N. N. Bogoliubov, B. L. Ioffe, L. D. Landau, B. V. Medvedev, D. V. Shirkov, and I. M. Shmushkevich for interesting discussions concerning this work.

[1] V. Ia. Fainberg and E. S. Fradkin, Dokl. Akad. Nauk SSSR **109**, 507 (1956), Soviet Phys. "Doklady" **1**, 455 (1956).

[2] B. L. Ioffe, J. Exptl. Theoret. Phys. (U.S.S.R.) **31**, 583 (1956), Soviet Phys. JETP **4**, 534 (1957).

[3] F. M. Kuni, Вестн. Ленингр. ун-та № 10, серия физики и химии (Bull. Leningrad Univ., No. 10, Phys. and Chem. Series) **2** (1957), p. 21.

[4] Chamberlain, Keller, Segrè, Steiner, Wiegand, and Ypsilantis, Phys. Rev. **102**, 1637 (1956).

[5] Cork, Lambertson, Piccioni, and Wenzel, Phys. Rev. **107**, 248 (1957).

[6] I. Ia. Pomeranchuk, J. Exptl. Theoret. Phys. (U.S.S.R.) **30**, 423 (1956), Soviet Phys. JETP **3**, 306 (1956).

[7] L. B. Okun' and I. Ia. Pomeranchuk, J. Exptl. Theoret. Phys. (U.S.S.R.) **30**, 424 (1956), Soviet Phys. JETP **3**, 307 (1956).

Translated by E. J. Saletan
136

SOVIET PHYSICS JETP VOLUME 34(7), NUMBER 3 SEPTEMBER, 1958

CALCULATION OF COORDINATE PROBABILITIES BY GIBBS METHOD

V. B. MAGALINSKII and Ia. P. TERLETSKII

Moscow State University

Submitted to JETP editor October 26, 1957

J. Exptl. Theoret. Phys. (U.S.S.R.) **34**, 729-734 (March, 1958)

Gibbs' statistical method is used to derive general formula which permits one to determine fully the stationary probability density as well as the transition probability density in a nonstationary process for an arbitrary generalized coordinate, provided the behavior of the mean value of the latter is known in the presence of (or after turning on) additional forces acting in the direction of this coordinate.

IT is well known that, using general methods of statistical mechanics, we can derive exact relationships which enable us to reduce a calculation of fluctuations and correlations of various quantities (among them time correlations) to a determination of average values of these quantities in the presence of (or after turning on) additional constant forces.[1-4]

It was shown in Ref. 5 that all the principal momenta determined in fluctuation theory, as well as in the theory of Brownian motion, can be computed by this method.

It will be shown below that not only momenta but also the corresponding coordinate probability densities can be exactly determined, provided one knows the behavior of these coordinates in the presence of additional constant forces or forces which were turned on at the initial instant.

1. STATIONARY PROBABILITY DENSITY OF A GIVEN VALUE OF A COORDINATE

Let X be the aggregate of all the canonical variables of the system, q(X) some generalized coordinate (from now on we confine ourselves to the one-dimensional case to simplify the derivation), and w(X) the stationary probability density in phase space. Then the probability density for q(X) to have a given value q is

$$W(q) = \int_{(X)} \delta\{q - q(X)\}\, w(X)\, dX$$

$$= \frac{1}{2\pi} \int_{-\infty}^{+\infty} e^{i\xi q} \int_{(X)} e^{-i\xi q(X)}\, w(X)\, dX\, d\xi. \qquad (1)$$

In the case of a canonical distribution we have $w(X) = \exp\{\Psi - H(X)/\Theta\}$, and consequently

$$\int_{(X)} e^{-i\xi q(X)} w(X)\, dX = \int_{(X)} \exp\{[\Psi - H(X) - aq(X)]/\Theta\}\, dX$$

$$= e^{(\Psi - \Psi(a))/\Theta} = e^{-\Delta\Psi(a)/\Theta}, \qquad (2)$$

where $a = i\xi\Theta$, and Ψ and $\Psi(a)$ are determined from the conditions

$$e^{-\Psi/\Theta} = \int_{(X)} e^{-H(X)/\Theta}\, dX,$$

$$e^{-\Psi(a)/\Theta} = \int_{(X)} \exp\{-[H(X) + aq(X)]/\Theta\}\, dX. \qquad (3)$$

Obviously Ψ has the meaning of the free energy of the original system, and $\Psi(a)$ has the meaning of the free energy of the system in the presence of an additional constant force $-a$ acting in the direction of the coordinate q(X). Thus, according to (1) and (2)

$$W(q) = \frac{1}{2\pi} \int_{-\infty}^{+\infty} \exp\left\{i\xi q - \frac{\Delta\Psi(a)}{\Theta}\right\} d\xi. \qquad (4)$$

This formula makes it possible to compute the sought probability density W(q), provided we know $\Delta\Psi(a)$ as a function of the force $a = i\xi\Theta$.

According to (3), the mean value of the coordinate q(X) over the ensemble with an additional force $-a$ is $\bar{q}^a = \partial\Psi(a)/\partial a$, hence

$$\Delta\Psi(a) = \int_0^a \bar{q}^\alpha d\alpha. \qquad (5)$$

Formula (5) enables us to determine $\Delta\Psi(a)$ from empirical data which give the dependence of the mean coordinate on the external force a in an isothermal process.

Let us illustrate what we said above using two simple examples.

(a) Coordinate probability of a harmonic oscillator. The equilibrium condition for an oscillator in the presence of an additional external α has the form

$$k\bar{q}^\alpha + \alpha = 0,$$

hence $\bar{q}^\alpha = -\alpha/k$ (k is the elastic coefficient). According to (5)

$$\Delta\Psi(a) = \int_0^a \bar{q}^\alpha d\alpha = -a^2/2k = (\Theta^2/2k)\,\xi^2. \qquad (5')$$

Substituting (5′) into (4) and integrating we get

$$W(q) = \sqrt{\frac{k}{2\pi\Theta}} \exp\left(-\frac{kq^2}{2\Theta}\right),$$

i.e., the Boltzmann distribution.

(b) Probability of volume V occupied by an ideal gas. In this case q = V, and $\bar{V}^\alpha$ is found from the equation of state $\bar{V}^\alpha = N\Theta/(p + \alpha)$

$$\Delta\Psi(\alpha) = \int_0^a \bar{V}^\alpha d\alpha = N\Theta \ln\left(1 + \frac{a}{p}\right) = N\Theta \ln\left(1 + i\frac{\bar{V}}{N}\xi\right),$$

where $\bar{V} = N\Theta/p$ is the equilibrium value of the volume. Finally we find

$$W(V) = \frac{1}{2\pi} \int_{-\infty}^{+\infty} \frac{e^{iV\xi}}{(1 + i\bar{V}\xi/N)^N}\, d\xi$$

$$= \frac{1}{V}\left(N\frac{V}{\bar{V}}\right)^N \frac{\exp(-NV/\bar{V})}{(N-1)!}. \qquad (4'')$$

In the case of small fluctuations ($|V - \bar{V}|/\bar{V} \ll 1$), (4″) becomes a Gaussian distribution.

2. TRANSITION PROBABILITY DENSITY

Let $W(q, t; q_0, t_0)$ be the probability density of transition of the system from the point q_0 at the instant t_0 to the point q at the instant t, and let $W_0(q_0)$ be the probability density of the initial value of the coordinate. Further, let us introduce the notation:

$$W_1(q, t; q_0, t_0) = W(q, t; q_0, t_0)\, W_0(q_0). \qquad (6)$$

The function $W(q, t; q_0, t_0)$ is uniquely determined by its characteristic function $\varphi_1(\xi, t; \eta, t_0)$ so that

$$W_1(q, t; q_0, t_0) = (2\pi)^{-2} \int_{-\infty}^{+\infty}\int_{-\infty}^{+\infty} e^{i\xi q + i\eta q_0} \varphi_1(\xi, t; \eta, t_0)\, d\xi\, d\eta. \qquad (7)$$

The characteristic function φ_1 is in turn determined if all the moments of the quantities q and q_0 are known, namely:

$$\varphi_1(\xi,\ t;\ \eta,\ t_0) = \sum_{j,k} \overline{q_t^j q_0^k}\,(-i\xi)^j\,(-i\eta)^k / j!k!, \qquad (8)$$

where

$$\overline{q_t^j q_0^k} = \iint W_1(q,\ t;\ q_0,\ t_0)\, q^j q_0^k\, dq\, dq_0. \qquad (9)$$

To compute these momenta, we make use of the general statistical method of Gibbs.

If we let X^0 be the aggregate of all the canonical variables at the initial instant, and X^t be the canonical variable of the same phase points at time t, then

$$\overline{q_t^j q_0^k} = \int_{(X_0)} q^j(X^t)\, q^k(X^0)\, w(X^0)\, dX^0, \qquad (10)$$

where $w(X^0)$ is the probability density of the initial phase X^0 and X^t are assumed to be expressed in terms of X^0, t, and t_0 in accordance with the canonical equations of mechanics with the Hamiltonian function $H(X): X^t = X(X^0, t_0, t)$. In the case of the Gibbs canonical distribution

$$w(X^0) = \exp\{\Psi_0 - H(X^0)/\Theta\}.$$

Let us introduce (so far, purely formally) an auxiliary function $Z(\alpha, t; \beta, t_0)$, which we define as

$$Z(\alpha,\ t;\ \beta,\ t_0) = \int_{(X^0)} \exp\{-[H(X^0) + \alpha q(X^t) + \beta q(X^0)]/\Theta\}\, dX^0. \qquad (11)$$

By simple differentiation we find

$$\overline{q_t^j q_0^k} = \frac{1}{Z_0}(-\Theta)^{j+k}\left[\frac{\partial^{j+k} Z(\alpha,\ t;\ \beta,\ t_0)}{\partial\alpha^j \partial\beta^k}\right]_{\alpha=\beta=0}, \qquad (12)$$

where

$$Z_0 \equiv Z(0,\ t;\ 0,\ t_0) = \int_{(X^0)} e^{-H(X^0)/\Theta} dX^0 = e^{-\Psi_0/\Theta}. \qquad (13)$$

Substituting (12) into (8) we find the characteristic function

$$\varphi_1(\xi,\ t;\ \eta,\ t_0) = \frac{1}{Z_0}\sum_{j,k}\left[\frac{\partial^{j+k} Z(\alpha,\ t;\ \beta,\ t_0)}{\partial\alpha^j\partial\beta^k}\right]_{\alpha=\beta=0} \times \frac{(i\xi\Theta)^j (i\eta\Theta)^k}{j!k!} = \frac{1}{Z_0} Z(a,\ t;\ b,\ t_0), \qquad (14)$$

where the notation $i\xi\Theta = a$, $i\eta\Theta = b$ is introduced. We now determine $Z(\alpha, t; \beta, t_0)$. Writing

$$Z(\alpha,\ t;\ \beta,\ t_0) = \exp\{-\Psi(\alpha,\ t;\ \beta,\ t_0)/\Theta\}, \qquad (13')$$

we have by virtue of (11)

$$\int_{(X_0)} \exp\{[\Psi(\alpha,\ t;\ \beta,\ t_0) - H(X^0) - \alpha q(X^t) - \beta q(X^0)]/\Theta\}\, dX^0 = 1 \qquad (15)$$

for any t.

Differentiating (15) with respect to time we get

$$\partial\Psi(\alpha,\ t;\ \beta,\ t_0)/\partial t = \alpha \bar{q}^{\alpha,\beta}, \qquad (16)$$

$$\Psi(\alpha,\ t;\ \beta,\ t_0) = \alpha(\bar{q}_t^{\alpha,\beta} - \bar{q}_0^{\alpha,\beta}) + \Psi(\alpha,\ t_0;\ \beta,\ t_0),$$

where

$$\bar{q}_t^{\alpha,\beta} = \int_{(X^0)} q(X^t) \exp\{[\Psi(\alpha,\ t;\ \beta,\ t_0) - H(X^0) - \alpha q(X^t) - \beta q(X^0)]/\Theta\}\, dX^0. \qquad (17)$$

Quantity $\bar{q}_t^{\alpha,\beta}$ can be interpreted as a macroscopic coordinate which is obtained as a result of averaging of q(X) over the ensemble separated from the original equilibrium ensemble by the following process:

(a) Before the time $t = t_0$, the system was acted on by a constant force $-(\alpha + \beta)$ so that the system was in equilibrium, having an equilibrium coordinate $\bar{q}_0^{\alpha+\beta}$ and a corresponding free energy

$$\Psi(\alpha,\ t;\ \beta,\ t_0) = \Psi_0 + \int_0^{\alpha+\beta} \bar{q}^{\lambda} d\lambda \qquad (18)$$

[see (5)].

(b) Starting from the time t_0, the system continues to be acted on only by the constant force $-\alpha$; as a result, the system comes out of equilibrium and undergoes a transition.

Thus $\bar{q}_t^{\alpha,\beta}$ can be interpreted as an average displacement of the coordinate q(X) during the time $t - t_0$ under the action of a constant force $-\alpha$. According to (a), the initial value of the coordinate is $\bar{q}_0^{\alpha,\beta} = \bar{q}_0^{\alpha+\beta}$.

Substituting (13), (13'), (14), (16), and (18) into (7), and taking (6) into account, we obtain the final formula for the transition probability density:

$$W(q,\ t;\ q_0,\ t_0) = \frac{1}{(2\pi)^2 W_0(q_0)} \int_{-\infty-\infty}^{+\infty+\infty} \exp\left\{i\xi q + i\eta q_0 - \frac{\Delta\Psi(a,\ t;\ b,\ t_0)}{\Theta}\right\} d\xi\, d\eta, \qquad (19)$$

where

$$\Delta\Psi(a,\ t;\ b,\ t_0) = a(\bar{q}_t^{a,b} - \bar{q}_0^{a+b}) + \int_0^{a+b} \bar{q}_0^{\lambda} d\lambda. \qquad (20)$$

The initial probability density is found from formulae (4) and (5).

Thus, if $\bar{q}_t^{a,b}$ and $\bar{q}^{\lambda}$ are known from the phenomenological equations of motion or from the empirical data, we can obtain an expression for $W(q, t; b, t_0)$ by substituting the value of $\Delta\Psi(a, t; b, t_0)$ found from (20) into (19) and integrating.

In this way the suggested method makes it possible to solve a much wider class of problems than can be done with the known methods of the theory of Brownian motion.

If the system is subjected to the action of forces independent of the coordinate q, the transition probability density depends only on the magnitude of the displacement $q - q_0$, i.e.,

$$W(q, t; q_0, t_0) = W(q - q_0; t - t_0).$$

Using arguments analogous to those cited above, we obtain the following formula for the transition probability density:

$$W(q - q_0; t - t_0) = \frac{1}{2\pi}\int_{-\infty}^{+\infty} \exp\{i\xi(q - q_0) - \Delta\Psi(a, t; t_0)/\Theta\}\, d\xi, \qquad (19')$$

$$\Delta\Psi(a, t; t_0) = a\overline{\Delta q}_t^a, \quad a = i\xi\Theta, \qquad (20')$$

and $\overline{\Delta q}_t^a$ is the mean displacement of the coordinate $q(X)$ during the time $t - t_0$ under the action of an additional constant force $-a$.

Let us illustrate the method developed above with a simple example of a Brownian particle in the gravitational field.

According to the above, the mean displacement $\overline{\Delta q}_t^a$ which we are interested in obeys the phenomenological equation

$$m\ddot{\overline{\Delta q}}_t^a + \gamma\dot{\overline{\Delta q}}_t^a = g - a$$

with homogeneous initial conditions. (Here m is mass, γ the coefficient of friction, and g the acceleration due to gravity.) The solution of this equation for $t = 0$ is

$$\overline{\Delta q}_t^a = \frac{g-a}{m\varkappa}t - \frac{g-a}{m\varkappa^2}(1 - e^{-\varkappa t}), \quad \varkappa = \frac{\gamma}{m}. \qquad (21)$$

Substituting the value of $\Delta\Psi(a, t; t_0)$ found from (21) and (20′) into (19′) and carrying out the integration we easily find

$$W(q - q_0; t) = \sqrt{\frac{m\varkappa^2}{4\pi\Theta f(t)}}\exp\left\{-\frac{m\varkappa^2[q - Q(t)]^2}{4\Theta f(t)}\right\} \qquad (22)$$

Here

$$Q(t) = \frac{g}{m\varkappa}t - \frac{g}{m\varkappa^2}(1 - e^{-\varkappa t})$$

is the mean coordinate of the particle at the instant t,

$$f(t) = \varkappa t - (1 - e^{-\varkappa t}).$$

Formula (22) describes a Gaussian distribution which spreads with time; its center moves according to the laws of mechanics.

It should be mentioned that the transition probability density $W(q - q_0; t)$, (22), which was obtained above on the basis of general principles of statistical mechanics, also satisfies a corresponding equation of Einstein — Fokker — Planck

$$\frac{\partial W}{\partial t} = D(t)\left(\frac{\partial^2 W}{\partial q^2} - \frac{g}{\Theta}\frac{\partial W}{\partial q}\right), \qquad (23)$$

being its source function. The diffusion coefficient $D(t)$ depends on time and is equal to the mean velocity of the particle when it is acted on by an additional constant external force equal to unity.

For $t \gg \kappa^{-1}$ (diffusion mode) $D(t) \to \Theta/\gamma$ and equation (23) takes on its usual form.

For $t \ll \kappa^{-1}$ (inertial mode) formula (22) gives

$$W(q - q_0; t)\, dq = \sqrt{\frac{m}{2\pi\Theta}}\exp\left(-\frac{mv^2}{2\Theta}\right) dv \qquad (24)$$

[where $v = (q - q_0)/t$], i.e., Maxwell distribution corresponding to the fact that before the collisions take place, the particle undergoes inertial motion.

[1] J. W. Gibbs, Principles of Statistical Mechanics (Collected Works, 1), New York, Longmans Green and Co., 1928.

[2] V. V. Vladimirskii, J. Exptl. Theoret. Phys. (U.S.S.R.) 12, 199 (1942).

[3] V. V. Vladimirskii and Ia. P. Terletskii, J. Exptl. Theoret. Phys. (U.S.S.R.) 15, 258 (1945).

[4] Ia. P. Terletskii, Динамические и статистические законы физики, (Dynamic and Statistical Laws of Physics) Moscow State University Press, 1949.

[5] Ia. P. Terletskii, Вестник МГУ (Bulletin, Moscow State Univ.) No. 4, 119 (1957).

Translated by N. Meshkov
137

ON THE ENERGY SPECTRUM OF SUPERCONDUCTORS

L. P. GOR'KOV

Institute for Physical Problems, Academy of Sciences, U.S.S.R.

Submitted to JETP editor November 18, 1957

J. Exptl. Theoret. Phys. (U.S.S.R.) **34**, 735-739 (March, 1958)

A method is proposed, based on the mathematical apparatus of quantum field theory, for the calculation of the properties of a system of Fermi particles with attractive interaction.

IT was shown in the work of Cooper[1] that if the interaction of electrons in a metal leads to an effective mutual attraction for two electrons close to the Fermi surface, then the pair of particles which possess mutually opposite momenta and spins can have bound states with negative coupling energies. In the works of Bardeen, Cooper and Schreiffer[2,3] and of Bogoliubov[4] a systematic theory of superconductivity has been erected on this principle. It was shown that the ground state of a system of interacting Fermi particles is located below the normal state with a filled Fermi sphere and, in consequence, is separated from the excited states by a gap in order of magnitude equal to the energy of coupling of the individual pair.

In the present work, a method is proposed, based on the physical idea of Cooper, which permits us, with the help of the apparatus of quantum field theory, to obtain all the results by a short and simple method.

We shall start out from a Hamiltonian in the form[2] which is written in the case of second quantization:

$$\hat{H} = \int \left\{ -\left(\psi^+ \frac{\Delta}{2m} \psi\right) + \frac{g}{2} (\psi^+ (\psi^+ \psi)\psi) \right\} d^3x, \qquad (1)$$

where

$$\psi_\sigma(\mathbf{x}) = V^{-1/2} \sum_{k\sigma} a_{k\sigma} s_{\sigma\alpha} e^{i\mathbf{k}\mathbf{x}}; \quad \psi_\beta^+(\mathbf{x}') = V^{-1/2} \sum_{k\sigma} a_{k\sigma}^+ s_{\beta\sigma}^* e^{-i\mathbf{k}\mathbf{x}'}$$

satisfy the usual commutation relations:

$$\{\psi_\alpha(\mathbf{x}),\ \psi_\beta^+(\mathbf{x}')\} = \delta_{\alpha\beta}\,\delta(\mathbf{x}-\mathbf{x}'),$$
$$\{\psi_\alpha(\mathbf{x}),\ \psi_\beta(\mathbf{x}')\} = \{\psi_\alpha^+(\mathbf{x}),\ \psi_\beta^+(\mathbf{x}')\} = 0. \qquad (2)$$

We shall consider the interaction to be equal to zero everywhere except in a region of energy of the particles 2κ around the Fermi surface, from $\epsilon_F - \kappa$ to $\epsilon_F + \kappa$.

We transform to the Heisenberg representation, in which the operators ψ and ψ^+ depend on the time and satisfy the following equations:

$$\{i\partial/\partial t + \Delta/2m\}\psi(x) - g(\psi^+(x)\psi(x))\psi(x) = 0,$$
$$\{i\partial/\partial t - \Delta/2m\}\psi^+(x) + g\psi^+(x)\,(\psi^+(x)\psi(x)) = 0. \qquad (3)$$

We determine the Green's function $G_{\alpha\beta}(x-x')$ as an average over the ground state of the system:

$$G_{\alpha\beta}(x-x') = -i\langle T(\psi_\alpha(x),\ \psi_\beta^+(x'))\rangle, \qquad (4)$$

where T is time-ordering operator.

For the derivation of the equation for the function $G(x-x')$ we take it into consideration that the ground state of the system differs from the usual state with a filled Fermi sphere by the presence of bound pairs of electrons. In the ground state, all the pairs are at rest as a whole. (This means that the interaction between particles is considered only insofar as it enters into the formation of the bound pairs. We neglect scattering effects.) A sort of "Bose condensation" of pairs takes place in the case in which the momentum of their motion as a whole is equal to zero, just as in a Bose gas such a condensation takes place by virtue of the statistics for the particles themselves. This circumstance permits us to write down in a definite way the mean form $\langle T(\psi(x_1)\,\psi(x_2)\times\psi^+(x_3)\,\psi^+(x_4))\rangle$, which appears in the equations for $G(x-x')$ by virtue of (3).

For example, we have

$$\langle T(\psi_\alpha(x_1)\psi_\beta(x_2)\psi_\gamma^+(x_3)\psi_\delta^+(x_4))\rangle =$$
$$-\langle T(\psi_\alpha(x_1)\psi_\gamma^+(x_3))\rangle\langle T(\psi_\beta(x_2)\psi_\delta^+(x_4))\rangle$$
$$+\langle T(\psi_\alpha(x_1))\psi_\delta^+(x_4))\rangle\langle T(\psi_\beta(x_2)\psi_\gamma^+(x_3))\rangle \qquad (5)$$
$$+\langle N|T(\psi_\alpha(x_1)\psi_\beta(x_2))|N$$
$$+2\rangle\langle N+2|T(\psi_\gamma^+(x_3)\psi_\delta^+(x_4))|N\rangle,$$

where $|N\rangle$ and $|N+2\rangle$ are the ground states of the system with numbers of particles N and N + 2. The quantity

$$\langle N|T(\psi\psi)|N+2\rangle\langle N+2|T(\psi^+\psi^+)|N\rangle, \qquad (5a)$$

evidently has the order of the density of the number of pairs, while $\langle T(\psi\psi^+)\rangle$ is the particle number density.

It is easy to show that the quantities thus introduced can be written in the form

$$\langle N|T(\psi_\alpha(x)\psi_\beta(x'))|N+2\rangle = e^{-2i\mu t}F_{\alpha\beta}(x-x'),$$
$$\langle N+2|T(\psi^+_\alpha(x)\psi^+_\beta(x'))|N\rangle = e^{2i\mu t}F^+_{\alpha\beta}(x-x'). \quad (6)$$

The function $G(x-x')$ depends only on the difference $x-x'$, because of the homogeneity of the problem. So far as the additional dependence on t in Eq. (6) is concerned, its origin is seen from the general quantum mechanical formula for the time derivative of an arbitrary operator $\hat{A}(t)$:

$$\frac{\partial}{\partial t}\langle N|\hat{A}(t)|N+2\rangle = i(E_N - E_{N+2})\langle N|\hat{A}(t)|N+2\rangle.$$

The value of the energy difference $E_{N+2} - E_N$ is obviously equal to $2\mu\,(\partial E/\partial N = \mu)$.

Making use of Eq. (3), we obtain equations for the functions $\hat{G}(x-x')$ and $\hat{F}(x-x')$:

$$\{i\partial/\partial t + \Delta/2m\}\hat{G}(x-x')$$
$$-ig\hat{F}(0+)\hat{F}^+(x-x') = \delta(x-x'),$$
$$\{i\partial/\partial t - \Delta/2m - 2\mu\}\hat{F}^+(x-x') \quad (7)$$
$$+ig\hat{F}^+(0+)\hat{G}(x-x') = 0.$$

Here terms are omitted which correspond to the first two terms in Eq. (5), inasmuch as they only change μ, which one can neglect, and the notations

$$F^+_{\alpha\beta}(0+) = e^{-2i\mu t}\langle\psi^+_\alpha(x)\psi^+_\beta(x)\rangle \equiv \lim_{x\to x'(t>t')} F^+_{\alpha\beta}(x-x')$$

and introduced, and correspondingly,

$$F_{\alpha\beta}(0+) = e^{2i\mu t}\langle\psi_\alpha(x)\psi_\beta(x)\rangle.$$

The complex conjugate yields

$$(F^+_{\alpha\beta}(0+))^* = -F_{\alpha\beta}(0+). \quad (8)$$

We transform in Eqs. (7) to the Fourier components of all functions, for example,

$$G_{\alpha\beta}(x-x') = (2\pi)^{-4}\int G_{\alpha\beta}(p\omega)\exp\{ip(x-x')$$
$$-i\omega(t-t')\}\,d\omega d^3p.$$

Denoting $\omega - \mu = \omega'$, we find

$$(\omega' - \xi_p)\hat{G}(p\omega) - ig\hat{F}(0+)\hat{F}^+(p\omega) = 1,$$
$$(\omega' + \xi_p)\hat{F}^+(p\omega) + ig\hat{F}^+(0+)\hat{G}(p\omega) = 0, \quad (9)$$

where

$$\xi_p = p^2/2m - \mu \approx v_F(p - p_F),$$

and p_F is the Fermi momentum. In what follows, we shall only have ω' in the formulas, hence we shall omit the prime.

It follows from Eq. (8) that $\hat{F}(0+)$ and $\hat{F}^+(0+)$ have the following matrix form:

$$\hat{F}^+(0+) = J\begin{pmatrix}0&1\\-1&0\end{pmatrix} \equiv J\hat{I};\ \hat{F}(0+) = -J\hat{I},$$
$$\hat{I}^2 = -\hat{E}; \quad (10)$$

equal both to $\hat{F}^+(p\omega)$ and $\hat{F}(p\omega)$, and the Green's function, in accord with (9), is proportional to the unit matrix. Substituting (10) in (9), we obtain

$$(\omega^2 - \xi_p^2 - g^2J^2)F^+(p\omega) = -igJ,$$
$$(\omega - \xi_p)G(p\omega) = 1 + igJF^+(p\omega). \quad (11)$$

Hence

$$F^+(p\omega) = -ig\frac{J}{\omega^2 - \xi_p^2 - \Delta^2};$$
$$G(p\omega) = \frac{\omega + \xi_p}{\omega^2 - \xi_p^2 - \Delta^2}, \quad (12)$$

where

$$\Delta^2 = g^2J^2.$$

As is evident from the first equation of (11), $F^+(p\omega)$ is determined with accuracy up to a solution of the homogeneous equation of the form $A(p)\delta(\omega^2 - \xi_p^2 - \Delta^2)$. It is not difficult to verify the fact that this term reduces in the expression for $G(p\omega)$ to an arbitrary imaginary part. In other words, Eqs. (11) determine only the real part of the Green's function.

We determine the rule for circling the poles in (12), making use of a theorem given by Landau,[5] according to which the imaginary part of the Green's function of a Fermi system is positive for $\omega < 0$ and changes sign in the transition from negative to positive frequencies.

As a result, we obtain

$$F^+(p\omega) = -igJ/(\omega - \varepsilon_p + i\delta)(\omega + \varepsilon_p - i\delta), \quad (13)$$
$$G(p\omega) = u_p^2(\omega - \varepsilon_p + i\delta)^{-1} + v_p^2(\omega + \varepsilon_p - i\delta)^{-1}, \quad (14)$$

where $\epsilon_p = \sqrt{\xi_p^2 + \Delta^2}$ and the functions μ_p^2 and v_p^2 are equal to

$$u_p^2 = \frac{1}{2}\left(1 + \frac{\xi_p}{\varepsilon_p}\right);\quad v_p^2 = \frac{1}{2}\left(1 - \frac{\xi_p}{\varepsilon_p}\right) \quad (14')$$

For the determination of the quantity Δ, we make use of the fact that

$$J = (2\pi)^{-4}\int F^+(p\omega)\,d\omega\,d^3k. \quad (15)$$

Substituting (13), we obtain the equation

$$1 = -\frac{g}{2(2\pi)^3}\int\frac{d^3k}{\sqrt{\xi_k^2 + \Delta^2}}(|\xi| < \varkappa). \quad (16)$$

For small $g < 0$ (attraction), this equation has a solution of the form

$$\Delta = 2\varkappa e^{-1/z\rho},$$

where

$$\rho = p_F |g| m / 2\pi^2.$$

The positive pole in (14) determines the excitation spectrum which, as is shown, has a gap of magnitude Δ. These results coincide with those obtained in Refs. 2 — 4.

The chemical potential μ is connected with the particle number density by the relation

$$N/V = \langle \psi^+(x)\psi(x)\rangle = -i(2\pi)^{-4}\int G_{\alpha\alpha}(p\omega)\, e^{i\omega\delta}\, d\omega d^3p, \quad (17)$$

with accuracy up to small exponential terms: $\mu = \epsilon_F$.

The method laid out also permits us to make use of it for temperatures differing from absolute zero. In this case we consider the mean Green's function (thermodynamically averaged)

$$G_{\alpha\beta}(x - x')$$

$$= -i\sum_n \exp\left\{\frac{\Omega + \mu N - E_n}{T}\right\} \langle n | T(\psi_\alpha(x)\psi^+_\beta(x')) | n\rangle,$$

where Ω is the thermodynamic potential in the variables T, V, μ. As is well known, the result of averaging does not depend on whether it is carried out with the use of a Gibbs distribution or over the stationary state with a given energy. This corresponds to the choice of the quantity $\overline{E}$ as a thermodynamic variable, in place of the temperature T. Taking the averaging in such a fashion we get the earlier equations (11) for the quantities G, F^+ and F, with this difference, that the corresponding averaging of T products are taken not over the ground state of the system but over a state with total energy E equal to the energy of the system at a given temperature. Equations (11), as we have already noted above, determine uniquely only the real part of the Green's function $G(p\omega)$, which is evidently equal to the real part of Eq. (14). We write down the general solution for the function $F^+(p\omega)$:

$$F^+(p\omega) = -igJ/(\omega - \varepsilon_p + i\delta)(\omega + \varepsilon_p - i\delta) + A_1(p, T)\,\delta(\omega - \varepsilon_p) + A_2(p, T)\,\delta(\omega + \varepsilon_p). \quad (18)$$

We have made use of the fact that $1/(x \mp i\delta) = 1/x \pm \pi i\delta(x)$. The value of the quantities $A_1(p,T)$ and $A_2(p,T)$ can be obtained from the relations between the real and imaginary parts of the Green's function,[5] which has the following form at temperatures different from zero:

$$\mathrm{Re}\, G(\omega) = -\frac{1}{\pi}\int_{-\infty}^{\infty} \coth\frac{x}{2T}\,\frac{\mathrm{Im}\, G(x)}{\omega - x}\, dx.$$

We obtain

$$A_1(p, T) = A_2(p, T) = -(\pi\Delta/\dot{\varepsilon}_p)\, n(\varepsilon_p)$$

and for the Green's function,

$$G(p\omega) = u_p^2(\omega - \varepsilon_p + i\delta)^{-1} + v_p^2(\omega + \varepsilon_p - i\delta)^{-1} + 2\pi i n(\varepsilon_p)[u_p^2\,\delta(\omega - \varepsilon_p) - v_p^2\,\delta(\omega + \varepsilon_p)], \quad (19)$$

where $n(\epsilon_p)$ has the form of the Fermi distribution of excitations at the given temperature:

$$n(\varepsilon_p) = [\exp(\varepsilon_p/T) + 1]^{-1}.$$

The excitation spectrum is then

$$\varepsilon_p = \sqrt{\xi_p^2 + \Delta^2}, \quad (20)$$

where Δ is a function of the temperature. Condition (15), upon substitution of $F^+(p\omega)$ in the form (18) in it, gives a relation which determines the magnitude of the gap in its temperature dependence:

$$1 = \frac{|g|}{2(2\pi)^3}\int \frac{d^3k\,(1 - 2n(\varepsilon_k))}{\sqrt{\xi_k^2 + \Delta^2(T)}}, \quad (|\xi| < \varkappa). \quad (21)$$

Equation (21) was obtained by Bardeen, Cooper and Schrieffer[3]; it was found that the magnitude of the gap $\Delta(T)$ vanishes at $T = T_c \sim \Delta(0)$. We shall show briefly how calculation of thermodynamical quantities is carried out by our method.

The heat capacity per unit volume is equal to

$$Vc_V = (\partial\overline{E}/\partial T)_V.$$

The quantity

$$\overline{E}/V = \left\langle\left\{-\left(\psi^+\frac{\Delta}{2m}\psi\right) + \frac{g}{2}(\psi^+(\psi^+\psi)\psi)\right\}\right\rangle$$

is expressed by the function of G, F^+ and F with accuracy up to inconsequential (constant in temperature) terms in the following fashion:

$$\overline{E} = 2V(2\pi)^{-3}\int \xi_p[v_p^2(1 - n(\varepsilon_p)) + u_p^2 n(\varepsilon_p)]\, d^3p + gVJ^2.$$

The total contribution to the heat capacity at such temperatures gives the interval $|\xi_p| \ll \varkappa$. Substituting here for the functions u_p^2 and v_p^2 their expressions (14′), and making use of Eq. (21), we get for the heat capacity

$$c_V = 2(2\pi)^{-3}\int \varepsilon_p \frac{\partial n(\varepsilon_p)}{\partial T}\, d^3p,$$

i.e., the ordinary formula for heat capacity of a gas of Fermi excitations with a spectrum (20). Computation of the heat capacity and the value of the gap in its temperature dependence was given in Ref. 3.

The author expresses his gratitude to Academician L. D. Landau for his valued advice and in-

terest in the work. The author also acknowledges A. A. Abrikosov, I. M. Khalatnikov, I. E. Dzialoshinskii and L. P. Pitaev for discussion of the results of this work.

[1] L. Cooper, Phys. Rev. **104**, 1189 (1956).
[2] Bardeen, Cooper and Schrieffer, Phys. Rev. **106**, 162 (1957).
[3] Bardeen, Cooper and Schrieffer, Phys. Rev. **108**, 5 (1957).
[4] N. N. Bogoliubov, J. Exptl. Theoret. Phys. (U.S.S.R.) **34**, 58 (1958); Soviet Phys. JETP **7**, 41 (1958).
[5] L. D. Landau, J. Exptl. Theoret. Phys. (U.S.S.R.) **34**, 262 (1958); Soviet Phys. JETP **7**, 182 (1958).

Translated by R. T. Beyer
138

THE THERMODYNAMICAL THEORY OF RESONANCE AND RELAXATION PHENOMENA IN FERROMAGNETICS

G. V. SKROTSKII and V. T. SHMATOV

Ural Polytechnic Institute

Submitted to JETP editor October 18, 1957

J. Exptl. Theoret. Phys. (U.S.S.R.) **34**, 740-745 (March, 1958)

The methods of irreversible thermodynamics are applied to derive the time variation of magnetization of ferromagnetics. The role of spin-lattice relaxation in the phanomenon of ferromagnetic resonance is discussed. The resultant equations are compared with those of Landau-Lifshitz and Bloch.

1. In the observation of ferromagnetic resonance, the ferromagnetic specimen is placed in a constant magnetic field $H_0 = H_z$. This magnetizes the sample to saturation. A radiofrequency field $\mathbf{h}$ is then applied perpendicular to $\mathbf{H}_0$. The amplitude of the field $\mathbf{h}$ is usually taken to be small ($h \ll H_0$); therefore, the magnetization vector $\mathbf{M}$ differs only slightly in direction from $\mathbf{H}_0$. In experiments on the study of relaxation in perpendicular fields, a strong radiofrequency field of high amplitude was applied. This produced a significant deviation of $\mathbf{M}$ away from $\mathbf{H}_0$.

For the determination of the frequency dependence of the components of the magnetization M_x, M_y, M_z of the ferromagnetic, there are used the equations of Landau-Lifshitz[1], Bloch,[2] or various modifications of these equations,[3] which are frequently put together without sufficient basis.

In the present paper, it is shown that as a result of the application of irreversible thermodynamics, one can obtain (under very simple and general assumptions) equations for the change in the magnetization with time, with consideration both of spin-spin and spin-lattice relaxations, and the role of the latter in the phenomenon of ferromagnetic resonance can also be judged.

From the viewpoint of thermodynamics, we can divide the system of spin moments, which correspond to the magnetic properties of the ferromagnetics, into a separate subsystem with temperature T (the spin system). We shall consider the remaining degrees of freedom of the entire system [analogously to what was done in the thermodynamic theory of paramagnetic relaxation[4]] to be thermostatted, the temperature of which (T_0) we shall consider fixed in the current research. We can show that the latter assumption is related to the conclusions made below and it is easily based on them.

If the subset is found in thermal equilibrium with the thermostat or is isolated completely from it, and the magnetization $\mathbf{M}$ has a non-equilibrium value, which does not correspond to the field $\mathbf{H}$, then we shall call the process of the approximation

of M to the equilibrium value the internal or spin-spin relaxation (correspondingly isothermal or adiabatic).

Another form of relaxation will take place if the magnetization of the subsystem M has a constant equilibrium value M_0 while its temperature $T > T_0$. In this case the system will go over to the equilibrium state by a transfer of heat to the thermostat. In what follows, we shall call this process the external or spin-lattice relaxation. Processes of internal and external relaxation usually take place simultaneously and are connected with one another.

The thermodynamic theory of relaxational phenomena, which takes into account both forms of relaxation, was developed in the works of Shaposhnikov and was applied to paramagnetics.[5-7]

2. For a sufficiently rapid change in the field H, the subsystem of spin moments will be found in a non-equilibrium state. The temperature T of the subsystem and the magnetization M do not satisfy the equation of state, which in this case determines a certain value of the field H*

$$\mathbf{H}^* = \mathbf{H}^*(T, \mathbf{M}), \tag{1}$$

which differs from H. The difference $\mathbf{H}^* - \mathbf{H}$ can be regarded as some additional magnetic field, in the presence of which the subsystem would be in an equilibrium state. By the definition of the field H*, we have, always,

$$[\mathbf{M}\mathbf{H}^*] = 0. \tag{2}$$

In order to take into account the internal relaxation, we write down the expression for the change in the entropy of the non-equilibrium state of the subsystem, which can be represented in the form (see Ref. 8)

$$TdS = dU - \mathbf{H}d\mathbf{M} + (\mathbf{H} - \mathbf{H}^*)\,d\mathbf{M},$$

where U is the internal energy of the subsystem. The first two terms in the right hand side of the latter equation determine the equilibrium part of the entropy change:

$$T(dS)_p = dU - \mathbf{H}d\mathbf{M}, \tag{3}$$

while the latter gives the non-equilibrium part. Therefore, for the measurement of the entropy in the subsystem, we find

$$Td\Delta S/dt = (\mathbf{H} - \mathbf{H}^*)\,d\mathbf{M}/dt.$$

In the approximation of irreversible thermodynamics,[9] the components of the "current" M_k are linear functions of the components of the "force" $(H_k - H_k^*)$, i.e.,

$$\dot{M}_k = \sum_{i=1}^{3} L_{ik}(H_i - H_i^*), \tag{4}$$

where L_{ik} is the tensor of kinetic coefficients whose components are functions of the magnetization for ferromagnetics. Symmetrizing L_{ik}^* and antisymmetrizing L_{ik}^a the parts of the tensor L_{ik} satisfy the Onsager relations:

$$L_{ik}^s(\mathbf{M}) = L_{ik}^s(-\mathbf{M});\ L_{ik}^a(\mathbf{M}) = -L_{ik}^a(-\mathbf{M}). \tag{5}$$

For a magneto-isotropic ferromagnetic, placed in a field $H_0 = H_Z$, one should, generally speaking, assume the presence of an axial anisotropy; therefore

$$L_{ik}^s = \lambda_i \delta_{ik}, \quad i, k = 1, 2, 3, \tag{6}$$

where $\lambda_1 = \lambda_2 = \lambda_\perp$, $\lambda_3 = \lambda_\parallel$.

The components of the antisymmetric part of the tensor L_{ik}^a form an axial vector L which, according to (5), is an odd function of the magnetization. The latter requirement can be satisfied by assuming

$$\mathbf{L} = \gamma\mathbf{M}, \tag{7}$$

where the coefficient γ can depend on the temperature.

Now Eq. (4) can be written in the form

$$\dot{M}_k = \lambda_k\{H_k - H_k^*(T, \mathbf{M})\} + \gamma[\mathbf{M}\mathbf{H}]_k. \tag{8}$$

Here the term in curly brackets defines the relaxation process in the spin system. If we neglect this term, then Eq. (8) coincides in form with the equation of motion of a system of noninteracting magnetic momenta in an external magnetic field. In this latter case, the factor γ has the meaning of a magnetomechanical ratio γ_0. In the presence of interaction in the subsystem, γ is generally different fro n γ_0. The dependence of γ on temperature, which is experimentally observed, does not contradict the thermodynamic calculation.

If we do not take the transfer of heat from the spin system to the "lattice" into consideration, then Eq. (8) describes the change in magnetization with time, brought about by the gyroscopic properties of the magnetic momentum and the process of spin-spin relaxation. In order to introduce time relaxation into Eq. (8), we expand the expression for $\mathbf{H}^*(T, \mathbf{M})$ in a series about the equilibrium state of the spin system. Limiting ourselves to the first powers of $\vartheta = T - T_0$ and $\mathbf{m} = \mathbf{M} - \mathbf{M}_0$ in the expansion, we get

$$\tau_k^T \dot{m}_k + m_k = \chi_k^T h_k + \tau_k^T \gamma[\mathbf{M}\mathbf{H}]_k + (\partial M_k/\partial T)_H \vartheta, \tag{9}$$

where $\mathbf{h} = \mathbf{H} - \mathbf{H}_0$. The isothermal susceptibility χ_k^T is found from the derivatives

$$(\partial H_k/\partial M_k)_T = 1/\chi_k^T;\ (\partial H_k/\partial M_i)_T = 0 \text{ для } i \neq k, \tag{10}$$

taken at the equilibrium position. Here, $\chi_1^T = \chi_2^T = \chi_\perp^T$, $\chi_3^T = \chi_\parallel^T$, and the times of isothermal spin-spin relaxation τ_k^T are determined from

$$\tau_k^T = \chi_k^T/\lambda_k. \quad (11)$$

In the case of an isothermal process in the spin system, $\vartheta = 0$ and Eq. (9) describes the change in magnetization with time, without any additional conditions.

For adiabatic change of the state of the spin system, we find for the time of adiabatic spin-spin relaxation τ_k^S:

$$\tau_k^S = \chi_k^S/\lambda_k, \quad (12)$$

where χ_k^S is the adiabatic susceptibility. It is now easy to find that

$$\tau_k^S/\tau_k^T = \chi_k^S/\chi_k^T = C_M/C_H, \quad (13)$$

where C_H and C_M are the specific heats of the spin system, for constant $\mathbf{H}$ and $\mathbf{M}$, respectively.

3. The quantity of heat dQ transferred to the spin system of the lattice in the time dt we set equal to

$$dQ = \alpha\vartheta dt.$$

Then, by Eq. (3),

$$\dot{\vartheta} + \frac{\vartheta}{\tau_M} = \frac{T_0}{C_M}\left(\frac{\partial \mathbf{H}}{\partial T}\right)_M \dot{\mathbf{m}}, \quad (14)$$

where $\tau_M = C_M/\alpha$ is the time of external, spin-lattice relaxation for constant magnetization. Considering the magnetization $\mathbf{M}$ in Eq. (14) as a function of $\mathbf{H}$ and T, we can put this equation in the form

$$\dot{\vartheta} + \frac{\vartheta}{\tau_H} = \frac{T_0}{C_H}\left(\frac{\partial \mathbf{M}}{\partial T}\right)_H \dot{\mathbf{h}}. \quad (15)$$

Here $\tau_H = C_H/\alpha$ is the time of external, spin-lattice relaxation for constant $\mathbf{H}$.

Eliminating ϑ from Eqs. (9) and (14), after simple transformations, we get the equation for the change in the magnetization with time:

$$\tau_k^T \tau_M \ddot{m}_k + (\tau_H + \tau_k^T)\dot{m}_k + m_k = \tau_M \chi_k^T \dot{h}_k + \chi_k^T h_k + \tau_k^T \tau_M \gamma [\dot{\mathbf{M}}\mathbf{H}]_k + \tau_k^T \gamma [\mathbf{M}\mathbf{H}]_k, \quad (16)$$

which takes into account the internal and the external relaxation.

In order to clarify the role of the spin-lattice relaxation, we rewrite the last equation in the form

$$\tau_H \frac{d}{dt}\{\tau_k^S \dot{m}_k + m_k - \chi_k^S h_k - \gamma\tau_k^S [\mathbf{M}\mathbf{H}]_k\} + \{\tau_k^T \dot{m}_k + m_k - \chi_k^T h_k - \gamma\tau_k^T [\mathbf{M}\mathbf{H}]_k\} = 0. \quad (17)$$

It follows from (13) that if we set $C_H = C_M$, then $\tau_k^S = \tau_k^T = \tau_k$, and therefore Eq. (17) can be written as

$$\tau_H dA/dt + A = 0.$$
$$A = \tau_k m_k + m_k - \chi_k h_k - \gamma\tau_k [\mathbf{M}\mathbf{H}]_k. \quad (18)$$

As is seen from (18), the spin-lattice relaxation in this case appears only in transient processes, since the stationary solution of (18)

$$\tau_k m_k + m_k = \chi_k h_k + \gamma\tau_k [\mathbf{M}\mathbf{H}]_k \quad (19)$$

takes only the spin-spin relaxation into account.

For ferromagnetics below the Curie point,[10] the ratio

$$\frac{C_H}{C_M} = 1 + H_0 \frac{\partial M}{\partial T} \Big/ \left(H_{ex} \frac{\partial M}{\partial T} - C_{dip}\right)$$

differs from unity only in the third decimal place, since the ratio of H_0 to the intensity of the field of exchange forces H_{ex} is of the order 10^{-3}, while the specific heat of the dipole interaction $C_{dip} \ll H_{ex}|\partial M/\partial T|$. Above the Curie point, the ratio

$$C_H/C_M = 1 + CH_0^2 T^{-2}/(CH_{ex}^2 T^{-2} + C_{dip}),$$

where C is the Curie constant, which differs from unity only in the sixth decimal place.

The closeness of the ratio of C_H/C_M to unity is brought about, as follows from what was said above, from the presence in the ferromagnetics of a strong field of exchange forces. Therefore, the specific heat of the spin system is so large that the radiofrequency field at small amplitude does not succeed in raising its temperature in any appreciable amount. As a result, the spin-lattice relaxation effect is shown to be insignificant and practically escapes observation.

On the other hand, in the case $\tau_H\omega_0 \gg 1$, where ω_0 is the resonance frequency, it is seen from (17) that, neglecting the group of terms in the second curly brackets, we obtain the equation

$$\tau_k^S \dot{m}_k + m_k = \chi_k^S h_k + \tau_k^S \gamma [\mathbf{M}\mathbf{H}]_k,$$

which takes into account only the spin-spin relaxation. In similar fashion we obtain, in the other limiting case when $\tau_H\omega_0 \ll 1$:

$$\tau_k^T \dot{m}_k + m_k = \chi_k^T h_k + \tau_k^T \gamma [\mathbf{M}\mathbf{H}]_k.$$

Therefore, for ferromagnetics, the spin-lattice relaxation can exist independently of the magnitude of the ratio C_H/C_M only upon satisfaction of the condition $\tau_H\omega_0 \approx 1$, which usually does not hold.

4. Neglecting the spin-lattice relaxation, we shall start out in what follows from Eq. (8) which, taking (2) into account, can be written in the form

$$\dot{M}_k = \lambda_k \left(H_k - \frac{H^*}{M} M_k \right) + \gamma [\mathbf{MH}]_k. \quad (20)$$

Since $\mathbf{H}^*$ and $\mathbf{M}$ are connected by the equation of state, then, in the approximation assumed,

$$M/H^* = M_0/H_0 = \chi_0, \quad (21)$$

where χ_0 is the static susceptibility and M_0 is the equilibrium magnetization corresponding to the field H_0. Introducing the longitudinal and transverse relaxation times

$$T_\perp = \chi_0/\lambda_\perp; \; T_\parallel = \chi_0/\lambda_\parallel, \quad (22)$$

we rewrite (20), keeping (21) in mind:

$$\begin{aligned} \dot{M}_{x,y} &= \gamma [\mathbf{MH}]_{x,y} - (M_{x,y} - \chi_0 H_{x,y})/T_\perp, \\ \dot{M}_z &= \gamma [\mathbf{MH}]_z - (M_z - \chi_0 H_z)/T_\parallel. \end{aligned} \quad (23)$$

The equations obtained above differ from the Bloch equations (which are applicable in the theory of nuclear magnetic resonances) by the presence of the terms $\chi_0 H_x$ and $\chi_0 H_y$. In ferromagnetic substances, the vector $\mathbf{M}$ in weak radiofrequency fields and even for resonance is close in its direction to $\mathbf{M}_0$, as a consequence of the large width of the absorption lines. Therefore, the components M_x and M_y are small, and it is not possible to neglect the terms $\chi_0 H_x$ and $\chi_0 H_y$. The equations, in a form that coincides with (23), were set up in Ref. 11 for the description of the phenomenon of ferromagnetic resonance.

5. At temperatures far removed from the Curie point ($T < \Theta$), the external field H_i does not appreciably change the magnitude of the vector of spontaneous magnetization $\mathbf{M} = \mathbf{M}_S$, producing only a change in its direction. If we require constancy of the magnitude of the vector $\mathbf{M}$, then it follows from (8) that

$$\sum_{k=1}^{3} \lambda_k M_k (H_k - H_k^*) = 0 \quad (24)$$

whence, by (2),

$$\mathbf{H}^* = \xi (\mathbf{MH}) \mathbf{M}/M^2, \quad (25)$$

where

$$\xi = \left[1 + \left(\frac{\lambda_\parallel}{\lambda_\perp} - 1 \right) \frac{M_z H_z}{\mathbf{MH}} \right] \Big/ \left[1 + \left(\frac{\lambda_\parallel}{\lambda_\perp} - 1 \right) \left(\frac{M_z}{M} \right)^2 \right]. \quad (26)$$

In this case, we can write Eq. (8) in the form

$$\begin{aligned} \dot{M}_{x,y} &= \gamma [\mathbf{MH}]_{x,y} - \lambda_\perp M^{-2} [\mathbf{M} [\mathbf{MH}]]_{x,y} \\ &+ \lambda_\perp (1 - \xi) (\mathbf{MH}) M^{-2} M_{x,y}; \\ \dot{M}_z &= \gamma [\mathbf{MH}]_z - \lambda_\parallel M^{-2} [\mathbf{M} [\mathbf{MH}]]_z \\ &+ \lambda_\parallel (1 - \xi) (\mathbf{MH}) M^{-2} M_z. \end{aligned} \quad (27)$$

For $\lambda_\perp = \lambda_\parallel = \lambda$, Eqs. (28) transform to the Landau-Lifshitz equations, as is seen from Eq. (26). The Landau-Lifshitz equations are widely used in the theory of ferromagnetic resonance. On the other hand, in weak radiofrequency fields, where $\mathbf{h} \ll \mathbf{H}_0$,

$$M_z H_z/\mathbf{MH} \approx 1; \quad M_z^2/M^2 \approx 1$$

the coefficient $\xi \approx 1$, and the equations (27) are simplified:

$$\begin{aligned} \dot{M}_{x,y} &= -\lambda_\perp M^{-2} [\mathbf{M} [\mathbf{MH}]]_{x,y} + \gamma [\mathbf{MH}]_{x,y}, \\ \dot{M}_z &= -\lambda_\parallel M^{-2} [\mathbf{M} [\mathbf{MH}]]_z + \gamma [\mathbf{MH}]_z. \end{aligned} \quad (28)$$

The right side of the equation for $\dot{M}_Z$ is equal to zero in this case; the solutions of Eq. (28) do not contain the constant λ, and coincide with the solutions of the Landau-Lifshitz equation in the case of weak fields for $\lambda_\perp = \lambda$.

If we assume that $\lambda_\perp \neq \lambda_\parallel$, then the difference of (23) from the Landau-Lifshitz equation can exist only in the case of strong radiofrequency fields, where $\xi \neq 1$.

Since the solution of the Landau-Lifshitz equation and Eq. (23) coincide in the case of weak rf fields, and they also coincide with Eq. (27), then the phenomenon of ferromagnetic resonance in weak fields is shown to be very insensitive to the detailed form of the equation employed for their description. Preference for this or that form of the equation can be made only upon observation of nonlinear effects, for example, observation of the change of the z component of the magnetization.

[1] L. D. Landau and E. M. Lifshitz, Phys. Z. Sowjetunion 8, 153 (1935).

[2] F. Bloch, Phys. Rev. **70**, 460 (1946).

[3] R. Wangsness, Phys. Rev. **104**, 857 (1956).

[4] C. J. Gorter, Paramagnetic Relaxation (Elsevier, New York, 1947).

[5] I. G. Shaposhnikov, J. Exptl. Theoret. Phys. (U.S.S.R.) **18**, 533 (1948).

[6] I. G. Shaposhnikov, J. Exptl. Theoret. Phys. (U.S.S.R.) **19**, 225 (1949).

[7] I. G. Shaposhnikov, Uc. Zap. Molotov State Univ., vol. 8, No. 1 (1953).

[8] M. A. Leontovich, Введение в термодинамику (Introduction to Thermodynamics), GITTL, 1956.

[9] S. R. deGroot, Thermodynamics of Irreversible Processes (Interscience, New York, 1951).

[10] N. Bloembergen and S. Wang, Phys. Rev. **93**, 72 (1954).

[11] R. Wangsness and F. Bloch, Phys. Rev. **89**, 728 (1953).

Translated by R. T. Beyer
139

Letters to the Editor

LATERAL DISTRIBUTION FUNCTION OF PHOTONS AT CASCADE SHOWER MAXIMUM

V. V. GUZHAVIN and I. P. IVANENKO

Moscow State University

Submitted to JETP editor November 6, 1957

J. Exptl. Theoret. Phys. (U.S.S.R.) **34**, 746-747 (March, 1958)

In an earlier publication[1] of the authors, the electron lateral distribution function (LDF) was calculated using the moment method. Knowledge of the photon LDF is necessary for analysis of cosmic-ray measurements, especially for interpretation of data on extensive air showers. Molière[2] calculated the photon LDF at the cascade electron-photon shower maximum neglecting ionization losses. Although the calculations of Molière have been often criticized, it can be stated that their result is correct for $r \ll 1$. Eyges and Fernbach[3] calculated the photon LDF by finding graphically a function such that its first few moments coincide with the moments of the required function. The function obtained is correct for $r \gtrsim 1$.

We calculated the photon LDF using the moment method. We made use of the fact that the LDF $N_\Gamma(x_r)$ of photons with energy $> E$ is proportional to $(\ln x_r)/x_r$ for $x_r \to 0$,[2] where $x_r = Er/E_s$, $E_s = 21$ Mev. The function $x_r N_\Gamma(x_r)$ can be approximated by the sum of polynomials

$$x_r N_\Gamma(x_r) = \mathrm{Ei}(-\alpha\sqrt{x_r}) \sum_{n=0}^{N} a_n R_n(\alpha x_r). \qquad (1)$$

where $R_n(\alpha x_r)$ are polynomials orthogonal in the interval $(0, \infty)$ with weight function $\mathrm{Ei}(-\alpha\sqrt{x_r})$. The polynomials $R_n(\alpha x_r)$ and the conjugate orthogonal polynomials $R_n^+(\alpha x_r)$ are determined from the conditions[1]

$$\int_0^\infty x_r^{2n'} \mathrm{Ei}(-\alpha\sqrt{x_r})\, R_n(\alpha x_r)\, dx_r = \begin{cases} \gamma & \text{for } n' = n \\ 0 & \text{for } n' < n, \end{cases}$$

$$\int_0^\infty \mathrm{Ei}(-\alpha\sqrt{x_r})\, R_n(\alpha x_r)\, R_{n'}^+(x_r)\, dx_r = \delta_{nn'}. \qquad (2)$$

The explicit expressions for R_0, R_1, R_2, are

$$R_0(\alpha x_r) = (\gamma/2L_0)\,\alpha^2;$$

$$R_1(\alpha x_r) = (\gamma/2L_1)\,\alpha^6\,[-A_1 + L_0 \alpha\alpha x_r];$$

$$R_2(\alpha x_r) = (\gamma/2L_2)\,\alpha^{10}\,[(A_1A_4 - A_2A_3) - (A_0A_4 - A_2A_2)\,\alpha\alpha x_r + L_1\alpha^2(\alpha x_r)^2], \qquad (3)$$

where

$$L_0 = A_0; \quad L_1 = A_0A_3 - A_1A_2;$$
$$L_2 = A_6L_1 + A_5(A_2A_2 - A_0A_4) + A_4(A_1A_4 - A_2A_3);$$
$$A_n = \Gamma(2 + 2n)/(2 + 2n).$$

Using formulae (3) we obtain the following expressions for the coefficients a_n:

$$a_0 = 1/\gamma; \quad a_1 = (1/\gamma)\,[-L_0^{-1}A_2\alpha^{-4} + \overline{x_\Gamma^2}];$$

$$a_2 = (1/\gamma)\,[L_0^{-1}(A_5A_2 - A_3A_4)\,\alpha^{-8} + L_1^{-1}(A_1A_4 - A_0A_5)\,\alpha^{-4}\overline{x_\Gamma^2} + \overline{x_\Gamma^4}],$$

where $\overline{x_\Gamma^n}$ is the n-th moment of the function $N_\Gamma(x_r)$.

The coefficient α can be found from the condition that the highest moment of the required function in the expansion of Ref. 1 is equal to the corresponding moment of the weight function $\mathrm{Ei}(-\alpha\sqrt{x_r})$.

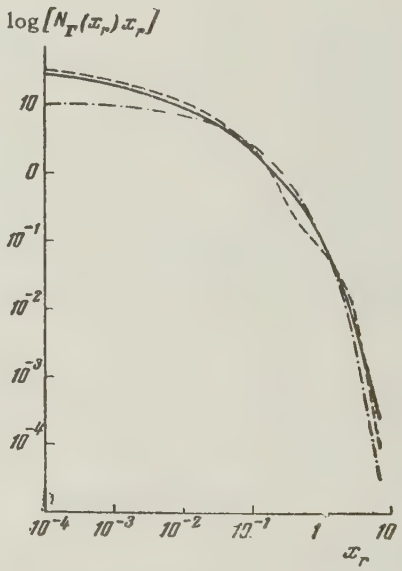

FIG. 1

Results of the calculation of the photon LDF are shown in Fig. 1 (solid curve) where the Molière curve (dashed) is also included. The curves differ by less than 20% up to $x_r \sim 0.1$. It should be noted that the curves are similar up to $x_r \sim 0.01$. For $x_r \sim 1$ the curves differ by a factor of two, but the Molière distribution is already inaccurate in that region. Our curve is shown also in Fig. 2, where the points correspond to calcula-

tions of Eyges and Fernbach. The functions differ by less than 10% for $x_r \sim 1-5$. The photon LDF calculated by us using the first three moments differs from the more accurate function by less than 10%.

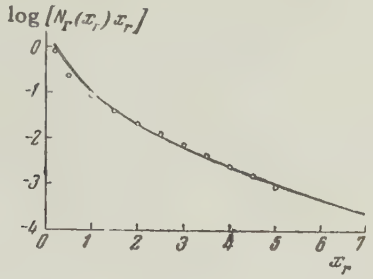

FIG. 2

The electron LDF[1] is also shown in Fig. 1 (dot-dash curve). It should be noted that, even for $x_r = 10^{-4}$ which corresponds to distances of 2×10^{-5} radiation units for particles with energy $\geq 10^8$ ev (i.e. distances < 0.5 cm in air at sea-level), the values of the photon LDF are only three times larger than those of the electron LDF, in spite of the fact that for $x_r \to 0$ the function $x_r N_\Gamma(x_r)$ diverges as $\ln x_r$, while $x_r N_p(x_r)$ remains finite.

[1] V. V. Guzhavin and I. P. Ivanenko, Dokl. Akad. Nauk SSSR **113**, 533 (1957), Soviet Phys. "Doklady" **2**, 131 (1957).

[2] G. Molière, Phys. Rev. **77**, 715 (1950).

[3] L. Eyges and S. Fernbach, Phys. Rev. **82**, 23 (1951).

Translated by H. Kasha
140

MOTION OF ELECTRON ALONG SELF-INTERSECTING TRAJECTORIES

G. E. ZIL' BERMAN

Submitted to JETP editor November 14, 1957

J. Exptl. Theoret. Phys. (U.S.S.R.) **34**, 748-749 (March, 1958)

In Ref. 1 we derived an equation for the motion of an electron with arbitrary law of dispersion $E(k)$ in a magnetic field ($H = H_z$) and obtained (following I. M. Lifshitz and Kosevich[2]) with the aid of the quasi-classical approximation the following equation

$$S(E, k_3) = 2\pi\alpha_0^{-2}(n + 1/2), \quad \alpha_0^2 = \hbar c / eH,$$

for the energy levels of an electron moving in closed trajectories (the intersections of the surface $E(k) = \text{const}$, and the plane $k_3 = \text{const}$). In the present work we shall consider a case when the trajectory has a form of a closed self-intersecting curve ("figure eight"). However, the consideration given below pertains also to the case when the "figure eight" has a narrow neck and when it breaks up into two closed regions.

Near the point of self-intersection it is impossible to employ the quasi-classical approximation. For the region near such a point (where the trajectory can be represented by two hyperbolas, which degenerate into straight lines upon exact self-intersection), it is necessary to write the exact solution. A similar problem was solved in Ref. 3. It turns out that near the point of self-intersection the exact solution is expressed in terms of degenerate hypergeometric functions, similar to the manner in which the solution near the point of the classical turn is expressed in terms of the Airy functions. The "joining" of the quasi-classical solution (away from the point of self-intersection) and the exact solution (in the vicinity of this point) gives a quantization condition in the form

$$S = 4\pi\alpha_0^{-2}(n + 1/2 + \gamma_{1,2}(\lambda)); \tag{1}$$

here S is the total area of the curve, $\gamma_{1,2}(\lambda)$ are functions, to be determined below, of the quantity

$$\lambda = (\varkappa_0/\varepsilon)^2 \sqrt{R/\varkappa_0}, \tag{2}$$

where $\kappa_0 = \kappa_{10} a_1$, κ_{10} is the value of κ_1 at the boundary (for exact self-intersection $\kappa_{10} = 0$), $\epsilon = a/\alpha_0$, R is the radius of curvature of the trajectory at the point of self-intersection ($\sqrt{\kappa_0/R}$ is the slope of the tangent at the point of self-intersection for $\kappa_{10} = 0$, or the slope of the asymptote of the hyperbola in the case of inexact self-intersection). The quantities γ_1 and γ_2 are determined in the following manner

$$\gamma_1 = -\frac{1}{8} - \varphi_1 - \frac{\lambda}{4}\ln\left|\frac{\lambda}{4e}\right|, \quad \gamma_2 = -\frac{1}{8} - \varphi_2 - \frac{\lambda}{4}\ln\left|\frac{\lambda}{4e}\right|,$$
$$R_1 e^{i\varphi_1} = 1/\Gamma\left(\frac{1}{4} + i\,\frac{\lambda}{4}\right), \quad R_2 e^{i\varphi_2} = e^{-i\pi/4}/\Gamma\left(\frac{3}{4} + i\,\frac{\lambda}{4}\right) \tag{3}$$

In order to gain an idea of the splitting of the energy levels upon gradual deformation of the "figure eight," it is enough to consider the following cases.

(1) When $\lambda < 0$ and $|\lambda| \gg 1$, corresponding to two individual regions (κ_{10} is imaginary), $\gamma_1 = \gamma_2 = 0$. Then the area of each region is determined by the usual equation $S = 2\pi\alpha_0^{-2}(n + 1/2)$, and the total area is

$$S = 4\pi\alpha_0^{-2}(n + 1/2) \tag{4}$$

(2) When $\lambda = 0$ (exact self-intersection, $\kappa_{10} = 0$), $\gamma_1 = -\gamma_3 = 1/8$. In this case the area of the entire curve is expressed by the formula

$$S = 4\pi\alpha_0^{-2}(n + 1/2 \pm 1/8). \quad (5)$$

Both levels, corresponding to a given value of n, are separated by a distance that is one quarter as small as that of the levels corresponding to neighboring n and equal γ. The levels are thus equidistant in pairs.

(3) When $\lambda \gg 1$ (wide neck, κ_{10} large), $\gamma_1 = -\gamma_2 = 1/4$. Formula (1) for the total area now becomes $S = 4\pi\alpha_0^{-2}(n + 1/2 \pm 1/4)$, which can also be written in the usual form

$$S = 2\pi\alpha_0^{-2}(n + 1/2). \quad (6)$$

The levels are again equidistant, but at distances half as small than in the case of two individual regions [formula (4)]. The levels are no longer equidistant when the curve is nearly self-intersecting and the conditions for the applicability of the quasiclassical approximation are no longer satisfied.

Let us consider the de Haas — van Alphen effect for trajectories with self intersection. The first two (most significant) terms of the oscillating portion of the number of electron states (with energy from 0 to E) will be of the form

$$\sin\left(\frac{1}{2}\alpha_0^2 S_m - \frac{\pi}{4}\right)\cos 2\pi\gamma_m$$
$$\frac{1}{2\sqrt{2}}\sin\left(\alpha_0^2 S_m - \frac{\pi}{4}\right)\cos 4\pi\gamma_m; \quad (7)$$

S_m is the extremal value of the area, and γ_m is the corresponding value of γ.

When $\gamma = 0$ (two individual regions), the oscillation takes place with a frequency corresponding to the cross-section area of the individual region. Then, as γ increases (merging of the regions and formation of one common region), the first term diminishes and the term with double the frequency starts assuming an ever increasing role. When $\gamma = 1/4$ (merging regions), the first term vanishes, i.e., the frequency of oscillations already corresponds to the total area of the curve.

The author takes this opportunity to thank I. M. Lifshitz for discussion of this work.

[1] G. E. Zil'berman, J. Exptl. Theoret. Phys. (U.S.S.R.) **32**, 295 (1957), Soviet Phys. JETP **5**, 208 (1957).

[2] I. M. Lifshitz and A. M. Kosevich, Dokl. Akad. Nauk SSSR **96**, 963 (1954); J. Exptl. Theoret. Phys. (U.S.S.R.) **29**, 730 (730 (1955), Soviet Phys. JETP **2**, 636 (1955).

[3] G. E Zil'berman, J. Exptl. Theoret. Phys. (U.S.S.R.) **33**, 387 (1957), Soviet Phys. JETP **7**, 299 (1958).

Translated by J. G. Adashko
141

ANGULAR DISTRIBUTION IN THE REACTIONS $K^+ \to 2\pi^+ + \pi^-$ *and* $K^+ \to 2\pi^0 + \pi^+$

V. N. GRIBOV

Leningrad Physico-Technical Institute, Academy of Sciences, U.S.S.R.

Submitted to JETP editor November 19, 1957

J. Exptl. Theoret. Phys. (U.S.S.R.) **34**, 749-751 (March, 1958).

BY angular distribution we shall understand the dependence of the disintegration probability on the angle ϑ between the relative momentum of the identically charged π mesons $\mathbf{k}_{12} = \mathbf{p}_1 - \mathbf{p}_2$ and the momentum of the third meson $\mathbf{p}_3$.

As is known,[1,2] neglecting the interaction of the π mesons in the final state, the matrix elements for both decays do not depend on ϑ with an accuracy up to terms $\sim k_{12}^2 p_3^2$, since the angular momenta ℓ, L (Refs. 1 and 2) can assume the values $\ell = L = 0, 2, 4, \ldots$, and the contribution of the corresponding states to the matrix elements are $\sim k_{12} p_3$. The latter is due to the fact that the particles in states with $\ell, L \neq 0$, in order to leave the region of their creation, have to overcome the centrifugal barrier, whose penetration coefficient is proportional to $k_{12}^{\ell} p_3^{\ell}$.

However, in the presence of interaction the particles can go into a state with $\ell, L \neq 0$ and give a contribution to the angular distribution without passing the centrifugal barrier. This case arises when the particles, created in a state with $\ell = L = 0$, leave the region of their creation, whereupon one of the pairs of particles 1 and 3 or 2 and 3 gets close and interacts. In such an interaction the angular momenta ℓ and L are not conserved, but the total angular momentum is conserved. This makes possible the transition from a state with $\ell, L = 0$ to a state $\ell, L \neq 0$ with the same total angular momentum. It can be shown[3] that the am-

plitude of such a transition is determined by the amplitudes of the scattering of the pairs of particles from each other and is proportional to $\sqrt{E}$ (E is the relative kinetic energy of three π mesons) for transitions into states with arbitrary, possible l and L. For sufficiently small energy, the contribution of these processes to the angular distribution is thus more important than the direct passage through the centrifugal barrier. In this case the angular distribution is determined not by the specific character of the disintegration interaction, but by the amplitudes for the scattering of one π meson from another.

In order to find the angular distribution in this case, it is sufficient to know the wave functions of the system of three π mesons in the small region of radius r_0 where the particles are created. It is shown in Ref. 3 that $\psi(2\pi^+, \pi^-)$ can in this region be written, for example, in the form

$$\psi(2\pi^+, \pi^-) = \left\{1 - ik_{12}a_2 - \frac{i}{3}(k_{12}+k_{23})(a_2+2a_0) + J\frac{\varkappa^2}{9}(5a_2^2+11a_2a_0+2a_0^2)\right\} f^{(-)} + \left\{-\frac{i}{3}(k_{13}+k_{23})(a_2-a_0) + J\frac{\varkappa^2}{9}(13a_2^2-11a_2a_0-2a_0^2)\right\} f^{(+)} + O(\varkappa^2) + O(\varkappa^3); \quad (1)$$

$f^{(-)}, f^{(+)}$ are the wave functions of the systems $(2\pi^+, \pi^-)$ and $(2\pi^0, \pi^+)$, respectively, at zero energy; a_0, a_2 are the amplitudes for the scattering of a π meson from a π meson at zero energy in states with isotopic spin 0 and 2; J is a known function of k_{12}/κ and ϑ; $\kappa = \sqrt{m_\pi E/\hbar}$. An analogous formula holds for $\psi(2\pi^0, \pi^-)$. With the help of these formulae, the matrix elements for both disintegrations can be expressed through the matrix elements at zero energy $\langle f^{(\mp)}|\hat{W}|\psi_{K^+}\rangle$ and the amplitudes a_2 and a_0.

The result of raising the respective expressions to the second power depends essentially on whether or not "time-parity" is conserved in these disintegrations. If "time-parity" is conserved then the $\langle f^{(\mp)}|\hat{W}|\psi_{K^+}\rangle$ are real. In this case the angular distribution differs from a spherically symmetric one only by terms of order κ^2, inasmuch as the terms of first order in 1 are purely imaginary. Using an approximation to the expression for J, limiting oneself to lowest powers in $\cos\vartheta$, and integrating over the energy of the third particle, one obtains for the disintegration probabilities the expressions

$$dW^{(-)}(\vartheta) = W^{(-)}\{1+\cos^2\vartheta\,(mE/\hbar^2)\,[0.07a_2^2 + 0.1a_2a_0 - 0.07a_0^2 + \rho(0.25a_2^2 - 0.32a_2a_0 + 0.07a_0^2) + 0.03(a_2-a_0)^2\rho^2]\}\,d\cos\vartheta,$$

$$dW^{(+)}(\vartheta) = W^{+}\{1+\cos^2\vartheta\,(mE/\hbar^2)\,[0.1a_2^2 + 0.03a_2a_0 + 0.03a_0^2 + \rho^{-1}(0.12a_2^2 - 0.17a_2a_0 + 0.05a_0^2)]\}\,d\cos\vartheta;$$

$$\rho = W^-/W^+.$$

If "time-parity" is not conserved the $\langle f^{(\pm)}|\hat{W}|\psi_{K^+}\rangle$ are complex. In this case the angular and energy distribution changes already in terms of first order of κ. In this case, taking into account only terms of first order, we obtain for the absolute squares of the matrix elements the expressions

$$|\langle\psi(2\pi^+, \pi^-)|\hat{W}|\psi_{K^+}\rangle|^2 = W^-\{1-(2\rho/3)(k_{13}+k_{23})(a_2-a_0)\sin\varphi\},$$

$$|\langle\psi(2\pi^0, \pi^+)|\hat{W}|\psi_{K^+}\rangle|^2 = W^+\{1-(4/3\rho)k_{12}(a_2-a_0)\sin\varphi\};$$

φ is the relative phase of $\langle f^{(+)}|\hat{W}|\psi_{K^+}\rangle$ and $\langle f^{(-)}|\hat{W}|\psi_{K^+}\rangle$.

In all the preceding formulae, the π mesons are taken to be nonrelativistic. In order to take into account the relativistic corrections it is sufficient to change in the final formulae, the angle ϑ to the angle ϑ' between the momentum p_3 and the relative momentum of the identically-charged π mesons in the system of their center of mass.

[1] R. Dalitz, Phil. Mag. **44**, 1068 (1953); Phys. Rev. **94**, 1046 (1954).

[2] E. Fabri, Nuovo cimento **11**, 479 (1954).

[3] V. N. Gribov, Nucl. Phys. **5**, 653 (1958).

Translated by R. Lipperheide
142

USE OF MOVING HIGH-FREQUENCY POTENTIAL WELLS FOR THE ACCELERATION OF CHARGED PARTICLES

A. V. GAPONOV and M. A. MILLER

Gorkii State University

Submitted to JETP editor November 25, 1957

J. Exptl. Theoret. Phys. (U.S.S.R.) **34**, 751-752 (March, 1958).

THE motion of charged particles (charge e, mass m, $e/m = \eta$) in high-frequency electromagnetic fields $\mathbf{E}(\mathbf{r})e^{i\omega t}$, $\mathbf{H}(\mathbf{r})e^{i\omega t}$ may be approximately represented as small oscillations $\mathbf{r}_1 = -(\eta/\omega^2)\mathbf{E}(\mathbf{r}_0)e^{i\omega t}$ relative to a comparatively slowly-varying mean position $\mathbf{r}_0(t)$. In the non-

relativistic case, the coordinate $\mathbf{r}_0(t)$ satisfies the equation[1]

$$\ddot{\mathbf{r}}_0 = -\nabla\Phi(\mathbf{r}_0); \quad \Phi(\mathbf{r}_0) = (\eta/2\omega)^2 |\mathbf{E}|^2. \qquad (1)$$

As previously shown,[1] absolute minima of the potential $\Phi(\mathbf{r}_0)$ exist in heterogeneous fields of definite configuration. Localization of particles with charge of any sign is possible in the potential wells that correspond to these minima. Upon using oscillations with various frequencies we obtain, generally speaking, a time-varying potential contour $\Phi(\mathbf{r}_0, t)$. In such a manner we may, in particular, bring about accelerated motion of the potential wells and, as a result, produce acceleration of the charged particles localized therein.[2]

We consider two cylindrical waves, progressing in opposite $(\pm z)$ directions. If their frequencies and amplitudes are identical, they form a standing wave $\mathbf{E}_0(x,y,z)e^{i\omega t}$, where $\mathbf{E}_0(x,y,z)$ is a real function. Let the structure of this field be such that the potential corresponding to it, $\Phi_0 = (\eta/2\omega)^2 |\mathbf{E}_0(x,y,z)|^2$, has absolute minima (for example, a wave of type TM_{01} in a circular waveguide, of type TM_{11} in a rectangular waveguide, etc.). For a displacement of the potential wells along z it is necessary to change the phase of one wave from its opposite; in particular, their displacement with constant velocity v_0 is brought about when two waves with different frequencies $\omega_{1,2} = \omega_0 \pm \Delta\omega$ are combined. Limiting ourselves to nonrelativistic motion $(|\Delta\omega| \ll \omega_0)$ and neglecting the difference in field structure of the opposing waves, we obtain for the total field

$$\mathbf{E} = \mathbf{E}_0(x, y, z - v_0 t)\, e^{i(\omega t - z\Delta h)}, \qquad (2)$$

where $2\Delta h = h(\omega_1) - h(\omega_2)$, and $h(\omega)$ is the propagation constant. The potential Φ corresponding to this field has the form $\Phi = \Phi_0(x, y, z - v_0 t)$. The displacement velocity of the potential wells

$$v_0 = 2\Delta\omega / [h(\omega_1) + h(\omega_2)] \qquad (3)$$

turns out to be proportional to the difference in frequencies of the opposing waves, so that the capture and consequent acceleration of a particle is brought about by varying the frequency of the generator which excites one of the waves.

In the case of a relativistic velocity v_0, the potential wells (in the accompanying frame of reference) are somewhat deformed. However, as before, their displacement velocity is determined by the relationship (3).

Inasmuch as in the accompanying frame of reference an accelerated particle is at all times oscillating with the frequency of the external field, the effectiveness of such an accelerator is less than that of the usual linear one. In fact, the ratio of the "actual field" $(\nabla_z\Phi)/\eta$ to the corresponding field in a linear accelerator with identical value of permissible intensity E_{max} is equal to

$$\eta^{-1} |\nabla_z\Phi| / E_{max} \approx h\eta E_{max} / 2\omega^2 = {}^1/_2 h |\mathbf{r}_1|_{max} \ll 1.$$

However, an accelerator with high-frequency potential wells does have definite advantages. First of all, the application of transverse magnetic waves (TM), which give rise to three dimensional potential wells, obviates the necessity for supplementary focusing of the particles in the transverse plane. Furthermore, since the effect of the capture and acceleration of particles does not depend on the sign of their charge, it is possible to apply this principle for the acceleration of quasi-neutral plasma bunches. Finally, the utilization of waves with any phase velocity, both greater and smaller than the velocity of light, is permissible. Consequently, instead of periodic structures, application of the customary smooth waveguides is allowed. It certainly follows by implication that in such a waveguide, as immediately apparent from (3), the equality $v_0 = c$ is unattainable.

In conclusion, we note that in the presence of a supplementary focusing magnetic field (H_z = const) in the accelerator, waves of the transverse electric type (TE and TEM) may be applied. In this case the expression for the potential Φ will have the form

$$\Phi = |\mathbf{E}|^2\eta^2 / 4(\omega^2 - \omega_H^2); \quad \omega_H = |\eta| H_z/c.$$

---

[1] A. B. Gaponov and M. A. Miller, J. Exptl. Theoret. Phys. (U.S.S.R.) **34**, 242 (1958), Soviet Phys. JETP **7**, 168 (1958).

[2] M. A. Miller, On the Focusing of Electron Bundles by means of High-Frequency Fields, delivered at the Second All-Union Conference of the Ministry for the Advanced Study of Radioelectronics, Saratov (1957).

Translated by J. S. Wood
143

FISSION OF U^{238}

M. N. NIKOLAEV, V. I. GOLUBEV, and I. I. BONDARENKO

Submitted to JETP editor November 25, 1957

J. Exptl. Theoret. Phys. (U.S.S.R.) **34**, 752-754 (March, 1958)

In connection with the problem of the operation of many types of nuclear reactors, it becomes interesting to study the fission of U^{238} by fission neutrons in large masses of uranium. In this work we describe measurements, performed in 1954, of the total number D of fissions of U^{238}, that take place in an infinite block of uranium when a single fission neutron is admitted into the block.

The experiment was set up in the following manner. A disc of U^{235} ("converter") was placed in the center of a hollow sphere of natural uranium (outer radius 25 cm, inner radius 5 cm). A collimated beam of thermal neutrons, from the reflector of the reactor of the atomic electric station, was aimed at the converter, which served as a source of fission neutrons.

A system of shields made of cadmium and boron prevented the thermal neutrons from entering inside the uranium sphere. The effect of the neutrons over the cadmium was eliminated by measurements in which the neutron beam was covered with a sheet of cadmium. A vertical channel filled with uranium inserts was drilled through the upper hemisphere, and detectors could be placed between the inserts.

The detector employed were flat fission chambers with layers of natural and enriched uranium. Comparison of the counts of these chambers in an identical flux of thermal neutrons made it possible to calculate the distribution of fissions of U^{238} and U^{235} from the measured distributions.

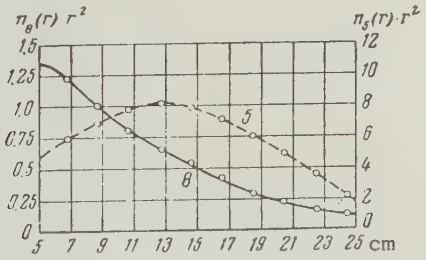

The diagram shows the distributions obtained in this manner. For convenience, the ordinates represent the quantities $n(r)r^2$. The values of these quantities, measured in the absence of a uranium sphere, are taken to be unity. During these measurements, the positions of the converter and of the shields remained the same as before. Were the uranium sphere used in these experiments infinitely thick and consisting of pure U^{238}, the value of D would satisfy the equation

$$D = N\sigma_{f8}\int_{r_0}^{\infty} n_8(r)\,r^2\,dr, \qquad (1)$$

where M is the number of nuclei per cm^3, $n_8(r)$ is the distribution of U^{238} fissions normalized in the manner indicated above, σ_{f8} the cross section for the fission of U^{238} by the fission neutron. The latter quantity was taken to be 0.31 ± 0.01 barns, a value previously obtained.*

Actually, in order to determine D it is necessary to take into account the fission of the U^{235} contained in the sphere, and the number of neutrons capable of fissioning U^{238} which may leak from the sphere. Corrections for these effects, which do not play an important role in our problem, were introduced by using the measured distribution of the U^{235} fissions and the value of the leakage, which was measured by means of an effective fission chamber with layers of U^{238}; the chamber was located at a large distance from the sphere.

The value of D was thus found to be 0.17 ± 0.01. Knowing D, it is possible to determine k_∞ for pure U^{238}:

$$k_\infty = D\nu_8/(1 + D\nu_8), \qquad (2)$$

where ν_8 is the average number of neutrons, liberated by fission of U^{238}. Taking $\nu_8 = 2.85 \pm 0.06$ (Ref. 2), we obtain $k_\infty = 0.325 \pm 0.011$.

If the distribution of the neutrons, capable of fissioning U^{238}, is expressed in terms of the Peierls single-group kinetic equation, D will be related to the known parameters α and β of this equation by

$$D = \sigma_{f8}N/(\alpha - \beta). \qquad (3)$$

Using this relation and selecting one of the parameters such as to make the experimental distribution of the U^{238} fissions in the sphere fit best the values calculated by means of an exact solution of the kinetic equation, it is possible to determine the parameters α and β. Thus, we obtained $\alpha = 0.201 \pm 0.007$ and $\beta = 0.115 \pm 0.004$. The distribution of the U^{238} fissions, calculated with the aid of these parameters, is shown on the diagram (solid curve).

The procedure employed in these experiments can be used for the measurement of the transport parameters of various substances at various energies. For example, we placed a source of 0.8 —

1.0 photoneutrons (Na — Be) in the center of a uranium sphere, measured the distribution of the Np^{237} fissions, and were able to determine the transport parameters of U^{238} for a group of neutrons with energies 0.5 — 1.0 Mev. The values obtained in this case were $\alpha = 0.22 \pm 0.01$ and $\beta = 0.187 \pm 0.008$.

*This value is in excellent agreement with the results of measurements made by Leachman and Schmitt[1] (0.307 ± 0.005 barns).

[1] R. B. Leachman and H. W. Schmitt, J. Nucl. Energy **4**, 38 (1957).

[2] Kuz' minov, Kutsaeva, and Bondarenko, Атомная энергия (Atomic Energy) (in press).

Translated by J. G. Adashko
144

CONCERNING THE SYNTHESIS OF THE SHAPE OF THE FERMI SURFACE IN METALS

M. Ia. AZBEL'

Physico-Technical Institute, Academy of Sciences, Ukrainian S.S.R.

Submitted to JETP editor November 26, 1957

J. Exptl. Theoret. Phys. (U.S.S.R.) **34**, 754-755 (March, 1958)

THE synthesis of the shape of the Fermi surface $\epsilon(\mathbf{p}) = \epsilon_0$ (where ϵ and $\mathbf{p}$ are the energy and quasi momentum of the conduction electron, and ϵ_0 is the limiting Fermi energy) from the experimental results is a task of great importance to the theory. I. M. Lifshitz and A. V. Pogorelev proposed[1] a method of such a synthesis from the extremal areas S_{ext} of the cross-sections of the Fermi surface. These areas can be determined from the periods of the oscillations of the magnetic susceptibility χ in the de Haas — van Alphen effect.

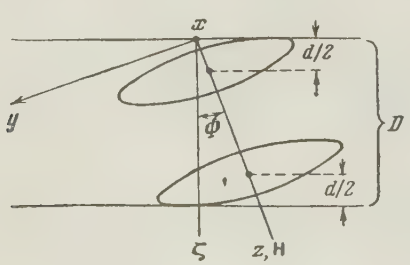

As a rule, however, harmonic analysis of the experimental curves of $\chi(H)$ is a rather difficult task, owing to the large number of harmonics. In this work we propose a method whereby S_{ext} and the radius vector of the surface $\mathbf{p}$ can be determined directly as a function of the direction $\mathbf{p}/p$ for various harmonics.

Let us examine the de Haas — van Alphen effect in a film in a constant magnetic field oriented in an arbitrary manner.

For brevity we shall assume that the Fermi surface is a single closed convex surface. Then, if the orbit corresponding to the central cross-section "is not contained" in a film of thickness D, i.e.,

$$D < d = \left| \int_{t_0'}^{t_0''} v_\zeta \, dt_2 \right|_{p_z=0,\ \varepsilon=\varepsilon_0} = \left| \cos\Phi \int_{t_0'}^{t_0''} v_z \, dt_2 + \sin\Phi \frac{2cp_x^{max}}{|eH|} \right|_{p_z=0,\ \varepsilon=\varepsilon_0},$$

$$v_\zeta(t_0') = v_\zeta(t_0'') = 0; \quad v_\zeta'(t_0') < 0; \quad v_\zeta'(t_0'') > 0$$

(t is the time of one electron revolution in the orbit, $\mathbf{v} = \nabla_p \epsilon$ is the electron velocity, and the other symbols are as indicated in the diagram), then all the electrons collide with the surface, and the amplitude of the quantum oscillations of χ is proportional to at least the second power of $\mu H/\epsilon_0$ (where μ is the Bohr magneton for the conduction electron. The second power is obtained under the case which is most favorable in this sense, namely of specular reflection of the electrons from the surface — see Ref. 2.)

If, however, the orbit corresponding to the central cross-section "is contained" in the film (D > d), with

$$(l/D)\cos\Phi\,(\mu H/\varepsilon_0)^{1/2} \ll 1$$

(ℓ is the mean free path of the electrons), then the electrons corresponding to the central cross section and contributing to the quantum oscillations will not collide with the surface. They satisfy the relation

$$\bar{v}_z(p_z) \approx \bar{v}_z(0) + \bar{v}_z'(0)\, p_z \sim v\,(\mu H/\varepsilon_0)^{1/2}.$$

Their energy spectrum coincides in the quasi-classical case with the spectrum in the bulk metal, and the amplitude of the corresponding quantum oscillations is proportional, as can be readily seen, to $(\mu H/\epsilon_0)^{3/2}$. In this case the magnetic moment differs from the magnetic moment of the bulk metal[3] only in that instead of D the formulas contain D − d, corresponding to those electrons

which do not collide with the surface. In a magnetic field parallel to the surface, the formula for the magnetic moment, for any kind of reflection from the surface, coincides with formula (14) of the work by Kosevich and Lifshitz.[4]

Consequently, if one investigates $\chi_q(H)$ in a film with $D < \ell$, then, by determining the successive values of the magnetic field H for which there are sharp increases in the quantum oscillations with a given period, for all possible directions of H, we determine d and S_{ext} for each of the surfaces individually (we mean here the closed surfaces into which $\epsilon(p) = \epsilon_0$ is resolved), without resorting to harmonic analysis. (The applicability of the above arguments to this case is obvious.)

The values of $d = D$ in a parallel field make it possible to determine

$$p_x^{max} = |eHD|/2c$$

for the central cross-section of the above surfaces, at all directions x in the plane of the film, i.e., to construct directly all the cross-sections $\epsilon(p) = \epsilon_0$ and $p_y = 0$. A set of monocrystallographic films with a varying orientations of the crystallographic axes relative to the surface would make it possible to plot $\epsilon(p) = \epsilon_0$.

The values of S_{ext}, as already indicated, also make it possible to synthesize the Fermi surface by the Lifshitz-Pogorelov method.

[1] I. M. Lifshitz and A. V. Pogorelov, Dokl. Akad. Nauk SSSR **96**, 1143 (1954).

[2] I. M. Lifshitz and A. M. Kosevich, Izv. Akad. Nauk SSSR, ser. fiz. **19**, 395 (1955).

[3] I. M. Lifshitz and A. M. Kosevich, Dokl. Akad. Nauk. SSSR **96**, 963 (1954); J. Exptl. Theoret. Phys. (U.S.S.R.) **29**, 730 (1955), Soviet Phys. JETP **2**, 636 (1956).

[4] A. M. Kosevich and I. M. Lifshitz, I. M. Lifshitz, J. Exptl. Theoret. Phys. (U.S.S.R.) **29**, 743 (1955), Soviet Phys. JETP **2**, 646 (1956).

Translated by J. G. Adashko
145

CALORIMETRIC DETERMINATION OF THE HALF-LIFE OF Ra^{226}

G. V. GORSHKOV, Z. G. GRITCHENKO, and N. S. SHIMANSKAIA

Radium Institute, Academy of Sciences, U.S.S.R.

Submitted to JETP editor December 6, 1957

J. Exptl. Theoret. Phys. (U.S.S.R.) **34**, 756-757 (March, 1958)

In the determination of the half-lives of long-lived isotopes by the calorimetric method, one measures the thermal effect Q of the radioactivity of a known weight p of a given isotope. The half-life T is determined from the relation $T = (\ln 2) \cdot pN_0\epsilon/AQ$, where N_0 is Avogadro's number, A the atomic weight of the isotope, and ϵ the energy liberated by the isotope in the calorimeter in a single decay event. The decay constants of Pu^{239} (Ref. 1) and Ac^{227} (Ref. 2) were measured relatively recently by such a calorimetric method.

Many investigators have used this method to determine T for Ra^{226}. They measured the thermal effect of radium, either free of its short-lived derivatives[3] or in equilibrium with these derivatives.[4,5] Unfortunately, the Ra contents in the measured compounds was determined in these investigations indirectly, usually on the basis of γ measurements. In addition, for the most part, the accuracy of the calorimetric measurements themselves was insufficient (1—4%), as was the accuracy with which ϵ was calculated for the elements of the Ra^{226} series.

We made precise calorimetric measurements of three equilibrium compounds of radium, subjected to 10 (Ra I, Ra II) and 15 (Ra III) additional crystallizations to eliminate possible contaminations. The purity of these compounds was controlled by means of a spectral method, which detected the presence of only insignificant impurities of certain elements of the second group of the periodic table.[6] The total contamination α did not exceed, in all three cases, 0.2% (by weight).

The results of direct weighing of radium bromide before sealing the compounds, and the Ra^{226} content in these compounds, are given in the table. The table lists also the results of the calorimetric measurements performed with the aid of a double static calorimeter.[9] The last column of the table gives the determined values of $Q_{\alpha+\beta}/p$ — the thermal effect of α- and β-radiation per gram of radium. In the calculation of these quantities, account is taken of the absorption of γ-rays in the compound itself (self absorption), in the protective container, in the glass of the ampoules, and in the walls of the calorimetric cylinder itself.

The increasing thermal effect due to accumulation of Po^{210} and RaE in the compounds was also accounted for.

Compound	Weight of salt, mg	Weight of Ra, mg	Thermal effect mcal/hr	Thermal effect of 1 g of Ra, mcal-hr
Ra I	274.8	160.7	20.96	129.2
Ra II	305.8	178.8	23.19	129.9
Ra III	256.3	149.9	19.55	129.9
				129.7

On the basis of the latest experimental data on α and β spectra of the elements of the radium series, we calculated ϵ for the equilibrium compound Ra^{226}. It turned out to be 25.335 Mev ($\pm 0.3\%$). Using this value, we obtained for the half-life of Ra^{226} a value $T = 1577 \pm 9$ years. This gave respectively for a value $z = 3.71 \pm 0.02 \times 10^{10}$ decays/sec-g, the specific activity z. The latter is connected with T by the simple relation $z = 1.847 \times 10^{21}/T$.

The values of z and T we determined are close to those adopted by the International Commission[8] ($z = 3.70 \times 10^{10}$, $T = 1580$ years), but differ noticeably from the values recently obtained by Kohman, Ames, and Sedlet[9] and Sebaoun[10] ($z = 3.61 - 3.62 \times 10^{10}$ ($\pm 0.5 - 0.6\%$); $T = 1617 - 1622$ years). In these two investigations the number of particles emitted by the equilibrium[10] or non-equilibrium[9] radium compound was measured directly. To explain the causes of such a discrepancy, it would be desirable to repeat the determination of these important quantities z and T of Ra^{226}, using the above methods as well as other possible methods.

[1] J. Stout and W. Jones, Phys. Rev. 71, 582 (1947).

[2] N. S. Shimanskaia and E. A. Iashugina, Атомная энергия (Atomic Energy) 1, 133 (1957).

[3] V. Hess, Wien. Ber. IIa, 121, 1419 (1912).

[4] S. Watson and M. Henderson, Proc. Roy. Soc. A118, 318 (1928).

[5] G. V. Gorshkov and N. S. Shimanskaia, Атомная энергия (Atomic Energy) 1, 86 (1956).

[6] Z. Gritchenko and T. Il'inskaia, Фонд РИАНа, Отчет 1957 (Fund of Radium Inst. Acad. Sci., Report for 1957).

[7] N. S. Shimanskaia, Тр. Радиевого ин-та (Trans. Radium Inst.) 7, 198 (1956).

[8] Curie, Debiern et al., Revs. Mod. Phys. 3, 427 (1931).

[9] Kohman, Ames, and Sedlet, NNES PPR V14B PII, 1657 (1949).

[10] W. Sebaoun, Ann. phys. 1, 680 (1956).

Translated by J. G. Adashko
146

ROLE OF INTERELECTRON COLLISIONS IN METALS IN THE INFRARED REGION OF THE SPECTRUM

G. P. MOTULEVICH and A. A. SHUBIN

P. N. Lebedev Physics Institute, Academy of Sciences, U.S.S.R.

Submitted to JETP editor December 7, 1957

J. Exptl. Theoret. Phys. (U.S.S.R.) 34, 757-758 (March, 1958)

As is known, the contribution of interelectron collisions to the value of the surface impedance of the metal is insignificant in the low-frequency region. However, as the frequency increases, this contribution increases, as was already noted, for example, in Ref. 1. Calculations pertaining to the infrared region of the spectrum were made by Pitaevskii[2] and Gurzhi.[3] It follows from these calculations that the interelectron collisions lead to the appearance of an additional term of the form B/λ^2 in the real part of the surface impedance. Here B is a factor that is independent of the wavelength of the light λ. The measurements we performed on the optical constants of silver[4] show that this additional term is substantial in the spectral region we investigated ($1 - 6\mu$). The diagram shows the dependence of the real part of the surface impedance R on λ. The dots indicate the experimental data for cR/π. The solid line represents the curve of $(c/\pi)(R_0 + B/\lambda^2)$ for $(c/\pi)R_0 = 0.96 \times 10^{-2}$ and $(c/\pi)B = 1.40 \times 10^{-2}\mu^2$. Here R_0 and B are independent of λ, and c is the velocity of light. It can be seen that the experimental points fit the solid curve well (diagram). A measurement of the real part of the surface impedance in the infrared region of the spectrum, using the same method, makes it possible to clarify the role of the interelectron collisions.

For silver, as follows from the experimental data,[4] the spectral region $1 - 6\mu$ is subject to the inequalities $\omega_0^2 \gg \omega^2 \gg \nu_0^2$, where ω_0 is the limit

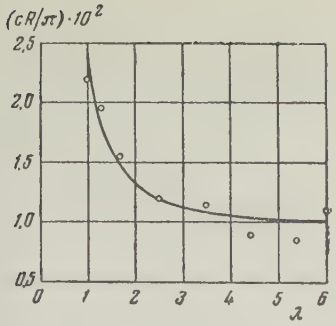

Dependence of real part of surface impedance of silver on the wavelength. Abscissa – $cR/\pi = 4n/(n^2 + \kappa^2)$, where $n - i\kappa$ is the complex index of refraction of the metal.

of the internal photoeffect, ω the frequency of the light, and ν_0 the frequency of the collisions between the electrons and the lattice. Therefore, making the important assumption that the Fermi surface is isotropic, we can determine the concentration of the conduction electrons M and the electron velocity v on the Fermi surface by using the expressions obtained for a clearly pronounced anamolous skin effect.[1] Here the reflection of the electrons from the surface of the metal is assumed to be diffuse. We have already determined N earlier, using our measurement data, (for silver $N = 5.2 \times 10^{22}\,cm^{-3}$); allowance for the term due to the interelectron collisions makes it possible to employ the quantity R_0 for the determination of v. We obtained $v = 2.4 \times 10^8$ cm/sec for silver.

Measurements of the optical constants of tin and lead in the spectral region $1 - 6\,\mu$ has shown that the contribution of the interelectron collisions to the real part of the surface impedance is substantial for these metals, too. However, the processing of the results obtained for these metals is made complicated by the circumstance that the inequality $\omega^2 \gg \nu_0^2$ is not satisfied in the above spectral region, by virtue of which it is impossible to employ the expressions obtained for the sharply-pronounced anomalous skin effect. Considerably less reliable are the calculations of the surface impedance or optical constants of the metal in the region where $\omega \sim \nu_0$. We used the expressions for the real and imaginary parts of the surface impedance, obtained for this region by Dingle.[5] Assuming that in this region the interelectron collisions lead to the appearance of a term B/λ^2 in the expression for R, we can determine for these metals not only N, but also v. Such a treatment yielded the following microscopic parameters: for tin, $N = 4.2 \times 10^{22}\,cm^{-3}$ and $v = 2.6 \times 10^8$ cm/sec (this value was obtained for $cR_0/\pi = 2.9 \times 10^{-2}$ and $cB/\pi = 24 \times 10^{-2}\,\mu^2$); for lead, $N = 3.8 \times 10^{22}\,cm^{-3}$ and $v = 4.0 \times 10^8$ cm/sec (this value was obtained for $cR_0/\pi = 5.1 \times 10^{-2}$ and $cB/\pi = 11.2 \times 10^{-2}\,\mu^2$).

In Ref. 4 we determined the upper limit of N for these metals, using a limiting formula which, as is clear from what has been said above, is not valid. Therefore, the estimate obtained there for the upper limit is too rough and is improved here. However, even these data should be considered as approximate, for we used in the calculation theoretical formulas which cannot be considered very reliable. To obtain more reliable values of these microscopic parameters it is necessary to measure the optical constants of Sn and Pb at low temperatures, at which ν_0 become substantially smaller.

In conclusion I express my gratitude to V. L. Ginzburg for discussing the results of this work.

[1] V. L. Ginzburg and G. P. Motulevich, Usp. fiz. nauk **55**, 469 (1955).

[2] L. P. Pitaevskii, J. Exptl. Theoret. Phys. (U.S.S.R.) **34**, 942 (1958), Soviet Phys. JETP **7** (in press).

[3] R. N. Gurzhi, J. Exptl. Theoret. Phys. (U.S.S.R.) **33**, 451, 660 (1957), Soviet Phys. JETP **6**, 352, 506 (1957).

[4] G. P. Motulevich and A. A. Shubin Оптика и спектроскопия (Optics and Spectroscopy) **2**, 633 (1957).

[5] R. B. Dingle, Physica, **19**, 311 (1953).

Translated by J. G. Adashko
147

ABSORPTION OF POLARIZED MU⁻ MESONS BY NUCLEI

E. I. DOLINSKII and L. D. BLOKHINTSEV

Moscow State University

Submitted to JETP editor December 9, 1957

J. Exptl. Theoret. Phys. (U.S.S.R.) **34**, 759-761 (March, 1958)

As was shown in Ref. 1, the angular distribution of neutrons produced upon capture of polarized μ^- mesons by free protons is of the form $1 + \alpha \cos\theta$. In this work we have calculated the coefficient α for the case of absorption of μ^- mesons by protons bound in the nuclei, for the scalar (s), vector (v), tensor (t) and pseudo-vector (a) versions of the four-fermion interaction of μ mesons with nucleons. The shell model is used and the recoil of the nucleus is neglected. Since the nucleons in the nucleus acquire energies on the

order of several Mev by capture of a μ^- meson, the calculation is made in the nonrelativistic approximation with respect to the nucleons. The interaction of the emitted neutron with the nucleus was taken into account with the aid of a complex potential, which made it possible to take into account a definite neutron-absorption probability in the nucleus. It must be noted here that our value of α may be too low, owing to the superposition of an isotropic background of neutrons from the decay of the compound nucleus, formed as a result of absorption of the neutron, on the anisotropic angular distribution of the neutrons emitted from the nucleus directly after the μ^- capture. This effect calls for an additional evaluation.

The wave function of the proton was taken in the form

$$\psi_P = R_{njl}(r)\,\Omega_{jlj_z}(\mathbf{r}/r), \quad j = l \pm 1/2,$$

where n, j, and ℓ are the quantum numbers that characterize the subshell in the nucleus, and $\Omega_{j\ell j_Z}$ is a spherical spinor.[2] If the spin-orbit interaction of the neutron with the nucleus is neglected, the wave function of the neutron becomes

$$\psi_{Ns_z} = \sum_{L=0}^{\infty} i^L (2L+1)\, a_L(r)\, P_L(\mathbf{k}_N\mathbf{r}/k_N r)\,\chi_{s_z} \qquad (1a)$$

which is asymptotically represented by a combination of a plane wave with a converging one (creation condition[3]). If the spin-orbit interaction is taken into account

$$\psi_{Ns_z} = 4\pi \sum_{IL l_z} i^L a_{IL}(r)\,(\chi_{s_z}\Omega^*_{IL l_z}(\mathbf{k}_N/k_N))\,\Omega_{IL l_z}(\mathbf{r}/r),$$
$$I = L \pm 1/2, \qquad (1b)$$

with an analogous asymptotic representation. The wave function of the neutrino was assumed plane, the dependence of the μ^--meson wave-function coordinates on the K orbit was neglected. We introduce the following notation

$$b_{L\lambda njl}(k_N) = \int_0^\infty a^*_L(r)\, j_\lambda(k_\nu r)\, R_{njl}(r)\, r^2\, dr,$$

$$b_{IL\lambda njl}(k_N) = \int_0^\infty a^*_{jL}(r)\, j_\lambda(k_\nu r)\, R_{njl}(r)\, r^2\, dr,$$

where j_λ is a spherical Bessel function and k_ν is the wave number of the neutrino

$$\varphi_{ik} = f_{ii} + f_{kk} + 2\mathrm{Re}\, f_{ik},\ \eta_{ik} = h_{ii} + h_{ik} + 2\mathrm{Re}\, h_{ik}$$

(i, k ≡ s, v, t, a; for a definition of f_{ik} and h_{ik} see Ref. 1);

$$A_{njl}(k_N) = \sum_{L\lambda}(2L+1)(2\lambda+1)(C^{l0}_{L0\lambda0})^2 |\, b_{L\lambda njl}(k_N)|^2;$$

$$B_{njl}(k_N) = \mathrm{Re}\sum_{L\lambda}[(2L+1)(2L+2)(2L+3)(2\lambda+1)$$
$$\times(2\lambda+2)(2\lambda+3)]^{1/2} \times \{C^{l0}_{L0\lambda0} C^{l0}_{L+10\lambda+10} W(L+1\,l\,1\lambda;$$
$$\lambda+1\,L)\, b_{L\lambda njl}(k_N)\, b^*_{L+1\lambda+1njl}(k_N) + C^{l0}_{L+10\lambda0} C^{l0}_{L0\lambda+10} W(Ll\,1\lambda;$$
$$\lambda+1\,L+1)\, b_{L+1\lambda njl}(k_N)\, b^*_{L\lambda+1njl}(k_N)\};$$

$$C_{njl}(k_N) = \sum_{IL\lambda}(2I+1)(2L+1)$$
$$\times(2\lambda+1)\,[C^{l0}_{L0\lambda0} W(Is\lambda l;\, Lj)]^2\, |\, b_{IL\lambda njl}(k_N)|^2;$$

$$D_{njl}(k_N) = (2/(2l+1)) \sum_{IL\lambda}(2I+1)$$
$$\times(2\lambda+1)\,(C^{l0}_{L0\lambda0})^2\, |\, b_{IL\lambda njl}(k_N)|^2;$$

$$E_{njl}(k_N) = \frac{(-)^I}{3} \sum_{IL\lambda I'L'\lambda'} (-)^{\sigma_{L'\lambda'}}(2I+1)(2I'+1)(2L+1)$$
$$\times(2L'+1)(2\lambda+1)(2\lambda'+1)\, C^{l0}_{L0\lambda0} C^{l0}_{L'0\lambda'0} C^{10}_{L0L'0} C^{10}_{\lambda0\lambda'0}$$
$$\times W(I'j\,1\lambda;\,\lambda' I)\, W(I's\,1L;\,L'I)\, W(Is\,\lambda l;\,Lj)$$
$$\times W(I's\,\lambda' l;\,L'j)\,\mathrm{Re}\,[b^*_{IL\lambda njl}(k_N)\, b_{I'L'\lambda' njl}(k_N)],$$

where

$$\sigma_{L'\lambda'} = \begin{cases} 0 \text{ for } L' = L \pm 1,\ \lambda' = \lambda \pm 1 \\ 1 \text{ for } L' = L \pm 1,\ \lambda' = \lambda \mp 1 \end{cases} \Bigg\} I = L \pm 1/2$$
$$I' = L' \pm 1/2,\quad s = 1/2$$

$$F_{njl}(k_N) = 4(-)^l \mathrm{Re} \sum_{IL\lambda I'L'\lambda'} (-)^{l+l'} i^{L+\lambda-L'-\lambda'}(2I+1)$$
$$\times(2I'+1)(2L+1)\times(2L'+1)(2\lambda+1)$$
$$\times(2\lambda'+1)\, C^{10}_{\lambda0\lambda'0} C^{l0}_{L0\lambda0} C^{l0}_{L'0\lambda'0}$$
$$\times \Big\{ W(lj1s;\ sl) \sum_{gf}(2g+1)\, C^{10}_{g010} C^{f0}_{g010} C^{f0}_{L0L'0} W(L's\,fI;\,I'L)$$
$$\times X(\lambda1\lambda';\,LgL';\,l1l)\, X(LgL';\,IfI';\,s1s)$$
$$+ 2 \sum_{gfphr}(2g+1)(2f+1)(2p+1)(2h+1)$$
$$\times C^{10}_{h0L0} C^{r1}_{L'011} C^{r1}_{h011} W(\lambda'1pL;\,fh)\, X(l\lambda L;\,jgI;\,s1s)$$
$$\times X(l\lambda'L';\,jfI';\,s1s)\, X(jfI';gpL'\,ILs)$$
$$\times X(ph\lambda';\,L'r1;\,g1\lambda) \Big\} b^*_{IL\lambda njl}(k_N)\, b_{I'L'\lambda' njl}(k_N),$$

where W are the Racah coefficients; for a definition of the quantities X, see Ref. 4.

Accurate to a constant factor independent of n, j, and ℓ, the probability of emission of a neutron with energy $E_N = \hbar^2 k_N^2/2m$ at a given angle θ, upon absorption of a μ^- meson by protons in a closed subshell characterized by the quantum numbers n, j, and ℓ, is given for the superposition of the s, v, t, and a versions by the following formulas. In case (1a)

$$W_{njl}(k_N;\,\theta) = \frac{2j+1}{2l+1}[(\varphi_{sv} + 3\varphi_{ta})\, A_{njl}(k_N)$$
$$+ (-\eta_{sv} + \eta_{ta})\, B_{njl}(k_N)\cos\theta]. \qquad (2)$$

In case (1b)

$$W_{njl}(k_N;\theta) = (2j+1)\{[(\varphi_{sv}-\varphi_{ta})C_{njl}(k_N)+\varphi_{ta}D_{njl}(k_N)] + [(-\eta_{isv}+\eta_{ita})E_{njl}(k_N)+\eta_{ita}F_{njl}(k_N)]\cos\theta\}. \quad (3)$$

The total effect due to all closed subshells in the nucleus is obtained by summation of (2) and (3) over n, j, and ℓ. Formulas (2) and (3) describe also the absorption of a μ^- mesons by a single proton located in above the closed shells (in this case the factor (2j + 1) must be omitted). One would expect these formulas to be a good approximation for the twice-magic nuclei (for example, $_{20}Ca^{40}$). The details of the calculation and numerical estimates for specific nuclei will be given in a separate article.

We are sincerely grateful to I. S. Shapiro for attention to this work and for discussion of the result.

[1] Shapiro, Dolinskii, and Blokhintsev, Dokl. Akad. Nauk. SSSR **116**, 946 (1957), Soviet Phys. "Doklady" **2**, 475 (1957); Nucl. Physics **4**, 273 (1957).

[2] Berestetskii, Dolginov, and Ter-Martirosian, J. Exptl. Theoret. Phys. (U.S.S.R.) **20**, 527 (1950).

[3] A. Sommerfeld, Atomic Structure and Spectral Lines Vol. 2. (Russian Transl.) GITTL, Moscow, 1956 [Probably: Methuen, London, 1929].

[4] A. Simon and T. A. Welton, Phys. Rev. **90**, 1036 (1953).

Translated by J. G. Adashko
148

POSSIBLE ASYMMETRY OF PARTICLES AND ANTIPARTICLES IN WEAK INTERACTIONS

A. A. ANSEL' M and V. M. SHEKHTER

Leningrad Physico-Technical Institute, Academy of Sciences, U.S.S.R.

Submitted to JETP editor December 9, 1957

J. Exptl. Theoret. Phys. (U.S.S.R.) **34**, 761-762 (March, 1958)

RECENT experimental data concerning the $\beta-\nu$ correlation[1] show that the positron decays of Ne^{19} and A^{35} may be explained as a mixture of A and V covariants of the β-interaction, while the electron decays of He^6 and the free neutron are dependent on T and, evidently, S covariants. Analogously, associated with the positron decays of Co^{58}, experiment gives a weak interference due to Fermi and Gamow-Teller interactions, while this interference is strong in the electron decays of Au^{198} and Sc^{46}. If we consider that all the experiments are valid, then the indicated facts sharply contradict existing theory. Indeed, if we assume that the processes $n \rightleftarrows p + e^- + \overline{\nu}'$ and $p \rightleftarrows n + e^+ + \nu$ occur as a result of different interactions, this indicates a denial of the symmetry of particles and antiparticles in weak interactions. In addition, antiparticles no longer bear an exact resemblance to the particles with opposite charge. For example, their masses may differ by the order of magnitude of g^2, the square of the weak-interaction constant.

The self-adjoint relativistic invariant Hamiltonian for β decay, in which e^-, e^+, ν, and ν' enter asymmetrically, may be written in the form

$$H = \sum_{i=1}^{5}(\overline{\Psi}_p O_i \Psi_n)[\Phi^+_{e^-}\gamma_4 O_i(g_i + g'_i\gamma_5)\Phi^+_{\nu} + \Phi^+_{e}\gamma_4 O_i(f_i + f'_i\gamma_5)\Phi_{\nu} + \Phi_{e^+}\gamma_4 O_i(\lambda_i + \lambda'_i\gamma_5)\Phi^+_{\nu} + \Phi_{e^+}\gamma_4 O_i(\mu_i + \mu'_i\gamma_5)\Phi_{\nu}] + \sum_{i=1}^{5}(\bar{\Psi}_n O_i \Psi_p)\cdot \quad (1)$$
$$\times[\Phi_{\nu}\gamma^4(g^*_i - g'^*_i\gamma_5)O_i\Phi_{e^-} + \Phi^+_{\nu}\gamma_4(f^*_i - f'^*_i\gamma_5)O_i\Phi_{e^-} + \Phi_{\bar{\nu}}\gamma_4(\lambda^*_i - \lambda'^*_i\gamma_5)O_i\Phi^+_{e^+} + \Phi^+_{\nu}\gamma_4(\mu^*_i - \mu'^*_i\gamma_5)O_i\Phi^+_{e^+}].$$

In addition, in the case of the neutrino field, $\Phi_\nu(x)$ and $\Phi^+_{\overline{\nu}}(x)$ are respectively the positive and negative frequency components of $\Psi_\nu(x)$, so that

$$\Phi_{\nu} = -i\int S^+(x-x')\gamma_4\psi_{\nu}(x')\,d^3x', \qquad \Phi^+_{\bar{\nu}} = -i\int S^-(x-x')\gamma_4\psi_{\nu}(x')\,d^3x' \quad (x_0 = x_0') \quad (2)$$

and analogously for electrons.

In (1), g_i, g'_i and μ^*_i, μ'^*_i refer to β^- and β^+ decays (the experiments may be satisfied, letting g_T, g_S (g_ν?) and μ_A, μ_V be unequal to zero), f^*_i, f'^*_i describe K capture, and λ^*_i, λ'^*_i describe the absorption of an antineutrino by a proton. It is easily seen that upon reflection of the spatial coordinates (P) the Hamiltonian preserves its form if the unprimed constants remain unchanged while the primed ones change sign; with reversal of time (T) it is necessary to substitute for every constant its complex conjugate; with charge conjugation (C), $g_i \rightleftarrows \mu^*_i$, $g'_i \rightleftarrows -\mu'^*_i$, $f_i \rightleftarrows \lambda^*_i$, $f'_i \rightleftarrows -\lambda'^*_i$. From this it is evident that the Hamiltonian (1) is invariant under PTC only when $g_i = \mu_i$, $g'_i = \mu'_i$, $= f_i = \lambda_i$, $f'_i = \lambda'_i$. We obtain

the usual theory of β decay if, in addition, $g_i = f_i$, $g_i' = f_i'$.

A similar breakdown into positive and negative frequency components may be carried out as well for the nucleon operators in (1). It is not clear, however, whether this has meaning, since as a result of the strong interaction with π mesons, β decay may pass through a virtual antinucleon state. In the presence of an external Coulomb field it must be contained in the projection operators $S^{\pm}$.

The Hamiltonian appears to be nonlocal, which leads to the fact that $[H(x_1), H(x_2)] \neq 0$ when x_1 and x_2 are separated by a space-like interval. Precisely speaking, instead of the function $S(x_1 - x_2)$, this commutator contains $S^{\pm}(x_1 - x_2)$, which do not vanish outside of the light cone. In the case where the operators S^+ and S^- refer to electrons, this indicates a violation of causality in weak interactions at distances of the order $\hbar/m_e c$; for a neutrino field there is no such localization (when the mass is equal to zero, the $S^{\pm}(x_1 - x_2)$ diminish outside of the light cone as $|x_1 - x_2|^{-3}$). This situation appears to raise a serious objection to ideas which have been expressed. However, since in weak interactions the theoretical principles previously considered absolute (conservation of parity and invariance with respect to charge conjugation) are in general violated, it becomes expedient to make an experimental verification of the developed scheme. In particular, it would be useful to compare carefully the β decay and K capture probabilities in the same nucleus with the values predicted by ordinary theory.

An analogous although more difficult experiment is the comparison of β decay with the absorption of an antineutron by a proton.*

After completion of the present paper, K. A. Ter-Martirosian informed the authors that similar considerations have been developed in an article by Arnovit and Feldman (at present unpublished).

We are grateful to V. N. Grilov and to K. A. Ter-Martirosian for their comments.

*If we maintain symmetry between the electron and positron then $g_i \lambda_i$, $f_i = \mu_i$, and the processes $\bar{\nu} + p = n + e^+$ and $n = p + e^- + \bar{\nu}$ must occur as a result of one and the same interaction.

[1] Perrmannsfeldt, Maxson, Stahelin, and Allen, Phys. Rev. **107**, 641 (1957).

[2] F. Boehm and A. H. Wapstra, Phys. Rev. **106**, 1364 (1957); Ambler, Hayward, Hopes, Hudson, and Wu, Phys. Rev. **106**, 1361 (1957); Postma, Huiskamp, Miedonia, Steenlaud, Tolhek, and Gorter, Physica **23**, 259 (1957); F. Boehm and A. H. Wapstra, Phys. Rev. **107**, 1462 (1957).

[3] Cowan, Reines, Harrison, Kruse, and McGuire, Science **124**, 103 (1956).

Translated by J. S. Wood
149

LIFETIME OF THE K_2^0 MESON

I. Iu. KOBZAREV and L. B. OKUN'

Submitted to JETP editor December 11, 1957

J. Exptl. Theoret. Phys. (U.S.S.R.) **34**, 763-764 (March, 1958)

GELL-MANN and Pais[1] predicted the existence of the long-lived neutral K meson (K_2^0), which was later discovered experimentally. In connection with the establishment of the noninvariance of weak interactions under space inversion and charge conjugation, the original arguments of Gell-Mann and Pais have to be modified, as was shown in a series of papers.[2] Below we shall assume that the weak interactions are invariant under time reversal and that the K_2^0 meson has negative "time-parity".

The following decays of K_2^0 will be possible (we shall denote the respective probabilities by w_n, where n is the number of the reaction):

1) $K_2^0 \to e^+ + \nu + \pi^-$, 4) $K_2^0 \to \mu^- + \nu + \pi^+$,
2) $K_2^0 \to e^- + \tilde{\nu} + \pi^+$, 5) $K_2^0 \to \pi^+ + \pi^- + \pi^0$,
3) $K_2^0 \to \mu^+ + \nu + \pi^-$, 6) $K_2^0 \to \pi^0 + \pi^0 + \pi^0$.

The decays 1, 2 and 3, 4 are the analogs of the decays

7) $K^+ \to e^+ + \nu + \pi^0$, 8) $K^+ \to \mu^+ + \nu + \pi^0$,

whereas the decays 5, 6 are analogous to the τ^+ decays

9) $K^+ \to \pi^+ + \pi^+ + \pi^-$, 10) $K^+ \to \pi^+ + \pi^0 + \pi^0$.

Here it is essential that in the decays 5, 6, as in the decays 9, 10, the outgoing π mesons are in the S state.

It has been shown[3] that if the decays of all strange particles take place by way of the decays of Λ hyperons, then the rule $\Delta T = \frac{1}{2}$, considered earlier in connection with the π-mesonic decays of strange particles, applies also to their leptonic decays. We use this rule to calculate the probabilities of the different decays of the K_2^0 meson, and

to estimate its lifetime. With the help of the rule $\Delta T = \frac{1}{2}$ we easily obtain

$$w_1 = w_2 = w_7, \quad w_3 = w_4 = w_8; \tag{1}$$

$$w_6/w_5 = {}^3/_2, \quad w_{10}/w_9 = {}^1/_4,$$
$$(w_5 + w_6)/(w_9 + w_{10}) = 1. \tag{2}$$

The ratios (2), however, do not take into account the mass difference of $\pi^{\pm}$ and π^0 mesons. The correction due to this mass difference was considered by Dalitz,[4] who allowed for it not only in the phase volumes, but also in the corresponding matrix elements, using essentially perturbation theory. In this work we consider the corrections only in the statistical weights. The statistical weight for the decay of a particle with mass M into three particles with masses m_1, m_2, m_3 is proportional to

$$\rho \sim m_1 m_2 m_3 (m_1 + m_2 + m_3)^{-5/2} \quad (M - m_1 - m_2 - m_3)^2.$$

Denoting the statistical weights of the respective decays by ρ_n, we obtain:

$$\rho_5/\rho_9 = 1.09, \quad \rho_{10}/\rho_9 = 1.20, \quad \rho_6/\rho_9 = 1.31.$$

Using these ratios we obtain, instead of (2),;

$$w_6/w_5 = 3\rho_6/2\rho_5 \approx 2, \quad w_{10}/w_9 \approx \rho_{10}/4\rho_9 \approx 0{,}30, \tag{3}$$
$$(w_5 + w_6)/(w_9 + w_{10}) \approx ({}^2/_5\rho_5 + {}^3/_5\rho_6)/({}^4/_5\rho_9 + {}^1/_5\rho_{10}) = 1{,}2.$$

Using the data on the lifetime of the K^+ meson[5] ($\tau_{K^+} = 1.17 \times 10^{-8}$ sec) and on the abundance of the different types of K^+ decays[6] ($K_{\mu 3} \sim 5.9\%$, $K_{e3} \sim 5.1\%$, $K_{\pi 3} \sim 7.9\%$), we find that the lifetime of the K_2^0 meson must be equal to

$$\tau_{K_2^0} = \tau_{K^+} \cdot 100/(2 \cdot 5.9 + 2 \cdot 5.1 + 1.2 \cdot 7{,}9)$$
$$= 3.8 \cdot 10^{-8} \text{ sec}, \tag{4}$$

and the probabilities of the different decays must add up to the total disintegration probability of the K_2^0 meson in the percentages, respectively,

$$w_1 = w_2 \sim 16\%; \quad w_5 = w_4 \sim 19\%;$$
$$w_5 \sim 10\%; \quad w_6 \sim 20\%. \tag{5}$$

The experimental verification of these results [relations (1), (3), (4), and (5)] could be useful for the clarification of the validity of the rule $\Delta T = \frac{1}{2}$ for the leptonic and non-leptonic decays of K mesons. We note that the experimentally established lower limit for the lifetime of the K_2^0 meson is equal to 3×10^{-8} sec, (Ref. 5) which is very close to the value obtained by us, but still below it.

In our investigation we neglected the probability of the decay $K \to 2\pi + \gamma$ and of other possible decays of the K_2^0 meson. The inclusion of these decays lowers, of course, somewhat the value for $\tau_{K_2^0}$ obtained by us.

[1] M. Gell-Mann and A. Pais, Phys. Rev. **97**, 1387 (1957).

[2] Ioffe, Okun', and Rudik, J. Exptl. Theoret. Phys. (U.S.S.R.) **32**, 396 (1957); Soviet Phys. JETP **5**, 328 (1957); Lee, Yang, and Oehme, Phys. Rev. **106**, 340 (1957); R. Gatto, Phys. Rev. **106**, 168 (1957); A. Pais and S. B. Treiman, Phys. Rev. **106**, 1106 (1957).

[3] L. B. Okun', J. Exptl. Theoret. Phys. (U.S.S.R.) **34**, 469 (1958), Soviet Phys. JETP **7**, 322 (1958). Report at the Venice Conference, 1957.

[4] R. H. Dalitz, Proc. Phys. Soc. **A69**, 527 (1956).

[5] Proc. Seventh Rochester Conference, 1957.

[6] Alexander, Johnston, and O'Ceallaigh, Nuovo cimento **6**, 478 (1957).

Translated by R. Lipperheide
150

POLARIZATION EFFECTS IN SCATTERING OF ELECTRONS BY PROTONS

G. V. FROLOV

Radium Institute, Academy of Sciences, U.S.S.R.

Submitted to JETP editor December 14, 1957

J. Exptl. Theoret. Phys. (U.S.S.R.) **34**, 764-766 (March, 1958).

AKHIEZER, Rozentsveig, and Shmushkevich[1] have shown that if the scattering of electrons by protons is considered in the first approximation with respect to e, but with account of all the meson-radiation corrections, the structure of the proton reduces to two real form factors $a(q^2)$ and $b(q^2)$. Here $q^2 = (p_1 - p_2)^2$, where p_1 and p_2 are the four-dimensional momenta of the electrons before and after the collision. In the same article, the authors calculated the cross section for the scattering of polarized electrons by polarized protons and the recoil-proton polarization which occurs when polarized electrons are scattered by unpolarized protons.

In this note we calculate the polarization of electrons, ξ_2^0, and recoil protons, Z_2^0, resulting from the scattering of a beam of electrons with polarization ξ_1^0 by protons with polarization Z_1^0, which makes it possible to determine a and b by means of suitable experiments. (The polari-

zation vectors ζ_1^0, Z_1^0, ζ_2^0, and Z_2^0 are the average values of the particle spin operators in a reference system in which the corresponding particle is at rest.) This makes it possible to determine a and b from suitable experiments. The calculations were made by the usual methods. We neglected everywhere the electron mass m compared with the proton mass M, and used an initial electron energy ϵ_1 in the laboratory system. It was also assumed that $\vartheta \gg m/\epsilon_1$, where ϑ is the electron scattering angle in the laboratory system.

We obtained the following expression for polarization of the recoil protons:

$$\mathbf{Z}_2^0 = \mathbf{k}\,[\alpha_{11}(\mathbf{k}\zeta_1^0) + A_{11}(\mathbf{k}Z_1^0) + A_{13}(\mathbf{l}Z_1^0)] + \mathbf{n}A_{22}(\mathbf{n}Z_1^0) + \mathbf{l}\,[\alpha_{31}(\mathbf{k}\zeta_1^0) + A_{31}(\mathbf{k}Z_1^0) + A_{33}(\mathbf{l}Z_1^0)];$$

$$\alpha_{11} = \frac{\gamma\eta\rho\tan(\vartheta/2)}{\eta+1}\left\{1-\eta+\mu-3\mu\eta+\xi(1+2\mu)+\frac{1}{\xi}\left(-\eta-2\mu\eta-\cot^2\frac{\vartheta}{2}\right)\right\},$$

$$A_{11} = \gamma\left\{1-\frac{\eta\rho\tan(\vartheta/2)(1+\mu)}{\eta+1}\left[1+2\eta+\cot^2\frac{\vartheta}{2}+\sin^2\frac{\vartheta}{2}+(2\eta/\xi)\cos^2\frac{\vartheta}{2}\right]\right\},$$

$$A_{13} = \frac{\gamma\eta\rho}{\eta+1}\left\{1+\mu\eta-\mu\xi-(1+\mu)\sin^2\frac{\vartheta}{2}+\frac{1}{\xi}\left[1-\eta(1+\mu)+2\eta(1+\mu)\sin^2\frac{\vartheta}{2}+\cot^2\frac{\vartheta}{2}\right]\right\},$$

$$A_{22} = \gamma\{1-\eta\rho(1+\mu)\tan(\vartheta/2)\},\quad \alpha_{31} = \frac{\gamma\eta\rho}{\eta+1}\left\{2+\mu-\mu\eta+\frac{1}{\xi}(1-\eta-2\mu\eta)\right\},$$

$$A_{31} = \frac{\gamma\eta\rho}{\eta+1}\left\{-1-\mu\eta+\mu\xi-(1+\mu)\sin^2\frac{\vartheta}{2}-\frac{1}{\xi}\left[1+\eta(1+\mu)-2\eta(1+\mu)\sin^2\frac{\vartheta}{2}+\cot^2\frac{\vartheta}{2}\right]\right\},$$

$$A_{33} = \gamma\left\{1-\frac{\eta\rho\tan(\vartheta/2)(1+\mu)}{\eta+1}\left[1+\eta+\cot^2\frac{\vartheta}{2}+\cos^2\frac{\vartheta}{2}-(2\eta/\xi)\cos^2\frac{\vartheta}{2}\right]\right\}.$$

The axes were chosen in the following manner: $\mathbf{k}$ is the unit vector in the direction of $\mathbf{p}_1$ of the incident electron beam, $\mathbf{n} = (\mathbf{p}_1 \times \mathbf{p}_2)/(\mathbf{p}_1 \times \mathbf{p}_2)$ is a unit vector normal to the scattering plane, $\mathbf{l} = \mathbf{k} \times \mathbf{n}$. The same notation is used as in Ref. 1:

$$\eta = q^2/4M^2,\quad \xi = \epsilon_1/M,\quad \mu = b/a,$$

$$\gamma = \{1 + (\zeta_{\mathrm{e}1}^0\mathbf{k})\,[M_{11}(\mathbf{Z}_1^0\mathbf{k}) + M_{13}(\mathbf{Z}_1^0\mathbf{l})]\}^{-1},$$

$$\rho = 2(1+\mu)\tan(\vartheta/2)/[1+\mu^2\eta+2\eta(1+\mu)^2\tan^2(\vartheta/2)],$$

$$M_{11} = \rho\tan(\vartheta/2)\,[\eta(1-\mu+1/\xi)-\xi],\quad M_{13} = \rho\eta(1/\xi-\mu).$$

For the polarization of the electrons, we obtained the following expression

$$\zeta_{\mathrm{e}2}^0 = \mathbf{k}\,[\beta_{11}(\mathbf{k}\zeta_{\mathrm{e}1}^0) + \beta_{13}(\mathbf{l}\zeta_{\mathrm{e}1}^0) + B_{11}(\mathbf{k}Z_1^0) + B_{13}(\mathbf{l}Z_1^0)]$$
$$+ \mathbf{n}\beta_{22}(\mathbf{n}\zeta_{\mathrm{e}1}^0) + \mathbf{l}\,[\beta_{31}(\mathbf{k}\zeta_{\mathrm{e}1}^0) + \beta_{33}(\mathbf{l}\zeta_{\mathrm{e}1}^0) + B_{31}(\mathbf{k}Z_1^0) + B_{33}(\mathbf{l}Z_1^0)],$$

where

$$\beta_{11} = \gamma\cos\vartheta,\quad \beta_{31} = -\gamma\sin\vartheta,$$

$$\beta_{22} = \gamma[1-\eta\rho(1+\mu)\tan(\vartheta/2)];$$

$$\beta_{13} = \beta_{22}\sin\vartheta,\qquad \beta_{33} = \beta_{22}\cos\vartheta,$$
$$B_{11} = \gamma\cos\vartheta M_{11},\qquad B_{31} = -\gamma\sin\vartheta M_{11},$$
$$B_{13} = \gamma\cos\vartheta M_{13},\qquad B_{33} = -\gamma\sin\vartheta M_{13}.$$

An examination of the resultant expressions leads to certain qualitative conclusions. It is easy to show that when polarized electrons are scattered by unpolarized protons, the longitudinal component of the electron polarization remains unchanged. On the other hand, the polarization of the recoil protons is in this case entirely due to the longitudinal component of the electron polarization. In scattering of unpolarized electrons by polarized protons, the electrons are longitudinally-polarized.

The author is grateful to Professor I. M. Shmushkevich, at whose suggestion this work was performed.

[1] Akhiezer, Rozentsveig, and Shmushkevich, J. Exptl. Theoret. Phys. (U.S.S.R.) **33**, 765 (1957), Soviet Phys. JETP **6**, 588 (1958).

Translated by J. G. Adashko
151

CONTRIBUTION TO THE THEORY OF SURFACE IMPEDANCE OF METALS IN ANOMALOUS SKIN EFFECT

M. Ia. AZBEL'

Physico-Technical Institute, Academy of Sciences, Ukrainian S.S.R.

Submitted to JETP editor December 17, 1957

J. Exptl. Theoret. Phys. (U.S.S.R.) **34**, 766-767 (March, 1958)

REFERENCES 1 and 1a contain the development of a theory of the surface impedance under conditions of anomalous skin effect, when the least characteristic quantity of the problem is the skin depth δ (small compared with the mean free path ℓ of the electron, compared with the distance vT traversed by the electrons during one period T of the high frequency field, and compared with the Larmor radius r in the presence of a constant magnetic field). The electrons in the metal were considered there as an ideal gas of Fermi quasi particles with a dispersion law $\epsilon = \epsilon(\mathbf{p})$ (ϵ is the energy and $\mathbf{p}$ the quasi momentum of the quasi particle).

Actually, the interaction between electrons is far from being small, and this leads to the need of describing the conduction electrons as a Fermi liquid.

The formulas for the current density and the kinetic equation were written for this case by Silin,[2] starting with the theory of a Fermi liquid as proposed by Landau[3]

$$\mathbf{j} = \frac{2e}{h^3}\int \frac{\partial \varepsilon_0}{\partial \mathbf{p}}\left(f' - \frac{\partial f_0}{\partial \varepsilon_0}\hat{L}f'\right)d\mathbf{p};$$

$$i\omega f' + \left(v_z\frac{\partial}{\partial z} + \frac{e}{c}[\mathbf{v}\times\mathbf{H}]\frac{\partial}{\partial \mathbf{p}}\right)\left(f' - \frac{\partial f_0}{\partial \varepsilon_0}\hat{L}f'\right) - I\left(f' - \frac{\partial f_0}{\partial \varepsilon_0}\hat{L}f'\right)$$

$$= -\frac{\partial f_0}{\partial \varepsilon_0}e\mathbf{v}\mathbf{E}; \quad \hat{L}f' = \int \Phi(\mathbf{p}, \mathbf{p}')f'(\mathbf{p}')\,d\mathbf{p}'.$$

Here f' is an addition to the equilibrium Fermi function $f_0(\epsilon_0)$, $\mathbf{v} = \partial\epsilon_0/\partial\mathbf{p}$ is the velocity of the electrons in the equilibrium state, $\Phi(\mathbf{p}, \mathbf{p}')$ is the function that characterizes the interaction, I is the collision integral, and z the direction of the inward normal to the metal surface.

It was shown in Refs. 1 and 1a that when $\hat{L} \equiv 0$, only electrons with $v_z \ll v$ are of significance in the determination of the surface impedance, for it is exactly at these values of v_z that the function f' has a sharp maximum near the surface at the distances of interest to us. But for such values of v_z, obviously, $|(\partial f_0/\partial\epsilon_0)\hat{L}f'| \ll |f'|$, so that the singularity in v_z disappears when integrating over the momenta (compare with the proof of the possibility of introducing the free-path time in anomalous skin effect for all temperatures, in Ref. 1a). This means that in the zeroth approximation with respect to the anomaly, the only one of real importance, the Fermi-liquid theory gives exactly the same results as the Fermi-gas theory.

The correctness of the above statement can also be readily verified directly, by replacing

$$\hat{L}f' = \int \Phi(\mathbf{p}, \mathbf{p}')f'(\mathbf{p}')\,d\mathbf{p}' \approx \int \Phi(v_x, v_y, 0; \mathbf{v}')f'(\mathbf{p}')\,d\mathbf{p}'$$

(the validity of such a replacement in the zeroth approximation with respect to the anomaly, i.e., with respect to $\max(\delta/\ell, \delta/r, \delta\omega/v)$, can be verified by substitution), and by carrying out calculations analogous to those of Ref. 1a.

Note added in proof. After this work was completed, an article by Silin [V. P. Silin, J. Exptl. Theoret. Phys. (U.S.S.R.) **33**, 1282, (1957), Soviet Phys. **6**, 985 (1958)] appeared, in which another method was used to obtained the very same result for the particular case of no constant magnetic field.

[1] G. E. H. Reuter and E. H. Sondheimer, Proc. Roy. Soc. **195**, 336 (1948).

[1a] M. Ia. Azbel' and E. A. Kaner, J. Exptl. Theoret. Phys. (U.S.S.R.) **30**, 811 (1956), **32**, 896 (1957); Soviet Phys. JETP **3**, 772 (1956), **5**, 730 (1957).

[2] V. P. Silin, J. Exptl. Theoret. Phys. (U.S.S.R.) **34**, 707 (1958), Soviet Phys. JETP **7**, 486 (1958) (this issue).

[3] L. D. Landau, J. Exptl. Theoret. Phys. (U.S.S.R.) **30**, 1058 (1956), Soviet Phys. JETP **3**, 920 (1956).

Translated by J. G. Adashko
152

INVESTIGATION OF THE $\pi^+ + d \rightarrow 2p$ REACTION FOR 174–307 Mev π^+ MESONS

B. S. NEGANOV and L. B. PARFENOV

Joint Institute for Nuclear Research

Submitted to JETP editor December 18, 1957

J. Exptl. Theoret. Phys. (U.S.S.R.) **34**, 767-769 (March, 1958).

USING ganged telescopes of scintillation counters, we investigated the reaction

$$\pi^+ + d \rightarrow 2p \qquad (1)$$

at pion energies of 174, 200, 227, 262, and 307 Mev. A beam of π^+ mesons was obtained by irradiating a hydrogen-containing target with a beam of protons, extracted from the synchrocyclotron of the Joint Institute for Nuclear Research. The yield of reaction (1) was determined by the difference of the counting rate of double coincidences from D_2O and H_2O targets. The measured differential cross sections for four angles, in the center of mass system, are represented in the table (E_π is the pion energy in the c.m.s.).

The angular distributions of the protons can be represented in the form $A + \cos^2\theta$ with the following coefficients, obtained by the least-squares method.

$E_\pi = 140$ Mev; $d\sigma/d\Omega = [(0.31 \pm 0.03) + \cos^2\theta] \times (2.54 \pm 0.15)\cdot 10^{-27}$ cm²/sterad, $\sigma = (10.4 \pm 0.8)\cdot 10^{-27}$ cm².

$E_\pi = 160$ Mev; $d\sigma/d\Omega = [(0.35 \pm 0.03) + \cos^2\theta] \times (1.76 \pm 0.11)\cdot 10^{-27}$ cm²/sterad, $\sigma = (7.6 \pm 0.6)\cdot 10^{-27}$ cm².

$E_\pi = 180$ Mev; $d\sigma/d\Omega = [(0.49 \pm 0.03) + \cos^2\theta] \times (1.05 \pm 0.06)\cdot 10^{-27}$ cm²/sterad, $\sigma = (5.4 \pm 0.4)\cdot 10^{-27}$ cm².

$E_\pi = 205$ Mev; $d\sigma/d\Omega = [(0.49 \pm 0.06) + \cos^2\theta] \times (0.66 \pm 0.04)\cdot 10^{-27}$ cm²/sterad, $\sigma = (3.4 \pm 0.3)\cdot 10^{-27}$ cm².

$E_\pi = 236$ Mev; $d\sigma/d\Omega = [(0.59 \pm 0.07) + \cos^2\theta] \times (0.32 \pm 0.02)\cdot 10^{-27}$ cm²/sterad, $\sigma = (1.9 \pm 0.2)\cdot 10^{-27}$ cm²

[σ is the total cross section of reaction (1)].

The total cross sections for the reaction

$$p + p \rightarrow d + \pi^+, \qquad (2)$$

calculated on the basis of the detailed-balance principle, are 3.05 ± 0.23, 2.50 ± 0.18, 1.93 ± 0.14, 133 ± 0.12, and 0.80 ± 0.08 millibarns at proton energies of 633, 690, 743, 812, and 903 Mev respectively. The dependence of the total cross section of reaction (2) on the pion energy in the c.m.s. is represented on the diagram.

Differential Cross Section in Units of 10^{-27} cm²/sterad (statistical errors)

E_π, Mev	θ 30°	45°	60°	90°
140	2.62±0.11	2.11±0.19	1.56±0.08	0.75±0.06
160	1.82±0.10	1.56±0.06	1.06±0.05	0.61±0.04
180	1.22±0.03	1.10±0.03	0.86±0.03	0.47±0.02
205	0.77±0.05	0.67±0.05	0.54±0.03	0.30±0.03
236	0.42±0.03	0.35±0.01	0.29±0.02	0.18±0.02

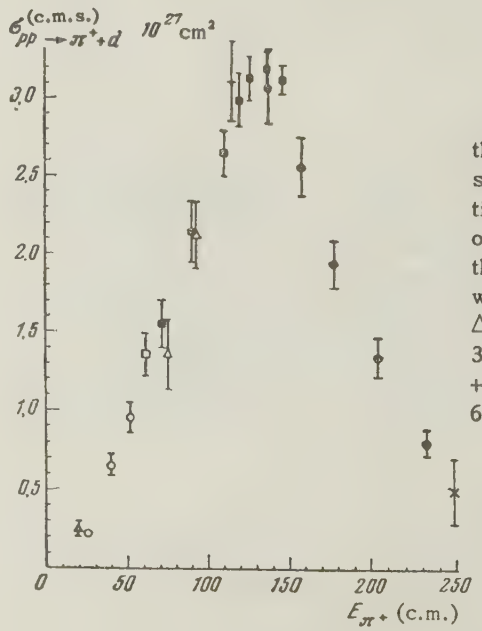

Dependence of the total cross-section of the reaction on the energy of the π^+ meson in the c.m.s. ● – our work; ■ – Ref. 1. △ – Ref. 2. □ – Ref. 3; ○ – Ref. 4; + – Ref. 5; ▲ – Ref. 6; × – Ref. 7.

The data obtained confirm the conclusion reached earlier by Meshcheriakov and Neganov[1] concerning the resonant character of the investigated reaction. The maximum of the excitation function is obtained at $E_n = 135$ Mev. These results are in agreement with the Mandel'shtam theory (Birmingham, Private Communication, 1957).

The change in the angular distribution at energies above resonant is apparently the result of the increase in the relative role of the transitions $^3P_{1,2} \rightarrow {}^3S_1$ and $^3F_{2,3} \rightarrow {}^3S_1$, which lead to the production of mesons in the d state. This assumption can be verified by polarization experiment and also by a further analysis and refinement of the angular distribution at a pion energy of 230

Mev in the laboratory system, at which a term proportional to $\cos^4\theta$ apparently appears in the angular distribution. From the point of view of the resonance model of pion production in nucleon-nucleon collisions, this means that the p state of the system (isobar nucleon), which precedes the radiation of a meson in the d state, start assuming an important role. In this case the amplitude of the $^1S_0 \rightarrow {}^3S_1$ transition should be small, since this transition corresponds to the d state of the isobar-nucleon system.

[1] M. G. Meshcheriakov and B. S. Neganov, Dokl. Akad. Nauk SSSR **100**, 677 (1955).

[2] H. L. Stadler, Phys. Rev. **96**, 496 (1954).

[3] T. H. Fields et al., Phys. Rev. **95**, 638 (1954).

[4] Durbin, Loar, and Steinberger, Phys. Rev. **84**, 581 (1951).

[5] C. E. Cohn, Phys. Rev. **105**, 1582 (1957).

[6] Clark, Roberts, and Wilson, Phys. Rev. **83**, 649 (1951).

[7] Batson, Culwich, and Riddiford, Rochester Conference Report, 1957.

Translated by J. G. Adashko
153

ELECTRON-NEUTRINO CORRELATION IN THE NEGATIVE DECAY OF Na^{24}

N. A. BURGOV and Iu. V. TEREKHOV

Submitted to JETP editor December 20, 1957

J. Exptl. Theoret Phys. (U.S.S.R.) **34**, 769 (March, 1958)

EXPERIMENTS for the determination of the electron-neutrino correlation through the use of resonant scattering of γ rays were proposed in Ref. 1. In the same reference, we calculated the dependence of the additional cross-section of the resonant scattering on the angle between the registered γ quanta for the β^--decay of Na^{24}. We have now carried out experiments using a gaseous source of Na^{24}.

The experimental setup was similar to that used in Ref. 2, with certain modifications. We employed FEU-33 instead of FEU-19 photomultipliers, which made it possible to dispense with broadband amplifiers and reduce the resolution time of the coincidence circuit to 3×10^{-9} sec. The source of γ-rays was metallic-sodium vapor containing radioactive Na^{24}. The source was kept at a temperature of 1,000°, corresponding to ~ 1 atmos vapor pressure of metallic sodium.

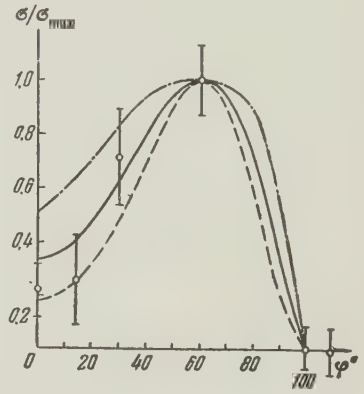

Dependence of the cross-section on the angle. Solid curve – $\lambda = 0$, dotted – $\lambda = -1$, dash-dot – $\lambda = 1$

The diagram shows the results obtained. The average value of the correlation constant λ from one series of experiments is -0.3. The values of λ range from 0 to -1 with a probability of 80%.

The measured maximum resonant-scattering cross section at an angle of 120° between the registered γ-quanta was $(3.1 \pm 0.4) \times 10^{-24}$ cm^2.

The lifetime of the level is $\sim 2 \times 10^{-13}$ sec. The estimated average time between two collisions of the recoil nucleus in the source is $\sim 10^{-11}$ sec, and the recoil nuclei can therefore be considered free and the calculations made in Ref. 1 are thus confirmed.

[1] N. A. Burgov, J. Exptl. Theoret. Phys. (U.S.S.R.) **33**, 655 (1957), Soviet Phys. JETP 6, 502 (1958).

[2] N. A. Burgov and Iu. V. Terekhov, Атомная энергия (Atomic Energy) 2, 514 (1957).

Translated by J. G. Adashko
154

ENERGY SPECTRUM OF A BOSE GAS

V. M. ELEONSKII and P. S. ZYRIANOV

Polytechnic Institute of the Ural

Submitted to JETP editor, December 6, 1957

J. Exptl. Theoret. Phys. (U.S.S.R.) **34**, 770-771 (March, 1958)

RECENTLY papers have appeared in the literature[1,2] concerning the energy spectrum of a system of Bose particles. This problem is of great interest in connection with the phenomenon of superfluidity of He^4 at low temperatures. It can be shown that the basic results of these papers essentially do not go beyond the framework of the method of collective interactions or the theory of perturbations in the second quantization as developed by Bogoliubov.[3] We investigate below the problem of finding the energy spectrum of a system of Bose particles by means of expanding the interaction kernels in series of moments. In some cases this method proves to be more convenient than the method of expanding the interaction kernels into a Fourier series.

In the second quantization the Hamiltonian of the system has the form:

$$H = \frac{\hbar^2}{2m}\int \nabla\psi^*\nabla\psi d\mathbf{r} + \frac{1}{2}\int \rho(\mathbf{r})\, G(\mathbf{r}-\mathbf{r}')\,\rho(\mathbf{r}')\, d\mathbf{r}d\mathbf{r}',$$

where $\rho(\mathbf{r}) = \psi^*(\mathbf{r})\psi(\mathbf{r})$. Introducing the new variable $\boldsymbol{\xi} = \mathbf{r} - \mathbf{r}'$, we rewrite the operator of the potential energy in the form

$$^1/_2\int \rho(\mathbf{r})\, G(\boldsymbol{\xi})\,\rho(\mathbf{r}-\boldsymbol{\xi})\, d\mathbf{r}\, d\boldsymbol{\xi},$$

expanding $\rho(\mathbf{r}-\boldsymbol{\xi})$ in a series of powers of $\boldsymbol{\xi}$ we obtain

$$H = -\frac{\hbar^2}{2m}\int \nabla\psi^*\nabla\psi\, d\mathbf{r} + \frac{1}{2}\sum_{n=0}^{\infty}\frac{(-n)^n}{n!}\int \rho(\mathbf{r})\, G(\boldsymbol{\xi})\,(\boldsymbol{\xi}\nabla)^n\rho(\mathbf{r})\, d\mathbf{r}\, d\boldsymbol{\xi}. \quad (1)$$

For weakly excited states one can replace in the Bose operator ψ those operators, which refer to the ground state, by the numbers $\sqrt{\rho}$ (ρ — particle density, with the volume of the system taken as equal to unity); then

$$\psi \sim \sqrt{\rho} + \sum_{\neq 0} a_k e^{i\mathbf{kr}}, \quad (2)$$

where a_k are Bose operators. Substituting (2) in (1), we obtain, with an accuracy to terms quadratic in the operators,

$$H = H_0 + \sum_{k>0}\left(\frac{\hbar^2k^2}{2m} + \frac{1}{2}A(k)\right)(a_k^+a_k + a_{-k}^+a_{-k}) + \sum_{k>0} 2\,(B(k)\,a_ka_{-k} + C(k)\,a_k^+a_{-k}^+), \quad (3)$$

where

$$H_0 = \frac{1}{2}G_0(0)\rho^2 - \rho\sum_{k>0}\left\{\sum_{n=1}^{\infty}\frac{(-1)^n}{n!}G_n(k) + G_0(0)\right\},$$

$$A(k) = 4G_0(0)\rho + 2\rho\sum_{n=1}^{\infty}\left\{\frac{(-1)^n}{n!}G_n(k) + \frac{1}{n!}G_n(k)\right\},$$

$$B(k) = \rho G_0(0) + \rho\sum_{n=1}^{\infty}\frac{(-1)^n}{n!}G_n(k), \quad C(k) = \rho G_0(0) + \rho\sum_{n=1}^{\infty}\frac{1}{n!}G_n(k), \quad G_n(k) = \int G(\xi)\,(ik\xi)^n d\xi.$$

In the case of the central forces $A(k)/2 = 2B(k) = 2C(k)$.

The quadratic expression (3), after diagonalization with respect to the central forces, gives the following eigenvalues for the energy:

$$E_k = \left\{\left(\frac{\hbar^2k^2}{2m}\right)\left[\frac{\hbar^2k^2}{2m} + 4\pi\rho\sum_{l=0}^{\infty}\frac{(-1)^l}{(2l+1)!}k^{2l}\int_0^{\infty}G(\xi)\,\xi^{2l+2}d\xi\right]\right\}^{1/2}. \quad (4)$$

In the case of completely hard spheres with diameter a we assume for the repulsive forces

$$G(\xi) = (\hbar^2/ma^2)\,\delta(\xi - a). \quad (5)$$

Then Eq. (4) gives the results of Brueckner and Sawada[1]

$$E(x) = \left(\frac{\hbar^2}{2ma^2}\right)x\left[x^2 + 2\lambda^2\frac{\sin x}{x}\right]^{1/2}, \quad (6)$$

where $x = ka$, $\lambda^2 = 8\pi\rho a^3$.

The values of λ^2 were determined in Ref. 1 by an integral equation. For the values of a and ρ assumed there for liquid helium, its value is close to our value of λ^2, since in Ref. 1 the dependence of λ^2 on ρa^3 is almost linear. The first term of the expansion of $\sin x/x$ in (6) leads to the results found by Lie, Huang, and Yang with the use of a pseudopotential for completely elastic spheres with diameter a.

In Refs. 1 and 2 the weak forces of attraction between the helium atoms were neglected. In the simplest case it is not difficult to take them into account by adding to (5) the potential for the forces of attraction. For the sake of simplicity we use the following expression instead of (5):

$$G(\xi) = (\hbar^2/ma^2)\,\delta(\xi - a) - U_0\eta(\xi), \quad (7)$$

where

$$\eta(\xi) = \begin{cases} 0, & \xi < a \\ 1, & a < \xi < b \\ 0, & \xi > b; \end{cases}$$

U_0 is the depth of potential well, and $b - a = d$ is the width of potential well. Knowing the binding energy E_0 per atom of He^4 at a temperature close to the absolute zero (the experiment gives for this energy the value $\sim \kappa 7°K$, where κ is the Boltzmann's constant), and using the known results of quantum mechanics, a relationship can be established between the binding energy and the width and depth of the potential well. Then only one parameter (with the exception of ρ and a) will appear in the energy spectrum of the system. This relation is expressed by the equation

$$d = d_0 \left(\frac{U_0}{2E_0} - 1\right)^{-1/2} \tan^{-1}\left(-\sqrt{\frac{U_0}{2E_0} - 1}\right),$$

$$d_0 = \left(\frac{mE_0}{\hbar^2}\right)^{-1/2}.$$

Use of the potential (7) instead of (6) leads to the following energy spectrum:

$$E(x) = \left(\frac{\hbar^2}{2ma^2}\right) x \left[x^2 + 2\lambda^2 \frac{\sin x}{x} - \gamma^2 x^{-3}\left(\sin\left(1 + \frac{d}{a}\right)x - \sin x\right) + \gamma^2\left(1 + \frac{d}{a}\right)x^{-2}\cos\left(1 + \frac{d}{a}\right)x - \gamma^2 x^{-2}\cos x\right]^{1/2}, \quad (8)$$

$$\gamma^2 = 4\pi U_0 \rho a^5 m/\hbar^2.$$

This form of the spectrum yields a better approximation to the experimental curve $E(x)$ for He^4 than equation (6), as is shown by an analysis of the relationship (8).

Note added in proof (February 21, 1957). Taking exchange forces into account leads to a change of parameter $\lambda^2 = 16\pi\rho a^3$. In the limit of $k \to 0$ this change is equivalent to the introduction of an effective mass $m^* = m/2$.

[1] K. A. Brueckner and K. Sawada, Phys. Rev. **106**, 1128 (1957).

[2] Lie, Huang, and Yang, Phys. Rev. **106**, 1135 (1957),

[3] N. N. Bogoliubov, J. Phys. (U.S.S.R.) **2**, 23 (1947).

Translated by P. F. Schmidt
155

THE ANTIFERROMAGNETIC ORIENTATION OF MAGNETIC MOMENTS IN THE ALLOY* Ni_3Fe

M. V. DEKHTIAR

Moscow State University

Submitted to JETP editor July 24, 1957

J. Exptl. Theoret. Phys. (U.S.S.R.) **34**, 772-773 (March, 1958)

THE influence of ordering the atoms on the magnetic structure of the alloy Ni_3Fe has been studied by Shull and Wilkinson[1] by means of neutron diffraction. These authors discovered the effect of the magnetic state of the alloy on the intensity of the superlattice lines which are observed as a result of the atomic ordering. The intensity of these lines is weakened when the neutron diffraction is observed on a magnetized sample. On this basis, the authors have concluded that the rearrangement of the atoms is accompanied by the appearance of a magnetic superlattice. The nature of the latter, however, remained unclear.

We have shown earlier[2] that the observed anomalies accompanying the variation of the magnetic properties with temperature permit the detection of structural changes in single phase alloys caused by ordering processes. In the present paper the temperature dependence of the saturation magnetization I_S, the remanent magnetization I_r and of the coercive force H_C of the alloy Ni_3Fe is investigated over a wide temperature range.

The investigated sample, with a diameter of 4.5 mm, was enclosed in a thin quartz tube, evacuated to 10^{-4} mm Hg, and quenched together with it in water after two hours of annealing at 1200°C. The experimental points in the region from 300 to 600°C were obtained for closely spaced values of the temperature (at intervals of 10 to 15°C) in order to determine more accurately the shape of the temperature dependence of I_S, I_r and H_C. The sample was kept one hour at each temperature before taking a reading.

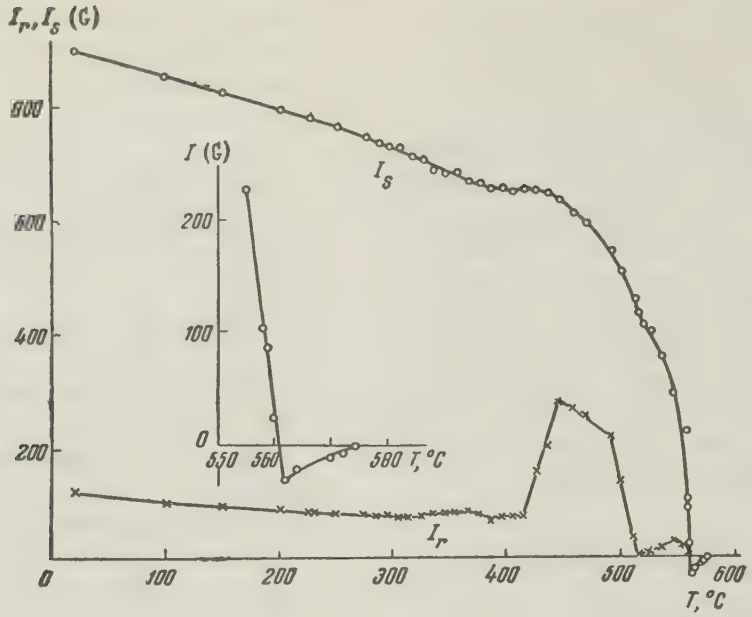

The figure shows the temperature dependence of I_s and I_r. A plateau appears on the I_s curve in the region from 385 to 435°C. Over a temperature range of about 50°C, the decrease in I_s with rising temperature is compensated by an increase in I_s caused by the establishment of an order at close range in the distribution of the atoms in the crystal lattice of the quenched disordered alloy.

Another indication of the establishment of order at close range is given by the threefold increase in I_r over the range 415 — 434°C, whereas I_r stays practically constant over the temperature range from room temperature to 415°C. H_c varies approximately in the same manner. These results are in agreement with the anomalous dependence of the thermal capacity over the same temperature range.[3]

In the narrow region from 490 to 510°C the residual magnetic moment per unit volume measured at field H = 0 decreases sharply from 240 gausses to almost zero (see drawing). The saturation magnetization at this temperature still remains at about 50% of the value of I_s at room temperature. At higher temperatures, saturation is not reached in the fields investigated by us; a compensation point is found on the I(T) curve (according to Néel,[4] see drawing). If in a field H = 135 oersted the magnetic moment per unit volume at 555°C is 0.25 I_s at room temperature, then on raising the temperature by another 5°C it suddenly drops to zero. On increasing the temperature further, the magnetic moment in a field of the indicated intensity has a negative value.

The presence of a compensation temperature in the I(T) curve and the appearance of negative magnetic moments above this temperature show the existence of an uncompensated antiferromagnetic orientation of the spin moments. One may assume that the latter appears close to 510°C, where a sharp drop of I_r to zero is observed.

The transition of the alloy from the ferromagnetic to the paramagnetic state occurs in the neighborhood of 574°C.

The observed changes in the magnetic structure of the alloy Ni_3Fe near 510°C and 574°C appear to correspond to the two maxima in the curve of thermal capacity vs. temperature shown in the paper by Leech and Sykes.[3]

The anomalous temperature variation of the magnetic properties of the alloy Ni_3Fe exemplifies the process of atomic ordering and the change in magnetic structure, which is connected, as we have shown, with the transition of the alloy Ni_3Fe from the ferromagnetic to the ferrimagnetic state.

The results of our investigation are in agreement with the papers by Smart[5] and Pratt,[6] who discuss the possibility of rearrangements which are caused not by the disappearance of the magnetic structure, but by changes in it.

*Uncompensated antiferromagnetism.

[1] C. G. Shull and M. K. Wilkinson, Phys. Rev. **97**, 304 (1955).

[2] M. V. Dekhtiar, Физ металлов и металлов (Phys. of Metals and Metal Research) **3**, 56 (1956).

[3] P. Leech and C. Sykes, Phil. Mag. **27**, 742 (1939).

[4] L. Néel, Ann. de phys. **3**, 137 (1948).

[5] J. S. Smart, Phys. Rev. **90**, 55 (1953). See also Антиферромагнетизм (Antiferromagnetism), edited by S. V. Vonsovskii, IIL, 1956, page 178.

[6] G. W. Pratt, Phys. Rev. **106**, 53 (1957).

Translated by P. F. Schmidt
156

NUCLEAR MAGNETIC MOMENTS OF Sr^{87} *AND* Mg^{25}

A. G. KUCHERIAEV, Iu. K. SZHENOV, Sh. M. GOGICHAISHVILI, I. N. LEONT' EVA, and L. V. VASIL' EV

Submitted to JETP editor December 25, 1957

J. Exptl. Theoret. Phys. (U.S.S.R.) **34**, 774-775 (March, 1958)

THE gyromagnetic ratio of the Sr^{87} nucleus was measured by us by the atomic-beam magnetic-resonance method.[1] Since the beam consisted of strontium atoms, intramolecular interactions could be disregarded and the diamagnetic correction[2] could be evaluated accurately. The beam was 378 cm long and was detected by surface ionization on an incandescent tungsten wire, upon which an oxygen jet was blowing. Under optimum conditions the coefficient of surface ionization was about 20 percent. The Sr^{87} ions were separated out by a magnetic analyzer and recorded with an electron multiplier and a galvanometer with a sensitivity of 4×10^{-10}amp/mm. The galvanometer deflection due to the narrow strontium beam at mass 87 was 250 mm. The strontium beam was produced by heating metallic strontium to 740°C in an oven made of Armco iron.

The nuclear gyromagnetic ratio g was determined from the equation[1] $g = 1.3122 \times 10^{-3} f_r/H_r$, where f_r is the resonance frequency of the oscillating field that induces the transitions, and H_r is the corresponding resonance value of the strength of the static magnetic field in which the transitions occur. The resonance values f_r and H_r are those which correspond to the minimum intensity of the refocused beam. Measurements were made both at constant field and at constant frequency. The fluctuations in beam intensity were compensated by two methods: (a) alternate measurements of beam intensity with the oscillating field on and off, and (b) continuous recording of the beam intensity by an instrument with a fast response. The frequency f was measured with a type 528 heterodyne wavemeter by observing zero beats on an oscilloscope. The magnetic field strength H was measured by proton resonance in water; the resonance frequency ν_H of the protons was measured by the method indicated above. Since the position of the field-measuring probe did not coincide with the place in the field H where the atomic beam was exposed to the oscillating field, the measured value ν_H was corrected by adding to it the difference between the proton resonance frequencies of the field-measuring probe and of another probe located in the place of beam passage; this difference had been measured before installing the electromagnet in the apparatus. A sharp and deep resonance dip of the intensity of the refocused beam, amounting to 60 percent, was observed at frequencies around 1.07 Mcs and fields around 5800 oersted. To cancel out end effects of the oscillating field[3] the measurements were carried out at opposite directions of the field H.

The maximum error of measurement — determined by nonuniqueness under reversals of magnetism, by the inhomogeneity of the field, and also by the sharpness of the resonance curves — is estimated to be 0.12 percent. The average value of 26 measurements of the gyromagnetic ratio is

$$g(Sr^{87}) = 0.2423 \pm 0.0003,$$

which within the limits of the errors of the measurements agrees with the value obtained by Jeffries and Sogo by the method of nuclear induction. Because of the diamagnetism of the atom the true value H_{true} of the magnetic field strength at the nucleus is less than the measured H_r, so that $H_{true} = (1-\sigma) H_{meas}$, where σ is the magnetic shielding constant. According to Dickinson[5] $\sigma = 0.00345$ for strontium. With this correction and the known[6] value of the spin of the Sr^{87} nucleus, $I = 9/2$, we obtain for the magnetic moment of the Sr^{87} nucleus

$$\mu(Sr^{87}) = 1.0939 \pm 0.0014 \text{ nuclear magnetons.}$$

[1] Rabi, Zacharias, Millman, and Kusch, Phys. Rev. **53**, 318 (1938); Rabi, Millman, Kusch, and Zacharias, Phys. Rev. **55**, 526 (1939).

[2] W. E. Lamb, Jr., Phys. Rev. **60**, 817 (1941); N. F. Ramsey, Experimental Nuclear Physics, ed. by E. Segre, vol. I, part III, Sec. 4C., Wiley, N. Y., 1953.

[3] S. Millman, Phys. Rev. **55**, 628 (1939).

[4] C. D. Jeffries and P. B. Sogo, Phys. Rev. **91**, 1286 (1953).

[5] W. C. Dickinson, Phys. Rev. 80, 563 (1950).

[6] M. Heyden and H. Kopfermann, Z. Physik **108**, 232 (1938).

Translated by J. Heberle
157

NUCLEON-NUCLEON CROSS-SECTIONS AT HIGH ENERGIES

R. B. BEGZHANOV

Physics Institute, Academy of Sciences, Armenian S.S.R.

Submitted to JETP editor December 25, 1957

J. Exptl. Theoret. Phys. (U.S.S.R.) **34**, 775-776 (March, 1958)

USING the Alikhanian-Alikhanov magnetic spectrometer, the authors of Refs. 1 and 2 determined the cross section σ_a for the inelastic interaction between protons of average energy from 0.9 to 34 Bev and lead or carbon nuclei. From these data, on the basis of the optical model,[3] it is possible to determine the transverse cross-section $\bar{\sigma}$ of the nucleon-nucleon interactions at the above energies, and also to choose the most logical form of the distribution of the nucleons in the nucleus, first using the results of electromagnetic measurements and then determining the scale parameter from the resultant experimental cross-sections.

Hofstadter[4] used the scattering of high energy electrons by nuclei to establish that, for medium and heavy nuclei, the distribution of the protons can be represented by the so-called homogeneous smoothed distribution of the type

$$\rho(r) = \rho_0 \left\{ \exp\left[\frac{r-c}{z}\right] + 1 \right\}^{-1}, \qquad (1)$$

where $c = 1.08\,A^{1/3} \times 10^{-13}$ cm, $z = 0.53 \times 10^{-13}$ cm, ρ_0 is the density at $r = 0$, and A is the atomic weight. It was shown in Ref. 5 that, accurate to 3%, the radial distributions of the protons and neutrons are identical. On this basis one can assume that the distribution of the nucleons in the nucleus coincides with that of the protons (1), determined by experiments on electron scattering.

The measurements by Kocharian, Begzhanov, and Saakian[1,2] have that advantage, from the point of view of determining the nuclear dimensions, that they give the inelastic cross-section σ_a directly, dispensing with the entire formalism of the optical model.

Following Fernbach, Serber, and Taylor,[3] we calculate σ_a using the semi-classical target-parameter method. As it passes through the nucleus, the proton wave decays exponentially, with an absorption coefficient $K(r) = \rho(r)\bar{\sigma}$. The size and shape of the nucleus are determined by the density distribution $\rho(r)$. The total absorption is expressed by the integral with respect to the coordinate s along the proton trajectory.

The cross section σ_a equals here the interaction probability, integrated over the impact parameter b. Taking it into account that $r^2 = b^2 + s^2$, we have

$$\sigma_a = 2\pi \int_0^\infty \left\{ 1 - \exp\left[-2 \int_0^\infty K\left(\sqrt{b^2 + s^2}\right) ds \right] \right\} b\,db. \qquad (2)$$

Numerical calculation of this integral for various values of the parameter c yields σ_a as a function of $\bar{\sigma}$ for the homogeneous smoothed distribution (1).

Calculation of the transverse cross section for the inelastic interaction between protons and carbon or lead nuclei, using the smoothed model of the nucleus (1), shows that the experimental cross sections for either lead [$\sigma_a = (1740 \pm 90)$ millibarns] or graphite [$\sigma_a = (210 \pm 15)$ millibarns] coincide with the calculated values at $\bar{\sigma} = (32 \pm 3)$ millibarns. The errors indicated are statistical.[6]

The best agreement between the calculated and the experimental cross sections is obtained for $c = (1.13 \pm 0.04) \times 10^{-13} A^{1/2}$ cm. It is assumed here that the fall-off thickness for the nucleon density is the same as for the protons density.[4] Consequently, if assuming the smoothed model of the nucleus, the nuclear radius R determined in this manner agrees with the results of the electromagnetic measurements. At the same time, whether the homogeneous or the Gaussian model is used, it is impossible to select the same value of r_0 in the expression $R = r_0 A^{1/3} \times 10^{-13}$ cm for the investigated nuclei.

The value of $\bar{\sigma}$ indicated above corresponds to the total effective cross section for nucleon-nucleon interactions, at least up to energies of 34 Bev. The section $\bar{\sigma} = (21 \pm 4)$ millibarns[7] corresponds to the mean value for the production of particles (or mesons) in elementary interactions with energies ~ 50 Bev. According to Williams,[8] the nucleon-nucleon cross-section increases with energy and $\bar{\sigma} \sim 120$ millibarns at ~ 30 Bev. The mistake in this work was noted later on by the author himself.[7]

Our results are in good agreement with the experiments on the determination of nucleon-nucleon cross sections at energies up to 5.3 Bev (Ref. 9) and on nucleon-nuclide cross sections. It follows therefore that, in general, the fundamental properties of the interaction processes, at least up to 34 Bev, do not differ from the interaction in the energy range attainable with modern accelerators.

The work was carried out under the supervision of Professor N. M. Kocharian. I thank M. L. Ter-Mikaelian for continuing interest in this work and for valuable comments, and also G. M. Garibian for reviewing the manuscript.

[1] N. M. Kocharian and R. B. Begzhanov, Dokl. Akad. Nauk Arm. SSR **25**, 3 (1957).
[2] Kocharian, Saakian, et al., Izv. Akad. Nauk Arm. SSR **10**, 81 (1957).
[3] Fernbach, Serber, and Taylor, Phys. Rev. **75**, 1352 (1949).
[4] R. Hofstadter, Revs. Mod. Phys. **28**, 214 (1956).
[5] Abashian, Cool, and Cronin, Phys. Rev. **104**, 855 (1956).
[6] R. B. Begzhanov and V. M. Kharitonov, Dokl. Akad. Nauk Arm. SSR **27**, 3 (1958).
[7] A. E. Brener and R. W. Williams, Phys. Rev. **106**, 1020 (1957).
[8] R. W. Williams, Phys. Rev. **98**, 1393 (1955).
[9] R. P. Shutt, Seventh Annual Rochester Conference on High Energy Nuclear Physics, N. Y. 1957.

Translated by J. G. Adashko
158

MEASUREMENTS OF THE SPIN-LATTICE RELAXATION TIMES OF Cr^{3+} IN CORUNDUM

P. P. PASHININ and A. M. PROKHOROV

P. N. Lebedev Physics Institute, Academy of Sciences, U.S.S.R.

Submitted to JETP editor December 28, 1957

J. Exptl. Theoret. Phys. (U.S.S.R.) **34**, 777 (March, 1958)

KNOWLEDGE of the spin-lattice relaxation times in ferromagnetic compounds has assumed particular significance in connection with recently developed investigations on the production of low-noise molecular amplifiers using ferromagnetics.

We measured the spin-lattice relaxation time for the Cr^{3+} ion in the lattice of corundum $Al_2O_3 - Cr_2O_3$ for the $\frac{3}{2} \rightarrow \frac{1}{2}$ electron transition (Ref. 1).

The measurements were carried out at 9370 Mc at two temperatures ($T = 300°K$ and $T = 77°K$), and the saturation effect in ferromagnetic resonant absorption was observed for the case when the constant field was parallel to the symmetry axis of the crystal.

The values obtained for the spin-lattice relaxation time, $T_1 = 1.4 \times 10^{-7}$ sec for $T = 300°K$ and $T_1 = 7 \times 10^{-4}$ sec for $T = 77°K$, make it possible to conclude that the basic mechanism of the relaxation in this temperature ranges consists of "Raman effect" processes, which lead to a temperature dependence of the spin-lattice relaxation time in the form $T_1 \sim T^{-7}$ (Ref. 2).

[1] A. A. Manenkov and A. M. Prokhorov, J. Exptl. Theoret. Phys. (U.S.S.R.) **28**, 762 (1955), Soviet Phys. JETP **1**, 611 (1955).
[2] I. H. Van Vleck, Phys. Rev. **57**, 426 (1940).

Translated by J. G. Adashko
159

CONCERNING THE HYPERON-NUCLEON INTERACTION

L. I. LAPIDUS

Joint Institute for Nuclear Research

Submitted to JETP editor December 31, 1957

J. Exptl. Theoret. Phys. (U.S.S.R.) **34**, 777-779 (March, 1958)

1. What little is known of the character of the forces between hyperons and nucleons is learned by analysis of hyperfragments or of the interactions between hyperons and nuclei.[1,2]

Parity nonconservation in hyperon decay can be used to study the interaction between hyperons and free nucleons, and also to investigate hypernuclei.

The direct method of establishing the spin-orbit dependence of the $Y - N$ forces can be the observation of the up-and-down asymmetry of the decay products relative to the scattering plane. The fact that the hyperons produced in $p - N$ and $K - N$ interactions are polarized is apparently evidence in favor of the presence of a (LS) dependence of the forces, but for direct proof the up-and-down asymmetry must be observed in the decay of hyperons that are polarized in elastic $Y - N$ scattering.

A study of the up-and-down assymetry with respect to the plane of hypernucleus production can be used to study the structure of the hypernucleus and for a direct determination of the spin of the hyperfragment. Proof that the spins of the baryons are compensated in ${}_{\Lambda}He^4$ would be the absence of such an asymmetry, which would be observed in ${}_{\Lambda}H^3$ at the same time.

2. Let us consider certain consequences of the unitarity and symmetry of the S matrix for $Y - N$ interactions. At Λ^0-particle energies below 150 Mev, only elastic scattering is possible in $\Lambda - N$

collisions. This situation was analyzed in connection with $N-N$ scattering. At Λ^0-particle energies above 150 Mev, the conversion of Λ particles into Σ hyperons becomes energetically feasible in addition to elastic scattering, and the unitary and symmetric S matrix covers the following processes

$$\begin{aligned}&\Lambda^0 p \to \Lambda^0 p\,(S_{11});\ \Sigma^+ n \to \Lambda^0 p\,(S_{12});\ \Sigma^0 p \to \Lambda^0 p\,(S_{13});\\ &\Lambda^0 p \to \Sigma^+ n\,(S_{21});\ \Sigma^+ n \to \Sigma^+ n\,(S_{22});\ \Sigma^0 p \to \Sigma^+ n\,(S_{23});\\ &\Lambda^0 p \to \Sigma^0 p\,(S_{31});\ \Sigma^+ n \to \Sigma^0 p\,(S_{32});\ \Sigma^0 p \to \Sigma^0 p\,(S_{33}),\end{aligned} \tag{1}$$

provided one considers the energy range where there is no additional pion production. In analogy with the procedure used for the combined analysis of scattering and photoproduction of pions with Compton effect on nucleons,[3] account of the symmetry and unitarity of the S matrix makes it possible to express the six independent elements of the S matrix in terms of the three scattering phases δ_1, δ_2, and δ_3 and the three mixing parameters φ, θ, and ψ.*

When the isotopic invariance of the amplitude is taken into account, the interactions between the Σ particles and the nucleons can be expressed in terms of the amplitudes R_3 and R_1 of the $\Sigma-N$ scattering in states with $T = 3/2$ and $T = 1/2$, the same as is done for $\pi-N$ scattering:

$$\begin{aligned}&3R_{22} = R_3 + 2R_1,\ 3R_{23} = \sqrt{2}\,(R_3 - R_1);\\ &3R_{33} = 2R_3 + R_1\,(R_{ik} = S_{ik} - \delta_{ik}).\end{aligned} \tag{2}$$

Comparison of (2) with the general expressions for a 3×3 S matrix, given in the appendix to Ref. 3, shows that if the isotopic invariance is taken into account (for arbitrary δ_1, δ_2, δ_3, and φ), we get

$$\cos^2\psi = 1,\ \cot\theta = \sqrt{2} \tag{3}$$

and the number of necessary parameters is reduced to four. Here

$$\begin{aligned}&S_{11} = e^{2i\delta_1}\cos^2\varphi + e^{2i\delta_2}\sin^2\varphi,\\ &S_{12}\sqrt{3} = \sqrt{2}\,ie^{i(\delta_1+\delta_2)}\sin 2\varphi \sin(\delta_1 - \delta_2),\\ &S_{13}\sqrt{3} = ie^{i(\delta_1+\delta_2)}\sin 2\varphi \sin(\delta_1 - \delta_2),\\ &3S_{22} = e^{2i\delta_1} + 2\,[e^{2i\delta_1}\sin^2\varphi + e^{2i\delta_2}\cos^2\varphi] = S_3 + 2S_1,\\ &3S_{23} = \sqrt{2}\,(S_3 - S_1);\ 3S_{33} = 2S_3 + S_1;\ |S_{11}|^2 = |S_1|^2.\end{aligned} \tag{4}$$

As can be seen from comparison of (2) and (4), information concerning δ_3 can be obtained from the data on the scattering of Σ^+ hyperons by protons. The quantities δ_1, δ_2, and φ characterize $\Lambda-N$ scattering, the $\Lambda \rightleftarrows \Sigma$ conversion, and also $\Sigma-N$ scattering in a state with isotopic spin $T = 1/2$.

Comparison of the expressions for S_{12} and S_{13} in (4) shows the correctness of the equation

$$S_{12} = \sqrt{2}\,S_{13}, \tag{5}$$

which can also be obtained directly, taking into account the isotopic invariance of the conversion of Λ particles into Σ hyperons.

Let us note the interesting circumstance that, in in this analysis, Eq. (5) results quantitatively from the isotopic invariance of the $\Sigma-N$ scattering. Conversely, were we to lean on (5), then we would obtain as the result

$$\sqrt{2}\,(S_{33} - S_{22}) = S_{23}, \tag{6}$$

which, on the other hand, follows directly from (2).

Equation (5) leads to a relation between the cross sections, and also to the equality of the polarizations of the Λ particles and the nucleons.

Generalization of the Vol' fenshteyn theorems[4,5] makes it possible to connect, for example, in the case of the $\Lambda \rightarrow \Sigma$ conversion, the azimuthal asymmetry of the nucleons and Σ hyperons, when the Λ particles are polarized, with the polarization of the same beams when the Λ particles are not polarized.

*Here we neglect mixing of the $^3P_2 \rightleftarrows {}^3F_2$ type.

[1] R. H. Dalitz, Rep. Prog. Phys. **20**, 165 (1957).
[2] N. Dallaporta and F. Ferrari, Nuovo cimento **5**, 111, 742 (1957).
[3] L. I. Lapidus, J. Exptl. Theoret. Phys. (U.S S.R.) **34**, 922 (1958), Soviet Phys. JETP **7** (in press).
[4] L. I. Baz', J. Exptl. Theoret. Phys. (U.S.S.R.) **32**, 628 (1957), Soviet Phys. JETP **5**, 521 (1957).
[5] L. I. Lapidus, J. Exptl. Theoret. Phys. (U.S.S.R.) **33**, 204 (1957), Soviet Phys. JETP **6**, 160 (1958).

Translated by J. G. Adashko
160

INTERACTION OF FIELDS IN THE OVERHAUSER EFFECT

V. M. KONTOROVICH

Institute of Radiophysics and Electronics, Academy of Sciences, Ukrainian S.S.R.

Submitted to JETP editor January 2, 1958

J. Exptl. Theoret. Phys. (U.S.S.R.) 34, 779-781 (March, 1958)

In this work we show, within the framework of the relaxation theory of Bloch,[1] that relaxation transitions can change substantially the character of the saturation when two resonant fields act simultaneously on a system with a discrete spectrum. According to Ref. 1, when saturation by the field changes the population of the resonant levels, a change takes place in the population of all the levels that are connected with the resonant ones through relaxation transitions (generalized Overhauser effect). Let us consider the interaction of two fields of frequencies ω_1 and ω_2, $|\omega_{pq} - \omega_1| \leq \Gamma$, $|\omega_{mn} - \omega_2| \lesssim \Gamma$, which have no common resonant level.*

We start with an equation for the addition $\hat{D}(t)$ to the equilibrium density matrix $\hat{\rho}^0$, which determines the resonant portion of the average dipole moment of the system, $\mathbf{d}(t) = \mathrm{Sp}(\hat{\mathbf{d}}\hat{D}(t))$. Let ω_{ab} be the frequency of a transition between levels a and b in the unperturbed system, and let the Hamiltonian of the perturbation be $\hbar\hat{V}(t)$, where

$$\hat{V}(t) = \hat{F}^{\pm}e^{\mp i\omega_1 t} + \hat{\Phi}^{\pm}e^{\mp i\omega_2 t}$$

(summation with respect to the $\pm$ sign). According to Ref. 1

$$(\partial/\partial t + i\omega_{ab})D_{ab} + \Gamma_{ab}(\hat{D}) \div i[\hat{V}(t),$$

$$\hat{D}]_{ab} = i(\rho_a^0 - \rho_b^0)V_{ab}(t). \qquad (1)$$

The relaxation is described by a linear transformation $\Gamma(\hat{D})$ of a definite type. The coefficients of this transformation represent the reciprocals of the relaxation times for the various transitions, and their final combinations need merely be considered by us as phenomenological parameters

$$\Gamma_{ab}(\hat{D}) = -\sum_{\tau\neq 0} 2\exp(\hbar\tau/kT)\Gamma_{ab}^{\tau}D_{a+\tau,b+\tau} + \Gamma_{ab}D_{ab}. \qquad (2)$$

If $\omega_{mn} \neq \omega_{pq}$ the first term must be retained only for $a = b$, for, in any event, when $a \neq b$ it does not contain resonant terms:

$$\Gamma_{ab} = \sum_{\tau}(\Gamma_{aa}^{\tau} + \Gamma_{bb}^{\tau}) - 2\Gamma_{ab}^{0}.$$

We seek the solution in the form

$$\hat{D}(t) = \hat{R} + \hat{P}^{\pm}e^{\mp i\omega_1 t} + \hat{Q}^{\pm}e^{\mp i\omega_2 t}, \qquad (3)$$

retaining only the resonance matrix elements

$$R_{aa} \equiv R_a, \quad P_{pq}^{+}, \; P_{qp}^{-}, \quad Q_{mn}^{+}, \; Q_{nm}^{-}.$$

From the equations for the diagonal terms of the system (1) we find, using the normalization condition $\Sigma R_a = 0$,

$$R_a = T_a^{\nu}\mathrm{Im}\,\nu + T_a^{\mu}\mathrm{Im}\,\mu, \quad \nu = P_{qp}^{-}F_{pq}^{+}, \quad \mu = Q_{nm}^{-}Q_{mn}^{+}. \qquad (4)$$

Here T_a are the coefficients of a transformation that is the inverse of $\Gamma'(D)$.†

We introduce

$$T_{ab} = T_a - T_b, \; \alpha_{ab}^{\pm} = \Gamma_{ab}^{+} \pm i\Delta\omega_{ab}, \; \gamma_{ab} = \rho_a^0 - \rho_b^0,$$

$$\Delta\omega_{pq} = \omega_{pq} - \omega_1, \; \Delta\omega_{mn} = \omega_{mn} - \omega_2.$$

For the "line form" we obtain

$$\frac{Q_{mn}^{+}}{\Phi_{mn}^{+}} = \frac{i\alpha_{mn}^{-}\{\gamma_{mn} - \gamma_{pq}s_{pq}(T_{mn}^{\nu}/T_{pq}^{\nu})\}}{|\alpha_{mn}|^2 + \Gamma_{mn}T_{mn}^{\mu}|\Phi_{mn}|^2\{1 - s_{pq}T_{mn}^{\nu}T_{pq}^{\mu}/T_{pq}^{\nu}T_{mn}^{\mu})\}}, \qquad (5)$$

where the saturation parameter is

$$s_{pq} = \Gamma_{pq}T_{pq}^{\nu}|F_{pq}|^2/(|\alpha_{pq}|^2 + \Gamma_{pq}T_{pq}^{\nu}|F_{pq}|^2);$$

a simple transformation of (5) produces a formula for P_{pq}^{+}/F_{pq}^{+}

It was shown in Ref. 1 that T_{mn}^{μ} and T_{pq}^{ν}, $1/\Gamma_{mn}$ and $1/\Gamma_{pq}$, which have the meanings of effective longitudinal and transverse relaxation times for the corresponding transitions, are positive. From the reciprocity theorem for the equivalent circuit for T_a, it follows that when $\hbar a/kT \ll 1$,

$$T_{mn}^{\nu} = {}_{i}T_{pq}^{\mu}, \; |T_{mn}^{\nu}|/T_{pq}^{\nu} < 1, \quad |T_{pq}^{\mu}|/T_{mn}^{\mu} < 1.$$

In this case, which usually holds for a nuclear spin system, the interaction of the fields, as can be seen from the denominator of formula (5), leads to a narrowing of the lines broadened by the saturation effect.

The extent of the effect is determined by the combination of the "crossover" relaxation times

$$\varkappa = (T_{pq}^{\mu}/T_{mn}^{\nu})/(T_{mn}^{\mu}/T_{pq}^{\nu})$$

and has no longer dependent on the distance between the resonant levels, in contradistinction with the effective level population. In connection with this, if $\varkappa$ is on the order of unity, the influence of the low-frequency resonant field on the resonant field of higher frequency should become noticeable.‡

In conclusion, I thank V. L. German and I. M. Lifshitz for discussion of the results.

*In the presence of a common resonant level, the situation becomes considerably more complicated, owing to the resonant contribution of the transitions through the common level, which acts as an intermediate one with the difference frequency.[1,2] In the usual electron-nuclear level scheme in the Overhauser effect, when the resonant fields for the electrons and nuclei have a common level, failure to take these transitions into account causes the constant hyperfine structure to tend to zero in the final result, which, as is known, gives a finite effect.[1] There is no common level if both resonant fields are due to electron transitions at different nuclear orientations.

†The prime indicates that one of the levels should be replaced by the normalization condition. Formally, the system of equations for T_a corresponds to a certain equivalent dc circuit.

‡We disregard level shifts (for example, the influence of polarization on nuclei on the position of the electron resonance[3]). We notice also that in experiments in which the Overhauser effect is measured with two fields,[4] there is no interaction between the fields, in view of the smallness of one of the resonant fields.

[1] F. Bloch, Phys. Rev. **102**, 104 (1956).

[2] S. H. Aulter and C. H. Townes, Phys. Rev. **100**, 703 (1955). V. M. Kontorovich and A. M. Prokhorov, J. Exptl. Theoret. Phys. (U.S.S.R.) **33**, 1428 (1957), Soviet Phys. JETP **6**, 1100 (1958). A. Javan, Phys. Rev. **107**, 1579 (1957).

[3] J. I. Kaplan, Phys. Rev. **99**, 1322 (1955).

[4] T. R. Carver and C. P. Slikhter, Phys. Rev. **102**, 975 (1956).

Translated by J. G. Adashko
161

ON THE THEORY OF PLASMA WAVES IN A DEGENERATE ELECTRON LIQUID

V. P. SILIN

P. N. Lebedev Physics Institute, Academy of Sciences, U.S.S.R.

Submitted to JETP editor January 2, 1958

J. Exptl. Theoret. Phys. (U.S.S.R.) **34**, 781-782 (March, 1958)

PLASMA waves in a degenerate electron gas were, apparently, first considered by Gol' dman.[1] However, the electrons in metals can hardly be considered as a gas. It is thus of interest to study the plasma oscillations of a degenerate electron liquid. According to Landau's theory of a Fermi liquid[2] the transport equation for the non-equilibrium correction δn to the distribution function of the quasi-particles (electrons) of a degenerate electron liquid has the form,[3]

$$\frac{\partial \delta n}{\partial t} + \mathbf{v}\frac{\partial}{\partial \mathbf{r}}\left\{\delta n - \delta\varepsilon\frac{\partial n_0}{\partial \varepsilon_0}\right\} + e\mathbf{E}\mathbf{v}\frac{\partial n_0}{\partial \varepsilon_0} = 0. \quad (1)$$

Here n_0 is the equilibrium distribution function, ϵ_0 the electron energy in the equilibrium state, and

$$\delta\varepsilon = \int \Phi(\mathbf{p},\mathbf{p}')\,\delta n(\mathbf{p}',\mathbf{r})\,d\mathbf{p}', \quad (2)$$

where Φ is typical for the theory of a Fermi liquid, reflecting the short-range correlation of the particles. Finally $\mathbf{E}$ is the electric field which is determined from the equation

$$\operatorname{div}\mathbf{E} = 4\pi e\int \delta n d\mathbf{p}. \quad (3)$$

In Eq. (1) collisions are neglected since it is assumed that the frequency of the plasma oscillations is much larger than the collision frequencies.

Considering solutions of Eq. (1) of the form $\delta n_{\mathbf{k}} e^{i(\mathbf{k}\cdot\mathbf{r})-i\omega t}$, and restricting ourselves to the case of long wavelengths, which allows us to expand in powers of k, we obtain from Eqs. (1) to (3), assuming that the Fermi surface is spherical, the following dispersion relation for the dependence of the frequency ω of the plasma waves on the wave vector at long waves

$$\omega^2 = \omega_0^2 + v_0 V_0\left(\frac{3}{5} + A_0 + \frac{4}{25}A_2\right)k^2, \quad (4)$$

where v_0 and p_0 are the velocity and momentum of an electron on the Fermi surface, and A_0 and A_2 coefficients in the expansion in Legendre polynomials

$$\frac{8\pi p_0^2\Phi}{3(2\pi\hbar)^2 v_0} = \sum_n A_n P_n(\cos\chi)$$

(χ is the angle between the vectors $\mathbf{p}$ and $\mathbf{p}'$). Finally

$$\omega_0^2 = 4\pi e^2\cdot 8\pi p_0^2 V_0/3(2\pi\hbar)^3,\ V_0 = v_0(1 + A_1).$$

For a perfect Fermi gas of electrons, $A_n = 0$ and (4) goes over into the corresponding formula of Gol' dman's paper. The author gave in Ref. 4 an estimate of the coefficient A_1 for a number of real metals. It was then shown that it was not at all allowed to neglect this quantity compared to unity.

It is useful to make an estimate for the coefficients A_n for the case when the function Φ is determined by the forward-scattering amplitude calculated in Born approximation for a screened Coulomb potential. In that case

$$A_n = \frac{4}{3\pi}\frac{e^2}{\hbar v_0}\frac{2n+1}{2}\int_{-1}^{1} dx\, P_n(x)\left\{\xi - \frac{1}{4}\frac{1}{1 - x + {}^1/_2\xi}\right\}$$

and correspondingly

$$A_0 = \frac{4}{3\pi}\frac{e^2}{\hbar v_0}\left\{\xi - \frac{1}{8}\ln(1+4\xi)\right\};$$

$$A_1 = \frac{1}{\pi}\frac{e^2}{\hbar v_0}\left\{1 - \frac{1}{2}\left(1+\frac{1}{2\xi}\right)\ln(1+4\xi)\right\};$$

$$A_2 = \frac{5}{2\pi}\frac{e^2}{\hbar v_0}\left\{1 + \frac{1}{2\xi} - \left(\frac{1}{3} + \frac{1}{2\xi} + \frac{1}{8\xi^2}\right)\ln(1+4\xi)\right\},$$

where $\xi = (p_0/\hbar k_D)^2 = \pi\hbar v_0/4e^2$, and $k_D = \sqrt{(4/\pi)}\, e^2/\hbar v_0 (p_0/\hbar)$ is the quantity which is the inverse of the screening radius. For most metals $v_0 \sim 10^8$ cm-sec^{-1} and hence $e^2/\hbar v_0 = 2.2$. Here $A_0 = 0.25$, $A_1 = 0.05$, and $A_2 = -0.05$.

If we consider anisotropic metals in the approximation $\omega_0^2/v_0^2 \gg k^2 \gg \omega_0^2/c^2$ (where c is the velocity of light), we can also speak of longitudinal waves,

$$\omega^2 = \frac{4\pi e^2}{k^2}\frac{2}{(2\pi\hbar)^3}\int\frac{dS}{v}(kv)(kV), \qquad (5)$$

where the integral is taken over the Fermi surface where dS is an element of that surface, and where

$$V = v + \frac{2}{(2\pi\hbar)^3}\int\frac{dS'}{v'}\Phi(p,p')v'.$$

The frequency of the plasma waves determined by equation (5) can also be found from the equation $k_\alpha k_\beta \epsilon_{\alpha\beta} = 0$, where $\epsilon_{\alpha\beta}$ is the dielectric constant of a degenerate electron liquid.[4]

Everything stated here can bear a relation to real metals only, apparently, if the energy of the plasma oscillation ($\sim\hbar\omega_0$) is small compared to the distance from the conduction band to the nearest filled band. One must then also take into account the contribution ϵ_0 to the dielectric constant, which comes not only from the conduction electrons.

We note finally that the dependence of the frequency of the plasma waves on the direction of the vector k can lead to a broadening of the line of discrete energy losses of electrons passing through non-cubic metals.

I express my gratitude to V. L. Ginzburg for a discussion of the present paper.

[1] I. I. Gol'dman, J. Exptl. Theoret. Phys. (U.S.S.R.) **17**, 681 (1947).

[2] L. D. Landau, J. Exptl. Theoret. Phys. (U.S.S.R.) **30**, 1058 (1956), Soviet Phys. JETP **3**, 920 (1956).

[3] V. P. Silin, J. Exptl. Theoret. Phys. (U.S.S.R.) **33**, 495 (1957), Soviet Phys. JETP **6**, 387 (1958).

[4] V. P. Silin, J. Exptl. Theoret. Phys. (U.S.S.R.) **33**, 1282 (1957), Soviet Phys. JETP **6**, 985 (1958).

Translated by D. ter Haar
162